« Agricultura non modo est ars, sed scientia »

(after Marcus Terentius Varro, ca. 37 BC, *Res Rusticae*, I. III.)

Promotors: Prof. dr. ir. Jan Pieters
Department of Biosystems Engineering,
Faculty of Bioscience Engineering,
Ghent University

Prof dr. ir. Bart Merci
Department of Heat, Flow and Combustion Mechanics,
Faculty of Engineering and Architecture,
Ghent University

Dr. ir. Peter Demeyer
Institute for Agricultural and Fisheries Research (ILVO)
Technology and Food Science Unit – Agricultural Engineering

Dean: Prof. dr. ir. Guido Van Huylenbroeck

Rector: Prof. dr. Anne De Paepe

Merlijn De Paepe

Experimental and model-based study of airflows and ammonia distributions in and around animal houses

Thesis submitted in fulfilment of the requirements
for the degree of Doctor (PhD) in Applied Biological Sciences

Dutch translation of the title:

Experimentele en modelgebaseerde studie van luchtstromingen en ammoniakdistributies in en rond stallen

Members of the jury:

Prof. dr. ir. Frank Devlieghere – Voorzitter(UGent, Vakgroep Voedselveiligheid en Voedselkwaliteit)
Prof. dr. ir. Ingmar Nopens – Secretaris (UGent, Vakgroep Wiskundige Modellering, Statistiek en Bio-informatica)
Dr. ir. Nico Ogink (Wageningen UR, Livestock Research)
Prof. dr. ir. Herman Van Langenhove (UGent, Vakgroep Duurzame Organische Chemie en Technologie)
Prof. dr. ir. Bart Sonck (UGent, Vakgroep Toegepaste Biowetenschappen)
Dr. lic. Lieve Herman (ILVO, Eenheid Technologie en Voeding)

Cover pictures:

Front: cows at ILVO, Eenheid Dier, Scheldeweg, Melle.
Back, from top to bottom: cattle barn scale model (see Chapters 2–3), Emission lab (Ch. 5–6), CFD model barn geometry with velocity vectors showing a ceiling-attached airflow (Ch. 4).
All pictures were taken by the author.

De Paepe M. (2014). Experimental and model-based study of airflows and ammonia distributions in and around animal houses. *PhD Thesis.* Ghent University, Belgium.

ISBN-number: 978-90-5989-698-7

SAMENVATTING

In dierhuisvestingssystemen kunnen diverse belangrijke eigenschappen rond het binnenklimaat worden onderscheiden: de temperatuur, de fijn stof- en gasconcentraties (incl. luchtvochtigheid), de luchtbeweging, het geluids- en lichtintensiteitsniveau. Ventilatie speelt hierbij een grote rol aangezien het noodzakelijk is om metabolisch gevormde warmte, CO_2, vocht en diverse schadelijke gassen te verwijderen en om de dieren bescherming te bieden tegen hitte- en koude-extremen buiten hun comfortzone. In dit opzicht heeft mechanische ventilatie reeds bewezen efficiënt te zijn. De werking hiervan is goed gekend en de ventilatiedebieten kunnen relatief gemakkelijk bepaald worden. Hoewel natuurlijke ventilatie een energie-efficiënte ventilatietechniek is, is het in de praktijk grotendeels onderbenut geraakt als gevolg van de beperkte beheersbaarheid van ventilatieniveaus en het bestaan van kennishiaten om deze beheersbaarheid te verbeteren.

De huidige kennis en meettechnieken laten geen nauwkeurige schattingen toe van de ventilatiedebieten en de emissies uit natuurlijk geventileerde stallen, wat te wijten is aan het ontbreken van een geschikte referentiemethode. Omdat de ventilatiedebieten in natuurlijk geventileerde stallen moeilijk te beoordelen zijn, zijn de daaraan gekoppelde emissieberekeningen ook zeer onzeker (met onzekerheden aanzienlijk hoger dan 10-20% geschat). Daarom is er verder onderzoek nodig om meettechnieken te ontwikkelen die nauwkeurig genoeg zijn, tevens om bestaande simulaties (bijv. modellen met CFD, voluit Computational Fluid Dynamics) te valideren en om meer consistente en nauwkeurige schattingen van deze emissies te verkrijgen.

Om aan deze eisen te voldoen, wordt in de literatuur gepleit voor een betere synergie tussen wiskundige modellering, fysische modellering en veldmetingen van ventilatiedebieten. Dit is vooral belangrijk in het licht van de wetgeving (zowel Europees als regionaal) die specifieke emissiereducties oplegt. Ammoniak (NH_3) kan worden gezien als de hoofdrolspeler in deze emissiereductieplannen. Momenteel wordt er voornamelijk gefocust op rundveestallen, die in de praktijk hoofdzakelijk natuurlijk geventileerd worden, omdat deze sector nog niet in

dezelfde mate als de varkens- of pluimveehouderij aangespoord is om hun emissies te verminderen. Een toenemende belangstelling voor de ontwikkeling van emissiearme rundveestallen en de rol van natuurlijke ventilatie hierbij is al een feit in Nederland. Aangezien dit naar alle waarschijnlijkheid ook meer aan belang zal winnen in Vlaanderen, moet deze trend en de behoefte aan een beter begrip grondig worden voorbereid. Vooral omdat de vraag naar dierlijke producten blijft groeien, is het van primair belang om natuurlijk geventileerde systemen verder te bestuderen, met name met betrekking tot hun interne luchtstromingen en emissies. De verdelingen van binnenklimaatparameters en emissiefenomenen zijn echter zeer complex en moeilijk te achterhalen vanwege hun vele invloedsfactoren. Dit leidt ertoe dat hun kwantificering een voortdurende uitdaging blijft. In het bijzonder geldt dit voor de bijdrage van de mestkelder, vanwege zijn kritische functie als bronlocatie van enkele belangrijke verontreinigende gassen.

Om deze redenen was de algemene doelstelling van dit proefschrift om meer inzicht te bekomen in een selectie van knelpunten in het huidige onderzoekslandschap, in het bijzonder met betrekking tot de complexe luchtstromingen onder natuurlijk geventileerde omstandigheden en het NH_3 massatransport vanuit de mestkelder. Als gevolg van werklast, technische uitdagingen en aanzienlijke kosten is het continu meten van luchtsnelheden en gasconcentraties moeilijk in de praktijk. Daarom bevat dit proefschrift onder meer de ontwikkeling van experimentele opstellingen die toelaten om gecontroleerde kwantitatieve studies onder steady-state condities uit te voeren, alsook de ontwikkeling en verificatie van daaraan verwante CFD modellen. Het onderzoek werd vooral gericht op rundveestallen (hoewel niet strikt), vanwege het feit dat natuurlijke ventilatie meestal in deze sector wordt toegepast.

In het eerste deel van het thesisonderzoek werden windtunnelexperimenten uitgevoerd voor een aantal ontwerpen van een stal op schaal 1:60, om een beter inzicht te verkrijgen in het complexe natuurlijke ventilatieproces in en rond stallen. Dit luik bestond uit luchtsnelheidsmetingen in de I.C.E. windtunnel van de Universiteit Gent.

In **hoofdstuk 2** werd het kwantitatieve effect bepaald van een aantal typische hoogten van ventilatieopeningen op de interne luchtsnelheden in zes schaalmodelontwerpen. De luchtsnelheden werden gemeten op acht posities, met nadruk op de twee zijdelingse ventilatieopeningen en de centrale posities onder de nokopening. Het effect van de

verschillende stalontwerpen op de windafwaartse luchtsnelheden werd hierbij eveneens onderzocht.

Uit deze experimenten kon worden besloten dat het wijzigen van de hoogte van de ventilatieopening de interne luchtstromingen aanzienlijk verandert. In de praktijk passen veehouders de ventilatiedebieten reeds aan door de ventilatieopeningen te openen of af te dekken met behulp van windschermen. Onze resultaten, verkregen onder isotherme omstandigheden, dus zonder opwaartse druk (of trekschouweffect), geven aan dat het vergroten van een inlaatopening aan de windzijde de snelheid van de inkomende luchtstroming doet verlagen, terwijl wel hogere luchtsnelheden waargenomen worden nabij de uitlaat. Het vergroten van de inlaatopening, of volledig openstellen van de wand, leidde tot 40% lagere inlaatsnelheden, maar meer dan 200% hogere snelheden door de uitlaatopening. Opmerkelijk is dat in het midden van de stal de luchtsnelheden nauwelijks beïnvloed werden door het ontwerp. Alleen bij het verwijderen van de achterste wand werden 3 à 4 maal hogere snelheden waargenomen t.h.v. het centrum van de stal.

Deze eerste studie was beperkt tot omstandigheden van loodrechte windinval. Om de realiteit van variërende windhoeken aan te pakken, was het doel van **hoofdstuk 3** om een kwantitatieve uitspraak te doen over het effect van de windinvalshoek op de binnenluchtsnelheden. Daartoe werden twee stalmodellen bestudeerd; de twee ontwerpen die over symmetrische ventilatieopeningen beschikten. De impact van de verschillende windinvalshoeken op de binnenluchtsnelheden kon grotendeels worden toegeschreven aan de relatieve positie van de kopgevels t.o.v. de windrichting. Deze positie bleek cruciaal en kan de gemeten trends in luchtsnelheden verklaren. Bij het draaien van de inkomende wind, namen de geschatte debieten doorheen de inlaat-en uitlaatopeningen geleidelijk af in beide schaalmodellen. Tot windinvalshoeken < 45° bleek ook dat het open staltype beter in staat was het ventilatiedebiet tussen de in- en uitlaatopening te behouden. Voor de praktijk betekent dit dat een natuurlijke geventileerde stal met open zijwanden een meer uniforme snelheidsverdeling binnenin toelaat. Bijkomend werden er lineaire regressies opgesteld die de opgemeten luchtsnelheden konden relateren met de windinvalshoek, voor hoeken tussen 0° en 45 °.

Naast de waarde van de experimentele resultaten op zich, nl. een vertaling van reële luchtstromingsverschijnselen naar een kleinere schaal, kunnen de kwantitatieve datasets tevens dienen ter evaluatie en verbetering van CFD-berekeningen. CFD kan van onschatbare

waarde zijn om een beter begrip te verkrijgen van de interne luchtstromingen in de (geschaalde) rundveestallen.

In **hoofdstuk 4** werd het effect van de hoogte van de ventilatieopeningen op de interne luchtsnelheden onderzocht d.m.v. tweedimensionale CFD-modellering, waarbij gebruik werd gemaakt van dezelfde zes stalconfiguraties zoals beschreven in hoofdstuk 2. De resulterende luchtstromingspatronen en luchtsnelheden werden hierin voorgesteld, evenals de overeenkomst met de eerder verkregen experimentele resultaten. Vergelijking van de numerieke (= CFD) data met de experimentele data leidde tot een relatief goede overeenkomst. Het belangrijkste voordeel van de CFD-benadering bestond eruit om de inwendige luchtstromingen voor elk van de ontwerpen te visualiseren. Ondersteund met nog andere modellen kan deze informatie uiteindelijk helpen bij het verbeteren van de stalinrichting en van luchtgeleidingstechnieken.

Het tweede deel van dit proefschrift richt zich op het NH_3-transport t.h.v. de mestkelder en de roostervloer. **Hoofdstuk 5** beschrijft de ontwikkeling van een vernieuwende testinstallatie die geschikt is voor de studie van massatransport: het 'Emissie Lab', ook afgekort tot 'EmiL'. Dit speelt in op de behoefte aan meer intensieve metingen in de praktijk, waar de omstandigheden zoals het ventilatiedebiet, de temperatuur en de mesthoogte (of omgekeerd: de vrije luchtruimte in de mestkelder) vaak moeilijk te veranderen zijn of moeilijk voor langere periode constant te houden zijn. Het emissielab bevat een mestkelder met een NH_3-emitterende oplossing en is bedekt door een betonnen roostervloer typisch voor runderen. Een hier bovenop geplaatste windtunnel zorgt voor luchtsnelheden tussen 0 en 1 m s^{-1} boven de roostervloer. Eerst werden de opbouw en de technische kenmerken van het emissielab beschreven en werden zijn prestaties getest tijdens een reeks van referentie-experimenten. Het voornaamste doel van deze testen was de algehele variabiliteit van de prestaties van de testopstelling te beoordelen, zodat dit kon dienen als basis voor de beoordeling van latere experimenten. Tijdens dit verkennende experiment werden specifiek de stabiliteit van parameters zoals de pH en temperatuur van de NH_3-emitterende oplossing en de gasvormige NH_3-concentraties onderzocht. Zoals gewenst kon de pH van de oplossing stabiel gehouden worden op 8,0 ± 0,1, wat ook resulteerde in stabiele NH_3-emissies. Uit zowel de meetresultaten als een theoretische benadering bleek dat de variatie op de NH_3-massatransfercoëfficiënt van de mestkelder (‘*PTC*’, een maat voor de emissie) beperkt bleef tot 13%. De *PTC*-waarden varieerden van $2{,}1 \times 10^{-3}$ tot maximaal $3{,}3 \times 10^{-3}$ m s^{-1}, wat ruim

binnen het bereik valt van de NH_3-massatransfercoëfficiënten gerapporteerd in de literatuur. Er kon dus worden besloten dat het emissielab betrouwbaar en geschikt is voor verdere experimenten met andere configuraties.

Emissie-experimenten met deze opstelling werden behandeld in **hoofdstuk 6**. Meer onderzoek was immers vereist met het oog op een steeds verdergaande verbetering van de luchtkwaliteit en op het verminderen van vervuilende emissies uit stallen met mestkelders; bijv. studies met betrekking tot de luchtlaag boven het mestoppervlak. Daarom is het essentieel om eerst te begrijpen wat de oorzaken zijn van verschillende luchtstromingspatronen in de mestkelder. Alzo werd het emissielab gebruikt om de impact van verschillende mesthoogten, luchtsnelheden en -richtingen op het NH_3- massatransport vanuit de mestkelder te bestuderen. De luchtstromingsrichting werd gewijzigd door de hoek van een klep boven de roostervloer te variëren (waarbij 0°: geen afbuiging van de wind, gezien de klep dan horizontaal staat, en 90°: volledige neerwaartse afbuiging van de wind naar de vloerspleten). De verschillende klephoeken kunnen staan voor de aan- of afwezigheid van verschillende obstakels in stallen in de praktijk, bijv. dieren, voederbakken en hokafscheidingen. De hoogte van de opgestapelde mest in de kelder is van belang omdat deze in de praktijk variabel is (wat ook leidt tot een variabele vrije ruimte tot aan de roostervloer, wat hier als parameter gebruikt is). Tijdens het ventilatieproces stroomt nl. lucht over/doorheen de roostervloer en in de mestkelder, waarbij het ventilatiedebiet rechtstreeks invloed heeft op de uiteindelijke gasemissies. Tenslotte kunnen de vermelde onderdelen van het interieur van de stal er eveneens voor zorgen dat er luchtstromingen in mindere of meerdere mate afgebogen worden en zo de mestkelder betreden. In de praktijk zijn deze drie factoren tegelijk aan het werk, dus is het van belang om de interactie tussen de bron van NH_3 (urine of mest) en het integrale effect van luchtstromingen op emissies te bestuderen.

De experimenten toonden aan dat het verlagen van de mesthoogte de NH_3-concentratie in de put niet beïnvloedde maar wel leidde tot significant lagere concentraties windafwaarts van de vloer. De NH_3-concentraties in de put werden niet beïnvloed door het verhogen van de luchtsnelheid boven de vloer. Hogere luchtsnelheden verlaagden de concentraties aan de windtunneluitlaat echter significant, maar leidden over het algemeen toch tot hogere emissiewaarden. Via de klep meer lucht in de kelder leiden, toonde duidelijke effecten: een neerwaartse luchtgeleiding (grotere klephoeken) leidde algemeen tot afnemende NH_3-

concentraties in de kelder en toenemende concentraties boven de roostervloer, wat uiteindelijk resulteerde in hogere emissies.

De NH_3-massatransfercoëfficiënt *PTC* steeg bij hogere ventilatiesnelheden of -debieten en bij grotere klephoeken, maar nam af bij een toenemende vrije ruimte boven het vloeistofoppervlak. Bij een klephoek van 0° zorgde een geleidelijke verlaging van deze bovenruimte van 0,90 m tot het minimum van 0,10 m tot een lineaire afname van de *PTC* met 45%. Deze trend werd ook waargenomen bij grotere klephoeken, maar dan minder uitgesproken. Het vergroten van de klephoek zelf toonde een toename van *PTC*, met een maximumwaarde waargenomen bij 45°. Globaal gezien varieerden de *PTC*-waarden tussen $9{,}8 \times 10^{-4}$ m s^{-1} en $5{,}1 \times 10^{-3}$ m s^{-1}. De effecten veroorzaakt door de diverse experimentele opstellingen leidden tot een globale variatiecoëfficiënt voor de *PTC* van 38%. Tevens werd een algemeen lineair model (GLM) ontwikkeld, dat de *PTC* waarden kon voorspellen, waarbij een groot deel van de variatie (82%) in de waargenomen *PTC* verklaard werd.

Driedimensionale CFD-simulaties van de emissielabexperimenten werden uitgevoerd in **hoofdstuk 7** om bepaalde aspecten, die niet ten volle kunnen worden gemeten tijdens experimentele studies, toch te kunnen visualiseren. Specifiek werden er twee mesthoogten, twee ventilatiedebieten en drie luchtstromingsrichtingen gemodelleerd. Het verhogen van de bovenruimte (= verlagen van de mesthoogte) leidde tijdens de experimenten niet tot significante effecten voor de NH_3-concentraties op zeven van de acht meetlocaties. De numerieke resultaten bevestigden deze experimentele bevinding. Ook op de andere vlakken legden de experimentele en de numerieke studies dezelfde effecten bloot. Meer lucht in de kelder geleiden, door het verhogen van de klephoek, leidde tot afnemende NH_3 concentraties in de kelder en toenemende concentraties boven de roostervloer, wat uiteindelijk zou leiden tot hogere emissies. Tenslotte werden de uitlaatconcentraties aanzienlijk verminderd door het verhogen van het ventilatiedebiet over de roostervloer. Wat de algemene trends betreft werd een goede overeenkomst gevonden tussen de experimentele en numerieke resultaten. Zowel het CFD-model als de experimenten toonden duidelijk aan hoe de verschillende luchtsnelheden en -richtingen de NH_3-concentratiegradiënt in en boven de mestkelder bepalen.

Het werd ook duidelijk dat de uitlaatconcentratie voor NH_3, die gebruikt wordt in de berekening van de emissie en de *PTC*, vaak hoger ingeschat werd door het CFD-model dan experimenteel bepaald. Dit kan te wijten zijn aan de beperkte representativiteit van de

puntmeting tijdens de experimenten. Het ontwikkelde CFD-model onthulde een gradiënt van NH_3-concentraties nabij de windtunnelvloer. Om nauwkeuriger te worden, zouden toekomstige emissiestudies in het algemeen dus baat hebben bij metingen op tal van meerdere locaties in de buurt van de luchtuitlaat.

De algemene discussie in **hoofdstuk 8** schetst de ruimere betekenis van de resultaten in de context van de thema's die aangekaart werden in de inleiding (hoofdstuk 1). De bevindingen van de ventilatiestudies op kleine schaal, nl. dat de windinvalshoek en de grootte van de ventilatieopeningen de inkomende ventilatiedebieten, de interne luchtsnelheden en de luchtstromingspatronen bepalen, zijn niet nieuw. De toegevoegde waarde van dit onderzoek ligt echter in het genereren van kwantitatieve data, zodat de verschillen tussen diverse ontwerpkeuzes beter onderscheiden kunnen worden. Kwantitatieve data zijn ook nuttig voor de ontwikkeling en verificatie van CFD-modellen, zoals aangetoond werd. Het ontwikkelde emissielab heeft zich daarenboven reeds bewezen als een uniek en waardevol platform voor de studie van luchtstromingen en massatransport op het niveau van de mestkelder. Een verdere optimalisatie van de opstelling is echter nog steeds mogelijk.

In dit proefschrift bleek het complementaire gebruik van experimentele platformen (op zowel kleine als grote schaal) met CFD-modellering een nuttige onderzoeksaanpak, die heeft bijgedragen tot een beter begrip van een aantal belangrijke factoren. Bovendien werd er aangetoond dat gecontroleerde windtunnelexperimenten een waardevolle techniek zijn om dit te bereiken, maar opnieuw vooral in combinatie met CFD-modellering. Een groot voordeel van de toegepaste CFD-modellering is de mogelijkheid om een brede en gedetailleerde weergave te verkrijgen van belangrijke parameters (bijv. luchtsnelheden, gasconcentraties, temperatuur, druk) in een willekeurige geometrie. CFD-modellering kan tevens helpen bij het optimaliseren van de testopstellingen.

Hoewel de huidige verkregen resultaten niet zomaar overdraagbaar zijn naar praktische toepassingen, kunnen gevalideerde CFD modellen wel worden gebruikt om allerlei fenomenen in verschillende geometrieën te onderzoeken, wat op zijn beurt zal leiden tot meer inzicht in (natuurlijke) ventilatie, luchtgeleidingstechnieken buiten de stal (bijv. windsingels, windschermen), emissiereductietechnologieën, enz. Het simuleren van de natuurlijke variabiliteit van wind blijft wel rekentechnisch complex.

De bevindingen van dit proefschrift kunnen dus worden beschouwd als een *proof of concept*, maar ze zorgen in ieder geval voor een wetenschappelijke basis en een aantal praktische

inzichten die de verdere optimalisatie van het ventilatieproces in natuurlijk geventileerde stallen ondersteunen (bijv. door het bouwen van nieuwe stallen volgens de meest geschikte gemiddelde windrichting) en leiden tot een beter begrip van (ammoniak)emissies uit stallen (bijv. de effecten van luchtsnelheid en luchtafbuiging nabij de roostervloer). Vooraleer de resultaten in de praktijk kunnen worden toegepast, worden echter een goede integratie met andere (reeds lopende) studies en verdere validatie aanbevolen. Met andere woorden zijn er aanvullende studies vereist, bijv. in praktijkstallen bezet door dieren, zodat eventuele interacties met het stalinterieur, de activiteit van de dieren of de variërende luchtpatronen kunnen worden geïdentificeerd.

SUMMARY

In animal housing systems, several important climate properties can be distinguished: temperature, dust (PM) and gas concentrations (including humidity), air movement, noise and light intensity levels. Ventilation plays a key role, since it is necessary to remove humidity and various harmful gases, and to provide protection against heat and cold extremes beyond the animals' comfort zone. With this respect, mechanical ventilation has proven to be efficient. Its working is well-known and the ventilation rates can be measured with relative ease. Although natural ventilation is an energy efficient ventilation technique, it has become largely underused in practice due to the existence of several knowledge gaps.

The current knowledge and measurement techniques do not allow for accurate estimates of ventilation rates and emissions from naturally ventilated barns, due to the lack of a standard reference method. Because the ventilation rate in naturally ventilated animal houses is difficult to assess, the related emission calculations for these houses are also highly uncertain (with uncertainties currently considerably higher than 10–20%). Therefore, further research and development are required to develop measurement techniques that are precise enough, also to validate simulation models (e.g., CFD or Computational Fluid Dynamics models), and to obtain more consistent and accurate emission estimates.

To meet these requirements, the literature argues in favour of a better synergy between mathematical modelling, physical modelling and field measurements of ventilation rates. This is especially important in the light of legislation (both European and regional), which imposes specific emission reductions. Ammonia (NH_3) can be seen as the protagonist in these emission reduction plans. Now, mainly cattle houses, which are in practice mainly naturally ventilated, are being focused at, since this sector has not been urged to reduce their emissions as much as the pig or poultry sector. With this respect, an increased interest in the development of low-emission cattle barns and the role of natural ventilation herein is already a fact in the Netherlands. Since this will probably have an influence on Flanders as well, this trend and the need for a better understanding should be thoroughly anticipated.

Summary

Particularly as demand for livestock products continues to grow, it is of primary importance to further study naturally ventilated systems, with regard to their internal airflows and emissions. However, the distributions of internal climate parameters and emission phenomena can be very complex, due to the many influencing factors. This makes their quantification a continuing challenge. In particular, this applies to the contribution from the slurry pit, due to its critical function as the source location of important pollutants.

Therefore, the general objective of this thesis was to achieve more insight into a selection of bottlenecks in the current research landscape, specifically regarding the complex airflows under naturally ventilated conditions and NH_3 mass transfer from the slurry pit. Continuous measurements of air velocities and gas concentrations are difficult in practice, due to the workload, the technical challenges and the considerable costs. Therefore, this thesis included the development of experimental set-ups that allowed controlled quantitative studies under steady-state conditions, as well as the development and verification of related CFD models. The research mainly focused on cattle houses (although not strictly), due to the fact that natural ventilation is mostly applied in this sector.

In the first part of the thesis, wind tunnel experiments were performed for a number of 1:60 scale model designs of a barn, in order to better understand the complex natural ventilation process in and around animal houses. This consisted of air velocity measurements using the Ghent University I.C.E. wind tunnel.

In **Chapter 2**, the quantitative effect of several common ventilation opening heights on the indoor air velocities was determined for six scale model designs. Internal air velocities were measured at eight positions, focusing at the two lateral ventilation openings and the central indoor positions beneath the ridge opening. The airflow obstruction (or windbreak) effect of the different barn designs on the leeward air velocity profile was also examined.

From these experiments it can be concluded that altering the ventilation opening heights significantly changes the indoor airflows. In practice, farmers already adjust airflow rates by opening or closing ventilation openings using windbreak screens. Our results that were obtained under isothermal conditions, i.e. without buoyancy, indicate that enlarging a windward ventilation opening (inlet) will lower the speed of the inlet air, should this be desired, although higher indoor air velocities were observed near the outlet. Enlarging the inlet opening, or completely opening up the wall, led to 40% lower inlet velocities, yet more than 200% higher outlet velocities. The larger inlet opening caused a higher airflow rate,

which was subsequently forced through the outlet opening. Noteworthy, at the centre of the house the air velocities were hardly affected by the design. Only in case of removal of the outlet wall, 3–4 times higher velocities were observed at the centre.

This first study was limited to conditions of perpendicular wind incidence. To address the reality of variable wind incidences, the objective of **Chapter 3** was to quantitatively report on the effect of the wind incidence angle on the indoor air velocities. To this end, two scale model barns were studied, i.e. the designs that featured symmetrical ventilation openings. The responses of different wind incidence angles on the indoor air velocities could largely be attributed to the relative position of the end walls towards the wind. This position is crucial and allows the measured air velocity trends to be explained. Upon rotation, the estimated airflow rates through the inlet and outlet openings gradually decreased in both scale models. It also became clear that, for wind incidence angles < 45°, the open-type barn is better at maintaining the airflow rate between the inlet and the outlet opening. In practice this would mean that naturally ventilated barns with open sidewalls allow for a more uniform indoor airflow distribution. Additionally, linear regressions were presented that relate the measured air velocity to the wind incidence angle, for angles ≤ 45°.

In addition to the value of these experimental results, being a small-scale representation of airflow phenomena in reality, the quantitative data sets can also serve the purpose of evaluating and improving corresponding CFD calculations. CFD can be of valuable help in order to obtain a more comprehensive understanding of the internal airflows in the scale-model cattle barns.

In **Chapter 4**, the effect of ventilation opening height on indoor air velocities was effectively investigated through two-dimensional CFD modelling, using the same six different ventilation opening configurations as described in Chapter 2. The resulting airflow patterns and indoor air velocities were presented, as well as the agreement with the previously acquired experimental results. Comparison with the experimental data led to relatively good agreement. The main advantage of the CFD approach was the ability to visualise the internal airflows for each of the designs. Eventually, this information, supported with other models, may assist in improving barn design and airflow guidance techniques.

The second part of the thesis focused on the NH_3 transfer process at the slurry pit level. **Chapter 5** describes the development of a novel real-scale test installation for mass transfer studies (the 'Emission Lab', or 'EmiL' in short). This addresses the need for intense

measurements in real life occupied barns, where the conditions such as the ventilation rate, temperature and slurry pit headspace height are often difficult to alter or maintain. The emission lab contained a slurry pit section with an NH_3 emitting solution, covered with a slatted floor as typical for cattle. A wind tunnel construction on top of the floor allowed for air velocities above the floor in the range of 0–1 m s^{-1}. First, its buildup was described and its technical characteristics and performance during a series of standardised experiments was tested. The main purpose of these tests was to assess the overall variability of the test installation's performance, as a basis for evaluation for further experiments. In this exploratory experiment, specifically the degree of stability of parameters such as solution pH and temperature and gaseous NH_3 concentrations was studied. As desired, the pH of the NH_3 emitting solution could be kept stable at 8.0 ± 0.1, resulting in stable NH_3 emissions. The measurement results as well as a theoretical approach showed that the variation on the pit transfer coefficient (*PTC*, a measure for the emission rate) was limited to 13%. The *PTCs* ranged from 2.1×10^{-3} to maximum 3.3×10^{-3} m s^{-1}, which is well within the range of NH_3 mass transfer values found in the literature. It could be concluded that the emission lab was reliable and suitable for further experiments with other configurations.

Actual emission experiments with this set-up were addressed in **Chapter 6.** In order to further mitigate both indoor air pollution as well as emissions from animal houses with slurry pits, more research was still required, e.g. regarding the air layer above the slurry surface. Understanding what causes different airflow patterns in the slurry pit is therefore essential. Therefore, the emission lab was used to study the impact of varying headspace heights, air velocities and direction on NH_3 mass transfer from the pit. The airflow direction was altered via the angle of a deflector above the slatted floor (0° meaning no change in airflow direction, since the deflector was in horizontal position then, while 90° implied a complete downward airflow deviation towards the floor slits). Different deflector positions can relate to the absence or presence of different obstacles in commercial barns, e.g. animals, feeding troughs, and pen boards. Because the manure build-up in the pit is variable in practice, it leads to a variable headspace height to the slatted floor. During the ventilation process air flows over the slatted floor, whereby the airflow rate also affects emissions. Finally, certain components of the animal house's interior may also lead to airflow entering the slurry pit, resulting in varying emission rates. In practice, these three factors are

simultaneously at work, so it is of importance to study the interaction between the NH_3 source and the integral effect that airflows may have on emissions.

It was found that increasing the headspace height did not affect the NH_3 concentrations in the pit but led to significantly lower NH_3 concentrations measured leeward from the floor. NH_3 concentrations in the pit were not affected by increasing the air velocity above the floor. Higher air velocities significantly reduced the wind tunnel outlet concentrations, but generally led to higher emission rates. Guiding more air into the pit led to clear effects: a more downward guidance (higher deflector angles) generally led to decreasing NH_3 concentrations in the pit and increasing concentrations above the pit, resulting in higher emissions.

The NH_3 pit transfer coefficient (*PTC*) was found to increase with higher airflow rates and deflector angles, but to diminish with increasing headspace height. At a deflector angle of 0°, gradually reducing the headspace height from 0.90 m to its minimum of 0.10 m, led to a linear decrease of the *PTC* by 45%. This trend was also seen at higher deflector angles, but less pronounced. Increasing the deflector angle itself showed an increase in *PTC*, with a maximum value at 45°. Overall, the *PTC* values ranged between 9.8×10^{-4} m s^{-1} and 5.1×10^{-3} m s^{-1}. The effects induced by the different experimental setups led to a global variation coefficient of *PTC of* 38%. A general linear model to predict *PTC* values was also presented, which explained a large part (82%) of the variation in the observed *PTCs*.

In order to visualise aspects that cannot be measured to the fullest extent during experimental studies, three-dimensional CFD simulations of the emission lab experiments were performed in **Chapter 7**. Specifically, two pit headspace heights, two airflow rates and three airflow directions were modelled. Increasing the headspace height during the experiments did not lead to significant effects for the NH_3 concentrations at seven of the eight measurement locations. The numerical results confirmed this experimental finding. Again, both the experimental and numerical studies observed the same effects. Guiding more air into the pit by increasing the deflector angle led to decreasing NH_3 concentrations in the pit and increasing concentrations above the slatted floor, which would eventually result in higher emissions. Finally, the outlet concentrations were significantly reduced by increasing the airflow rate over the slatted floor. Also in this case, the numerical results confirmed the experimental finding. Regarding the overall trends, good agreement was found between the experimental and numerical results. Both the CFD model and the

experiments confirmed that different airflow rates and directions clearly determine the NH_3 concentration gradient in and above the slurry pit.

It also became apparent that the outlet NH_3 concentration, used for the calculation of emission rates and pit transfer coefficients (*PTC)*, was very often estimated higher by the CFD model than determined experimentally. This could be due to the limited representativeness of the one-point measurement during the experiments. The developed CFD model in fact revealed a gradient of NH_3 concentrations near the wind tunnel floor. Future emission studies in general would thus benefit from measurements at several more locations near the outlet, in order to become more accurate.

The general discussion in **Chapter 8** displays the wider significance of the results in the context of the themes raised in the introduction (Chapter 1). The findings of the small-scale ventilation studies, i.e., that the angle of wind incidence and the size of the ventilation openings determine the incoming airflow rates, the indoor air velocities and the airflow patterns, are not new. However, the added value of this research is in the generation of quantitative data, so differences between various design choices can be better distinguished. Quantitative data are also useful for the development and verification of CFD models, which has been illustrated. The developed emission lab set-up has already proven to be a unique and valuable platform for the study of airflows and mass transfer at the slurry pit level. However, further optimisation of the set-up is still possible.

The complementary use of experimental platforms in this thesis (whether small or large-scale) with computational modelling proved to be a useful research approach, which has contributed to a better understanding of a number of key factors. Additionally, it has been proven that controlled wind tunnel experiments are a valuable technique to accomplish this, but again especially in combination with CFD modelling. A great advantage of the applied CFD modelling is the ability to generate a broad and detailed view of the parameters of interest (e.g. air velocities, gas concentrations, temperature, pressure) in any geometry. CFD modelling can also be of help in the optimisation of test constructions.

Although the present results are not directly transferable to practical applications, validated CFD models can be used to investigate various phenomena in multiple geometries, which in turn will lead to more insight into (natural) ventilation, outdoor air conduction techniques (e.g., shelterbelts), abatement technologies, etc. The simulation of wind's natural variability does remain computationally complex.

The findings of this thesis can therefore be considered as a proof of concept, but they certainly provide a scientific basis and some practical insights which support the further optimisation of the ventilation process in naturally ventilated barns (e.g., by placing new animal houses according to the average wind direction that is best suited) and the understanding of (NH_3) emissions from barns (e.g., the effect of near-floor air velocities and direction). However, before the findings can be applied directly in practice, integration with other (already ongoing) studies and further validation is recommended. In other words, additional testing is required, e.g. in commercial barns occupied with animals, so that possible interactions with the barn type and interior, the animal activity or the fluctuating airflow patterns can also be identified

TABLE OF CONTENTS

LIST OF SYMBOLS AND ABBREVIATIONS

A	free surface area of the ventilation opening, m²
A_{inlet}	free surface area of the inlet opening, m²
A_{outlet}	free surface area of the outlet opening, m²
A_{ridge}	free surface area of the ridge opening, m²
A_s	surface area of the air-solution interface, m²
AAQ	agricultural air quality
AMTC	ammonia mass transfer coefficient, m s^{-1}
AOZ	animal occupied zone
C	centre plane under the ridge in scale model
$C_{1\text{-}8}$	NH_3 concentration measured at positions 1 to 8, mg m^{-3}
C_a	bulk air NH_3 concentration, mg m^{-3}
C_d	discharge coefficient (typically 0.61 for openings with sharp edges), dimensionless
C_{in}	inlet concentration, mg m^{-3}
C_{out}	outlet concentration, mg m^{-3}
C_s	equilibrium NH_3 concentration in the gas phase in contact with the solution surface, mg m^{-3}
C_v	ventilation coefficient, dimensionless
CFD	Computational Fluid Dynamics
D	hydraulic diameter, m
DA	deflector angle, °
E	NH_3 emission rate, mg s^{-1}
g	gravitational constant, 9.81 m/s²
H_{inlet}	heights of bottom to top of the inlet opening, m
H_{outlet}	heights of bottom to top of the outlet opening, m
H_t	total height of the scale model; 0.15 m
HH	headspace height in slurry pit, m
I	inlet (front) ventilation opening of scale model
I	turbulence intensity, %
IAQ	indoor air quality

k	turbulence kinetic energy, $m^2\ s^{-2}$
K_D	dissociation constant, dimensionless
K_H	Henry's constant, dimensionless
L	left measurement position in scale model
L_t	characteristic length of the wind tunnel, m
M	middle measurement position in scale model
m	NH_3 mass fraction, $mg\ m^{-3}$
O	outlet (back) ventilation opening of the scale model
O_v	virtual origin, at front-left-bottom of the slatted floor
Δp	pressure difference over the opening, Pa
PTC	pit transfer coefficient for NH_3, $m\ s^{-1}$
Q	ventilation or airflow rate, $m^3\ s^{-1}$
R	right measurement position in scale model
Re	Reynolds number, dimensionless
sd	standard deviation
SM	scale model
SM1	standard scale model (with equally large inlet and outlet opening height)
SM2	standard scale model with closed ridge opening
SM3	standard scale with closed outlet opening
SM4	low-front scale model, with front wall 0.02 m in height
SM5	open-front scale model, without front wall
SM6	open house scale model, without front nor back wall
T	temperature, °C
T_{sol}	ammonium solution temperature, °C
T_{WT}	temperature in wind tunnel, °C
u	longitudinal component of air velocity (in the x direction), $m\ s^{-1}$
$\bar{u}$	average air velocity through a ventilation opening, $m\ s^{-1}$
$u_{1\text{-}6}$	air velocity in floor slit 1-6, $m\ s^{-1}$
u_r	reference air velocity (without scale model), $m\ s^{-1}$
$u_{slit\ L}$	air velocity in back left floor slit, $m\ s^{-1}$
$u_{slit\ R}$	air velocity in back right floor slit, $m\ s^{-1}$
u_{WT}	air velocity in wind tunnel, $m\ s^{-1}$

x length along the wind tunnel work section, m

y width along the wind tunnel work section, m

z height along the wind tunnel work section, m

Greek symbols

ε turbulence dissipation rate, $m^2\ s^{-3}$

v kinematic viscosity (of air), $m^2\ s^{-1}$

ρ_a air density, $kg\ m^{-3}$

ϑ wind incidence angle, i.e. the angle between the wind direction and a perpendicular to the upwind sidewall, °

φ relative humidity, %

ω specific turbulence dissipation rate, s^{-1}

CHAPTER 1. GENERAL INTRODUCTION

1.1. Impact of airflows in and around animal houses

1.1.1. INDOOR CLIMATE

In animal housing systems, several important climate properties can be distinguished: temperature, dust (PM) and gas concentrations (including humidity), air movement, noise and light intensity levels. Ventilation plays a great role in all of these, except for the light levels. An appropriate indoor air quality (IAQ) is essential for the health and general well-being of farmers and animals (Spoolder et al., 2000; Radon et al., 2002) and the productivity gain (Fisk et al., 1997). Over the years, several studies have shown the benefits of a uniform air distribution inside agricultural buildings (e.g., Boulard et al., 2002; Gebremedhin & Wu, 2005).

A controlled air stream is necessary for the adequate removal of heat, humidity and gases, such as carbon dioxide (CO_2) and ammonia (NH_3), as well as to provide protection against temperature extremes. The desired climate is different for each animal species and also depends on the weight and the developmental stage of the animal. The required ventilation rate is related to the animal activity, but is in practice generally determined by three parameters: the sensible heat, the humidity, and the internal CO_2 concentration (CIGR, 1994). Usually only the thermal optimum for the animals is considered (Ki et al., 2006).

Indeed, the indoor temperature in barns plays an important role. Animals have a specific zone of thermal comfort that depends primarily on their species, their physiology, the relative humidity and the ventilation rate (St-Pierre et al., 2003). Beyond this zone the animals encounter stress when trying to maintain their homoeothermic balance. Several authors have reported symptoms associated with temperature stress, such as reduced food intake, reduced growth and milk production, and a decrease in reproduction (Broucek et al, 1981; Bianca, 1976; Hahn, 1999; Jordan, 2003; Ravagnolo, 2000; Silanikove, 2000; West, 2003).

Heat exchange can occur in three ways: by conduction, convection and radiation. In naturally ventilated buildings, these internal parameters are directly linked to the outside climate parameters such as wind velocity, wind direction, outside temperature and insolation (Campen & Bot, 2001). It should also be remembered that a certain temperature (T) or relative humidity (RH) cannot be achieved independently of each other, since RH and T affect each other. RH can be calculated from the vapour pressure (P) and the saturated vapour pressure (P_S) at the prevailing temperature (Equation 1) (KNMI, 2001).

$$RH = P / P_S(T) \times 100\% \quad (1)$$

For an optimal production, the CIGR Committee (1994) recommends a relative humidity around 70–75%. In some animals' growth stages other humidity requirements are sometimes imposed. Excessive water vapour produced by the animals should be removed as quickly as possible, since high humidity may facilitate the growth of fungi and bacteria. However, a low moisture content can also be unfavourable, as this dries out the animals' mucous membranes and facilitates the production of fine dust (PM), which is known to carry bacteria (Bianca, 1976) and has negative health impacts (Van Ransbeeck, 2013).

Temperature and humidity do not only play an important role towards animal welfare, they can also have adverse consequences for the building construction. Condensation on the walls is likely to cause surface moulds, which decreases the viability of the building, and implies more intense maintenance (Boussery & Christiaens, 2002).

Also at legal level, demands are made concerning the quantity and quality of the internal climate. The European Council Directive 98/58/EC (EU, 1998), regarding the protection of farm animals, states that air circulation, particulate matter (PM) levels, temperature, relative air humidity and gas concentrations must be "kept within limits which are not harmful to the animals" (without assigning explicit values).

The ventilation of animal houses is related to atmospheric emissions of NH_3, CO_2, CH_4, N_2O, H_2S and PM (Jungbluth et al., 2001; Kim et al., 2008; Teye & Hautalla, 2008). Thus, not only is there a growing concern about the impact on indoor air quality, but also on the atmosphere (Aneja et al., 2008; Zhang et al., 2008a). This problem has increased in recent years, due to the specialisation and up-scaling of agriculture (Ogink & Aarnink, 2003).

The gas production from livestock has several origins: the CO_2 production by the animals' respiration and release from manure, the production of nitrous oxide (N_2O), ammonia (NH_3) and hydrogen sulphide (H_2S) from the fermentation of excrements, and the release of methane (CH_4) originating from ruminants' digestive systems and from manure storage (Ni et al., 2000; Landbouwrapport, 2005; VMM, 2011). These pollutants and their emissions are discussed in further detail in Section 1.1.5.

In the barn building, different zones related to the emission process can be identified, such as the slurry pit headspace, the floor surface, the animal occupied zone (AOZ), the human height level and the emission zone. Each of these zones features distinct pollutant transfer processes. Takai et al. (2013) have distinguished the following five processes:

(1) pollutant production in the substrate (manure and urine at floor level or in the slurry pit)
(2) transfer from the liquid to the gas phase
(3) transfer through the boundary layer
(4) mixing inside the building envelope (i.e., the AOZ, the human zone and above)
(5) transport to the wider environment (i.e., actual emissions).

Figure 1 shows a schematic overview of the separate pollutant sources, each contributing to the total emission. This immediately hints at the usefulness of a source-oriented approach of emission reductions.

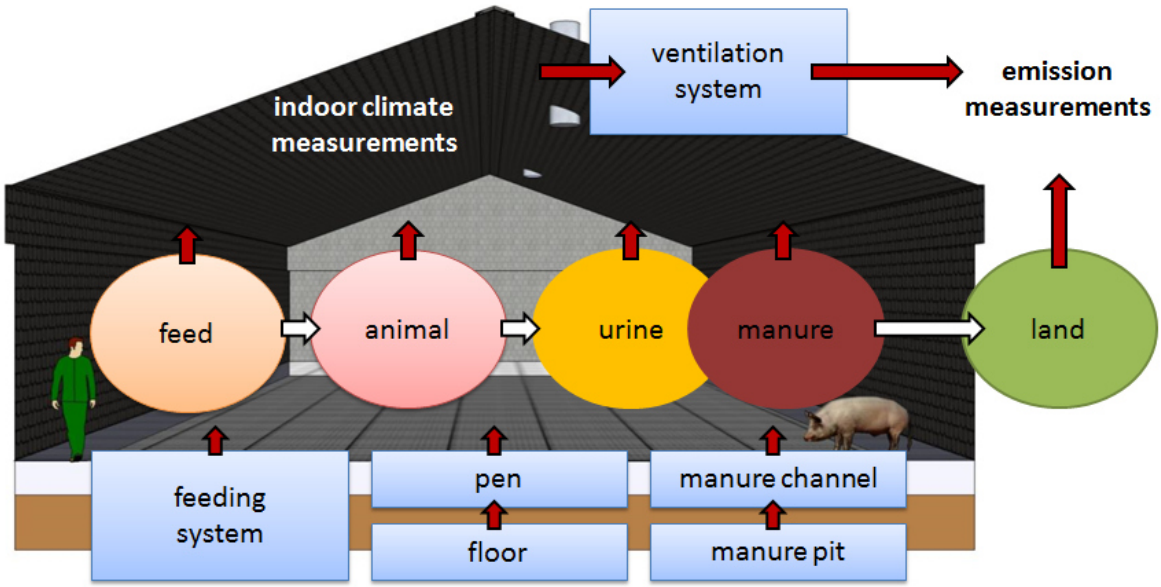

Figure 1 - Schematic overview of the typical elements and interactions in and around an animal house, and their impact on aerial emissions. (Source: Demeyer & De Paepe, previously unpublished)

1.1.2. VENTILATION SYSTEMS

To provide an adequate indoor climate for production purposes, animal houses rely amongst others on airflows generated through a ventilation system. There are two different major ventilation systems: mechanical and natural ventilation, according to the respective driving forces employed.

Mechanical ventilation

In mechanically ventilated (MV) buildings, a pressure difference is created mechanically through one or more fans (Figure 2). There is a large diversity of fan systems available on the market. In poultry housing examples are longitudinal (or front-end), lateral, tunnel, and ridge ventilation, or a combination thereof with inlet tubes or valves. In pig housing the variation is even greater, through the way the ventilation systems introduce fresh outside air into the barn: door (feeding corridor), valve, ceiling, pipe (i.e. the "fresh nose" system in farrowing units), valve, and floor channel ventilation (Stevens, 2007).

Mechanical ventilation systems are mostly automatically controlled according to specified needs, which makes them very effective at controlling the indoor climate. Therefore, precise control of indoor conditions should be possible under most weather conditions. This makes mechanical ventilation the most effective and commonly used ventilation technique, particularly for animals with a narrow thermal comfort zone. Thus, the need for climate control is considered to be an essential key factor for the preference of mechanical ventilated systems in practice (van 't Klooster, 1994). However, these systems suffer from a relatively high energy consumption and can also bring about noise (Algers et al., 1978), leading to the animals experiencing stress (Weeks, 2008). Also, their reliance on fossil energy means that natural ventilation is now more frequently investigated again (Norton et al. 2007). For instance, the average energy input for mechanical ventilation in growing pig housing is estimated around 28 kWh/animal/year (McCutcheon, 2013), but the power consumption of fans may vary strongly, depending on their efficiency, rotations per minute (RPM), pressure loss, and the accuracy in terms of settings (e.g., Schild & Mysen, 2009). Also noteworthy is the fact that mechanically ventilated buildings represent isolated industrial entities without transparency to the outer world/society in what is happening inside. This is

one of the reasons that the dairy sector is reluctant to introduce mechanically ventilated barns, for fear of damaging the public image of dairy production.

For research purposes, a great advantage of mechanical ventilation lies in the ease of control and measurement of the ventilation rates, by placing a free-rotating impeller anemometer in the fans' shaft. The impeller's rotations per unit time can be translated to a ventilation rate. Coupled with measurements of the difference in gas concentration between these outlet points and the incoming air, a reliable estimate of the emission rate can be provided.

Figure 2 - Example of a ceiling fan in a mechanically ventilated barn.

Natural ventilation

Another way to achieve a suitable indoor climate is by natural ventilation (NV), which is also a key method in the energy-efficient design of civil buildings (Khan, Su & Riffat, 2008). Regarding energy consumption and indoor noise, natural ventilation is indeed the technique listed by the EU as the BAT (Best Available Technique) for intensive animal rearing, where possible to apply (EPA, 2008; IPPC, 2013). Using naturally available resources, i.e., wind and buoyancy, this technique is also relatively low cost in comparison with mechanical ventilation. It also limits further emission of CO_2, in the likely event that otherwise mechanically ventilated fans are powered by fossil fuels. In this respect, the energy efficiency of natural ventilation systems is a major advantage. Additional advantages for the occupying animals are the silent operation of natural ventilation and the fact that natural ventilation is fail-safe, whereas power failures in mechanically ventilated systems interrupt

the operation of the fans. Under certain conditions (e.g., during warm weather) and for a prolonged period, this can result in the animals suffocating, leading to death by heat stress. On the other hand, this can also happen under natural ventilation conditions if the ventilation rates are insufficient.

Natural ventilation became rather underused in livestock farming and its implementation is currently mostly limited to dairy houses. This is partly due to important challenges related to complicated time-dependent effects that must be dealt with (Linden, 1999). In practice, these can lead to the need for more complex ventilation management strategies, especially in treating acute changes in the indoor microclimate, e.g. high temperature and air contaminant levels, due to dynamic outdoor conditions.

Naturally ventilated agricultural structures can be divided in (automatically) controlled and non-controlled systems (Hoff, 2004). An automatically controlled natural ventilation (ACNV) system offers the possibility to alter the airflow inlets and outlets through automation, according to the desired internal climate parameters (e.g., temperature). For example, wind screens spanning across the ventilation openings can be lowered. Another possible subdivision in naturally ventilated buildings lies in the open versus closed hangar design. In an open hangar design, one or more side walls remain fully open.

Natural ventilation has two driving forces: a pressure gradient created by wind and one created by temperature differences. A building that is exposed to the wind will experience a positive pressure at the windward side, due to the direct impact of the wind. A negative pressure or suction force is generated at the majority of the other sides of the building, as well as on the roof, depending on its slope. Due to this pressure difference, air in the building will be forced from the windward openings to the sheltered, or leeward, openings (Linden, 1999).

Yet, even when there is no wind, airflows may still occur due to a thermal gradient. Basically, this amounts to a difference in air density due to temperature differences between the interior and the exterior, which depends on heating caused by the heating system, convective and radiative fluxes, or by the metabolism of the occupying animals. Fresh air enters the building through the ventilation openings, heats up due to mixing with the indoor air, consequently rises and leaves the building through the ridge opening. This phenomenon is better known as buoyancy or the 'stack effect' (Khanduri et al., 1996; Linden, 1999). Since buoyancy increases with height, a roof pitch angle of at least 20° is suggested to accomplish

a sufficient effect (IPPC, 2003). Especially during conditions of low wind speed and high temperature it is important to make good use of the buoyancy effect (van 't Klooster, 1994). Generally, the effects of wind dominate over the buoyancy effects when wind speeds are above 2 m s^{-1} (Jardinier, 1980).

Additionally, in regions with warm climates designs of open hangars can be found (Figure 3). They mainly feature a roof to protect against direct sunlight.

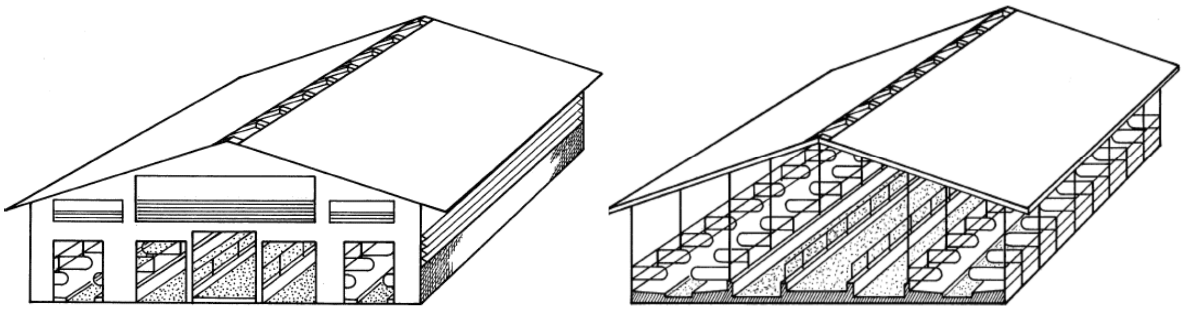

Figure 3 - Barns with typical lateral openings (left) and an open hangar design (right), as well as a ridge opening (Graves & Brugger, 1995)

1.1.3. VENTILATION RATE

The ventilation rate is expressed as the volumetric flow rate of outside air being introduced into the building, or indoor air exiting the building, and can be expressed in e.g. $m^3 s^{-1}$. Several calculation approaches exist. For mechanically ventilated buildings, the ventilation rate can be easily acquired by measuring the pressure difference between the outlet duct and the outside air, or through the rotations of an impeller fitted near the exhaust fan. This however, cannot be applied in naturally ventilated buildings, due to their large openings through which the wind direction also varies according to the external weather conditions. Therefore, other indirect methods were developed in order to determine natural ventilation rates.

For instance, when the pressure difference over a ventilation opening is measured, the wind-driven ventilation rate can be calculated using Equation 2 (ASHRAE, 2009):

$$Q_w = C_d A \sqrt{\frac{2 \Delta p}{\rho_a}} \quad (2)$$

where:

Q_w = wind-driven ventilation rate, $m^3\ s^{-1}$

C_d = discharge coefficient (typically 0.61 for openings with sharp edges)

A = opening surface area, m^2

Δp = pressure difference over the opening, Pa

ρ_a = air density, $kg\ m^{-3}$

Another approach involving anemometry allows for a simple calculation of the ventilation rate (Equation 3), e.g. in scale-model studies.

$$Q = \bar{u} \times A \tag{3}$$

where: $\bar{u}$ = average air velocity throughout the opening, $m\ s^{-1}$; A = opening surface area, m^2

The ventilation rate for buoyancy-driven natural ventilation using openings at two different heights (e.g. a side inlet and a ridge opening) can be estimated with Equation 3 (ASHRAE, 2009):

$$Q_b = C_d\ A \sqrt{2\ g\ H_d\ \frac{T_i - T_o}{T_i}} \tag{4}$$

where:

Q_b = buoyancy-driven ventilation rate, $m^3\ s^{-1}$

A = opening surface area, m^2 (assuming equal inlet and outlet areas)

g = gravitational constant, $9.81\ m/s^2$

H_d = height from midpoint of lower opening to midpoint of upper opening, m

T_i = average indoor temperature between inlet and outlet, K

T_o = outdoor temperature, K

However, in practice, the used techniques are mostly indirect methods based on energy or mass balance calculations, such as heat balance (Strøm, 1978; Pedersen et al., 1998) or moisture balance calculations (FAO, 2011) and the CO_2 mass balance method (Scholtens et al., 1994; Van 't Ooster, 1994; Pedersen et al., 1998). Also frequently applied in naturally ventilated barns is the tracer gas method (Demmers et al., 2000). Sulphur hexafluoride (SF_6) is the most widely used tracer gas, although it carries great global warming potential. Krypton (^{85}Kr) is also used as tracer gas, despite its human health hazard potential (Takai et

al., 2013). Tracer gas methods rely on the assumption that the ratio between the emission rates of the pollutant of interest (or air in whole) and the tracer gas is equal to the ratio between this pollutant and tracer gas concentrations (Ogink et al., 2013). However, due to the substantial effect of the sensor placements, even in a controlled laboratory environment the total error can be as high as 86% of the ventilation rate, when it is based on a single measurement point of the tracer gas (Van Buggenhout et al., 2007; Ozcan & Berckmans, 2010). Hence, to be representative for the total barn, tracer gas methods and the ratio method in particular should always be based on multiple sampling points. Tracer gas methods have an important limitation since they assume that the air and the tracer gases mix perfectly in the ventilated air volume, although perfect mixing can only be obtained under ideal conditions (Takai et al., 2013). For emission estimates itself, the tracer gas ratio method does not require perfect mixing throughout the barn, but the reliability of ratio methods applied to naturally ventilated barns with large openings still needs to be improved (Ogink et al., 2013).

For naturally ventilated piggery buildings, some important factors affecting ventilation and air exchange rates have already been identified: the type of ventilation system used, height of ventilation openings, animal stocking density and building size (Banhazi et al., 2008, 2010, 2011). These findings are likely to be useful for identifying the effects that influence ventilation rates in naturally ventilated cattle buildings as well. However, due to the large ventilation openings in naturally ventilated buildings and the dynamic conditions of airflows, it still remains difficult to measure their ventilation rates accurately (Albright, 1990; Hellickson & Walker, 1983; Kiwan et al., 2013; Müller et al., 2007; Ozcan, 2011), which has serious repercussions for the consistency and accuracy of emission estimates (Takai et al., 2013). While the standard uncertainty for short time basis building emissions (i.e., typically measured in a representative outlet section during a few minutes) in mechanical ventilation is reported to be at best 10–20% or more, in natural ventilation it is considerably higher due to the lack of a standard reference method and there may also be significant unquantifiable biases, such as the choice of measurement positions and the heat production of the animals (Calvet et al., 2013).

1.1.4. BUILDING INTERACTIONS

For naturally ventilated systems, the required ventilation rate is not only dependent on characteristics such as the outdoor-indoor temperature difference and wind velocity, but also the ventilation opening design, the wind incidence angle, and possible interference of the building's interior and its surroundings, e.g. other constructions or vegetation.

Ventilation openings

To achieve internal airflow at all, and at the required ventilation rate, it is of course essential to implement ventilation openings in the building. The ventilation openings in naturally ventilated barns are typically very wide, running alongside the entire building (Figure 4).

a)  b) 

Figure 4 - Examples of lateral ventilation openings: (a) large, (b) small and fitted with a tightly woven wind screen (green).

Due to these large ventilation openings in naturally ventilated barns, Takai et al. (2013) have stated that the difference between inside and outside air pressure can be extremely small, i.e. often 1 Pa or lower, with outdoor wind direction and speed playing the main roles for air exchange in the building. It was also stated that this results in rapidly fluctuating airflows, changing air inlet and outlet locations and non-homogeneous pollutant distribution.

A very important variable is the ventilation opening height, which can be fixed or made adjustable with the use of wind screens. The necessary height of the opening is then dependent on the used windbreak material, since its porosity can vary. Screens are certainly useful in the case of buildings with fully opened sidewalls, in order to avoid ventilation rates

that would exceed recommendations (Brouk, Smith & Harner, 2000). A completely opened ventilation opening is usually not recommended, as this would not shelter the animals sufficiently, except during warm summer conditions. Besides windbreak materials fitted inside the ventilation opening (e.g., adjustable screens, space boarding, or other materials), artificial or natural shelterbelts can also be implemented near the barn (e.g., hedges, rows of trees).

In addition to lateral openings, usually one or more ridge openings (Figure 3) are provided to release excessive heat, moisture and gases. Generally, a ridge width of 0.05 m is provided for every 3.00 m of building width, with a minimum of 0.15 m (Graves & Brugger, 1995). Adverse wind effects on the ventilation can be reduced or avoided by installing a wind deflector (or spoiler) along the open ridge, and/or a hood at the air inlet (Maton et al., 1985). They are commonly used in practice to increase the Venturi effect through the ridge.

Building position and orientation

Apart from the speed of the wind entering via the ventilation openings, the largest contributor to an efficient natural ventilation is the orientation of the building, specifically of the ventilation openings (e.g., Yu, Hou & Liao, 2002). As well as the building's shape and adjacent constructions (see below), the angle of wind incidence strongly affects the pressure distribution around the building. Therefore, building orientation is of essential importance in obtaining an optimum indoor air quality in naturally ventilated barns. Generally, and as a rule of thumb followed by many farmers, the barn is best oriented with its sidewalls perpendicular to the prevailing wind direction (as in Figure 5) (Hellickson & Walker, 1983; Choinière & Munroe, 1990). In case the end walls of the barn are oriented more perpendicularly to the prevailing wind, there is a risk of inadequate ventilation due to insufficient mixing of the incoming air with the barn's indoor air (Boussery & Christiaens, 2002). In Flanders, the wind is mostly south-western (40% of a typical year). When the barn is oriented to the southwest with its end wall, there is a risk that the airflow does not reach all parts of the building. This will then result in insufficient air renewal.

For open-front barns, the open side should face the south-east, in case of mostly south-western winds (Figure 6). In this case the wind mostly enters the building from the southeast

through the large open side, which avoids high-speed draughts. This orientation also takes maximal advantage of the incoming solar radiation.

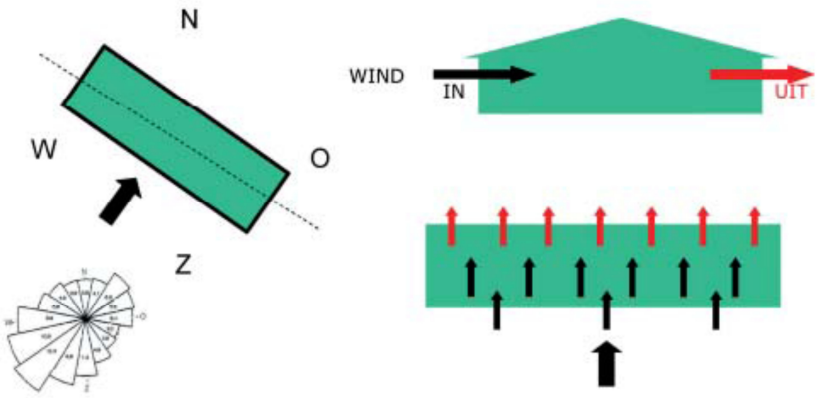

Figure 5 - Orientation of a barn construction with lateral ventilation openings (source: Boussery, 2002)

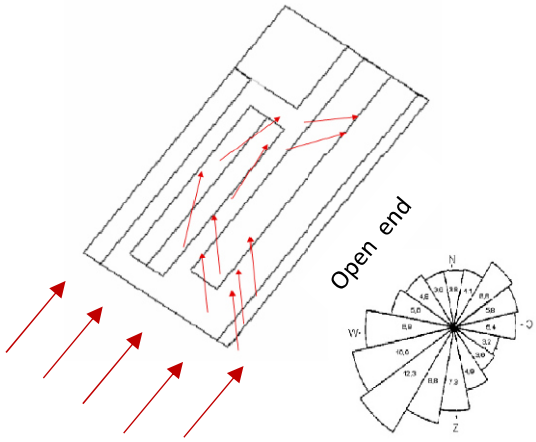

Figure 6 - Top view of an open-front barn construction, with the airflow depicted by arrows (after Boussery, 2002)

It is often possible that the airflow profiles through the large ventilation openings are not homogeneous, and in some cases not even unidirectional (Albright, 1990; Bartzanas et al., 2007; Norton et al., 2009). This can result in various air velocity and airflow profiles, depending on the wind velocity, wind direction and the geometry of the building itself. Figure 7 shows an example of possible airflow profiles as a function of the wind direction.

Natural ventilation also implies that air inlet and outlet locations can change over time (Takai et al., 2013)., i.e., a supposed inlet can become an outlet and vice versa, depending on the wind direction. A ventilation opening can even be an inlet and outlet opening at the same

time, especially in the case of single-sided ventilation (Linden, 1999). This again implies that the airflow rate is particularly difficult to estimate in these cases.

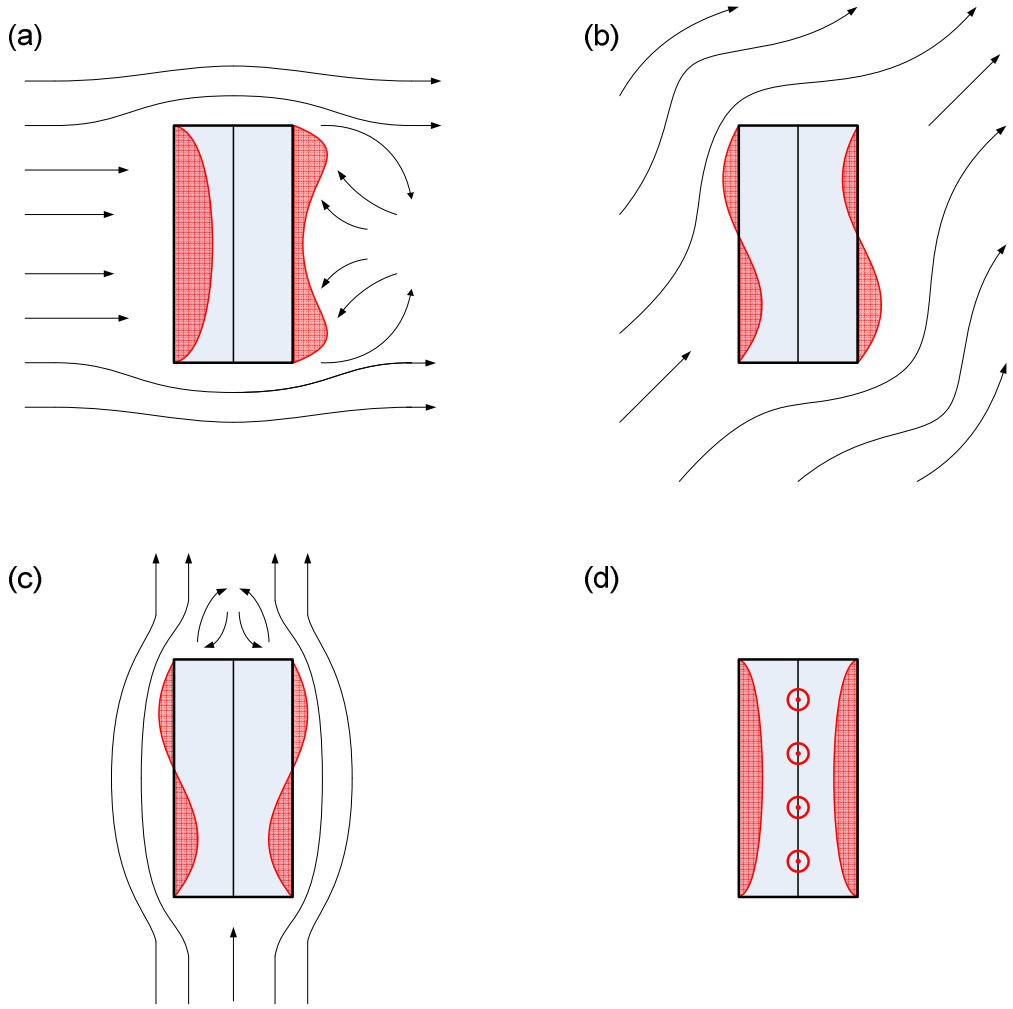

Figure 7 - Top view of the expected airflow profiles (–) through the ventilation openings under various wind incidence angles (a, b, c). (d) shows the airflow profile during wind calm periods, when the natural ventilation is purely caused by buoyancy. Source: Pollet (2009).

Building surroundings

To further complicate matters, internal airflows can be influenced by surrounding elements. For instance, a barn building should be relatively free-standing from possible surrounding constructions, such as other barns or a manure storage silo. Of course, new buildings are still necessary for the up-scaling of production, specialisation and continuing mechanisation. New buildings are often higher and larger in volume. This evolution tends to lead to buildings being placed in uniform series, which are often poorly integrated with existing

buildings and the surrounding landscape (i.e., a visual aspect for neighbours) (Ogink & Aarnink, 2003; Vande Ryse et al., 2007). The effect of such evolutions is two-fold. On the one hand, there is the possibility these result in excessive wind velocities between adjacent buildings; the so-called corridor (or Venturi) effect. This can cause over-ventilation, resulting in an internal temperature drop, large temperature fluctuations, high air velocity at animal height (draughts), an increased risk of disease, and potentially unnecessary heating costs. On the other hand, also under-ventilation can occur, by obstruction of the wind causing too low wind velocities, or unwanted wind rotations (Khanduri et al., 1998).

Barn interior

A comparatively smaller, yet not negligible effect on the internal airflow can be attributed to the barn's interior components. For example, cold incoming air can collide with roof rafters or pen partition walls, sometimes resulting in a downdraught towards the animals. This effect is however difficult to estimate. In any case, in general it is best to keep the air speed at animal level as low as possible, preferably below 0.2 m s^{-1} (BPEX, 2004). Pigs are more sensitive to these draughts than most other farm animals. Descending cold air additionally has an impact at slurry pit level, since it can enter the pit through the floor slats and induce air mixing in the pit's headspace, which in turn results in the release of polluted air toward the barn environment.

1.1.5. POLLUTANTS AND EMISSIONS

The choice and development of the ventilation system do not only have a large impact on the climate in the building, but also on the environment, through the related pollutant emissions. Apart from ventilation control purposes, the determination of the ventilation rate is also essential in order to calculate a building's emissions:

$$E = Q \times (C_{in} - C_{out}) \quad (5)$$

with E = emission rate (mg s^{-1}), $C_{in/out}$ = inside/outside concentration of the pollutant of interest (mg m^{-3}). The impact of farm systems on the environment also has clear implications on obtaining and maintaining an exploitation permit. This permit may be suspended or cancelled, in whole or in part, if the operator fails to comply with the applicable legislation or any specific conditions imposed within the permit.

Figure 8 shows the most important pollutant interactions with the atmosphere, our health, the environment and the climate. At a global scale, the increased frequency of extreme weather events, such as droughts and excessive rain, and the risk of new diseases in plants, animals and humans is to be expected and will also have an adverse effect on the profits generated by agricultural activities (IPCC, 2013).

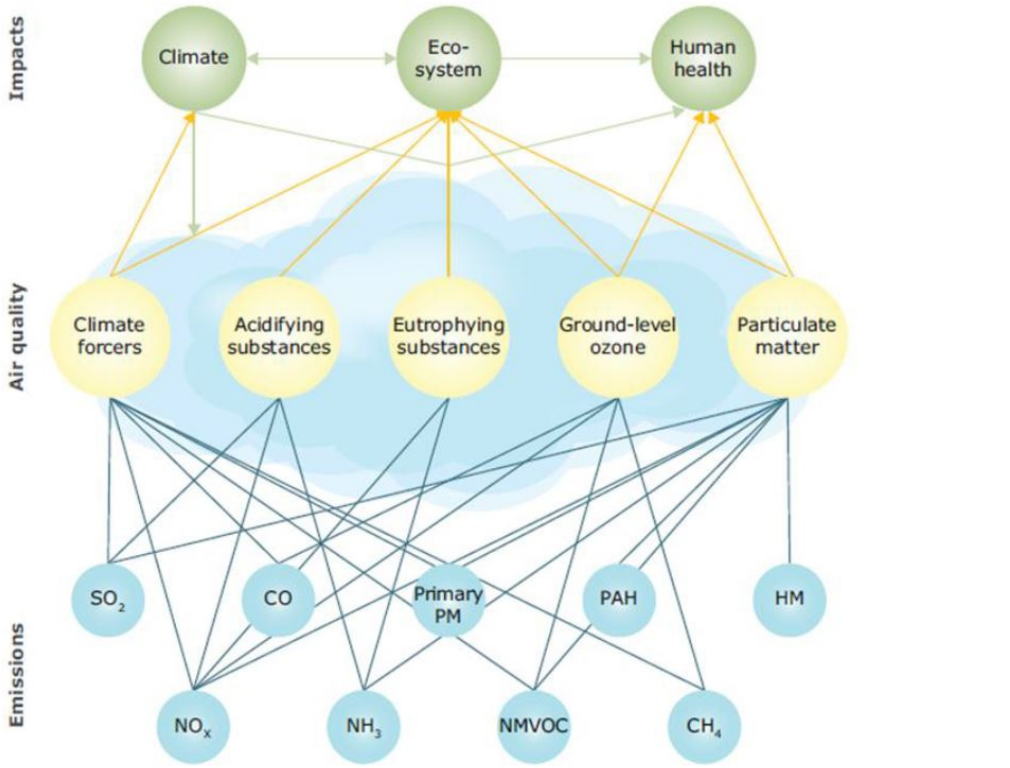

From left to right the pollutants shown are as follows: sulphur dioxide (SO_2), nitrogen oxides (NO_x), carbon monoxide (CO), ammonia (NH_3), particulate matter (PM), non-methane volatile organic compounds (NMVOC), polycyclic aromatic hydrocarbons (PAH), methane (CH_4), heavy metals (HM).

Figure 8 – Emitted pollutants and their impact on air quality, climate, ecosystems and health (EEA, 2013).

At a regional scale, the gaseous emissions from livestock production systems, contribute to eutrophication and acidification of natural areas (ApSimon et al, 1967; Schuurkes & Mosello, 1998) as well as to possible nuisance situations, such as odour (McGinn et al., 2003). Eutrophication is a result of nutrient pollution (e.g., nitrogen released into the air because of NH_3 volatilization and N_2O production) into natural waters and soils, which generally promotes excessive plant growth and decay, favours weeds over other species, and is likely to cause severe reductions in water quality. The largest acidifying potential lies in the

emissions of NH_3, sulphur dioxide (SO_2), and nitrogen oxides (NO_x) (Vandille & Janssen, 2012). The ever increasing intensification of agricultural activities is one of the issues that challenge the conservation of nature (or nature reserves) and landscapes in Flanders and Western Europe in general (Kuijken, 2006).

On a global scale, the greenhouse effect must be taken into account. It is a natural process by which thermal radiation from a planetary surface is absorbed by atmospheric greenhouse gases (GHG), and is re-radiated in all directions. Because a part of this re-radiation is directed towards the surface and the lower atmosphere, it results in an elevation of the average surface temperature. The primary greenhouse gases in the Earth's atmosphere are H_2O, CO_2, CH_4, N_2O, and ozone (O_3). Human activities, mainly the burning of fossil fuels and clearing of forests, have intensified this natural greenhouse effect, causing global warming (IPCC, 2013). The IPCC developed the Global Warming Potential (GWP) concept to compare the ability of each GHG to trap heat in the atmosphere relative to another gas. The GWP of a GHG is defined as the ratio of the time-integrated radiative forcing from the instantaneous release of 1 kg of a trace substance relative to that of 1 kg of the reference gas CO_2 (IPCC, 2013).

Standards for the quantity of GHG emissions are set by the Kyoto Protocol of 1997 and the European “2020” norm of 2012; the climate acts that aim to reduce GHG emissions in order to counter global warming. Takai et al. (2013) state that here is no doubt that GHG emissions from naturally ventilated livestock buildings will have a more central role in research activities in the coming years.

Below, the major gases emitted by animal housing systems are discussed. NH_3 emissions are discussed to a greater extent, since they are a focal point of this thesis.

NH_3

NH_3 is a major cause of indoor air pollution in livestock production systems which affects both animal and human health (Drummond, 1980; Preller, 1995). NH_3 is a toxic gas, so exposure to high levels may irritate skin, eyes, throat, and lungs and cause coughing (EEA, 2013), which stresses the importance of sufficient air renewal.

In livestock production systems, NH_3 is mainly a by-product of animal waste, as feed nitrogen which is not metabolized into animal protein, is excreted in the urine and faeces. In animal houses, ventilated either mechanically or naturally, the majority of these excrements pass through the slatted floors and end up in the slurry pit. There, further microbial activity can

release NH_3 into the air during decomposition processes (Tamminga, 1992; Gay & Knowlton, 2009). For traditional cow cubicle houses with slatted floors, up to 40% of NH_3 emissions can be traced back to the slurry pit, and about 60% to soiled floors (top surfaces and side faces of the slats) (Ogink & Kroodsma, 1996; PCM, 2008).

NH_3 emitted to the atmosphere is usually deposited on vegetation or other materials in the immediate vicinity; within a few kilometres from the source (Nieuwejaers et al, 2004; VMM, 2011). In Belgium, agricultural activities were responsible for 34% of the total acidifying emissions in 2008. Within this share, NH_3 contributed for 34% as well. In Europe, the agricultural sector is the major source of NH_3 emission, contributing up to 92% of the total emissions in 2011 (EEA, 2013) (see Figure 9). In Belgium, more than 90% of the NH_3 emission by agriculture can be attributed to livestock production, the remainder to the use of artificial fertilisers.

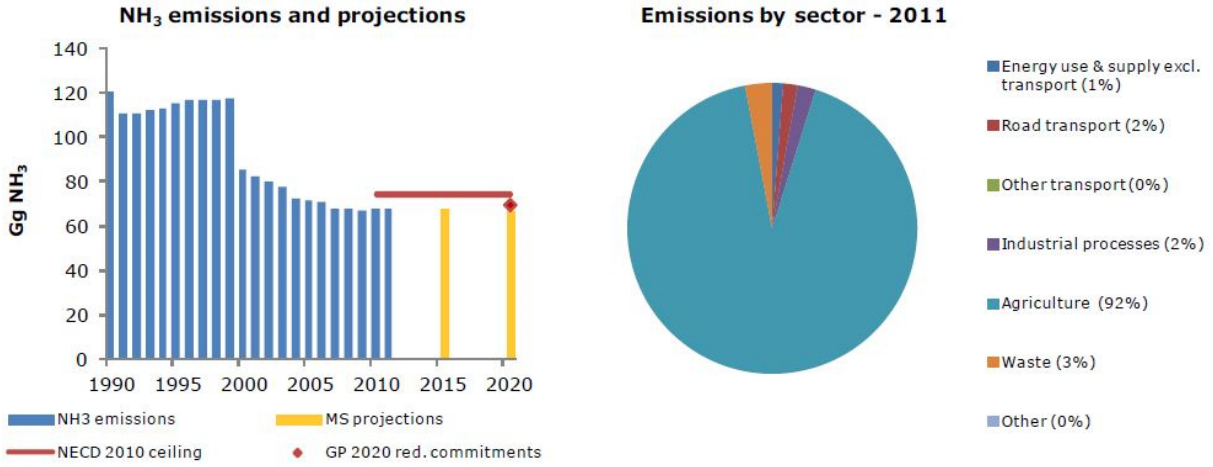

Figure 9 – NH_3 emissions and projections for Belgium, in total and by sector (EEA, 2013).

The NH_3 emission rate in 2008 was determined at 38 kton/year (VMM, 2008). In the period of 1990-2006 Flanders' NH_3 emissions had already decreased by approximately 55%. The reduction in emissions within the European agricultural sector is mainly due to a reduction in livestock numbers (especially cattle) since 1990, changes in the management of manure, direct manure injection in the field, and decreased use of nitrogenous fertilisers (European Environment Agency, 2012). Indeed, also in Flanders, the first large decrease was only observed since the year 2000, when the second MAP ("manure action plan") came into

force. Now, it is barns' manure storage that remains the largest NH_3 source in Flanders' agricultural sector.

The European NEC (National Emission Ceilings) Directive (2001/81/EC) imposes specific emission ceilings for the major pollutants to each EU member state. For the agricultural sector, this directive was especially important towards NH_3 emissions. The Belgian emission ceiling for NH_3 in 2010 was limited to 74 kton, of which 45 kton was attributed to Flanders (NEC reduction programme, 2006). In 2014, the European Commission will re-evaluate and adjust the emission ceilings, which may impose a stricter legislation to the agricultural sector. Additionally, more than 12% of Flanders' surface belongs to the Natura 2000 Network, which brings along obligations towards conservation objectives ("instandhoudingsdoelstellingen" (IHD) in Dutch). These are meant to help sustain Europe's most valuable habitats and species in these areas (LNE, 2013). Since the definitive procedures are not yet established, farmers near these vulnerable ecosystems (of which many are cattle farmers) are limited in up-scaling their activities.

To conclude, it is clear that NH_3 is of great importance for policy makers and should be further considered in agricultural air quality (AAQ) modelling (Zhang et al., 2008a). In Flanders, these concerns have already led to the introduction of low-NH_3-emission animal housing systems. As of 2003, new pig and poultry houses must integrate one of the NH_3 reduction techniques specified in a list of low-emission housing systems, which are appended to the VLAREM II legislation (VLM, 2013). This obligation does not apply to cattle housing, mainly because ventilation rates (and the related emission rates) in naturally ventilated systems are difficult to measure correctly, which is necessary in order to determine the effects of barn systems designed to be low in emission.

CO_2

CO_2 accumulates in the animal house due to respiration and by its release from manure. It is not toxic by itself, but high concentrations result in less readily available oxygen (O_2) in the air, which has adverse effects on production (Seppänen et al., 1999). The CO_2 concentration is best kept below 3000 ppm (Hinz & Linke, 1998). Generally, a ventilation rate based on the temperature and humidity levels is sufficient to control excessive indoor CO_2 and NH_3 levels (Groot Koerkamp et al., 1998). CO_2 from cow exhalation does not contribute to the extra greenhouse effect, because unlike fossil carbon, it only takes part in fast carbon cycle.

CH_4

The CH_4 formed during the digestive process in ruminants such as cattle, sheep and goats, who are able to acquire nutrients from plant-based food by fermenting it in a specialised stomach prior to digestion (principally through bacterial actions and requiring regurgitation), accounts for approx. 60% of the CH_4 emissions from livestock, while 40% can be attributed to manure storages (VMM, 2011). CH_4 emissions from livestock rearing account for approximately 77% of the total CH_4 emissions in Flanders (IPCC, 2013). CH_4 is a potent greenhouse gas: its global-warming potential (GWP) is 34 for a 100-year period. This means that if the same mass of CH_4 and CO_2 were introduced into the atmosphere, CH_4 will trap 34 times more heat than CO_2 over the next 100 years. Its short-term impact in a 20-year period is deemed even greater; with a GWP of 86 (IPCC, 2013).

N_2O

The majority of N_2O emissions can be attributed to agricultural activities, mainly application of synthetic fertilizers. N_2O is also emitted during the breakdown of nitrogen in livestock manure and urine, contributing for 5% of the agricultural emission (EPA, 2013). The emission largely depends on the manure storage system and the storage duration. Especially in litter-based manure systems, N_2O emission will occur as a result of mixed aerobic and anaerobic conditions. The N_2O production by Flanders' agriculture is 56% of the total N_2O emission (VMM, 2011). With a 100-year GWP of 310, it has a large impact on global warming.

H_2S

H_2S is formed under anaerobic conditions, so in agriculture its source is mainly manure storage. Although H_2S is not transported over large distances, it can interact with other compounds to contribute to odour**.** H_2S is best known for its characteristic odour of rotten eggs and at high concentrations it can be lethal. Even at low concentrations it is a respiratory irritant. A concentration of 20 ppm can already cause serious damage (eye tissue damage, lung disease, etc.) (Lambert et al., 2006). 5 ppm is seen as the maximum concentration in a barn (CIGR, 1994).

Particulate matter (PM)

According to EEA (2013), fine dust or PM is a mixture of microscopic aerosol particles (solid and liquid) covering a wide range of chemical compositions. PM_{10} ($PM_{2.5}$; PM_1) refers to

particles with an aerodynamic diameter of 10 (2.5; 1) micrometres or less. PM is either directly emitted as primary particles or forms in the atmosphere from emitted SO_2, NO_x, NH_3 and non-methane volatile organic compounds (NMVOCs). The main sources of PM in the animal rearing sector are the manure, feed, and parts of shed skin (Cambra-López et al., 2010; Van Ransbeeck, 2013). With regard to human health, PM_{10} and $PM_{2.5}$ can cause or aggravate cardiovascular and lung diseases, heart attacks, arrhythmias, cancer and premature death. It can also affect the central nervous system and the reproductive system. PM also affects global warming, mainly by cooling the climate, although in some cases it can still lead to warming (EEA, 2013). The current EU legislation has set the annual mean limit on PM_{10} at 40 µg/m³, with a maximum of 35 days of more than 50 µg/m³, and $PM_{2.5}$ at 20 µg/m³.

Odour

Apart from NH_3, barns often emit other odorous species, such as organic sulphur compounds (e.g., dimethyl sulphide (DMS)) and free fatty acids (FFA). An important aspect of this odour issue is the fraction of gaseous and/or volatile compounds between the gas phase and particles (PM). Different mechanisms lie at the base of possible interaction between particles and gaseous components, i.e., adsorption and absorption in the aqueous or apolar phase (Pankow, 1994; Bidleman et al., 2010; Bowman & Eskelsen, 2009). This can result in the absorption of odour in PM. Due to technical issues, most odour-sampling techniques do not take this into account, which can lead to an underestimation of odour emissions (Cambra-López et al., 2010). Although there is no clear evidence for this, Takai et al. (2013) state that there may possibly be fewer incidences of odour nuisance reported in conjunction with naturally ventilated livestock buildings, when compared to mechanically ventilated buildings. This may mainly be related to the type of animals normally raised in naturally ventilated buildings, compared to mechanically ventilated buildings. Indeed, mostly cattle buildings are naturally ventilated. However, in temperate and hot climate regions, pigs are also kept in naturally ventilated buildings. The main emission reduction techniques for odour are structural adaptations of the ventilation outlets (elevated outlets, air scrubbers). Adaptations of the immediate surroundings (wind screens or vegetative barriers) can lead to reduction of wind speeds (Bitog et al., 2012) and captation of particles (Asman, 2008), but have no proven effect on odour reduction (Pronk et al., 2013).

1.2. Experimental studies of natural ventilation and NH_3 mass transfer

1.2.1. AIRFLOW DISTRIBUTIONS IN NATURALLY VENTILATED BARNS

Direct measurements

As mentioned earlier, in commercial naturally ventilated barns the study of airflow patterns and the determination of ventilation rates has been proven to be a difficult task and involves uncertainties due to the instability of meteorological conditions, such as the external temperature and wind velocity (Kiwan et al., 2013). In a literature review by Ogink et al. (2013) it was suggested that the application of direct ventilation rate methods may be improved by combining local air velocity measurements with airflow pattern modelling, scale-model research and investigations using CFD or other techniques that provide the necessary air velocity data. Experimental buildings are often used to measure airflow characteristics, due to the ease of use and/or to exclude the effects of animal activity on the airflows (or vice versa) (e.g. Harral & Boon, 1997; Smith et al., 1999).

Recently, Kiwan et al. (2010) measured the horizontal air velocity through ventilation openings in two naturally ventilated dairy buildings, using an impeller anemometer. As was to be expected, the selection of measuring locations was found to be a crucial factor for accurate measurement. Lately, more and more studies are performed with multi-point 3D ultrasonic anemometers, which are robust and precise sensors that use ultrasonic sound waves to measure the air velocity. For example, Fiedler et al. (2013) used them to investigate external boundary conditions (the approaching wind direction and velocity, and obstructions due to other buildings) in two naturally ventilated dairy buildings. Still, it remains a serious challenge to know at which locations to measure in order to acquire representative results under all circumstances.

Scale-model approach

Performing scaled ventilation studies through wind tunnel experiments offers many advantages over field experiments. In a wind tunnel, naturally variable conditions such as the wind incidence angle and wind velocity can be kept constant, which is essential for a qualitative data acquisition and offers the possibility to correctly compare different

experiments. Also, the free wind velocity (or reference velocity, i.e., without a building present in the field or test section) can be clearly determined, which is essential to compose air velocity profiles. Furthermore, the use of wind tunnels is less time-consuming than field experiments, making it possible to perform more tests in a same amount of time, and also entails lower research costs, provided that the wind tunnel set-up is readily available. The works of e.g., Ogilvie & Boyd (1985), Lane-Serff (1989) and Savardekar (1990) have already shown that airflows on a full scale can be portrayed accurately using small-scale models in a wind tunnel (Linden, 1999). Several authors (e.g., Choinière & Munroe, 1994; Ikeguchi et al., 2001, 2005; Verlinde et al., 1998) have also illustrated that wind tunnel simulations offer the possibility to study wind-induced ventilation in animal houses. The flow patterns obtained within their scale models were suggested to be similar to those observed in reality, although no parallel measurements were done at real scale.

In wind tunnel studies, various approaches have already been taken in order to study the natural ventilation parameters. Besides air velocity measurements, several other methods can also characterise airflow patterns, such as pressure difference measurements and airflow visualisation by the use of smoke (e.g., Yu, Hou & Liao, 2002). Choinière & Munroe (1994) used smoke in wind tunnel experiments to visualise the airflow patterns in “naturally ventilated” scale model barns. They observed airflow patterns for buildings oriented at 0, 30, 60 and 90° to the wind direction. Optimal ventilation patterns were found for winds perpendicular to the ventilation openings. More recently, Lee et al. (2003, 2005) have obtained good results assessing airflow distributions in a greenhouse geometry with both a computational fluid dynamics model (CFD; see Sections 1.3 and 4.2.1) and particle image velocimetry (PIV; an optical method of flow visualisation carried out by seeding the flow with tracer particles and consequently illuminating them).

1.2.2. NH_3 MASS TRANSFER IN ANIMAL HOUSES

In order to better understand NH_3 emission processes, several research approaches can be found in the literature. They are mainly used to find suitable NH_3 mitigation techniques. Ogink et al. (2013) reviewed the methods for measuring emission rates from naturally ventilated livestock buildings, which can be listed as follows: separate determination of concentration and air exchange rate, tracer gas techniques, passive flux samplers (which rely on capturing NH_3 using tubes with acid coatings, at a rate proportional to the concentration and the airflow velocity through it), flux chambers (in the case of static/closed chambers: the emission from the surface covered by the chamber, e.g. a soiled floor, is calculated by the rate of increase in concentration over time inside the chamber), downwind measurements and dispersion modelling (e.g., the Gaussian plume dispersion model or the backward Lagrangian stochastic model, in combination with one-point or line measurements of the pollutant; see Ogink et al., 2013). The major experimental platforms are large-scale measurements in practice and scale-model studies, which are discussed below.

Direct measurements

Measurements in commercial barns (e.g., Cnockaert & Sonck, 2007; Monteny & Erisman, 1998; Wu, 2012; Ye et al., 2011; Zhang et al., 2005) should be the most representative but have the disadvantage that they may show relatively large NH_3 emission variations, due to differences in manure composition, pH, temperature, etc. Consequently, it is very difficult to compare various settings across different systems or periods of time.

A number of factors are known to effectively influence the NH_3 emission process, including the animals' diet (Philippe et al., 2011; Elzing & Monteny, 1997), the airflow patterns, velocities and directions near and in the slurry pit headspace (Elzing & Monteny, 1997), the floor type and opening ratio (Swierstra et al., 1995; Braam et al., 1997), manure management (e.g., the manure height with respect to the slatted floor) and manure properties such as temperature and pH (Monteny & Erisman, 1998), which can all be altered in favour of less NH_3 emissions. For NH_3 emission reduction purposes, a source-oriented approach is therefore deemed highly beneficial. For example, a solid floor with a manure scraper inhibits the pit ventilation and NH_3 emission, but can result in the animals losing grip and falling (Monteny & Erisman, 1998), either by the presence of faeces or the wet cleaning

process. This is another reason why, for the time being, new cattle barns are not required to integrate low-emission techniques. For slatted floors, e.g. Retz et al. (2010) investigated the impact of a wet, mechanical cleaning-method. However, by cleaning the slats no significant effect was detected on the NH_3 emission.

Pollutant emissions from surfaces, such as floors and manure pits, can also be determined through flux chambers, which appear to be useful for the evaluation of abatement technologies, potentially also usable to determine emissions of pollutants other than NH_3 (Takai et al., 2013). However, this still requires further development and validation against reference methods, due to spatial variability as a major limitation for the accurate quantification of emissions, unless a large number of measurements is performed in different places across the building (Ogink et al., 2013). For a good estimation of the NH_3 emissions from floors, Mosquera et al. (2010) recommend to measure near different floor sections throughout a number of days and under different weather conditions. Research has also shown that the emission mass transfer in the chambers varied with the chamber height and air velocity above the emission surface (Ogink et al., 2013).

Scale-model approach

A more controlled approach includes emission experiments in scaled laboratory set-ups. Several scale-model investigations on slurry pits have been performed for various settings (e.g. Morsing et al., 2008; Zhang et al., 2008b; Ye et al., 2008a, 2008b; Ye et al., 2009a, 2009b; Rong et al., 2009). For example, Ye et al. (2008a) performed experiments with a model pig house and found NH_3 emission rates to increase with higher airflow rates, increasing floor opening ratios and decreasing headspace heights in the slurry pit. A statistical model was developed for the NH_3 emission rate as a function of these variables (R^2 = 0.93). The NH_3 emission rate was found to be more sensitive to the airflow rate than to the floor opening ratio and headspace height in the pit. However, the tested headspace heights were relatively small. Ye et al. (2009b) studied the potential for emission reduction of an airflow deflector above the slurry pit of a scale-model pig house, using CO_2 as a tracer gas, but it was positioned above the end of the slatted floor and did not touch the floor during any of the tested angles. Ye et al. (2011) tested nine parameters in full-scale experimental pig rooms and found the five that explained most of the NH_3 emission variability from the

slurry pit (R^2 = 0.83) to be the airflow rate, floor system, slurry temperature, pit headspace height and curtains that divide the slurry pit into several parts.

These latest scale-model studies used chambers smaller than 0.20 m^3 in volume, and ammonium solutions with initial pH values between 8 and 10. In these studies, the determined NH_3 mass transfer coefficient (*AMTC*) values were within the range of 1.17×10^{-2} to 1.3×10^{-6} m s^{-1} as reviewed by Ni (1999). The literature clearly indicates that results from these scale-model experiments should be validated with full-scale experiments (Morsing et al., 2008). Likewise, Wu et al. (2012a) observed an NH_3 emission reduction from a relatively large (1:2 scale) model cattle barn of up to 85.2 %, by using partial pit ventilation, i.e. mechanically extracting air from underneath the slatted floor. It is however doubtful that this can be achieved in practice, where soiled floors still constitute a large source (60%) of NH_3 emissions (e.g., Ogink & Kroodsma, 1996), and because large pressure differences between the pit and the exhaust must be overcome, which would mean an undesirably high power consumption by the ventilation system.

1.3. Mathematical modelling using Computational Fluid Dynamics

Because a barn's internal environment is linked with ambient conditions, optimising and controlling natural ventilation systems is not easy and as such usually requires extensive experimentation, using sophisticated techniques in order to describe the flow phenomena (Boulard et al., 2002; Zhang et al., 2000). Therefore, an option is to supplement them with mathematical modelling, e.g. calculations of mass or heat balances. Mathematical modelling is the use of mathematics to describe complex phenomena, investigate key questions, explain real-world phenomena, test ideas, and finally make predictions (de Vries, 2001). Experimental approaches, model simulations and theoretical analyses can often complement each other (Figure 10). Ideally, the combination of experiments and modelling leads to a complete understanding of the studied phenomena.

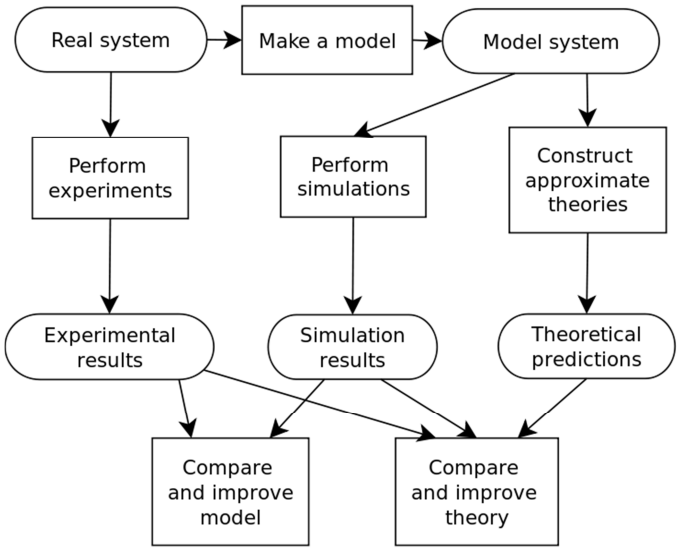

Figure 10 - Flowchart showing the possible interactions between experiments, model simulations and theoretical predictions (adapted from Allen & Tildesley, 1989).

Mathematical models can often be divided in 'black box' or 'white box' models or somewhere in between, according to how much a priori information is available. A black-box model is a system of which there is no a priori information available. Mathematical models can also take many forms, including (but not limited to) dynamical systems, statistical models, differential equations, and neural networks. In scientific computation an important role is played by computational fluid dynamics (CFD), a discipline that uses computers to solve situations governed by fluids (Quarteroni, 2009). The climate (including airflows) in agricultural buildings can be described through the physical laws of fluid motion, heat and

mass transfer, so can be effectively modelled using CFD (Norton et al., 2007). Therefore, CFD has been chosen to be applied in this thesis. The basics of CFD are further given in the "Materials and Methods" section of Chapter 4.

1.3.1. CFD MODELLING OF AIRFLOW DISTRIBUTIONS

In real-life experiments, point measurements using sensors are only able to provide limited information, due to their cost and for practical reasons (e.g., running out of space in the experimental set-up, or negatively influencing the studied airflow pattern by placing too many sensors). Using the mathematical approach of CFD, it is possible to model a domain of interest and generate information on many characteristics (air velocities, pressures, gas concentrations, etc.) throughout the whole domain of interest.

Historically, Nielsen (1974) was the first to apply CFD for room airflow predictions. The first CFD study on livestock buildings simply approximated the geometry as a two-dimensional rectangle (Choi et al., 1988). More complicated geometrical details of livestock buildings were introduced in a later era (e.g., Sun et al., 2004; Bjerg et al., 2008a; Bjerg & Andersen, 2010).

In 2007, Norton et al. reviewed the state of the art of the application of CFD in the agricultural industry, where it was clearly stated that airflows, heat and mass transfer processes in agricultural systems can be effectively modelled using CFD, offering solutions for flows in both spatial and temporal fields.

With regard to natural ventilation, Norton et al. (2009) performed extensive CFD modelling on the effect of the wind incidence angle for an experimental livestock building and for different inlet opening areas. Good qualitative agreement was found between numerical and experimental results. Also the climate distribution in naturally ventilated livestock buildings was comprehensively tested for different eave opening conditions and thermal conditions (Norton et al., 2010a-b-c-d).

Determining suitable measurement locations for the determination of ventilation rates in naturally ventilated buildings also requires good knowledge about the internal airflows. To obtain this, CFD modelling may again be useful (Takai et al., 2013). With regard to the CO_2 mass balance method used to calculate ventilation rates, CFD has been used to find the

optimum gas sampling positions for the outlet CO_2 concentrations and allowed to conclude that the gas sampling positions should be located adjacent to the openings or even within them (Wu, 2012; Wu et al., 2012b).

Natural ventilation in civil buildings has also successfully been modelled with CFD, e.g. by Nikas et al. (2009), Larsen et al. (2011), and Nikolopolous et al. (2012).

1.3.2. CFD MODELLING OF NH_3 MASS TRANSFER

CFD can also help to understand how airflow characteristics may influence the NH_3 emission. Bjerg et al. (2013) described the use of CFD methods to predict NH_3 emissions from naturally ventilated buildings as a task requiring significant expertise, therefore having a practical use mostly limited to targeted research and design purposes, e.g. related to low-emission buildings or techniques.

In cattle buildings with slatted floors, two main airflow circulations can be distinguished: one in the animal occupied zone (AOZ) and higher, and one in the slurry pit's headspace beneath the slatted floor (Wu, 2012). So far, CFD studies regarding airflow patterns and pollutant dispersion in dairy cow buildings (Norton et al., 2010a-b) have mostly been limited to the space above the slatted floor. Much less attention has been given to the airflow characteristics under the slatted floor, which is vital to the understanding of NH_3 transport from the slurry surface.

Zhang et al. (2008d) performed both experiments and CFD simulations to determine ventilation rates (and resulting emissions) for a small-scale slurry pit set-up. They suggested that the ventilation rates in a pig production building should be controlled to maintain a low inlet air momentum to reduce emissions. Sapounas et al. (2009) simulated the effect of forced pit ventilation on NH_3 emission from a naturally ventilated cattle barn, which warned for the effect of high air velocities on emission.

Using a 2D CFD model, Bjerg & Andersen (2010) demonstrated a potential reduction (of at least 30%) of NH_3 emissions from a naturally ventilated livestock building by adjusting the ventilation opening size according to outdoor wind conditions, in order to avoid over-ventilation (and increased NH_3 emission) during windy periods. They also found a further reduction by removing a minor mechanically expelled airstream from the slurry pit.

In CFD modelling studies, the slatted floor is usually simulated as a porous medium (Sun et al., 2004; Bjerg et al., 2008a-b). Wu et al. (2012c) simulated their scale model slurry pit by treating the slatted floor as a porous medium, as well as modelling it directly in full geometric detail. It was shown that direct modelling outperformed the simpler 'porous media' approach, since the latter gave worse predictions of the mean air velocities and turbulence kinetic energy in the pit headspace next to the upwind wall.

1.4. Problem statement

In livestock production buildings, ventilation is necessary to remove humidity and gases, and to provide protection against heat and cold extremes beyond the animals' comfort zone. With this respect, mechanical ventilation has proven to be very efficient. Its working is well-known and the ventilation rates can be measured with relative ease. Although natural ventilation is an energy efficient ventilation technique, it has become largely underused in practice due to the existence of several knowledge gaps. Because the ventilation rate in naturally ventilated animal houses is difficult to assess, the related emission calculations for these houses are also highly uncertain. This is especially important in the light of legislation (both European and regional), which imposes specific emission reductions. NH_3 can be seen as the protagonist in these emission reduction plans. Now, mainly (naturally ventilated) cattle houses are being focused at, since this sector has not been urged to reduce their emissions as much as the pig or poultry sector. With this respect, increased interest in developing mitigation measures in naturally ventilated animal housings is already a fact in the Netherlands. Since this will probably have an influence on Flanders as well, this trend and the need for a better understanding should be thoroughly anticipated. Particularly as demand for livestock products continues to grow throughout the world, it is of primary importance to further research naturally ventilated systems, with regard to their internal airflows and emissions. However, the distributions of internal climate parameters and emission phenomena can be very complex, due to the many influencing factors. This makes their quantification a continuing challenge. In the light of indoor air quality and a continued reduction of atmospheric pollution from barns, not only floor emissions are important, but more research on the slurry pit is advised as well, due to its critical function as a source location of important pollutants. The literature review has shown that several approaches are taken in the international research, such as direct measurements, scale-model studies and CFD modelling.

With this respect, ILVO and the Department of Biosystems Engineering of Ghent University currently cooperate in several closely related projects:

- The project 'NatVent' (IWT 2011-2014) has the aim to develop a reference technique and a practical measuring technique for the measurement and control of the ventilation rate in commercial naturally ventilated barns. Such a technique is deemed

necessary to validate the estimated emissions and their uncertainties in naturally ventilated buildings (e.g., Calvet et al., 2013).

- The project 'BLESpig' (IWT 2014-2017) studies the effects of the ventilation system and regimes on the indoor air quality and emissions of NH_3, odour and PM. One of its aims is to develop a model of the indoor climate and also includes gas measurement inside slurry pits. Additionally, it will investigate outdoor airflow conduction techniques, e.g., shelterbelts and external windbreaks. This project also involves a study of the effect of air scrubbers, in collaboration with prof. dr. ir. Herman Van Langenhove (Ghent University, BW11).
- The present project 'AirModel' (ILVO 2009-2013) addresses the indoor airflow patterns in naturally ventilated barns, as well as the NH_3 mass transfer originating from the slurry pit (see Section 1.5, Research objectives).

Figure 11 schematically shows the main focal points of the three different projects and how they are entwined.

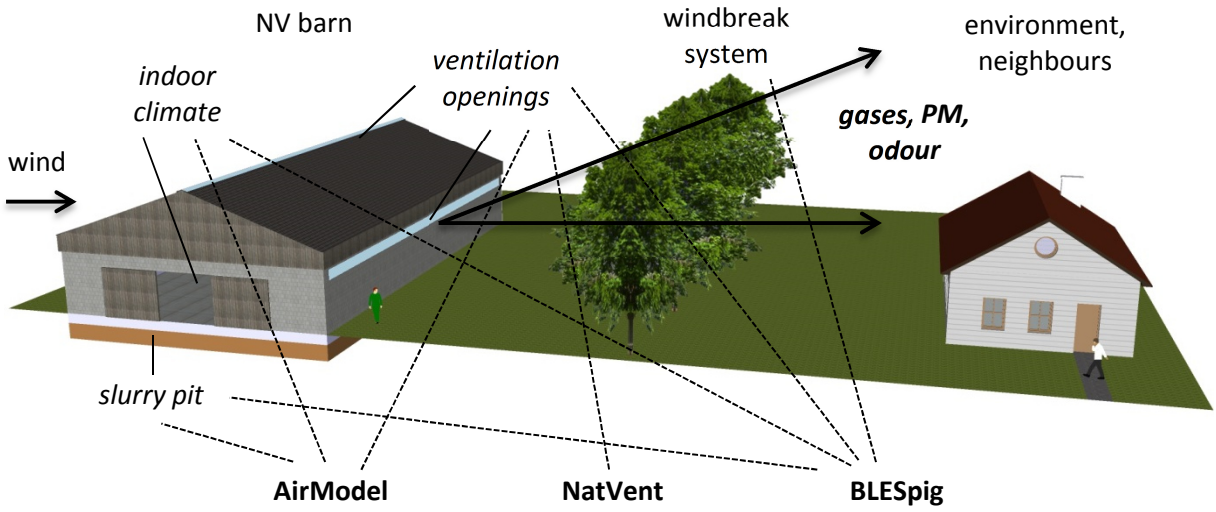

Figure 11 – Schematic of a naturally ventilated (NV) barn, its main emissions (in bold), a wind break system (here a row of trees, or shelterbelt) and a neighbouring house, illustrating the focus points of the mentioned research projects. (Source: Demeyer & De Paepe, previously unpublished)

1.5. Research objectives

As described in the previous section, naturally ventilated houses still struggle with problems regarding ventilation rate measurements and accurate emission calculations. The research in this thesis mainly focused on cattle houses (although not strictly), due to the fact that natural ventilation is mostly applied in this sector. The general objective of this thesis is to gain more insight in the complex processes of natural ventilation and NH_3 mass transfer, by measuring air velocities and NH_3 concentrations using different experimental set-ups and CFD models. A parallel objective is to investigate the feasibility of wind tunnel experiments, scale models and CFD modelling for the acquisition of scientifically funded knowledge that may lead to practical insights, which can help optimise naturally ventilated barns and simultaneously mitigate their emissions.

The main objectives of this thesis are:

- To quantify the effects of ventilation opening configurations on the air velocities and airflow rates using scale-model barns in a wind tunnel environment (Chapter 2).
- To additionally study the impact of the wind incidence angle on the indoor air velocities and airflow rates, using the previously developed scale-model barns (Chapter 3).
- To develop a CFD model that allows to visualise the airflow characteristics in greater detail and can be validated by the scale-model experiments (Chapter 4).
- To develop a real-scale experimental slurry pit that contains a steady NH_3 source and is covered by a slatted floor. First, its stability and performance will be investigated (Chapter 5). Second, it will be used to study the effect of varying pit headspace heights, air velocities above the slatted floor and airflow direction on the NH_3 mass transfer and emissions (Chapter 6).
- To develop a CFD model in order to obtain further insight in the NH_3 mass transfer at the slurry pit level, again to be compared with the experimental findings (Chapter 7).

1.6. Thesis outline

This thesis is divided into nine chapters. Chapter 1, "Introduction and problem statement", describes the impact of airflows in and around animal houses, the state of the art in the literature, and leads to the motivation for the work performed in this thesis. Furthermore, it describes the research objectives and hints at the taken approaches and used techniques.

The research results are divided into two parts.

Part I, entitled "Small-scale ventilation studies in a wind tunnel", describes the results of experiments that focus at the effect of some key factors in natural ventilation, i.e., the ventilation opening height (Chapter 2) and the wind incidence angle (Chapter 3). In Chapter 4, a complementary CFD modelling approach is taken.

Part II, entitled "NH_3 mass transfer studies at slurry pit level", ensues with the results of NH_3 measurements in an experimental slurry pit set-up using different configurations (Chapters 5 and 6). In Chapter 7, a related CFD model was developed.

Chapter 8, or "General discussion", discusses the wider significance of the results in the context of the themes raised in Chapter 1.

Finally, Chapter 9, "Framework, general conclusions and future research", situates the performed work, summarises its main conclusions and implications for practice, and provides an outlook for future potential and needs.

RESULTS

PART I: SMALL-SCALE VENTILATION STUDIES IN A WIND TUNNEL

Since ventilation plays a great role in obtaining a healthy indoor climate by removing heat and pollutants, sufficiently high ventilation rates are needed to properly accommodate the animals and farm workers. However, high ventilation rates are more likely to increase pollutant emissions towards the barn's environment. Since this is a delicate balance in practice, at times compromises must be made, whether they are in fact well-founded or not. Indeed, particularly for natural ventilation systems, there is still a need for a better understanding of the airflow distribution, ventilation rates and their effect on emissions. The in- and outgoing ventilation rates in these types of barns are especially difficult to determine, as are the ideal positions for pollutant monitoring, due to the large dimensions of the ventilation openings, the natural variability of wind and the lack of a widely applicable measurement method. Therefore, it is a continuing challenge to quantify the effect of different barn designs and wind characteristics on the ventilation rates and their related pollutant emissions.

In architectural studies, working with scale models in a wind tunnel environment has always had the advantage of combining the control of the incoming wind (speed, direction) with a relative ease of measurement, precisely because the geometries of interest are downsized. Since this acquired our interest, such a research path was chosen in part I of this thesis. Over the course of three chapters, a number of key factors in the natural ventilation process of a cattle barn are studied.

Chapter 2 starts with a series of experiments under perpendicular wind conditions, focussing on the effect of various ventilation opening sizes and configurations on the wind profile behind the scale-model barns, the indoor air velocities, and finally the ventilation rates through the large inlet, outlet and ridge openings.

In **Chapter 3**, the established wind tunnel set-up is used to additionally study the effect of the angle of wind incidence, which is another important factor in natural ventilation systems. Again, indoor air velocities and airflow rates are the focus of our measurements.

In **Chapter 4**, the road of the wind tunnel experimentation is actually abandoned, but instead a Computational Fluid Dynamics (CFD) modelling approach is taken. Specifically, the experiments with the varying ventilation opening configurations are now simulated with CFD, in order to better visualize the indoor airflow patterns and to acquire an even better understanding of the results.

CHAPTER 2. AIRFLOW MEASUREMENTS IN AND AROUND SCALE MODEL CATTLE BARNS: EFFECT OF VENTILATION OPENING HEIGHT

2.1. Introduction

In order to better understand the complex natural ventilation process in and around animal houses, wind tunnel experiments were performed for a number of scale model designs of a cattle barn. In this chapter, the objective was to quantify the effect of several common ventilation opening heights on the internal air velocities. The obstruction (or windbreak) effect of the different barn designs on the leeward air velocity profile was also examined.

Internal air velocities were measured at eight positions, focusing at the two lateral ventilation openings and the central indoor positions beneath the ridge opening. In addition to the value of the experimental results, being a small-scale representation of airflow phenomena in reality, the quantitative data set should also serve the purpose of evaluating and improving corresponding CFD calculations (see Chapter 4). Although usually both air velocity and pressure patterns are compared to computational models, at present only mean and fluctuating air velocities were recorded. However, the main advantage of this study is the realistic geometric representation of the building architecture, whereas sometimes a much more simplified scale model design is used (e.g., Jiang et al., 2003).

2.2. Materials and methods

2.2.1. GENERAL SET-UP

The wind tunnel experiments in this study were organized as a series of air velocity measurements in and around different designs of a scale model of a cattle barn. These designs differed in ventilation opening size or configuration (e.g., open vs. closed ventilation opening). Eight hotwire anemometers were placed inside the scale model, to register the

Chapter after published manuscript: De Paepe, M., Pieters, J.G., Cornelis, W.M., Gabriels. D., Merci, B., Demeyer, P. (2012). Airflow measurements in and around scale model cattle barns in a wind tunnel: Effect of ventilation opening height. *Biosystems Engineering*, 113, 22-32.

internal air velocities near the ventilation openings and in the centre of the scale model. Furthermore, air velocity profiles at the leeward side of the scale models were registered, and temperature and relative humidity inside the wind tunnel were monitored.

2.2.2. WIND TUNNEL

In this study a wind tunnel was used to generate a steady air flow. In this set-up, wind was the largest contributor to the 'natural' ventilation process inside the scale model, as opposed to buoyancy forces. All experiments were conducted in the wind tunnel of the International Centre for Eremology (I.C.E.), Ghent University, Belgium (Figure 1). A detailed description of the I.C.E. wind tunnel is given by Gabriels et al. (1997) and Cornelis et al. (2004). It is a closed-circuit low velocity boundary layer wind tunnel, made of sheet metal with a rectangular shaped work section of 12.00 m long (*x*) and 1.20 m wide (*y*), with a ceiling adjustable in height from 1.80 to 3.20 m (*z*). In this study, the ceiling of the wind tunnel was placed at its maximum height. An additional plywood floor was placed at a height of 0.30 m, effectively reducing the work section height to 2.90 m.

The roughness length, z_0, of the plywood floor was previously calculated from air velocity profiles and equal to 0.22×10^{-6} m (Cornelis & Gabriels, 2005). All experiments were carried out in a rough surface turbulent boundary layer. The boundary layer thickness was approximately 0.60–0.65 m (Cornelis et al., 2004). Thus, the 0.15-m high scale model used in this study was completely situated within the boundary layer. The dimensionless Reynolds number *Re* is given by

$$Re = \frac{uL_t}{v} \quad (1)$$

where L_t is a characteristic length in m, which is the average of the width and height of the wind tunnel work section, *v* is the kinematic viscosity of the fluid in $m^2\ s^{-1}$ and *u* is the longitudinal component of wind velocity (in the x-direction). For a rectangular pipe, turbulent regime occurs at Reynolds numbers above about 1400. So for L_t = 2.05 m and *v* = 14.6 × 10-6 $m^2\ s^{-1}$, the airflow becomes turbulent at wind velocities beyond 0.009 m s^{-1} and is therefore always fully turbulent in this wind tunnel (Dierickx et al., 2003).

2.2.3. SCALE MODELS

Standard model

A 1:60 cattle barn scale model was used (Figures 2-3). The design and dimensions were based on the model applied by Verlinde et al. (1998), who also performed experiments in the I.C.E. wind tunnel. This model was based on a real life naturally ventilated cattle building for 90 dairy cows, situated in Moortsele, Belgium. For our study the dimensions of the scale model have been slightly increased, resulting in 82 mm high sidewalls, a total height of 150 mm, a length of 677 mm, a width of 422 mm and an 18-degree roof slope. This resulted in a wind tunnel blockage ratio of 2.9%. A larger scale model would have given rise to a tunnel effect between the model and the wind tunnel wall (Verlinde et al., 1998), likely influencing the wind entering and exiting the house through the ventilation openings. Along the 5-mm wide ridge opening 5-mm high wind deflectors were added. This addition simulated 0.3-m high deflectors, as commonly used in practice to increase the Venturi effect. The scale model was placed in the wind tunnel work section at x = 7.67 m.

The main scale model was constructed using a welded aluminium frame. Three mm thick transparent polycarbonate sheets served as walls and roofs and were fixed onto the frame with smooth adhesive tape. Since the roof was removable from the lower module, draught tape was applied at the eaves to avoid air leakage between both modules.

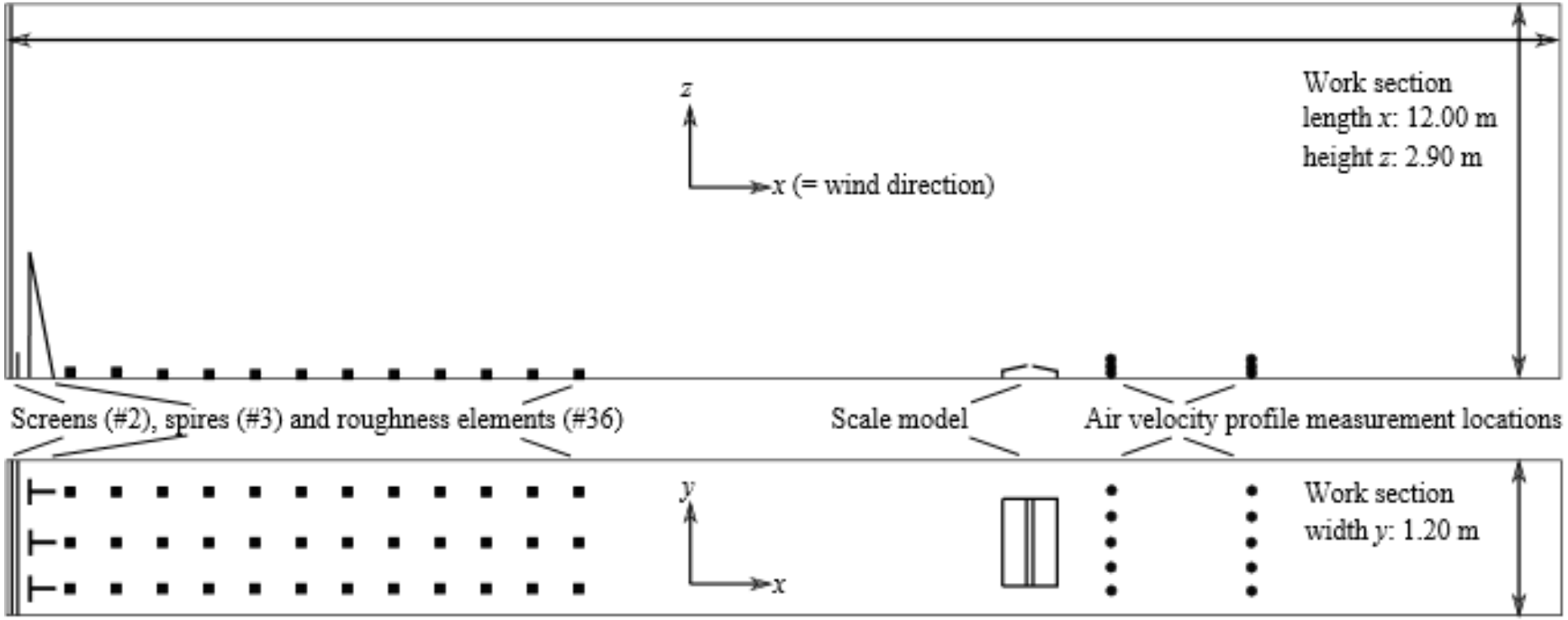

Figure 1 – Longitudinal cross section and top view of the wind tunnel work section, with x = 0 m at the far left and the scale model placed at x = 7.67 m. The black dots denote the positions where air velocity profiles were registered at x = 8.51 m and x = 9.59 m.

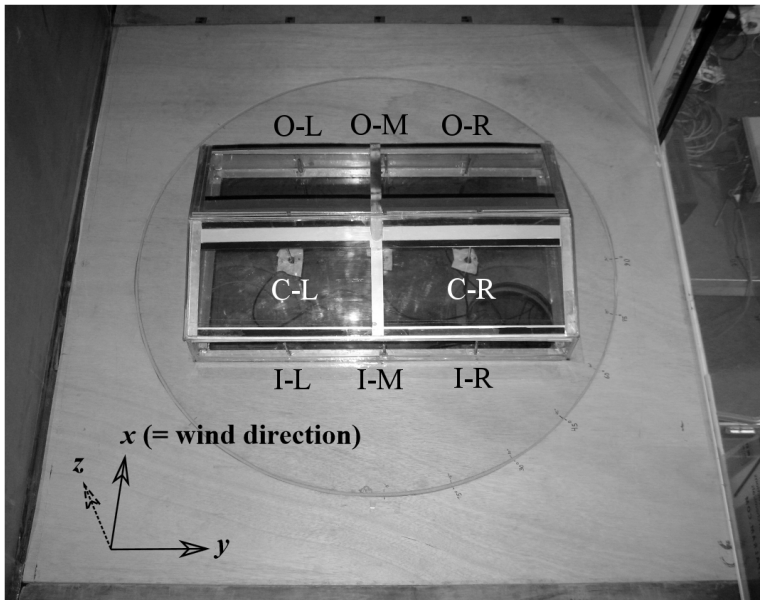

Figure 2 – Bird's eye view of the cattle barn scale model inside the I.C.E. wind tunnel. The letters mark the eight measurement locations, with C = centre plane, I = inlet, O = outlet, L = left, M = middle, R = right.

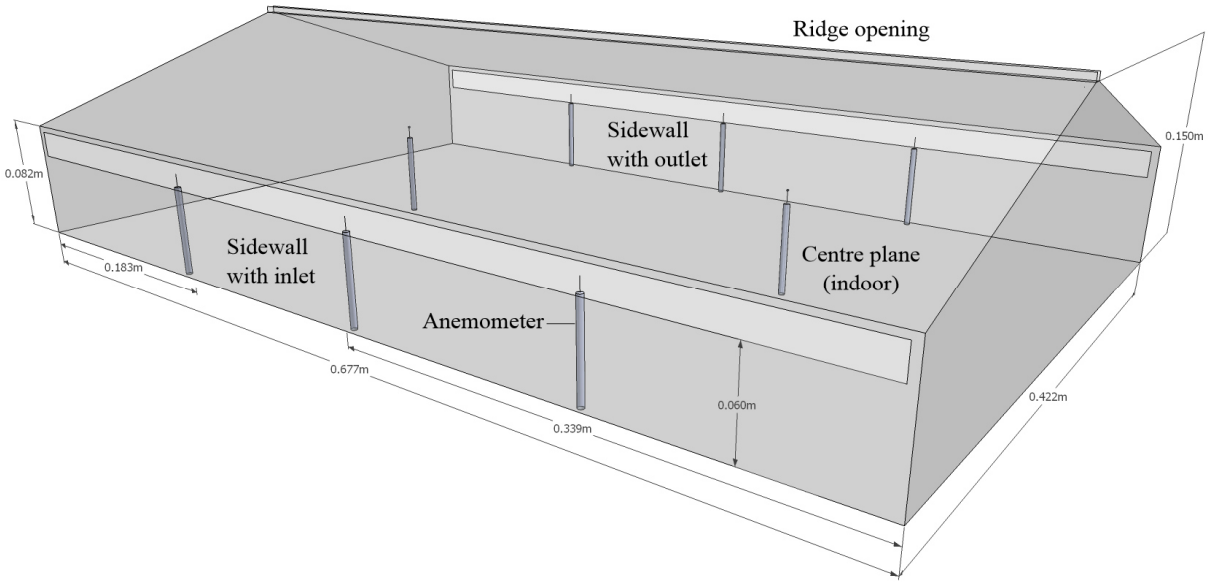

Figure 3 – Sketch of the cattle barn 1:60 scale model (standard design, SM1) dimensions (in m) and positions of the eight hotwire anemometers at a height of z = 0.06 m

Modifications to the standard model

Six variations of the main model were designed, each resulting in a different configuration of ridge or sidewall ventilation, i.e., with different sidewalls that vary in ventilation opening heights. The six scale model designs and their characteristics are presented in Table 1 and Figure 4. Each ventilation opening was 66 mm wide across the sidewall. SM1 is a scale model of a standard cattle barn, with 18 mm high ventilation openings beneath the eaves (1.08 m in full scale). SM2 only differs in the fact that the 5 mm wide ridge opening was closed. In SM3 the outlet opening at the back was closed. SM4 introduced a low front wall, only 20 mm in height. In reality such a 1.20 m high wall is sometimes used and still found adequate to protect the cattle housed inside. SM5, on the other hand, features a fully open front wall. Finally, in SM6 the back wall was also removed, leaving only the endwalls present. In reality, one or even more walls are sometimes fully opened during hot summer weather (e.g., Graves & Brugger, 1995). The standard scale model, SM1, will be regarded as the reference case with which the other designs can be compared.

Table 1 – The six scale model (*SM*) designs with (1) the height *H* above the tunnel floor of the ventilation opening from its lower end to (→) its upper end, and (2) the free surface areas A of the ventilation openings. [*]

Scale model		H_{inlet} (cm)	H_{outlet} (cm)	A_{inlet} (cm²)	A_{outlet} (cm²)	A_{ridge} (cm²)
SM1	Standard dairy house ($A_{inlet} = A_{outlet}$)	5.8 → 7.6	5.8 → 7.6	118.8	118.8	33.0
SM2	House with closed ridge ($A_{ridge} = 0$)	5.8 → 7.6	5.8 → 7.6	118.8	118.8	–
SM3	House with closed outlet ($A_{outlet} = 0$)	5.8 → 7.6	–	118.8	–	33.0
SM4	Low-front house ($A_{inlet} \approx 3x\ A_{inlet,\ SM1}$)	2.0 → 7.6	5.8 → 7.6	369.6	118.8	33.0
SM5	Open-front house ($A_{inlet} \approx 4x\ A_{inlet,\ SM1}$)	0.0 → 7.6	5.8 → 7.6	501.6	118.8	33.0
SM6	Open house; only end walls ($A_{inlet} = A_{outlet}$)	0.0 → 7.6	0.0 → 7.6	501.6	501.6	33.0

[*] 'Inlet' and 'outlet' refer to the ventilation opening on the sidewall, at the front and at the back of the model respectively; 'ridge' is the ridge opening. Sidewalls are perpendicular to the wind direction, whereas endwalls are parallel to it.

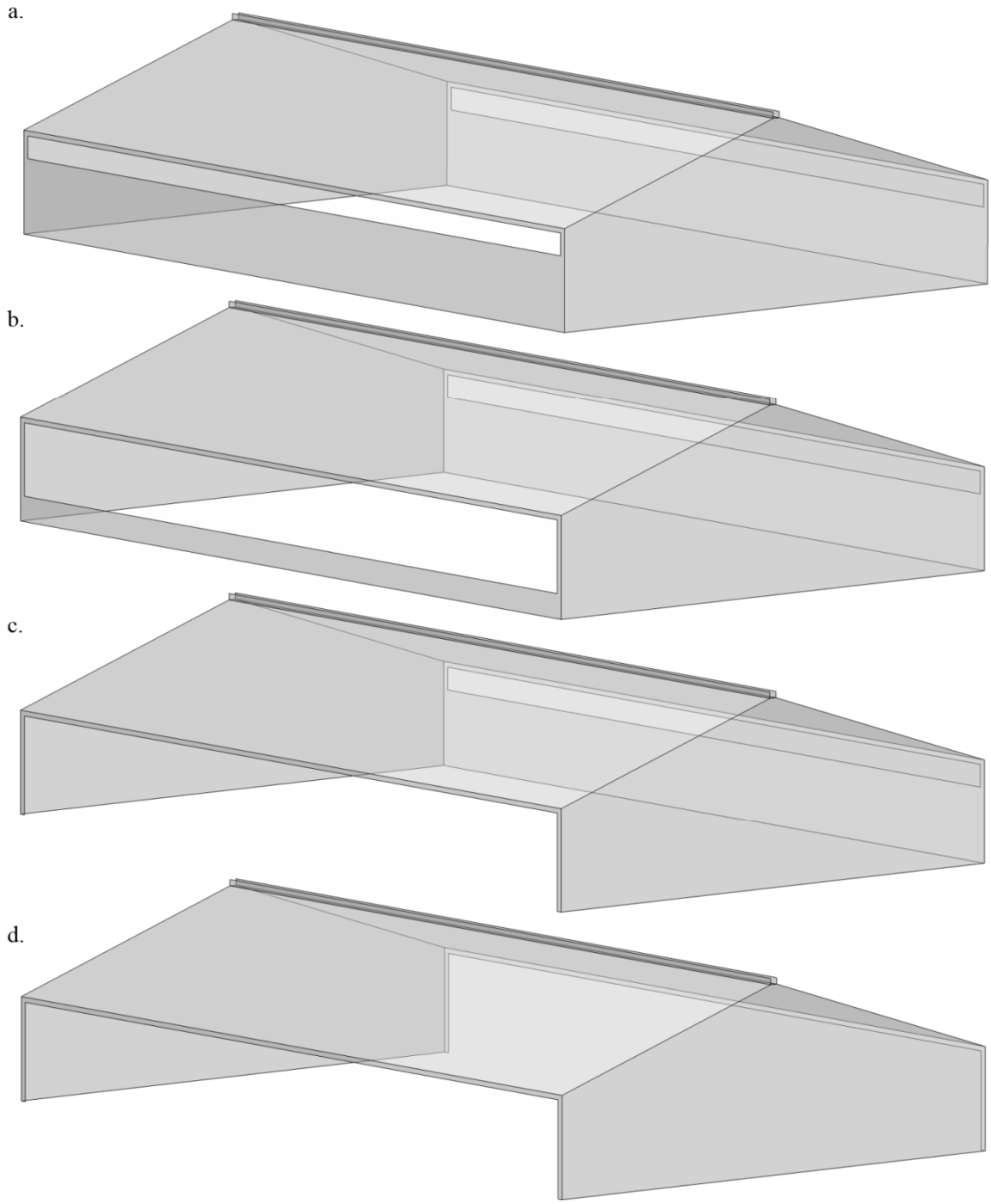

Figure 4 – Sketch of the different cattle barn scale model designs: (a) standard model SM1 (SM2 and SM3 were variations where the ridge or outlet, respectively, was closed); (b) low-front house SM4; (c) open-front house SM5; (d) open house SM6.

2.2.4. MEASUREMENTS AND PROCEDURES

Experimental conditions

The minimal free-stream air velocity generated by the wind tunnel (i.e., above the boundary layer and not affected by the tunnel surface or other objects) was 5.7 m s^{-1}. In order to obtain lower velocities, two permeable synthetic wind screens (agrotextiles) were placed at the work section entrance: one large screen, fully covering the inlet plane of the wind tunnel work section, and a smaller one (0.20 m high from the work section floor upward) placed 0.10 m leeward of the large screen. The screens manufactured by Vervaeke (Ruiselede, Belgium) were made of PE material and had the following characteristics: woven (tape/mono), yarn width 1000/600, opening size 1300 µm, opening area 35.7%, flow reduction coefficient (R_c) 80.4% (see 'screen F' in Dierickx et al., 2001). As a result, the reference air velocity u_r, measured near the work section entrance at x = 1.00 m, y = 0.60 m, z = 0.50 m, averaged 3.5 m s^{-1} during all experiments. This served as an assurance that the same initial air velocity was always applied. In this case the Reynolds number *Re* was about 491 000 (see Equation 1). To establish a symmetric and smooth work section, acrylic sheets were placed along the wall which contains window frames. These would otherwise result in a rougher wall texture. Air velocity profiles in the wind tunnel work section are further discussed below.

The mean 10-m height wind velocity measured at the national weather station of Uccle (Belgium) between the months of October and April, during which period cattle is mainly indoors, is 3.8 m s^{-1} (KMI, 2012). This corresponds to 2.5 m s^{-1} at a height z of 0.5 m, according to

$$u_z = u_{ref}\left(\frac{z}{z_{ref}}\right)^n \qquad (2)$$

with u_z = wind speed at height z (m), u_{ref} = wind speed at reference height z_{ref} (10 m) and n = topographic roughness factor of 0.14 (Anders, 1994).

This is comparable to the average reference air velocity u_r measured at the wind tunnel's work section entrance at 0.5 m height, i.e. 3.5 m s^{-1} (standard deviation of 0.1 m s^{-1}). A lower air velocity was technically not attainable.

Despite our scaled approach, several authors (e.g., Choinière & Munroe, 1994; Bottcher et al., 1986; Linden, 1999) argue that for a given building, airflow patterns behave in a similar fashion above a certain threshold Reynolds number. Choinière et al. (1988), having used

sidewall height as characteristic length L_t, recommended a Reynolds number above 5400 to maintain stable airflow patterns in scale model experiments, which was definitely the case in this study; *Re* exceeded 18000 since our sidewall height was 0.082 m.

The ambient temperature *T* and relative humidity *φ*, were also measured near the work section entrance at *x* = 1.00 m, *y* = 0.60 m, *z* = 0.50 m. These measurements were carried out with E+E type EE65 and EE33 transducers (E+E Elektronic, Engerwitsdorf, Germany). Due to varying atmospheric conditions, temperature and relative humidity in the wind tunnel fluctuated between 16.8°C and 23.3°C, and between 31.6% and 35.9%, respectively. During a single experiment, temperature showed a fluctuation of max. 0.1 °C, relative humidity of less than 0.2%.

All measurements of air velocity, temperature and humidity were conducted at a 1-Hz frequency, with a sample time of 120 s. This approach led to representative results (data not shown). To ensure a fully developed airflow in the work section, sampling was only started 100 s after starting the wind tunnel fan. All data were acquired using a type DTL 1232 logger (LHM Instrumentation, Belgium) equipped with Logwin32 software.

Obstruction effect of the scale model on the air flow pattern

To investigate the obstruction effect of the scale model on the leeward air flow pattern, air velocity profiles were registered at two locations along the wind tunnel work section, as shown in Figure 1: (1) at *x* = 8.51 m, which is at one scale-model width leeward of the scale model's back wall, and (2) at *x* = 9.59 m, which is at ten times the total height of the scale model ($10H_t$ = 1.50 m) in the leeward direction. Prior to these experiments, the initial profiles in the wind tunnel, i.e., without any scale model, were measured as well. Subsequently, the scale model was put into position and the air velocity profiles were measured again at the same positions.

Three unidirectional hot film anemometers (type EE65, E+E) were mounted along a pole at heights *z* = 0.05 m, 0.10 m and 0.20 m. The pole was consecutively placed at *y*-intervals of 0.20 m (with *y* in the lateral direction, see Figure 1). As only the horizontal components of the air velocity were considered, the probe windows were aligned towards the free flow direction.

Effect of ventilation opening height on air velocities in the scale models

Ventilation opening heights, as well as positions, clearly affect indoor air velocities (e.g., Morsing et al., 2002). To further investigate the quantitative effect of varying ventilation opening heights on the air velocities measured inside the scale model, six scale model designs were used in these experiments (see Table 1 and Figure 4).

Three small-scale 2D hot wire anemometers (type 8465, TSI Inc., Shoreview, MN, USA) were placed near both the sidewall ventilation openings. At these locations the air streams are predominantly horizontal. In the central (*y*,*z*)-plane containing the ridge, two omni-directional NTC anemometers (type 8475, TSI Inc.) were placed. All eight probes were inserted through perforations made in the floor plate of the scale model. The positioning of the probes inside the scale model can be seen in Figs 2 and 3. Each probe was calibrated and their accuracy was ± 0.1 m s $^{-1}$ in the selected air velocity range (0.125 – 5.00 m s^{-1} for types 8465; 0.05 – 2.50 m s^{-1} for types 8475). According to the manufacturer, their accuracy does not change when used between 18 and 28°C; outside this range 0.2% per °C must be added. These probes give no indication of the air stream direction.

Both type 8475 anemometers in the central (*y*,*z*)-plane containing the ridge were alternately placed at four heights *z*, i.e., at 0.03, 0.06, 0.10 and 0.14 m (Figure 5), while the other six probes near the inlet and outlet openings always remained at a fixed height of 0.06 m.

Airflow rates

In addition to the measured air velocity values, approximations of airflow rates *Q*, in m³ s^{-1}, were calculated for each ventilation opening (inlet, outlet and ridge opening) by multiplying the opening's free surface area *A* (in m²) by the average air velocity measured through it (in m s^{-1}), as in

$$Q = \bar{u} \times A \tag{3}$$

where $\bar{u}$ is the average air velocity in m s $^{-1}$.

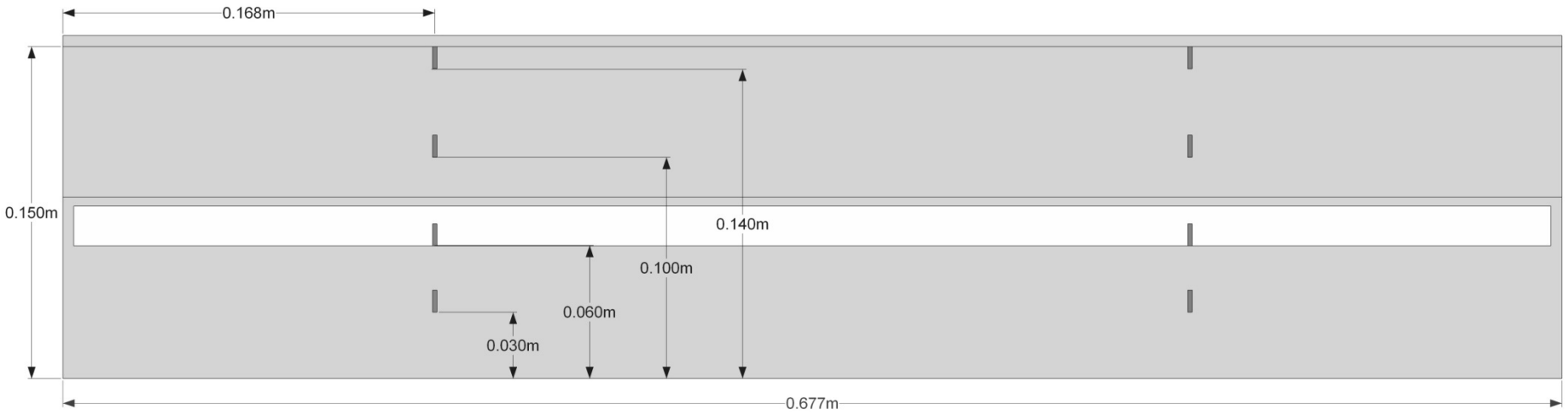

Figure 5 – Front view of the cattle barn scale model (standard model, SM1). The black rectangles mark the eight locations where air velocity was measured in the central (*y*,*z*)-plane under the ridge. On the left hand side were the $u_{C\text{-}L}$ values, on the right hand side $u_{C\text{-}R}$ values.

Statistical methods

The effect of measurement location and scale model configuration (fixed independent variables) on the air velocity u (dependent variable) was determined using two-way ANOVA. Since the interaction between location and scale model was always significant, one-way ANOVA was performed with the different combinations of both factors (measurement location and scale model) as separated groups. A Scheffé post-hoc test (Scheffé, 1959) was used to determine the significant differences between scale models within each fixed measurement location. Statistical analyses were performed using SPSS Statistics 19 (SPSS Inc. 2010, IBM corporation, New York, USA). Statistical significance was considered at $p < 0.05$.

2.3. Results and discussion

2.3.1. OBSTRUCTION EFFECT OF THE SCALE MODEL DESIGNS

Figure 6 shows the free flow air velocity profiles in the wind tunnel without any scale model present, measured at x = 8.51 m (Figure 6a) and x = 9.59 m (Figure 6b). Both profiles were statistically similar, as well as symmetric along the wind tunnel width y. Maximal air velocities were found at the centre (y = 0.6 m), which is the farthest possible position from the wind tunnel walls, thus experiencing minimal friction. The air velocity profile at x = 9.59 m shows only slightly lower u-values than the upstream one, at x = 8.51 m. The u-values at heights z = 0.05 m, 0.10 m or 0.20 m at any measured y-value differ at most by 0.3 m s^{-1} (= 6.5 % of the highest measured value, being 4.6 m s^{-1}). Note that these air velocities are higher than the reference air velocity of 3.5 m s^{-1}, near the work section entrance. This can be attributed to the three roughness spires at the work section entrance (Figure 1), which induce nearby wind velocity reductions.

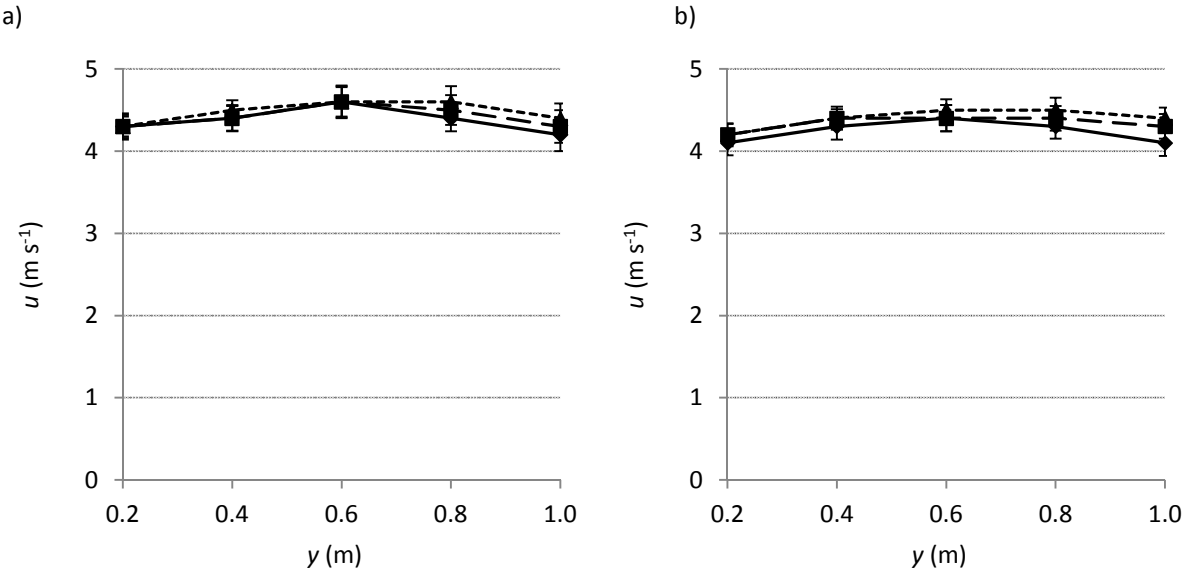

Figure 6 – The air velocity profile measured at (a) x = 8.51 m and (b) x = 9.59 m without any scale model present; at heights z = 0.05 m (♦, full line); z = 0.10 m (■, long dots); z = 0.20 m (▲, small dots). The error bars show one positive and negative standard deviation of the averaged air velocities.

Figure 7 shows the air velocity profiles leeward of the scale models at x = 8.51 m (one scale model width behind the model) for SM1, SM5 and SM6 and at x = 9.59 m (at 10 H_t) for SM1. The other scale model designs are not considered here. The default house SM1 gave rise to air velocity reductions of 70 to 83% in the leeward projection of the scale model (i.e., for y = 0.40 m to 0.80 m and z = 0.05 m to 0.10 m). Similarly, the wind breaking effect of the open-front scale model SM5 (Figure 7b) varied between 58 and 85% at the same heights. The air velocities around the default house SM1 and the open-front house SM5 (Figure 7a-b) statistically differed only at y = 0.80 m, and at (y,z) = (0.40 m, 0.20 m) and at (y,z) = (0.60 m, 0.20 m). This means that the height of the ventilation inlet did not matter, while both models featured the same outlet opening.

The completely open house scale model SM6 (Figure 7c), however, showed smaller reductions in its leeward projection: from 27 to 65%. In other words, scale model SM6 let the air flow pass through more effectively, which was to be expected.

At wind tunnel widths y = 0.20 m and 0.80 m, air velocities (Figure 7a-c) did not show statistical difference with those presented in Figure 6a, nor with each other, so the wind obstruction of the scale models had no effect at those widths. This is to be expected since streamlines also travel alongside obstructions.

At x = 9.59 m (= 10 H_t) leeward of the standard scale model SM1, the air velocity profile showed air velocity reductions of only 14 to 27% (Figure 7d), compared with the situation without a scale model (Figure 6b). Only at y = 0.20 m (Figure 7d) did air velocities not show statistical difference with those in Figure 6b, where the scale model was absent.

Overall, the air velocity reductions at height z = 0.20 m were less pronounced. This is consistent with the typical flow development pattern in a wind tunnel, where less friction is experienced the farther away from the floor or walls. In addition, z = 0.20 m is also the measuring height that is the farthest away from the scale model, the latter serving as an obstacle or friction agent as well.

These results clearly show the wind obstruction effect of a building's ventilation opening design upon its immediate leeward environment. These effects must be kept in mind should another barn be present in the vicinity. The latter could experience ventilation rates that are no longer sufficient to maintain an adequate indoor climate.

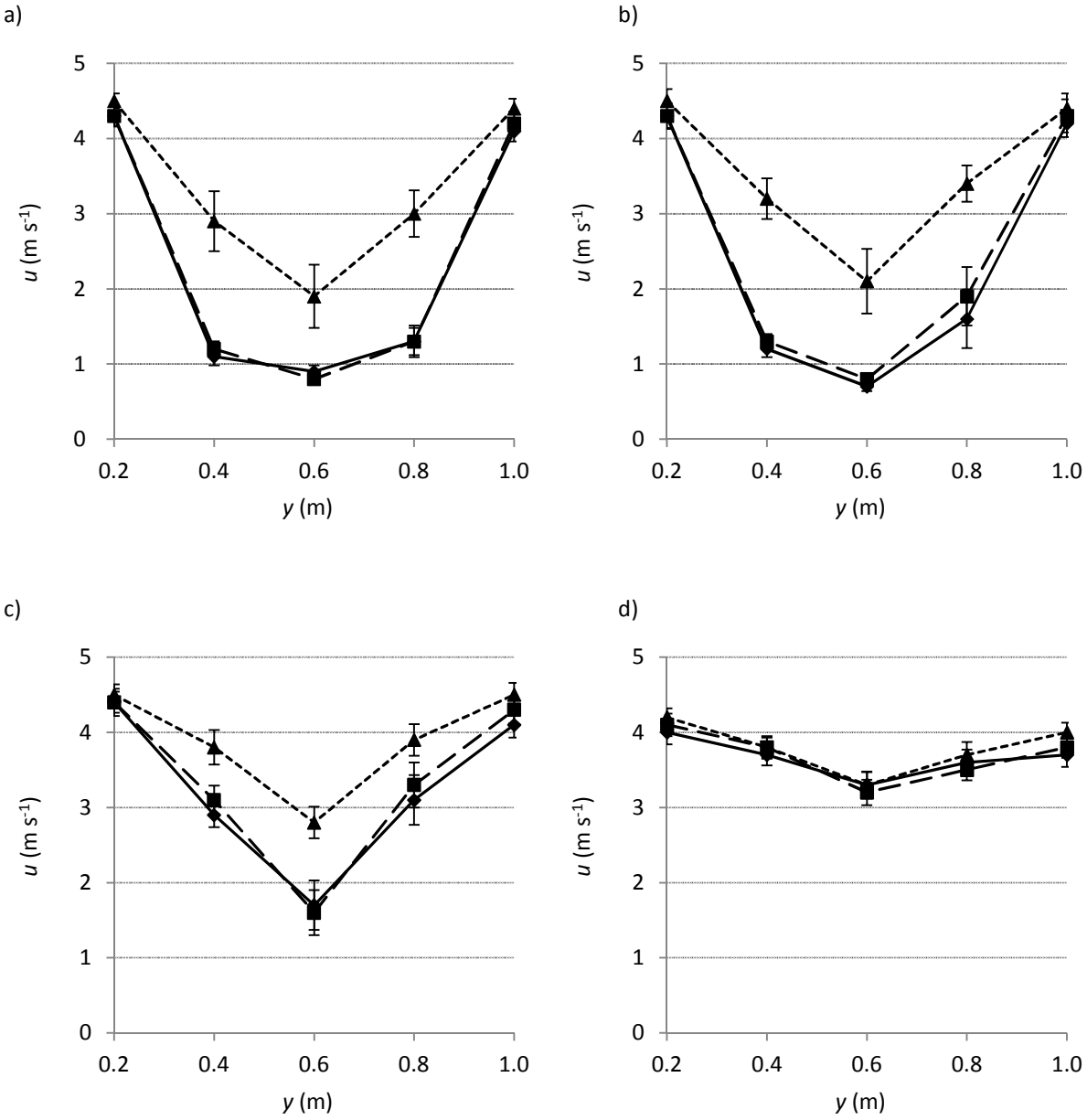

Figure 7 – (a) The air velocity profile one width (0.42 m) leeward of the standard scale model SM1, i.e., at x = 8.51 m; (b) idem leeward of open-front scale model SM5; (c) idem leeward of open house scale model SM6; (d) the air velocity profile at 1.50 m (10 H_t) leeward of standard scale model SM1, i.e., at x = 9.59 m; all at heights z = 0.05 m (♦, full line); z = 0.10 m (■, long dots); z = 0.20 m (▲, small dots). The error bars depict one positive and negative standard deviation of the averaged air velocities.

2.3.2. Effect of ventilation opening height on air velocities in the scale model

Air velocities

Figure 8 depicts the air velocities measured at a height of z = 0.06 m (i.e., the mid height of the ventilation opening in standard scale model SM1) inside the six scale model designs

which were all placed at x = 7.67 m. As in all cases the reference velocity u_r was 3.5 m s^{-1}. Encircled data points denote values that are not significantly different among scale model designs, at a given location (*Y* axis in the graph).

The standard scale model SM1 showed air velocity values between 3.7 and 4.0 m s^{-1} at the inlet opening (I), between 0.6 and 0.7 m s^{-1} in the centre (C) and between 1.5 and 2.3 m s^{-1} at the outlet opening (O). Closing the ridge opening (as in SM2) resulted in lower air velocities at the inlet opening (17 to 33% less compared with the standard model SM1), yet not significantly different values at the centre and outlet opening, except for position O-R, where a 10% increase was found. The similar values between SM1 and SM2 at the outlet can be explained by the fact that in this wind tunnel set-up mostly cross ventilation occurred in the scale models. Moreover, buoyancy (or stack effect) only played a minor role since the wind tunnel setup was isothermal during any given measurement. Closing the outlet (as in SM3) on the other hand, resulted in substantially reduced air velocity values, with reductions ranging from -45% in the centre to -86% at the inlet compared with SM1. The wind velocities in SM3 are overall the lowest air velocity values recorded during the experiments. The reason for this is a pressure build-up inside the model. The oncoming air flow tries to avoid this resistance obstacle. Lowering the front wall to a height of only 20 mm (as in SM4), resulted in 41 to 45% lower air velocities at the inlet, yet also in 44 to 66% higher values at the outlet, compared with standard model SM1. Fully opening the front wall (as in SM5) led to similar results as SM4. Only location I-M showed a difference of 0.2 m s^{-1}. This similarity could be expected, since both models differed only in minor respects, i.e., a front wall of 20 mm high (SM4) versus a completely absent front wall (SM5). The open barn (SM6), compared with SM1, showed lower values at the inlet (except for position I-M) but 252 to 339% higher velocity values at the centre and 37 to 111% higher values at the outlet. An explanation for these higher values may be the unhindered cross-ventilated airflow in SM6, as opposed to possible return flows at floor level in SM1.

The highest velocities at the inlet were found in the standard model SM1 and the open house SM6. The air velocity values at the inlet opening were generally slightly higher at the right side (I-R) than at the left (I-L). This was observed in all six scale model designs. The reason for these deviations is still unclear, since each scale model was symmetrically designed and carefully positioned. Also, the air velocity profiles in Figures 6 and 7 do not

show such a pronounced difference between left and right. At the outlet opening the highest velocities were found in the more open models SM4, SM5 and SM6. Except for scale models SM3 and SM6, the air velocities in the centre of the scale models did not differ significantly, ranging between 0.5 and 0.8 m s^{-1}. In the open house SM6, centre values lied around 2.5 m s^{-1}.

Inside the six scale model designs, the air velocities under the ridge opening near the gables (positions C-L and C-R) were not only measured at the standard height of z = 0.06 m, but also at three other heights of 0.03, 0.010 and 0.014 m (Figure 5). Table 2 shows the corresponding values for each scale model design. The highest and lowest values are denoted by a (+) or (–) sign.

These results follow the same trends as observed at the inlet and outlet openings. For both the left hand side (position C-L) and the right hand side (position C-R) maximal u-values were observed in the open house SM6, while minima were found in the closed-outlet model SM3. In general, a slight decrease in air velocity from z = 0.03 to 0.06 m can be observed, whereas there is a gradual rise in velocity towards z = 0.010 and 0.014 m, the latter being directly under the ridge opening (z = 0.015 m).

Similar values were observed between the standard scale model SM1 and model SM2, where the ridge opening was closed. This indicates that closing the ridge opening had no effect on the air velocities in the centre of the scale model, as opposed to clearly lowered values near the inlet and outlet openings (see Figure 8). The values for scale model designs SM4 (low-front house) and SM5 (open front house) are also very similar. This concurs with the observations at the inlet and outlet openings (see Figure 8).

The lowest possible position the anemometers could be placed at was at z = 0.03 m. The animal activity level in real life would be scaled down to an even lower height. At z = 0.03 m, air velocities were situated between 0.26 and 0.95 m s^{-1} for scale models SM1 to SM5, except for open house SM6, which showed relatively high velocities of around 2.50 m s^{-1}. In real life situations, air velocities between 2 to 3 m s^{-1} at cow level are beneficial during hot, humid conditions to help alleviate or minimize heat stress (Shearer et al., 1991). But generally, open-front houses or open houses are not suited for animals less than one year old or less than 300 kg in weight. Also, a notable rise in NH_3 emissions can be caused in the event that high indoor air velocities effectively result in excessive ventilation rates (e.g., Snell et al., 2003), which should therefore be avoided.

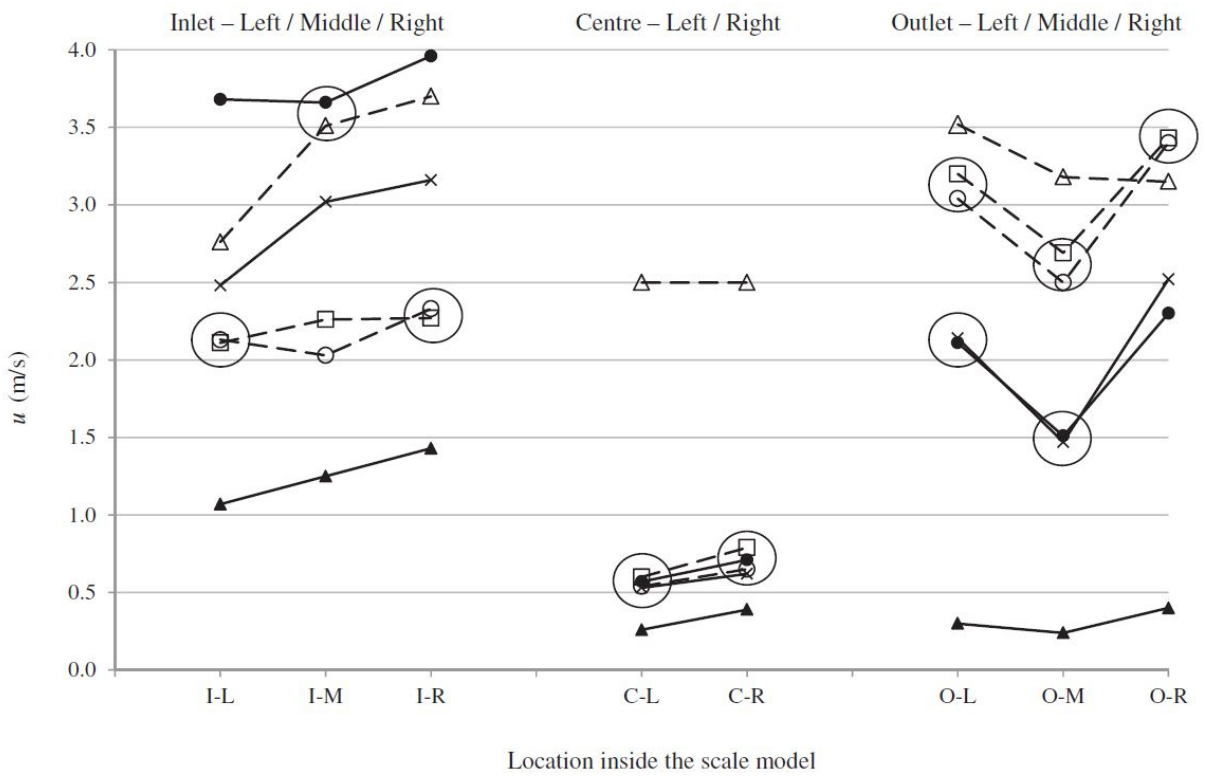

Figure 8 – Air velocities u (in m s–1) measured at *z* = 0.06 m inside the six scale model designs.

●, SM1; ×, SM2; ▲, SM3; ○, SM4; □, SM5; Δ, SM6; I, inlet; C, centre; O, outlet; L, left; M, middle; R, right. Connector lines between data points are purely for visual aid. Encircled data points denote values that are not significantly different among scale model designs, at a given location (p-level > 0.05).

Table 2 – Average air velocities *u* measured inside the six scale model designs, left (C-L) and right (C-R) at four different heights *z* in the central (y,z) plane under the ridge (Mean ± SD). (+) and (–) denote maximum and minimum values observed at each height z. Letters a-q indicate values that are not significantly different, within and between rows.

		Scale model					
	z (m)	SM1	SM2	SM3	SM4	SM5	SM6
$u_{C\text{-}L}$	0.03	0.75 ± 0.03 [a]	0.74 ± 0.04 [a, k]	0.26 ± 0.03(-) [l]	0.48 ± 0.05 [b]	0.49 ± 0.06 [b]	> 2.50 * (+)
(m s^{-1})	0.06	0.57 ± 0.03 [c]	0.53 ± 0.02 [c]	0.26 ± 0.02 (-) [l]	0.54 ± 0.05 [c]	0.60 ± 0.09	≈ 2.50 * (+)
	0.10	0.80 ± 0.04 [d]	0.70 ± 0.04 [a, k]	0.33 ± 0.02 (-)	0.76 ± 0.09 [d]	0.77 ± 0.09 [d, m]	1.67 ± 0.07 (+)
	0.14	1.53 ± 0.05 (+) [e, f]	1.44 ± 0.04 [e]	0.97 ± 0.03	0.91 ± 0.07	0.82 ± 0.07 (-) [m]	1.51 ± 0.07 (+) [f]
$u_{C\text{-}R}$	0.03	0.95 ± 0.02	0.89 ± 0.02 [g]	0.39 ± 0.02 (-) [n]	0.67 ± 0.03 [k]	0.63 ± 0.05 [k]	> 2.50 * (+)
(m s^{-1})	0.06	0.71 ± 0.02	0.62 ± 0.03 [i]	0.39 ± 0.01 (-) [n, p]	0.65 ± 0.04 [i]	0.79 ± 0.06	> 2.50 * (+)
	0.10	0.89 ± 0.03 [g]	0.86 ± 0.03 [g]	0.41 ± 0.01 (-) [p]	1.06 ± 0.08	0.99 ± 0.06 [q]	1.91 ± 0.05 (+)
	0.14	1.93 ± 0.06 (+) [j]	1.81 ± 0.05 [j]	0.74 ± 0.02 (-)	1.24 ± 0.04	1.04 ± 0.05 [q]	1.81 ± 0.07 (+) [j]

* The NTC anemometers used at the central plane under the ridge were calibrated to register air velocities up to 2.50 m s^{-1}.

Airflow rates

The average air velocities throughout each ventilation opening and the resulting airflow rates for all six scale model designs are shown in Table 3. The free surface areas A of the openings were previously given in Table 1. The results in Table 3 show that for each scale model design, the highest airflow rates *Q* were found at the inlet opening. The lowest values were found near the ridge opening, since it had a small free surface area A. Focusing on the airflow rates at the inlet opening, the highest value can be found in SM6 (where there is minimal wind resistance due to the open front and back walls), followed respectively by SM5, SM4, SM1, SM2 and finally SM3, where due to the closed outlet the lowest value was observed. This same sequence is maintained at the outlet opening and can be explained by the fact that larger ventilation openings in a wall will cause lower wind resistance over that wall. This also causes higher airflow rates when the ventilation opening surface area increases, as confirmed by the results given in Table 3, i.e., the rising airflow rates from SM4 to SM5 and finally SM6. These findings confirm what was previously identified statistically by Banhazi et al. (2008). At the ridge opening, the ventilation values do not differ very much, since its surface area A was only altered in SM2, where it was zero. The observed trends agree with common sense, thereby indicating that the numerical data are also useful for the evaluation of CFD models. It should however be noted that Q_{inlet} is not equal to the sum of Q_{outlet} and Q_{ridge}, due to the limited number of air velocity measurement points, which likely could not obtain a complete image of the airflow over the entire openings. Introducing more sensors, on the other hand, could disturb the 'normal' airflow pattern.

Table 3 – Average air velocities *u* and airflow rates *Q* for the six scale model designs, calculated from the average air velocity through the inlet opening, the ridge opening and the outlet opening.

Scale model	$u_{avg,\ inlet}$ ($m\ s^{-1}$)	$u_{avg,\ outlet}$ ($m\ s^{-1}$)	$u_{avg,\ ridge}$ * ($m\ s^{-1}$)	Q_{inlet} ($m^3\ s^{-1}$)	Q_{outlet} ($m^3\ s^{-1}$)	Q_{ridge} ($m^3\ s^{-1}$)
SM1	3.78	1.98	1.73	0.045	0.024	0.005
SM2	2.89	2.05	1.63	0.034	0.024	–
SM3	1.26	0.32	0.86	0.015	–	0.003
SM4	2.17	2.99	1.08	0.080	0.036	0.003
SM5	2.22	3.11	0.93	0.111	0.037	0.003
SM6	3.33	3.28	1.66	0.167	0.165	0.005

* Due to the confined space inside the scale model, these values were measured at z = 0.14 m, whereas the ridge opening itself was positioned at z = 0.15 m.

2.4. Conclusions and implications

The purpose of this research was to better understand the complex natural ventilation process in and around animal houses with different designs through air velocity measurements in 1:60 scale model variations of a cattle barn placed in a wind tunnel.

The obstruction or wind breaking effect exerted by the standard house upon its immediate leeward environment was 70 to 83% at scale model height. The open-front house showed a similar reduction in air velocities. The open house exhibited only reductions of 30 to 65%. The design of this model logically implied a smaller obstruction effect.

The quantitative effect of several common ventilation opening heights on the indoor air velocities was determined for six scale model designs. These effects could clearly be observed. Enlarging the inlet opening, or completely opening up the wall, led to 40% lower velocities near the inlet, but also more than 200% higher velocities at the outlet. The latter can be attributed to the larger inlet opening allowing for a higher airflow rate, which was subsequently forced through the outlet opening. At the centre of the house the air velocities were hardly affected by the construction. Only in case of removal of the outlet wall, 3–4 times higher velocities were observed at the centre.

From these experiments it can be concluded that altering the ventilation opening heights significantly changes the indoor airflows. In practice, farmers already adjust airflow rates by opening or closing ventilation openings using windbreak screens. This study quantitatively shows how influential these adaptations to openings can precisely be. Our results that were obtained under isothermal conditions, i.e. without buoyancy, indicate that enlarging a windward ventilation opening (inlet) will lower the speed of the inlet air, should this be desired, although higher indoor air velocities were observed near the outlet. Our set-up additionally provides a useful data set for the evaluation and improvement of CFD (Computational Fluid Dynamics) models. CFD also offers the possibility to predict the indoor microclimate, which was not included in the presently described wind tunnel experiments. Controlling the microclimate, especially at animal height and position, is what lies at the essence of any ventilation technique.

CHAPTER 3. AIRFLOW MEASUREMENTS IN AND AROUND SCALE MODEL CATTLE BARNS: EFFECT OF WIND INCIDENCE ANGLE

3.1. Introduction

In the previous chapter, wind tunnel experiments with 1:60 scaled cattle barns were performed in order to study the effect of the ventilation opening height on the ventilation efficiency. Indoor and outdoor air velocities were clearly affected, as well as the resulting airflow rates. For six different scale model designs it was clearly shown that larger ventilation openings resulted in higher airflow rates. However, this work was limited to conditions of perpendicular wind incidence. To address the reality of variable wind incidences, the objective of this chapter is to quantitatively report on the effect of the wind incidence angle on the indoor air velocities. Additionally, the effect of barn design was incorporated. To this end, two of the previously used scale-model barns were studied, i.e. the designs that featured symmetrical ventilation openings, either small or large (the most common sizes in commercial barns). The open-type barn is better at maintaining the airflow rate from the inlet to the outlet opening, due to its large openings which allow a fluid cross-ventilation (see Chapter 2, Table 2: SM6). It could be hypothesised that this similarity between ingoing and outgoing airflow rates can be maintained regardless of the wind incidence angle.

3.2. Materials and methods

3.2.1. WIND TUNNEL

The experiments were again conducted in the 12-m long closed-circuit wind tunnel of the International Centre for Eremology (I.C.E.), Ghent University, Belgium. A detailed description

Chapter after published manuscript: De Paepe, M., Pieters, J.G., Cornelis, W.M., Gabriels. D., Merci, B., Demeyer, P. (2013). Airflow measurements in and around scale model cattle barns in a wind tunnel: Effect of wind incidence angle. *Biosystems Engineering*, 115, 211-219.

of the I.C.E. wind tunnel has been given by Gabriels et al. (1997) and Cornelis et al. (2004). Acrylic sheets were placed along the wall that contained window frames, further improving the symmetry of the air velocity profile across the *y* axis in the wind tunnel work section (data not shown).

In Belgium, the main wind direction is from the southwest, with average wind speeds of 6–7 m s^{-1} at the coast, decreasing to 2–4 m s^{-1} in regions with greater altitude (KMI, 2012). In this experimental set-up, the reference air velocity, measured near the entrance of the wind tunnel work section, was 3.5 m s^{-1}. Overall, the experimental conditions were the same as described in Chapter 2.

3.2.2. SCALE MODELS

Two 1:60 cattle barn scale model designs were studied (Figure 1-2). These have been selected from the six designs (named SM1 through SM6) described in Chapter 2, since they featured symmetrical side openings. The aluminium-polycarbonate constructions featured 82 mm high sidewalls, a total height of 150 mm, a length of 677 mm, a width of 422 mm and an 18-degree roof slope. This resulted in a wind tunnel blockage ratio of 2.9%. Along the 5-mm wide ridge opening, 5-mm high wind deflectors were added, simulating 0.3-m high deflectors. It should be noted that the scaled barns were simplified: they did not feature heat sources (animal occupation), nor any interior structures.

Both model designs and their characteristics are presented in Figure 1 and Table 1. Each ventilation opening was 66 mm wide across the sidewall. SM1 is a scale model of a standard cattle barn, with 18 mm high ventilation openings beneath the eaves (1.08 m in full scale). SM6 had completely open front and back walls, leaving only the end walls (gable walls) present. The models were placed in the wind tunnel at a distance x = 7.67 m from the work section entrance.

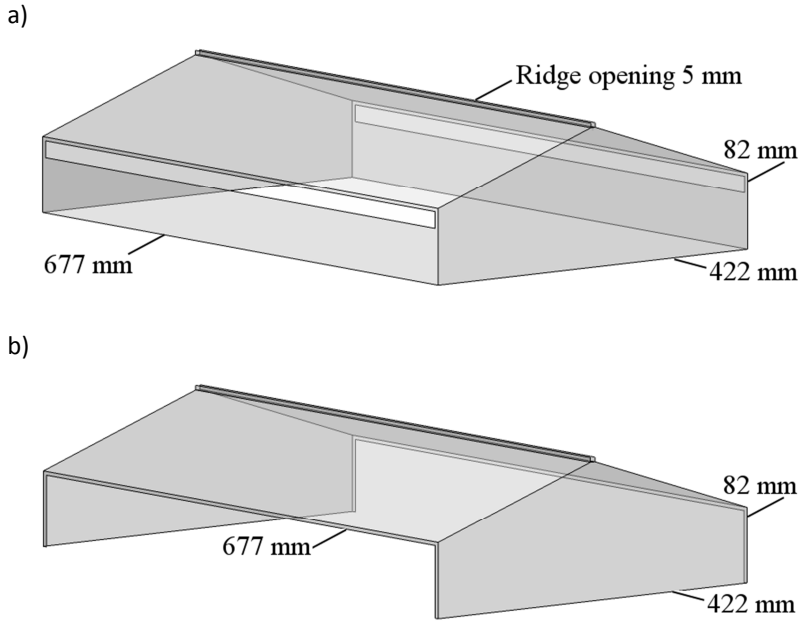

Figure 1 – Sketch of the two cattle barn scale-model designs: (a) standard model SM1, and (b) open building SM6, featuring approximately 4 times larger side openings. Labels 'SM1' and 'SM6' have been introduced in Chapter 2.

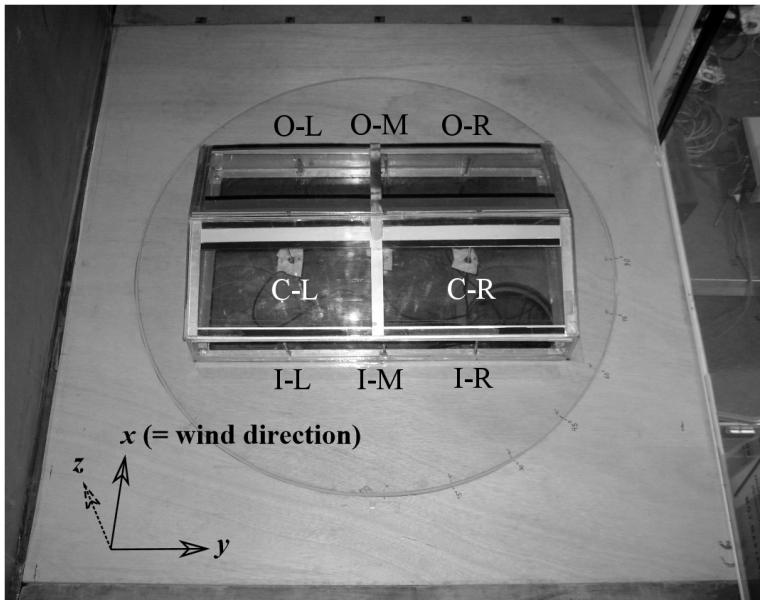

Figure 2 – Bird's eye view of scale model SM6 inside the I.C.E. wind tunnel. The letters mark the eight measurement locations, with C = centre plane, I = inlet, O = outlet, L = left, M = middle, R = right.

Table 1 – The two scale model designs with (1) the height *H* above the tunnel floor of the ventilation opening from its lower end to (→) its upper end, and (2) the free surface areas A of the ventilation openings. *

Scale model	H_{inlet} (cm)	H_{outlet} (cm)	A_{inlet} (cm²)	A_{outlet} (cm²)	A_{ridge} (cm²)
SM1	5.8 → 7.6	5.8 → 7.6	118.8	118.8	33.0
SM6	0.0 → 7.6	0.0 → 7.6	501.6	501.6	33.0

* 'Inlet' and 'outlet' refer to the ventilation openings in the sidewall, at the windward and leeward side of the model respectively, when $\vartheta = 0°$.

3.2.3. TURNTABLE

In order to simulate wind incidence angles other than the transversal flow generated by the wind tunnel, the scale model has been placed on a wooden turntable, 0.90 m in diameter. It was fitted in a floor plate of 1.20 m by 1.20 m, to suit the standard working section of the I.C.E. wind tunnel. Figure 3 shows a diagram of the experimental setup. The rotation angles were set manually using angular markings placed on the turntable. Ji, Tan, Kato, Bu and Takahashi (2011) recently described a novel method, allowing continuous rotation by coupling a turntable to a motorised rotating mechanism. However, since our study focuses on steady state flows, we chose instead to implement fixed angles.

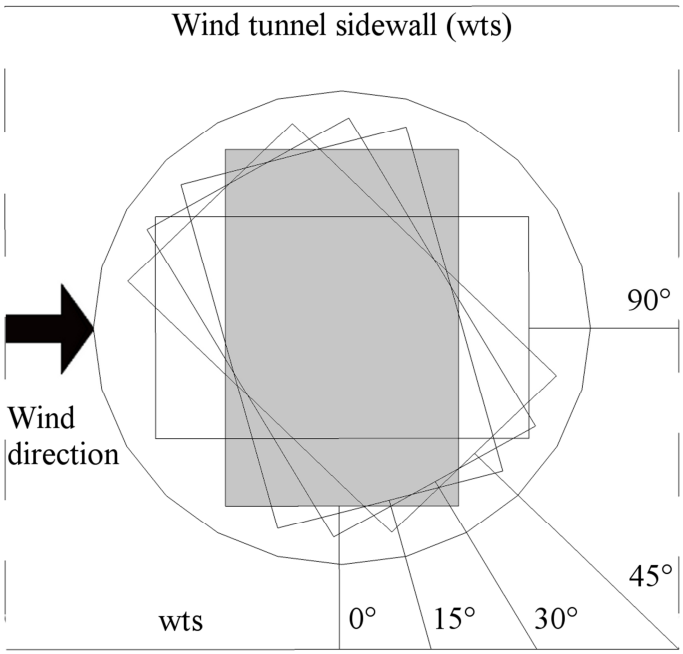

Figure 3 – Top view of the cattle barn scale-model (grey rectangle) placed on the turntable. Indicated are the five angles used to simulate different wind incidences. The four rectangles depict the respective resulting positions of the scale model.

3.2.4. MEASUREMENTS AND PROCEDURES

Experimental conditions

The reference air velocity, u_r, measured near the work section entrance at x = 1.00 m, y = 0.60 m, z = 0.50 m (i.e., above the boundary layer), averaged 3.5 m s^{-1} during all experiments, with a standard deviation of 0.1 m s^{-1}. The Reynolds number, *Re*, was about 491 000, based on the characteristic length, L_t (m), being the average of the width and height of the wind tunnel work section.

Near the work section entrance the ambient temperature, T, and relative humidity, φ, have also been measured, using E+E type EE65 and EE33 transducers (E+E Elektronic, Engerwitsdorf, Germany). Due to varying atmospheric conditions, temperature and relative humidity in the wind tunnel fluctuated between 16.8°C and 23.1°C, and between 29.8% and 32.5%, respectively. During a single experiment, the temperature showed a fluctuation of max. 0.1 °C, and relative humidity varied by less than 0.2%. The thermal and humidity effects can be neglected in the setup. The temperature difference caused by the anemometers was calculated to be approx. 1 °C, not influencing the airflow pattern inside the scale models, since they featured a very small stack height of 0.15 m.

All measurements were conducted at a frequency of 1Hz, with a sample time of 120 s. Sampling commenced at least 100 s after the wind tunnel fan started to ensure a fully developed airflow. All data were captured using a type DTL 1232 logger with Logwin32 software (LHM Instrumentation, Belgium).

Effect of wind incidence angle on indoor air velocities

Air velocities were measured at eight locations inside the two cattle barn models to investigate the quantitative effect of varying wind incidence angles. Three small-scale 2D hot wire anemometers (type 8465, TSI Inc., Shoreview, MN, USA) were placed near both sidewall ventilation openings. At these locations, the air streams were known to be predominantly horizontal. In the central (y,z)-plane containing the ridge, two omni-directional NTC anemometers (type 8475, TSI Inc.) were in place. All eight probes have been inserted through perforations made in the floor plate of the scale model. The positioning of the probes inside the scale model can be seen in Figure 2 and Table 2. Each probe has been calibrated and their accuracy was ± 0.1 m s^{-1} in the selected air velocity range (0.125–5.00

m s^{-1} for types 8465; 0.05–2.50 m s^{-1} for types 8475). The probes did not give an indication of the airflow direction.

The two type 8475 anemometers in the central (*y*,*z*)-plane containing the ridge have been placed consecutively at four heights (*z* = 0.03, 0.06, 0.10 and 0.14 m). The six other probes near the inlet and outlet openings remained at a fixed height, with the lowest point of the probe end at z = 0.06 m, resulting in the probe spanning the opening's height as it has been constructed in scale model SM1.

With this setup, both scale model designs have been subjected to five different wind incidence angles through rotation of the turntable: angles ϑ = 0, 15, 30, 45 and 90° have been tested. ϑ = 0° denotes the wind flowing perpendicular to the frontal (windward) ventilation opening, while with ϑ = 90° the wind impacts onto one of the end walls.

Table 2– Positions of the internal anemometers with reference to the bottom front left of the scale model.

Position	*x'* (mm)	*y'* (mm)	*z* (mm)
I-L	12	165	60
I-M	12	335	60
I-R	12	505	60
C-L	210	165	30/60/100/140
C-R	210	505	30/60/100/140
O-L	408	165	60
O-M	408	335	60
O-R	408	505	60

Airflow rates

Estimations of airflow rates *Q* have been calculated for each ventilation opening (inlet, outlet and ridge opening) by multiplying the opening's free surface area *A* (in m²) with the average air velocity measured in the respective ventilation opening, $\bar{u}$ (in m s^{-1}). For wind incidence angles of 15°, 30° and 45°, further multiplication with cos(ϑ) was introduced to make an approximation of the velocity vector aligned with the airflow generated by the wind tunnel. No *Q* values were estimated for ϑ = 90°, since the directional flow field is very variable in this configuration.

Statistical methods

The effect of measurement location and scale model configuration (fixed independent variables) on the air velocity *u* (dependent variable) was determined using two-way ANOVA. Since the interaction between location and scale model was always significant, a one-way ANOVA was performed with the different combinations of both factors (measurement location and scale model) as separated groups. A Scheffé post-hoc test (Scheffé, 1959) was applied to determine the significant differences between scale models within each fixed measurement location. Statistical analyses were performed using SPSS Statistics 19 (SPSS Inc. 2010, IBM corporation, New York, USA). Statistical significance was considered at $p < 0.05$.

3.3. Results and discussion

3.3.1. EFFECT OF WIND INCIDENCE ANGLE ON INDOOR AIR VELOCITIES

Figure 4 shows the average air velocities as measured by the eight probes at height z = 0.06 m inside the standard scale model SM1 (Figure 4a) and open building SM6 (Fig 4b), for the five different wind incidence angles (0, 15, 30, 45 and 90°). Circled data points denote values that are not significantly different among scale model orientations, at the given measurement location (*Y* axis in the graph).

During the rotation experiments with the standard scale model (SM1), air velocity values between 0.6 and 4.0 m s^{-1} have been observed at the inlet opening (I), between 0.2 and 1.0 m s^{-1} in the centre (C) and between 1.1 and 2.3 m s^{-1} at the outlet opening (O). A slight rotation of scale model SM1, such as 15°, changed the indoor air velocities observed at the centre of the model and near the outlet. No notable changes were observed near the inlet opening. A change started taking place at the central plane, where at the left position (C-L) decreasing values were measured, while at the right position (C-R) increasing values were noted. This trend is visible for all further angles. This phenomenon can be explained by the fact that, upon rotation, the position C-L became more and more obstructed by the left end walls (see Figure 5), resulting in a reduced velocity. This was in turn compensated at the opposite side (C-R), where higher air velocities were observed. This can be explained by the rotation of the right end walls, which gradually guided the air more towards the centre of the scale model, thereby passing measurement position C-R.

Further rotation of the scale model towards an angle of 30° gives similar results as with an angle of 15°. Only to the left of the outlet (O-L) again a small drop in air velocity between the cases of 15° and 30° was observed. The latter can also be explained by the obstruction effect at this position upon rotation. Figure 5 shows that the position O-L enters the obstruction zone (grey) when the scale model is placed at an angle of 30°. Further rotation resulted in a further decrease in air velocity at this position. This is consistent with computational modelling results by Norton et al. (2009), which showed that for a naturally ventilated barn with a 30° wind incidence angle this zone contained a secondary (i.e., lower-speed) wind-driven vortex.

The introduced obstruction effect helps to explain the variations measured throughout these experiments. Small differences in air velocities were found at the middle and right side of the inlet opening (I-M and I-R), since these positions were never obstructed, except at a 90° angle, where air velocities dropped with 64% and 84%, respectively. The same observation can be made for the right side of the outlet (O-R). The outlet's middle position (O-M), however, was gradually subjected to an increasing obstruction upon further rotation, thus experiencing decreasing air velocities.

At 90° the wind fully impacted upon the left end walls, thereby not directly passing through the ventilation openings, as in the previous configurations. This specific orientation leads to significantly lower air velocities near the inlet and outlet openings. However, a slight rise in air velocity was observed at the central position C-R. A possible explanation of this artefact was the unintended protrusion of the anemometer outside the scale model at this position, due to rotation of the model. The air also exited through the ridge opening (see Table 3 and below), which was perfectly aligned along the wind direction in this setup.

The experiments with the open building model SM6 (Figure 4b) showed largely similar results. The obstruction effect still explains most of the observations, yet some important differences can be noted. Upon rotation from 0° to 45°, the air velocities at I-L rose, possibly because the large ventilation openings allow the wind to pass relatively easily through the scale model. At the same time, the left end walls started to face the wind more and more, and became a much greater obstruction to the wind. This most likely created a high-pressure zone that diverted the air towards the large ventilation openings. At I-M and I-R small differences in air velocity can be seen up to a rotation angle of 15°, while at 90° significantly lower air velocities can be observed at these measuring points (75% and 64% respectively).

At the central position C-R no reductions in air velocities were observed, except at an angle of 90°. The air velocities measured near the outlet opening (O-L, O-M and O-R) show trends similar to those in the standard barn scale model SM1.

The air velocities under the 0.15-m high ridge opening (positions C-L and C-R) have not only been measured at height *z* = 0.06 m, but also at three other heights (z = 0.03, 0.10 and 0.14 m). Table 3 shows the air velocities measured in the centre of the scale model at two different points C-L and C-R, and at heights z = 0.03, 0.06, 0.10 and 0.14 m. In general, for scale model SM1 the same trends can be seen as described previously (see also Figure 4, positions C-L and C-R), where the focus was on 0.06 m height. In the case of open building SM6, the values measured at z = 0.03 m are similar to those at 0.06 m height. At heights z = 0.10 and 0.14 m, lower air velocities are measured, showing no clear trend with respect to scale model rotation, except for the obvious minimum values found for a 90° rotation. This can probably be attributed to the fact that the large ventilation openings in this open building impose less friction on the airflow at the lower heights. This would mean that direct cross-ventilation occurred between both ventilation openings, whereby airflows largely avoids passing through the upper area of the scale model. This phenomenon has also been observed in two-dimensional CFD simulations with this scale model design, where wind was simulated perpendicular to the ventilation openings (see Chapter 4).

3.3.2. EXPRESSION OF AIR VELOCITIES AS FUNCTION OF WIND INCIDENCE ANGLE

A linear regression analysis of the averaged air velocities through the inlet and outlet openings was carried out on the cosine of the wind incidence angle, ϑ, for both scale models. In Figure 6, the averaged air velocities through each ventilation opening were plotted as a function of cos(ϑ). Trend line fitting lead to good R^2 values, ranging between 0.57–0.97. With the resulting linear regression equations it was possible to predict the experimental air velocities within a maximum error of 5%. The values for 90° angles were not included in the regression, since at this angle the airflow patterns were fundamentally different. Therefore, care must be taken when trying to extrapolate the data towards wind incidence angles larger than 45°. Additionally, this model is only valid for the present experimental setup and the used reference air velocity of 3.5 m s^{-1}. Further experimental research is needed to acknowledge its validity for other reference air velocities.

Table 3 – Effect of wind incidence angle on average air velocities u inside standard house SM1, left (C-L) and right (C-R) at four different heights *z* in the central (*y,z*) plane under the ridge (Mean ± SD). Letters (a-t, a'-k') indicate values that are not significantly different, within and between rows.

Scale model		Rotation				
SM1	*z* (m)	0°	15°	30°	45°	90°
$u_{C\text{-}L}$	0.03	0.75 ± 0.03$^{a, b}$	0.43 ± 0.03$^{c, d}$	0.42 ± 0.04^{c}	0.46 ± 0.03$^{c, h, k}$	0.20 ± 0.02^{e}
(m s^{-1})	0.06	0.57 ± 0.03^{f}	0.39 ± 0.03^{d}	0.40 ± 0.03^{d}	0.39 ± 0.02^{d}	0.19 ± 0.01^{e}
	0.10	0.80 ± 0.04$^{g, h}$	0.67 ± 0.04^{i}	0.68 ± 0.03^{i,} j	0.48 ± 0.03^{k}	0.17 ± 0.02^{e}
	0.14	1.53 ± 0.05^{l}	1.44 ± 0.04^{l}	1.23 ± 0.05^{m}	0.60 ± 0.04^{f}	0.25 ± 0.01
$u_{C\text{-}R}$	0.03	0.95 ± 0.02^{n}	1.15 ± 0.04$^{o, p}$	1.19 ± 0.04^{o,q}	1.20 ± 0.04$^{m, q}$	0.83 ± 0.03^{g}
(m s^{-1})	0.06	0.71 ± 0.02$^{a, j}$	0.98 ± 0.02$^{n, r}$	1.04 ± 0.02^{s}	1.02 ± 0.02$^{r, s}$	0.78 ± 0.06$^{b, h}$
	0.10	0.89 ± 0.03	1.03 ± 0.04^{s}	1.12 ± 0.03^{p}	1.24 ± 0.04^{m}	0.65 ± 0.02^{i}
	0.14	1.93 ± 0.06^{t}	1.89 ± 0.06^{t}	1.72 ± 0.07	1.78 ± 0.10	0.65 ± 0.04^{i}
SM6	*z* (m)	0°	15°	30°	45°	90°
$u_{C\text{-}L}$	0.03	> 2.50 *	> 2.50 *	~ 2.50 *	0.94 ± 0.08$^{a'}$	0.48 ± 0.04$^{b'}$
(m s^{-1})	0.06	~ 2.50 *	~ 2.50 *	~ 2.50 *	0.93 ± 0.08$^{a'}$	0.52 ± 0.04$^{b'}$
	0.10	1.67 ± 0.07$^{c'}$	1.63 ± 0.06$^{c'}$	1.93 ± 0.11$^{d', i'}$	0.93 ± 0.06$^{a'}$	0.69 ± 0.05$^{e'}$
	0.14	1.51 ± 0.07$^{f'}$	1.35 ± 0.04$^{g'}$	1.51 ± 0.06$^{f'}$	0.90 ± 0.05$^{a'}$	0.75 ± 0.07$^{e'}$
$u_{C\text{-}R}$	0.03	> 2.50 *	> 2.50 *	~ 2.50 *	~ 2.50 *	1.30 ± 0.04$^{g'}$
(m s^{-1})	0.06	> 2.50 *	> 2.50 *	> 2.50 *	~ 2.50 *	1.53 ± 0.05$^{f'}$
	0.10	1.91 ± 0.05$^{d'}$	2.01 ± 0.06$^{h'}$	1.93 ± 0.06$^{d', i'}$	1.79 ± 0.05$^{j', k'}$	1.84 ± 0.08$^{k'}$
	0.14	1.81 ± 0.07$^{k'}$	1.97 ± 0.10$^{d', h', i'}$	1.74 ± 0.08$^{j'}$	1.97 ± 0.08$^{h', i'}$	1.93 ± 0.06$^{d', i'}$

* The NTC anemometers used at the central plane under the ridge were calibrated to register air velocities up to 2.50 m s^{-1}.

"~ 2.50" means about half of the raw data were slightly less than 2.50 m s^{-1}, while the other half reached the registrable limit of 2.50 m s^{-1}.

"> 2.50" means the majority of the raw data exceed 2.50 m s^{-1}.

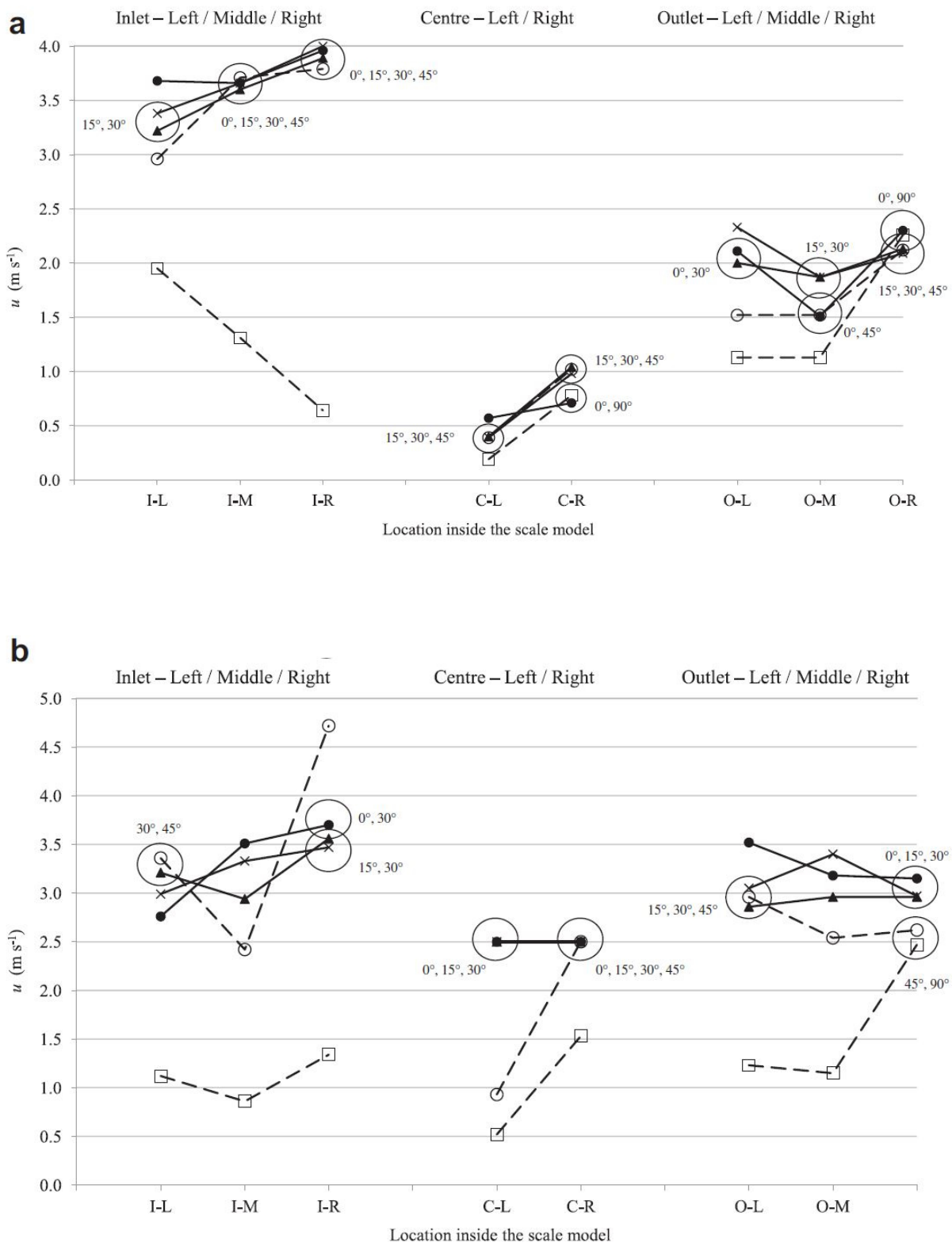

Figure 4 – Average values for air velocities u (in m s^{-1}) measured at height z = 0.06 m inside (a) standard model SM1, and (b) open building model SM6, exposed to five different wind incidence angles ϑ; ●, 0°; ×, 15°; ▲, 30°; ○, 45°; □, 90°; I, inlet; C, centre; O, outlet; L, left; M, middle; R, right. Connector lines between data points are purely for visual aid. Encircled data points denote values that are not significantly different among scale model designs, at a given location (p-level > 0.05).

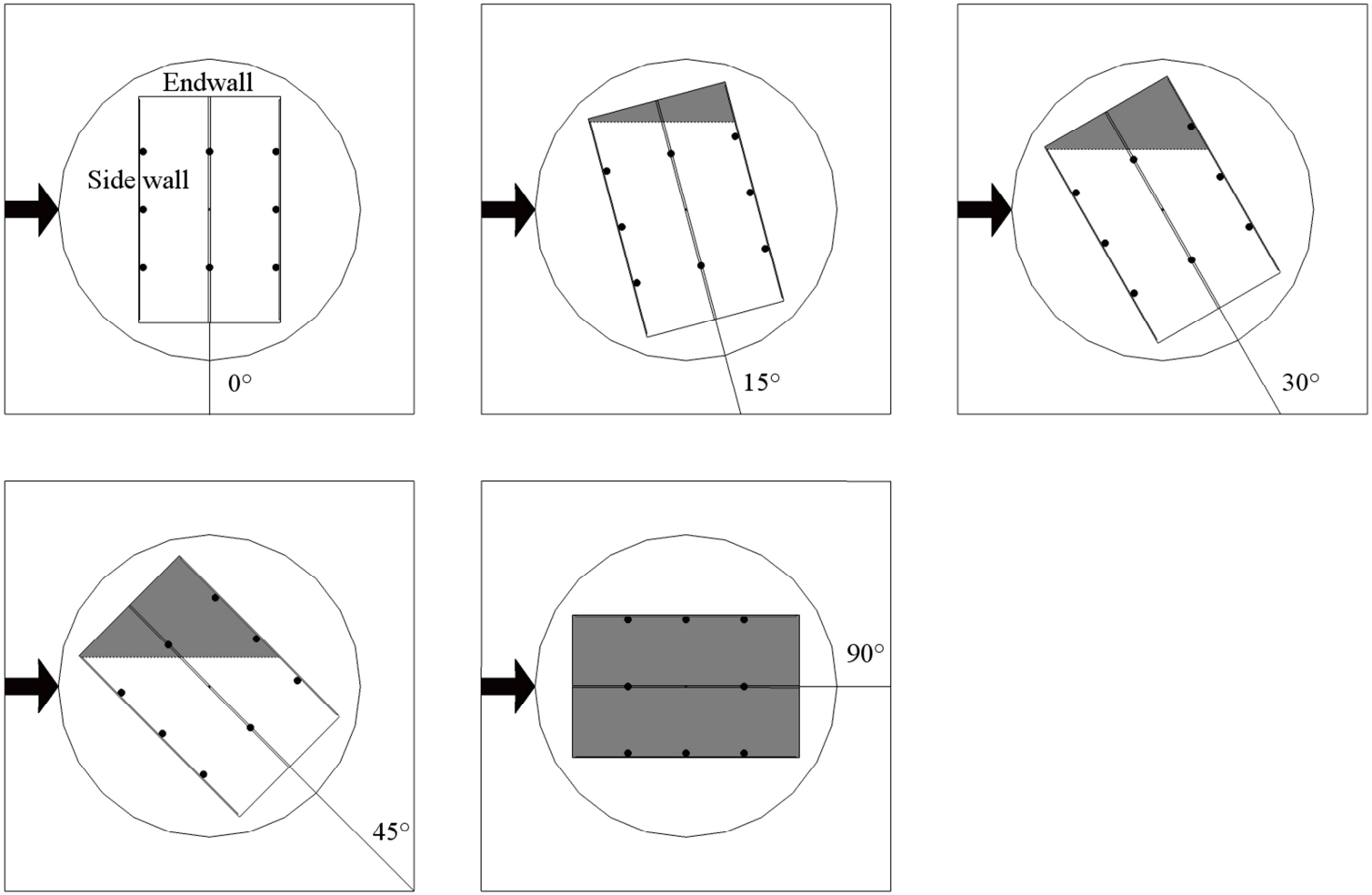

Figure 5 – Top view of the scale model barn under angles 0, 15, 30, 45 and 90°, respectively, with the wind following the black arrow. The grey areas indicate zones that experience leeward obstruction by the gradually rotated end walls. The eight measurement positions are indicated by black dots.

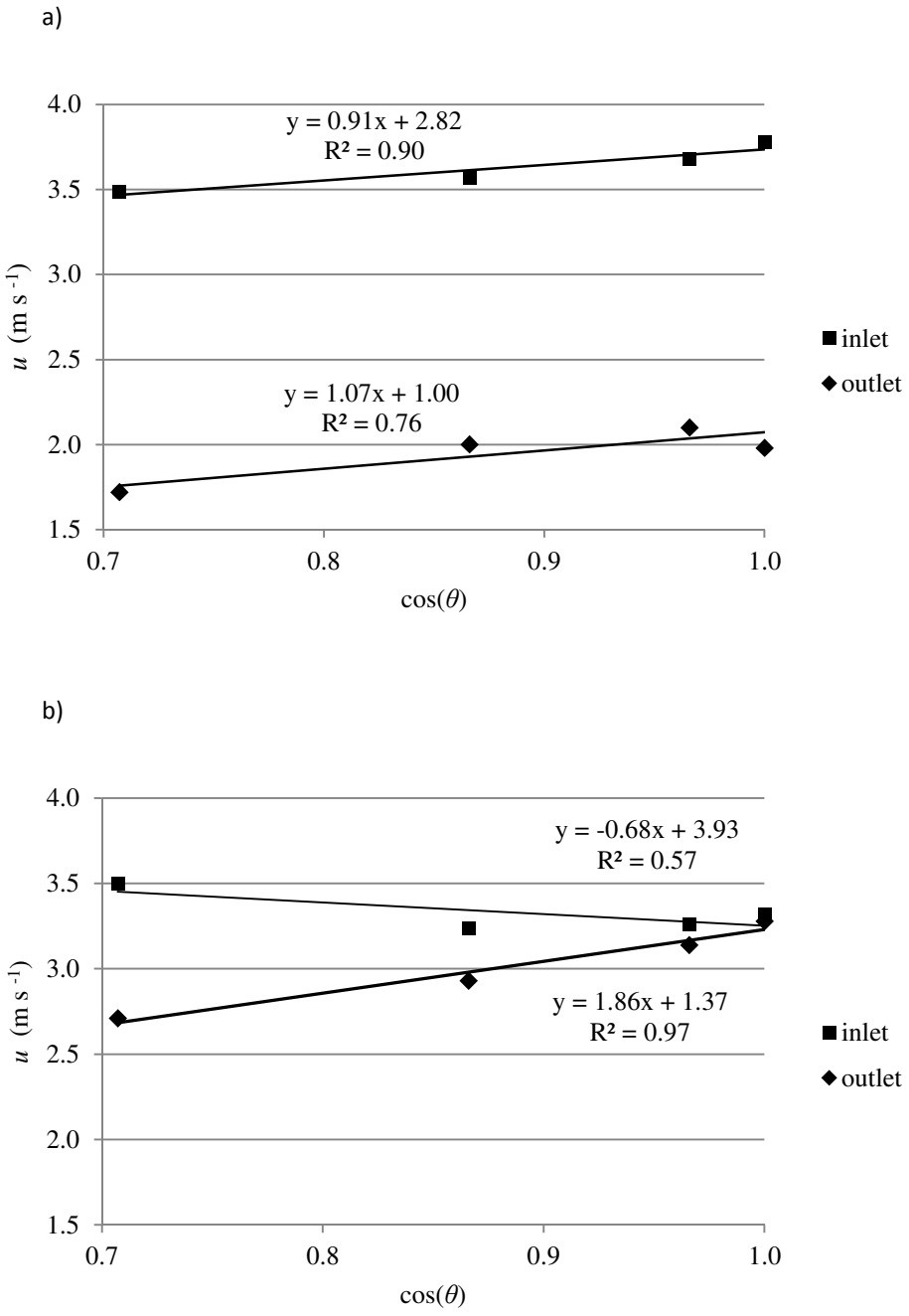

Figure 6 – Linear regression of the average air velocities at the inlet and outlet opening in function of cos(ϑ), for (a) standard barn model SM1, and (b) open-type barn SM6. The respective regression equations and R^2 values are also given.

3.3.3. CALCULATION OF AIRFLOW RATES

The average air velocities at each ventilation opening and the estimated airflow rates for both scale models are shown in Table 4. The free surface areas, A, of the openings were presented in Table 1.

The airflow rates through the inlet of scale model SM1 decreased only slightly (7%) for a rotation from 0° to 15°. Further rotation to 30° and 45° resulted in more significant decreases of the airflow rate with respectively 18 and 36%. At the extreme angle of 90°, net airflow rates are theoretically zero but this is of course not the case in reality. The outlet opening exhibited constant airflow rates for a rotation from 0° and 15°, and declining rates for further rotation to 30° and 45° (13 and 42% decrease respectively). At this angle, a single opening could have experienced both incoming air as well as outgoing air, since the openings were fully aligned with the wind.

In general, the same conclusions can be made for open building SM6, where airflow rates through the inlet and outlet opening remained constant for a rotation up to 15° and dropped more significantly at greater angles. A theoretical model by Zhang, Janni & Jacobson (1989) also showed consistently decreasing airflow rates upon rotation.

Table 4 also shows that for SM1 the airflow rates at the inlet opening are about twice those at the outlet. In contrast, the airflow rates in SM6 at the inlet opening were in general similar to those at the outlet for wind incidence angles < 45°. This is of course related to the open structure of SM6, causing less obstruction to the external airflow and allowing a more fluid cross-ventilation through this barn.

Airflow rates for the ridge opening were generally very low due to the small surface area A, and also very similar for all rotations.

Table 4 – Average air velocities *u* and airflow rate estimations *Q* through the inlet and outlet openings of standard barn SM1 and open house SM6.

Scale model	ϑ	cos(ϑ)	$u_{avg,\ inlet}$ (m s^{-1})	$u_{avg,\ outlet}$ (m s^{-1})	$u_{avg,\ ridge}$ (m s^{-1})	Q_{inlet} (m^3 s^{-1})	Q_{outlet} (m^3 s^{-1})	Q_{ridge} (m^3 s^{-1})
SM1	0°	1	3.78	1.98	1.73	0.045	0.024	0.006
	15°	0.97	3.68	2.10	1.67	0.042	0.024	0.005
	30°	0.87	3.57	2.00	1.48	0.037	0.021	0.004
	45°	0.71	3.49	1.72	1.19	0.029	0.014	0.003
	90°	0	1.30	1.51	0.45	-	-	-
SM6	0°	1	3.32	3.28	1.66	0.167	0.165	0.005
	15°	0.97	3.26	3.14	1.66	0.158	0.152	0.005
	30°	0.87	3.24	2.93	1.63	0.141	0.127	0.005
	45°	0.71	3.50	2.71	1.44	0.124	0.096	0.003
	90°	0	1.11	1.62	1.34	-	-	-

3.4. Conclusions and implications

Quantitative results of air velocity measurements have been presented for two 1:60 scale model cattle barns in a wind tunnel, with a reference air velocity of 3.5 ms^{-1}. The effect of five wind incidence angles on the indoor air velocities has been quantified. The responses in local air velocities could largely be attributed to the relative position of the end walls of the scale models towards the wind. This position is crucial and allows the measured air velocity trends to be explained, leading to a better understanding of the ventilation process. It must, however, be noted that the scale model barns are simplified in that they do not feature heat sources (animal occupation) nor any interior structures.

Upon rotation, the estimated airflow rates through the inlet and outlet openings gradually decreased in both scale models. It also became clear that, for wind incidence angles < 45°, the open-type barn is better at maintaining the airflow rate between the inlet and the outlet opening. Its large openings were indeed hypothesised to generate a fluid cross-ventilation. In practice this would mean that naturally ventilated barns with open sidewalls allow for a more uniform indoor airflow distribution. This of course depends on other factors as well.

Additionally, linear regressions were presented that relate the measured air velocities to the wind incidence angle, for angles ≤ 45°. The experimental set-up also provides useful data for the evaluation and possible improvement of CFD models.

CHAPTER 4. CFD MODELLING OF THE AIRFLOWS IN SCALE MODEL CATTLE BARNS: EFFECT OF VENTILATION OPENING HEIGHT

4.1. Introduction

Computational Fluid Dynamics (CFD) can be of valuable help in order to obtain a more comprehensive understanding of the internal airflows in the scale-model cattle barns during the wind tunnel experiments. Therefore, in this chapter the objective was to perform two-dimensional (2D) CFD simulations using the six different ventilation opening configurations (i.e., after the designs described in Chapter 2). The resulting airflow patterns and indoor air velocities will be visualised and compared with the previously acquired experimental results of the wind tunnel study in Chapter 2. This will allow us to investigate whether airflow patterns in (scale-model) naturally ventilated barns can be adequately described by CFD modelling.

4.2. Materials and methods

4.2.1. CFD

CFD is the scientific discipline of predicting fluid flow, heat and mass transfer, chemical reactions and related phenomena by solving the applicable differential equations numerically. The main advantage of using CFD is time and cost saving, by reducing the need for experimental data. CFD has become the most widely used simulation technique in the world (Lewis et al., 2004) and can offer both a spatial and a temporal solution in the considered domain.

CFD is able to predict parameters for existing models, as well as to design new ones, solve specific problems, etc. However, this can only be accomplished when the correct

Chapter extended after published manuscript: De Paepe, M., Pieters, J.G., Cornelis, W.M., Gabriels. D., Merci, B., Demeyer, P. (2013). Computational modelling and scale model validation of airflow patterns in naturally ventilated barns. In: *ISHS Acta Horticulturae*, 1008 – 1st International Symposium on CFD Applications in Agriculture. CIGR-AgEng, 2012, Valencia, Spain.

mathematical operations are applied and the domain of interest and its boundary conditions are well-defined.

Due to the ever-increasing computational power in the last three decades there has been a vast increase in the use of CFD tools in different engineering disciplines, e.g. aerospace applications, turbo-machinery, weather forecasting, electronic cooling arrangements, flow in heat exchangers, etc. In the 1980s, a solution for a reasonably sized three-dimensional fluid dynamics problem was rarely possible on a personal computer. Now, it is very common for researchers using such computers to solve reasonably sized fluid dynamics problems in three dimensions (Lewis et al., 2004).

For this thesis the thoroughly and systematically validated CFD code 'Fluent' (ANSYS, Inc.) was chosen; an advanced and the most widely adopted CFD tool. Fluent offers a wide range of mathematical models for transport phenomena (such as gas and heat transport). Using meshing software, such as Gambit, it is possible to model complex geometric structures to be used as the fluid flow domain.

Finite volume method

Fluent uses the finite volume method for its calculations, in which the domain is discretised into a finite number of control volumes. In these control volumes the following statements apply (Versteeg & Malalasekera, 2007):

- The fluid's mass is retained
- The change in moment is equal to the sum of the forces on a volume (Newton's second law)
- The change in energy is equal to the sum of the heat and work delivered to the volume (first law of thermodynamics)
- The conservation of species

In a CFD solver, such as Fluent, a system is modelled with these **laws of conservation**, which leads to a total solution for the considered domain, both temporally and spatially. Solving occurs by discretising the partial differential equations (associated with the various processes, e.g., convection and diffusion) in algebraic equations.

Navier-Stokes equations

The mathematical model of a fluid dynamics problem is governed by the Navier-Stokes equations. These fundamental equations represent the fluid as a continuum, include the conservation of mass, momentum and energy, and can be derived following either an integral or a differential approach. The integral form of the equations is derived using the Reynolds Transport Theorem and is discussed in many standard texts on fluid mechanics (Shames, 1982). In the differential approach followed by Lewis et al. (2004), a differential control volume is considered in the fluid domain and to represent the variation of mass, momentum and energy, a Taylor expansion is used.

For example, in order to derive a general conservation of the mass equation, a differential control volume as shown in Figure 1 is considered. The full derivation of the Navier-Stokes equations is, however, not in the scope of this thesis. Fluent solves these conservation equations for mass and moment for all fluid flows. If heat transfer occurs, the conservation of energy is also taken into account. When implementing multiple materials (e.g., emission gases), the preservation of species is also taken into account. In order to obtain a solution in the domain of interest, boundary conditions need to be defined. Some examples of boundary conditions are the incoming air velocity, the outgoing flow rate and wall properties.

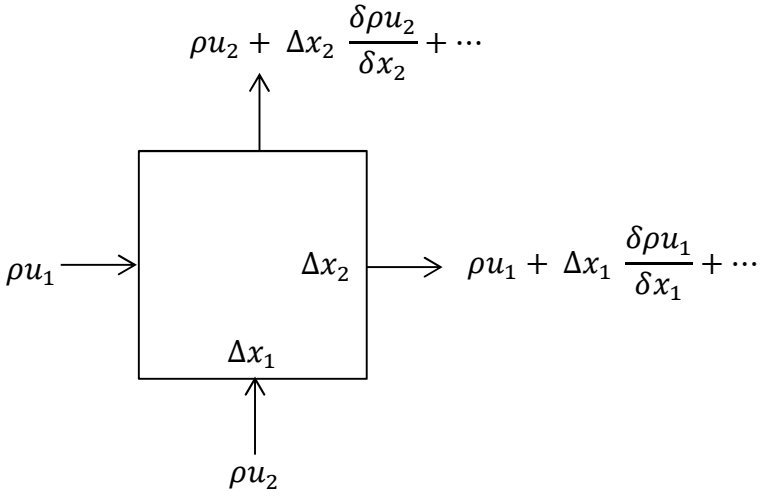

Figure 1 - Conservation of mass in a flow field, using an infinitesimal control volume (Lewis et al., 2004).

Turbulence models

For laminar flows, CFD solutions are generally very accurate. In all convection applications, turbulence becomes important for Reynolds or Rayleigh numbers beyond a certain value.

The prediction of turbulent flows, as these usually are in buildings, remains more difficult due to their complex nature. Turbulent flow is characterized by velocity fluctuations on a very small scale and with high frequency. This implies that the calculations for turbulent flows demand more computing power and time. In order to acquire an acceptable CFD model, the turbulence parameters should be approached as good as possible. Several turbulence models are available to approximate turbulent flow problems more properly.

The three major methods of dealing with these turbulence problems in CFD are the Reynolds Averaged Navier-Stokes (RANS) model, the Large Eddy Simulation (LES) model and the Direct Numerical Simulation (DNS) model. Of these three methods, DNS gives the best detailed and accurate description of the turbulent flown but it's disadvantage is that the current computing hardware is not yet available to handle large practical problems. The LES technique is computationally less intensive. The RANS method is the most widely used turbulence modelling approach, since a relatively small number of mesh cells (or their interlaying nodes) is required to compute the turbulence. Furthermore, the accuracy of the results are always highly dependent on the employed model and mesh (Lewis et al., 2004).

For a much more comprehensive explanation of CFD, the works of Lewis et al. (2004) and Versteeg & Malalasekera (2007) are highly advised.

4.2.2. GENERAL WORK FLOW IN CFD MODELLING

This section describes the typical procedure to be followed for a CFD simulation. A schematic overview is shown in Figure 2. First, the geometry of interest (i.e., a barn design) needs to be modelled according to the desired detail, which can range from a very coarse representation to a fully realistic detail. Consequently, this domain is split up in a finite number of elements, which together make up the computational mesh or grid. Also, boundary conditions need to be applied at the domain's borders of essence (e.g., an airflow velocity inlet, an atmospheric pressure outlet). Boundary conditions are in essence known values, be they experimentally acquired or theoretically assumed, which can be substituted in the governing equations of the fluid flow problem at hand, eventually leading to a solution for the whole computational domain of interest. This provides calculated values for air velocities, pressure, temperature, etc., for each of the defined mesh cells.

After investigation of the solution, the simulation can be fine-tuned through the optimisation of its parameters. This feedback loop coincides with the post-processing phase,

where the model's results are reported either in text form or visually on screen, for instance as iso-value contour plots or vector plots (showing both local flow velocity magnitudes and directions). This allows to scrutinise the resulting solution. Some CFD software packages also allow the export of the data to other modelling programs so that it can be processed even further.

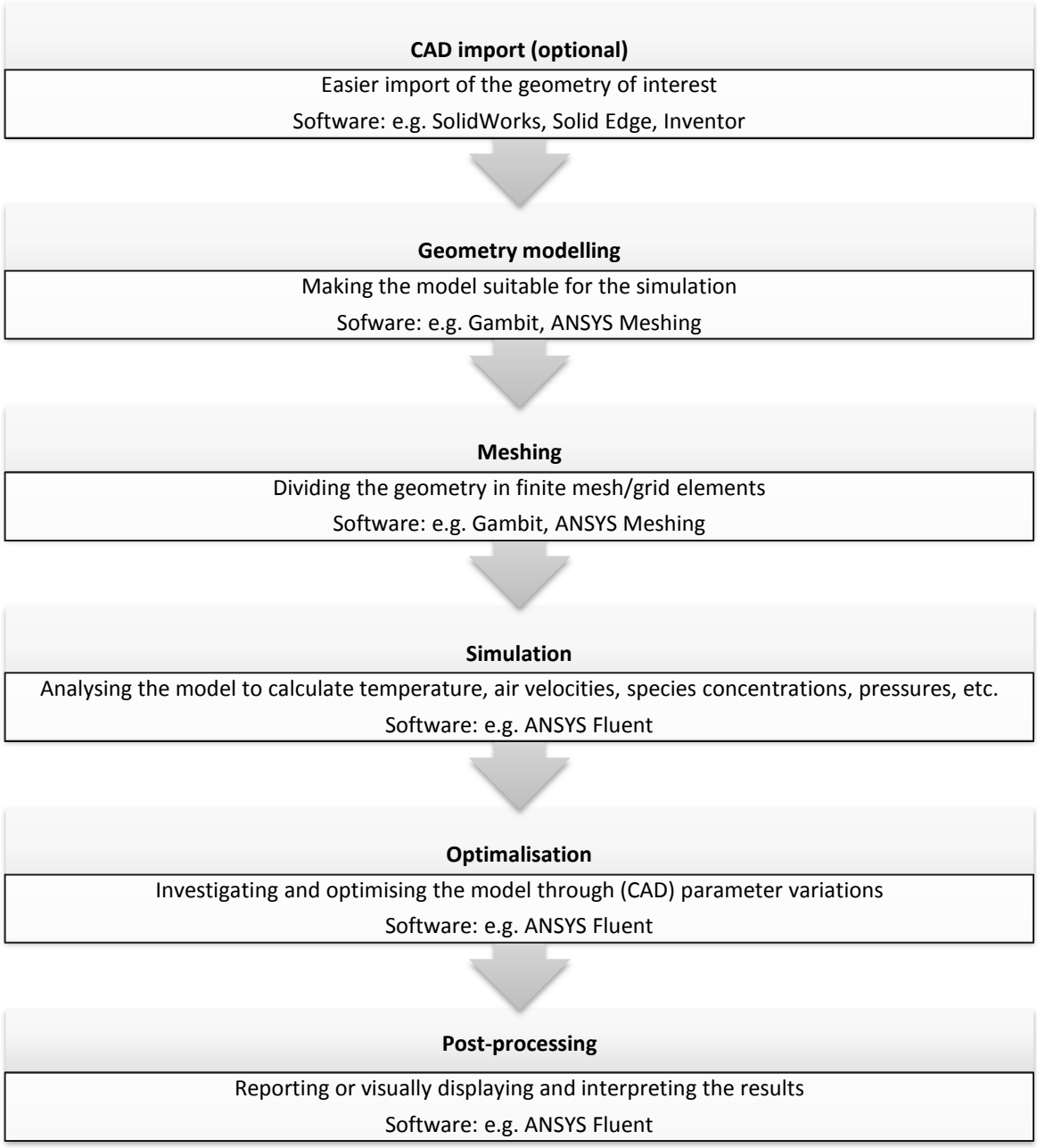

Figure 2 – Chart of the typical work flow during CFD modelling. Adapted from ANSYS, Inc.

4.2.3. SET-UP OF THE MODELLED CASES

In this study, RANS modelling with ANSYS Fluent 14.0 software was used to perform 2D simulations of natural ventilation with six different scale models of a barn (Figure 3) placed in a wind tunnel. The computational domain (Figure 4) in fact consisted of the second part of the wind tunnel work section. The first –windward– part was simulated beforehand. The exiting wind velocity profile of the developed flow in the first part of the wind tunnel was used as the inlet velocity profile for the computational domain (second part of the wind tunnel).

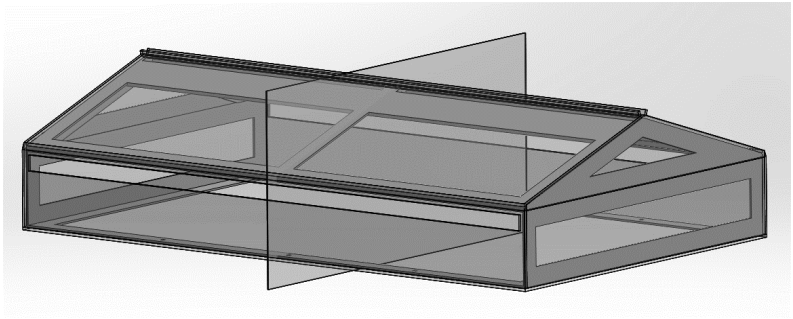

Figure 3 – CAD schematic of the scale model barn (type 'SM1') used in the wind tunnel experiments. The central section plane shows the two-dimensional geometry used in the CFD model. Source: Van Overbeke, P.

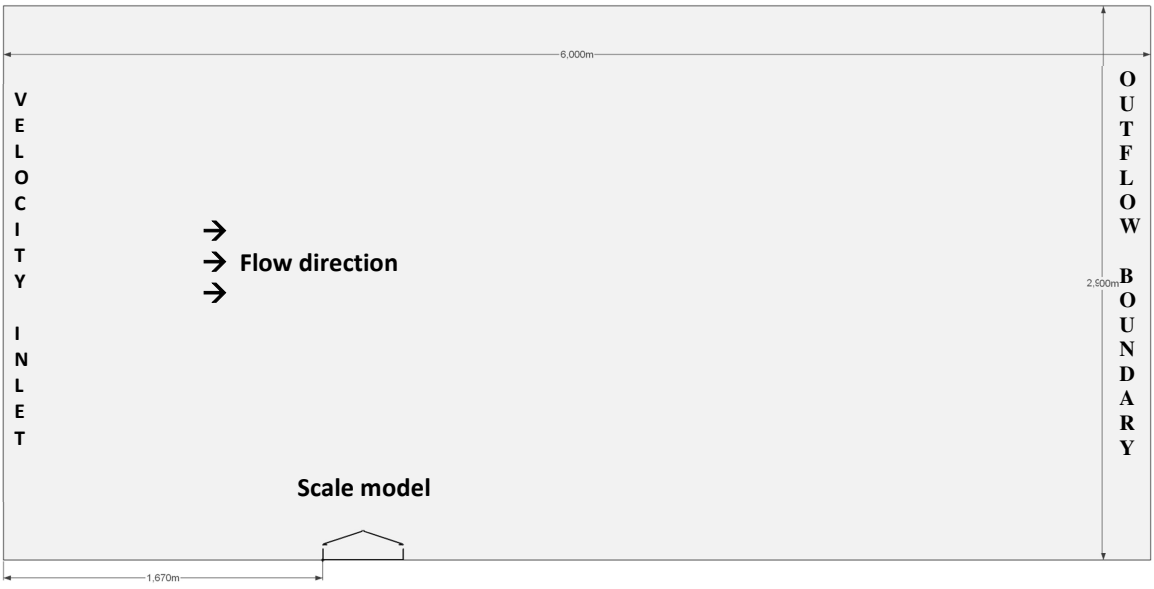

Figure 4 – Computational domain, i.e. the second half of a wind tunnel's test section (6 m x 2.9 m), with a scale model positioned at 1.67 m from the velocity inlet boundary.

The barn geometry is a 1:60 scale model of a typical Belgian barn (Figure 3), featuring two side openings with variable height and a 0.5 cm wide ridge opening. The six scale model (SM) designs were: ('SM1') standard barn with equal inlet and outlet openings 1.8 cm in height; ('SM2') standard barn but with closed ridge opening; ('SM3') standard barn but with closed outlet opening; ('SM4') low-front barn, with a 2-cm high front wall and 5.6 cm inlet opening height; ('SM5') open-front barn, i.e. without front wall, thus a 7.6 cm high inlet opening; ('SM6') open housing type barn, i.e. without front or back wall. The SM2 and SM3 models are not really applicable for livestock farming, but were taken into account in order to test the power of the CFD model.

Each CFD case featured one of the six scale model designs. The meshes contained approx. 140 000 triangular cells. More details are given in Figure 5. The boundaries and respective conditions are described hereafter (see 'Experimental validation'). Computations were carried out for isothermal conditions and with double precision. A steady-state calculation using the pressure-based solver and standard k-ω turbulence model was chosen. Lewis et al. (2004) define steady state problems as "problems that are independent of time, and a solution to such problems can be obtained using either the steady Navier-Stokes equations, along with an appropriate implicit fluid dynamics solver (Taylor & Hughes, 1981), or the unsteady state Navier-Stokes equations and the appropriate time-stepping (or time-marching) procedure (e.g., Donea & Huerta, 2003)". The advantage of the used steady state technique is its relatively fast calculation time. A limitation is the focus on averages, e.g. average air velocities, whereas peak values or fluctuations are not accounted for. Nevertheless, a good insight into the average behaviour of flow phenomena is still very worthwhile, since these generally suffice towards ventilation control strategies.

Convergence of the solutions was assumed at residuals between 10^{-3} and 10^{-6} (iterative convergence criteria). Post-processing of the CFD solution included the visualisation of air velocity contours and vectors. Inspection of these vectors enabled the distinct characterisation of flow paths in each of the six scale model designs.

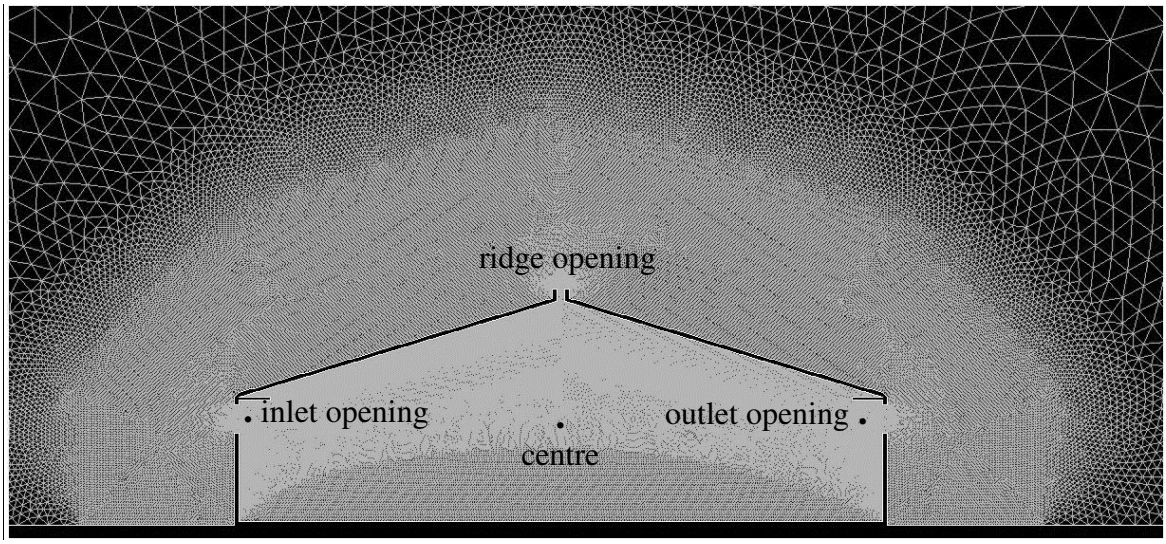

Figure 5 – Detail of the 2D computational mesh in and around a model barn (design 'SM1'). A virtual 'dome' surrounded the barn, in which the cell dimension was 0.1 cm. Outside the dome, the cell dimensions gradually rose to 1.0 cm. The three black dots (indoors) indicate the positions of air velocity readings.

4.2.4. EXPERIMENTAL VERIFICATION

CFD tools presents the user with an abundance of options for solving the mathematical basis, e.g., different turbulence models and iteration methods. However, even when the correct mathematical terms are accurately solved, the model scan sometimes still differ from reality. Some possible causes are solving laminar flow equations for turbulent flow conditions, neglecting the buoyancy force (stack effect), a much too simplified representation of the domain, or subdividing the domain into too few cells (a coarse mesh). Norton et al. (2007) found CFD apt for use in agricultural situations, but in order to avoid the above problems, it is necessary to perform verification or validation experiments, to make sure the proper mathematical background is being used and the parameters are predicted as accurately as possible. Verification of the CFD simulations can be done by comparing with various types of measurements, e.g. anemometry, thermometry and gas concentration monitoring. The CFD model can also be used to predict indoor air quality and the gaseous emission towards the environment. For instance, Venkatram et al. (2003), Bjerg et al. (2004) and Sun et al. (2004) have found good agreement between their CFD model results and real-life emission measurements.

In this study, the developed CFD model is compared with experimental air velocity measurements performed using six cattle barn scale models (Figure 2) in the Ghent University I.C.E. wind tunnel, featuring a 12.00 m long, 1.20 m wide and 2.90 m high work section. The experiments were performed under isothermal conditions and a constant, developed airflow. The airflow is always fully turbulent in this setup, with a Reynolds number *Re* of approximately 419 000. An airflow of 3.5 m s^{-1} impacted on each of the six scale model designs, perpendicular to the lateral ventilation openings (as in the computational domain shown in Figure 4). The hydraulic diameter of the wind tunnel was determined at 2.0 m, while the turbulence intensity was 3%, according to the equation $I = 0.16 \times Re^{-0.125}$.

Three calibrated hot-wire anemometers (type 8465, TSI Inc., Shoreview, MN, USA) were placed in the scale model. The measurement positions were at the centre of each inlet and outlet opening (see Figure 4), as well as centrally indoors. This yielded 18 data points, three for each scale model design. All measurements took place simultaneously and at a height of 6 cm, in line with the standard ventilation openings. The measurement frequency was 1 Hz. Velocity values were averaged over 120 s. The procedure of the wind tunnel experiments was further detailed in Chapter 2. The developed CFD model will be quantitatively assessed by comparing the computed air velocities with the average air velocities ± 2 standard deviations (SD) measured at the same positions during the experimental study in Chapter 2. The literature states that if the difference between computed and experimental values looks sufficiently small, the CFD model is considered to be validated (Versteeg & Malalasekera, 2007).

4.3. Results and discussion

The CFD simulations clearly showed that ventilation opening height and configuration affects the indoor air velocities. For instance, larger inlet openings led to lower air velocities near the inlet, but higher velocities at the outlet. Table 1 presents the CFD results, as well as the average air velocity values measured during the wind tunnel experiments (Chapter 2), plus and minus two standard deviations (SD), which was considered the evaluation criterion for the CFD model (Section 4.2.4.). In eleven of the eighteen cases the computed (or numerical) values were within the range of the experimentally determined air velocity ± 2 SD. In six cases the CFD model returned lower air velocities. The largest deviations were observed at

the lowest measured air velocities (< 0.6 m s^{-1}), resulting in relative differences of 50% when compared with the experimental avg. - 2SD. In one case, i.e. SM2 outlet, the computed air velocity was 10% higher than the experimental avg. + 2SD. These differences could not be attributed to any specific scale-model design, since they were found amongst five of the six scale models. Sørensen & Nielsen (2003) supposed that a two-dimensional CFD approach may be sufficient in the case of a full-width opening in a ventilated room, as was the case here. Still, the deviations observed in this study are probably due to the limitations of a 2D treatment of the flow. A 3D model could capture the flow more qualitatively, including possible lateral movements of flow vortices.

Table 1 – Air velocity magnitudes (in m s^{-1}) obtained through the 2D CFD models (i.e., numerical) as well as experimental values.

Scale model	Measurement Position	Numerical air velocity (m s^{-1})	Experimental air velocity (m s^{-1}), avg. ± 2 SD.
SM1	inlet	3.4	3.7 ± 0.4
	indoors	0.5	0.7 ± 0.2
	outlet	1.9	1.5 ± 0.4
SM2	inlet	3.2	3.0 ± 0.4
	indoors	0.2	0.6 ± 0.2
	outlet	2.1	1.5 ± 0.4
SM3	inlet	1.3	1.3 ± 0.4
	indoors	0.1	0.4 ± 0.2
	outlet	0.1	0.2 ± 0.2
SM4	inlet	1.5	2.0 ± 0.6
	indoors	0.2	0.6 ± 0.2
	outlet	2.6	2.5 ± 0.4
SM5	inlet	1.7	2.3 ± 0.8
	indoors	0.9	0.7 ± 0.2
	outlet	2.1	2.7 ± 0.4
SM6	inlet	2.7	3.5 ± 0.4
	indoors	1.8	2.5 ± 0.2
	outlet	3.3	3.2 ± 0.4

Figure 6 shows the major flow paths which could be identified visually in the CFD results. Each ventilation configuration gave rise to noticeably different airflow patterns; e.g., closing the ridge opening (as in SM2), led to a ceiling-attached jet flow with a backflow at lower heights. A closed outlet (SM3) induced strong recirculation and forced all air through the ridge opening. Larger inlet openings (SM4-5) also resulted in ceiling-attached flows. Finally, the open-type barn SM6 posed little wind obstruction, hence mainly cross-ventilation occurred. From these findings it can be concluded that in real-life situations, indoor ventilation should always be carefully assessed in order not to jeopardize indoor air quality and the animals' and worker's health.

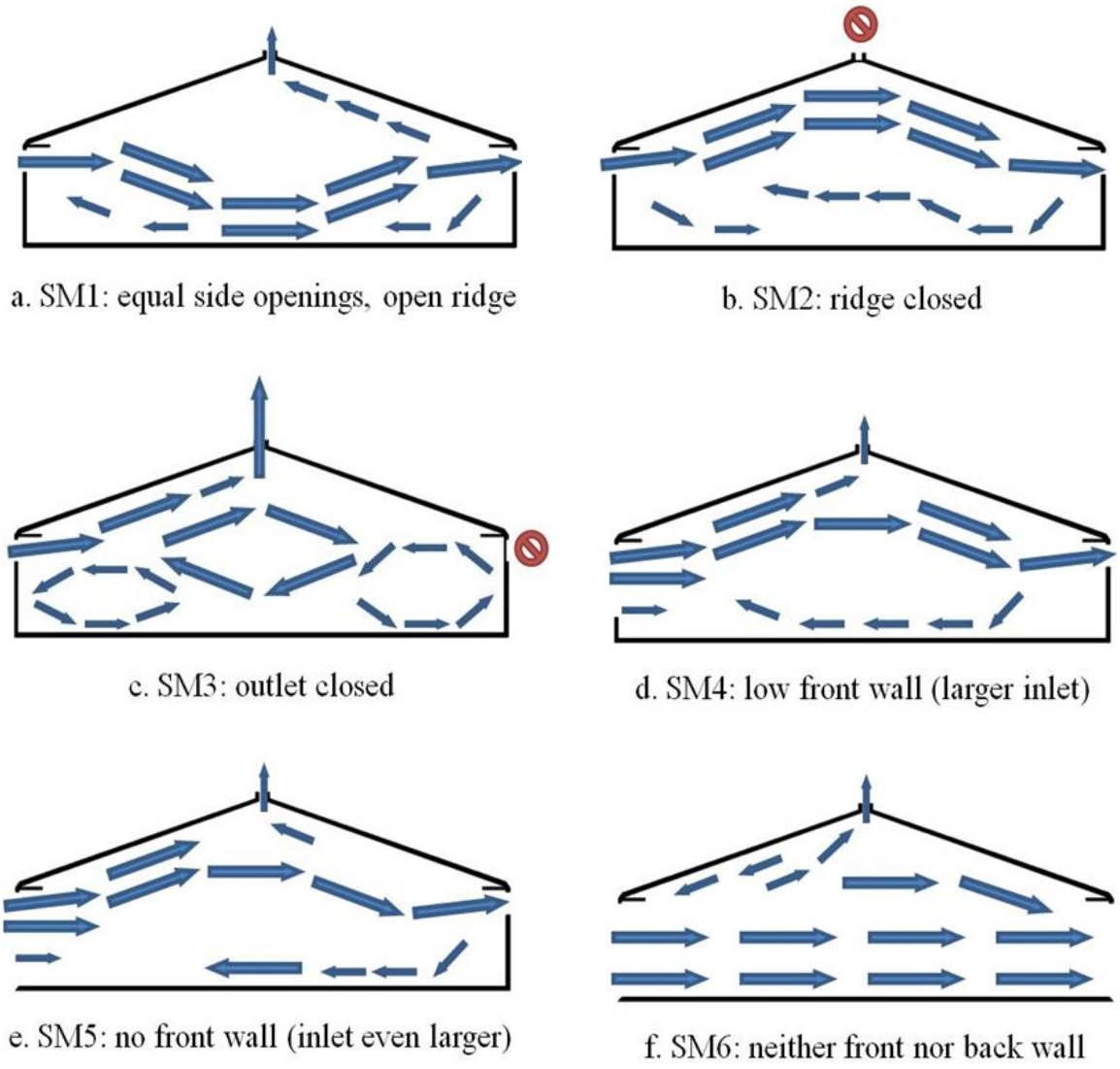

Figure 6 – Main airflow paths as visually observed in the two-dimensional CFD models of the six scaled cattle barn designs. The larger vectors indicate the paths with (relatively) higher velocities, while the small vectors show secondary, lower-speed motions.

4.4. Conclusions and implications

In this chapter the possibility to adequately describe the airflow patterns in six scale-model barn designs was investigated. To this end, a 2D CFD model was developed. Comparison with experimental air velocity data from the wind tunnel study (Chapter 2) generally led to good agreement, although there is still room for improvement in the model, especially at positions featuring low air velocities (< 0.6 m s^{-1}).

The CFD model showed that larger ventilation openings gave rise to lower air velocities near the inlet opening, but higher velocities at the outlet, which was also observed in the experimental study of Chapter 2. The model also revealed the main airflow paths, showing mainly ceiling-attached airflows in the cross-ventilation barn designs, except for the open-type barn where a straight flow between the inlet and outlet dominated.

The main advantage of the computational approach was the airflow visualisation for each of the six ventilation opening configurations. Eventually, this information supported with other CFD models may assist in improving barn design and airflow guidance techniques. It can be seen more and more that CFD is becoming a technology that partly or completely replaces experiments. It is however recommended to maintain a firm interaction between both. For instance, where experiments can at some points be difficult to interpret, a complementary CFD model will often help to clarify them. Ultimately, this may allow the research to move much faster towards a practical solution.

RESULTS

PART II: NH_3 mass transfer studies at slurry pit level

In the Introduction chapter, it also became clear that there is a need for more research regarding the complex mechanisms of emissions from animal houses, as well as mitigation options. Besides soiled floors as major source of NH_3 emissions, the slurry pit should not be underestimated and thus deserves more attention. However, performing reliable measurements in commercial barns requires an intense work load, significant costs and time, especially in confined spaces such as slurry pits and during the presence of animals. Therefore, the idea arose to develop a real-scale emission set-up, yet under controlled and reproducible laboratory conditions. This set-up should allow an easy measurement of the NH_3 emission and the calculation of NH_3 mass transfer coefficients under various circumstances.

Three chapters have been dedicated to this particular research path.

Chapter 5 describes the development of such a suitable set-up, that can serve as a useful platform to study NH_3 mass transfer between the pit and the room space. We will also demonstrate its ability to provide a stable NH_3 release, using a circulated ammonium source solution in combination with an automated pH control system.

In **Chapter 6**, the next step is to use this set-up in order to effectively investigate a number of interesting key factors in the NH_3 emission process originating from the slurry pit, i.e. the pit headspace height (or inversely, the manure height towards the slatted floor), the air velocity and the airflow direction at floor level. In this way, the degree of their impact on the emission can be quantified.

Finally, in **Chapter 7**, a selection of the previous experimental cases will be modelled using CFD, to acquire a more detailed understanding and to pave the way for further modelling studies.

The combined findings of Part II ultimately aim to contribute to the continuing efforts that are made to find useful emission mitigation techniques for animal houses.

CHAPTER 5. DEVELOPMENT OF AN EXPERIMENTAL SLURRY PIT SET-UP FOR THE STUDY OF NH_3 (EMISSION LAB, 'EMIL')

5.1. Introduction

In 2004 a preliminary test facility was built at ILVO, in order to investigate the transmission of NH_3 from animal manure through a slatted floor. Another objective at that time was to relate the emission with the manure height (or inversely, the headspace height in the slurry pit). Similar to Elzing & Montey (1997), who had worked with real manure and urine in a slurry pit set-up, liquid cow manure was used during this 2004 study. But, due to the low NH_3 concentrations emitted from this manure, no definitive conclusions could be formulated. Also of importance is the tendency of real manure to emit varying amounts of NH_3, in both space (throughout the soiled surface) and time (fresh versus older manure, effects of fluctuating airflows, pH, temperature, etc.). It would thus be very valuable to use a controlled source solution that is able to release NH_3 concentrations that are both steady and measurable. This way, other parameter effects can be revealed, such as the pit's design.

In the scale-model studies mentioned in Chapter 1 (e.g., Morsing et al., 2008) such an ammonium solution was used, but it was already fully mixed with the buffer solution since the start of the experiment and no special precautions were taken to compensate for any decreasing pH levels (which influence the emission rate). A better approach would thus be to build an automatic buffer dosage system that allows the addition of buffer solution whenever the pH drops below a certain threshold.

Therefore, in this chapter the objective is to develop a suitable test installation that satisfies the above mentioned needs to study NH_3 transfer processes in a large-scale section of a slurry pit. The degree to which stability of parameters such as pH, solution temperature and NH_3 concentration is attained during a 10-day long experiment will consequently be investigated. Also, the day-to-day variation on the pit transfer coefficient will be determined.

Chapter after manuscript submitted to *Biosystems Engineering*: De Paepe, M., Pieters, J.G., Merci, B., Demeyer, P. (2014). Real-scale test installation for the study of ammonia transfer processes at slurry pit level.

5.2. Materials and methods

The test installation was built in a large (approx. 4400 m³) frost-free workshop. It consists of a large-scale slurry pit section with a concrete slatted floor and covered with a wind tunnel system. The test installation is fully equipped to conduct and monitor controlled NH_3 emission experiments. All components are discussed in detail below. The test installation will be further referred to as the 'Emission Lab' or, in short, 'EmiL'.

5.2.1. SLURRY PIT AND WIND TUNNEL SET-UP

The geometry used in this study is a section of a slurry pit (Figures 1–3) with dimensions L 2.66 m × W 1.00 m × H 1.38 m. The slurry pit is covered by a typical concrete slatted floor for cows, with dimensions L 2.99 m × W 1.00 m × H 0.18 m, with 30 slits of length 0.49 m and width 0.04 m, resulting in an opening ratio of 20%.

The pit and floor combination is covered by an 8.00-m long wind tunnel (W 1.15 m × H 0.50 m), which consists of a steel frame, Plexiglas windows and a concrete-form-plywood floor, except for the slatted floor. The wind tunnel is placed symmetrically so the inlet is located at 2.50 m before the slatted floor, and the outlet at 2.50 m behind the floor.

A type IF35 suction fan (Fancom BV, Panningen, The Netherlands) was placed at the outlet of the wind tunnel. The inlet of the wind tunnel draws steady indoor air. The airflow rate could be set between 0 – 1350 $m^3\ h^{-1}$. Given the wind tunnel cross sectional area of 0.575 m², this results in possible air velocities above the slatted floor between 0 – 0.65 $m\ s^{-1}$.

The pit contains a custom built stainless steel container (L 2.65 m × W 1.00 m × H 0.19 m) mounted on a scissor lift table. This allows setting different pit headspace heights (*HH*) ranging from 10 to 90 cm. The free surface area, *A*, of this container is 2.40 m². To ensure air tightness around the container, an inflatable tube has been installed along its edges, closing all gaps near the pit walls.

Figure 1 shows a side view of the set-up, with the front panel removed. Figures 2–3 show a cross section and a top view, respectively.

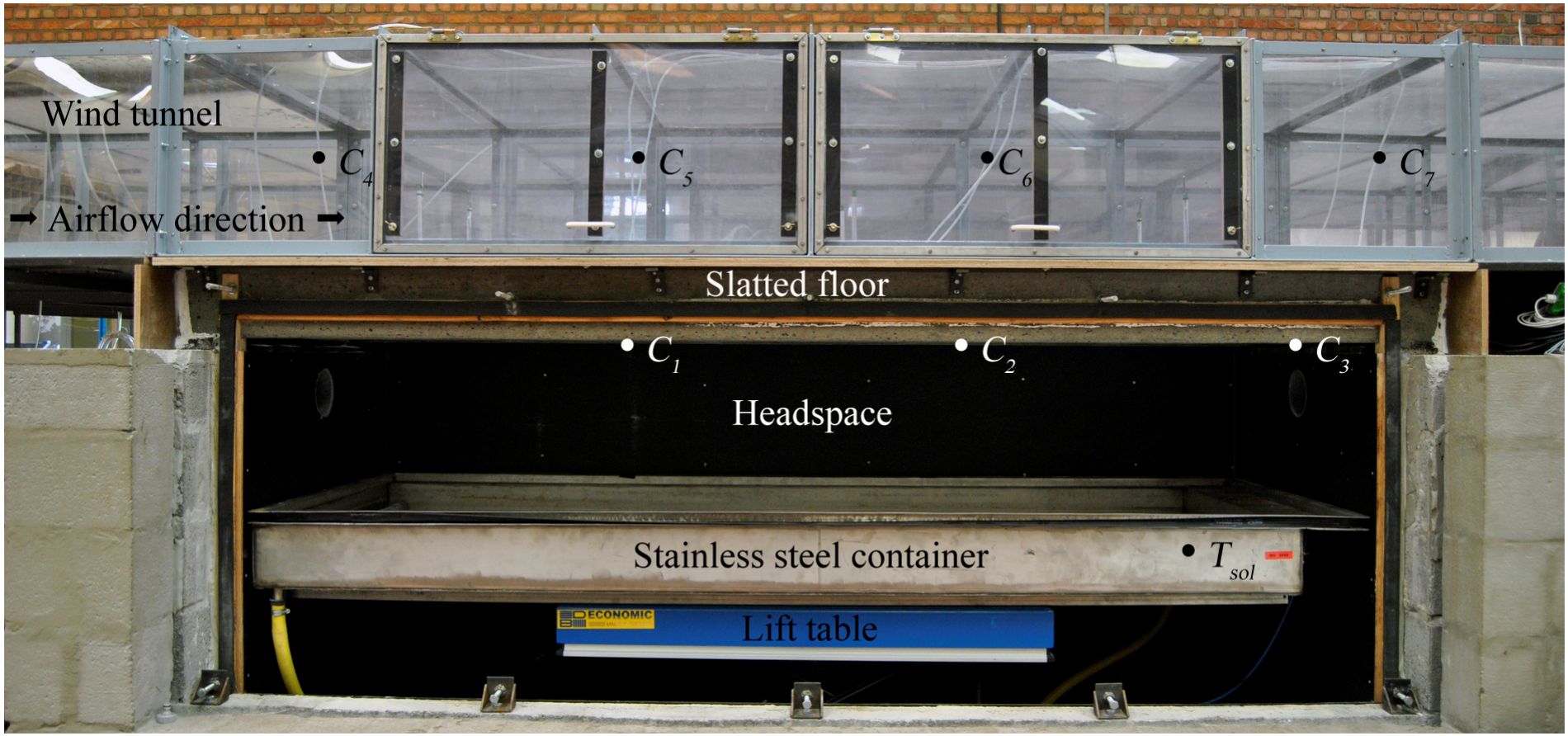

Figure 1 – Side view of the experimental slurry pit section covered by the wind tunnel (full length not shown). Inside is the stainless steel container on the scissor lift table. Denoted are the solution temperature (T_{sol}) and gas sampling positions $C_{1\text{-}7}$.

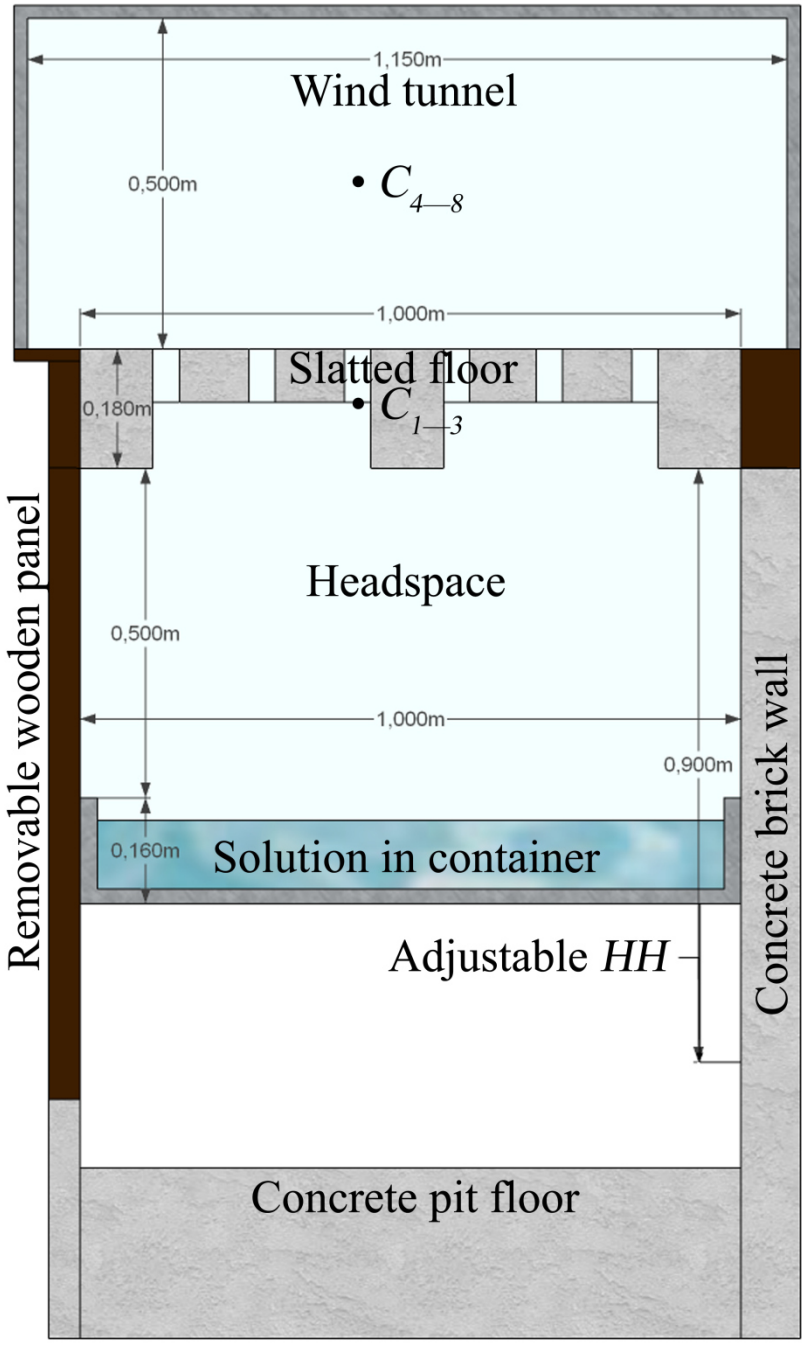

Figure 2 – Cross section of the set-up, showing the adjustable headspace height (*HH*) and the current setting at 0.50 m. The lift table has been omitted from the sketch.

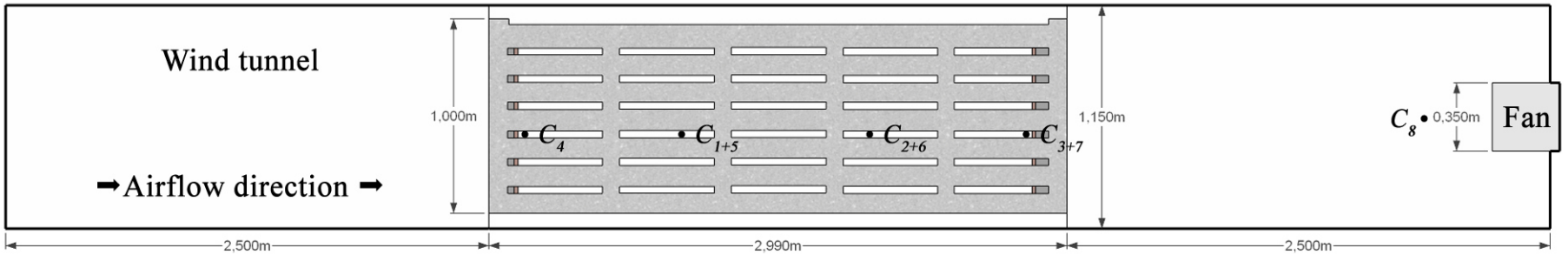

Figure 3 – Top view of the whole wind tunnel, with the slatted floor in the middle and the fan at the end.

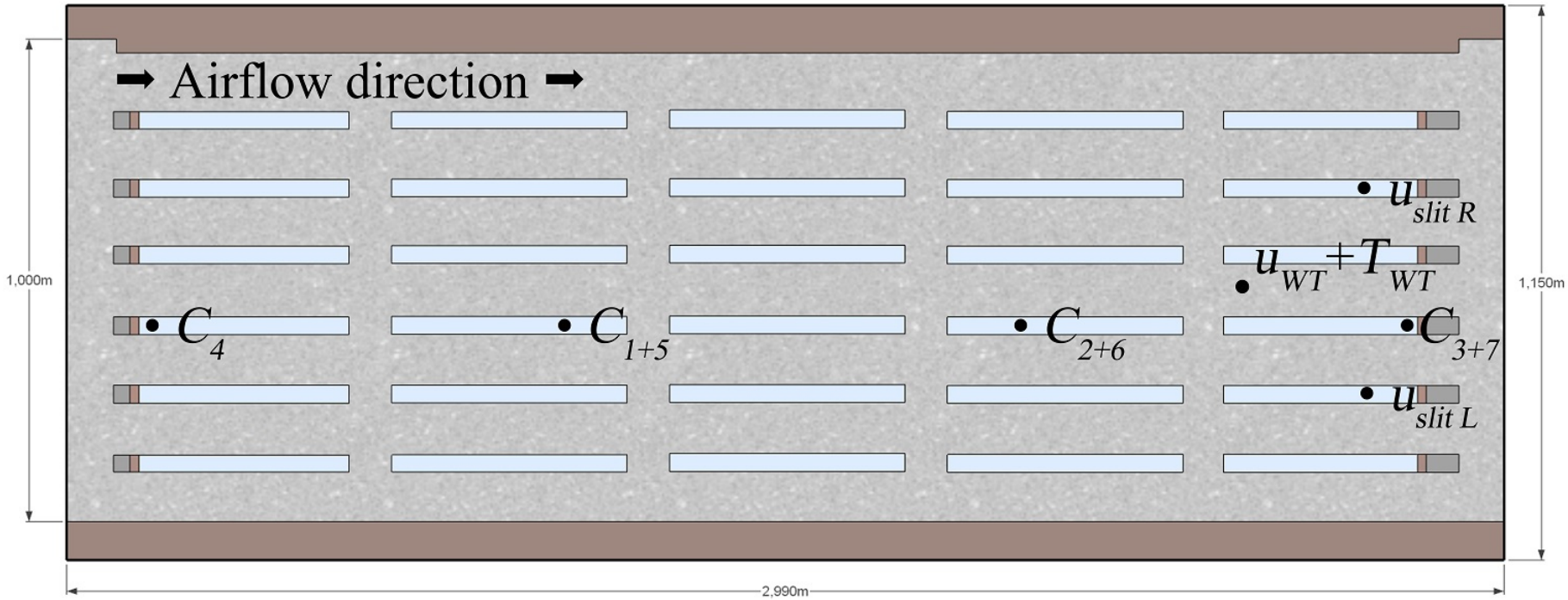

Figure 4 – Top view of the concrete slatted floor with the positions of anemometers (*u*), thermistors (*T*) and gas sampling positions (C_{1-7}). Position C_8 lies 1.75 m leeward of C_7, i.e. at the end of the wind tunnel in front of the suction fan.

5.2.2. AMMONIA SOURCE AND RELEASE CONTROL SET-UP

To study NH_3 transfer processes at slurry pit level, it is important to have an NH_3 source which is uniform over the total slurry pit surface and also generates a constant emission over the testing period.

As source a standardized NH_4^+-solution was used, since real manure generally portrays large variations in pH and ammonium concentration. Furthermore, actual cattle manure was found to emit too little NH_3 to be able to measure in this set-up. The stainless steel container in the pit was filled with 225 L of a standard 100 g L^{-1} ammonium chloride (NH_4Cl) solution, prepared by dissolving NH_4Cl in tap water. Thus, the total ammoniacal nitrogen (TAN) concentration was 33.7 g L^{-1} and although this was high, it was chosen to ensure measurable NH_3 concentrations throughout the whole set-up. As Snoek et al. (2012) found for urine puddles in dairy barns, the initial nitrogen concentration strongly contributes to the NH_3 emission, but the largest effect is still reserved for the pH of the solution.

A custom built pumping system provided a constant circulation of the NH_4Cl solution from and to the container, at a rate of approx. 0.5 L/s. This circulation allowed a constant pH monitoring and also the possibility to adjust the pH by injecting a buffer solution. Also, the pumping generated turbulence and maximized the homogeneity of the NH_4Cl solution throughout the container volume, and the uniformity of the emission surface. An ink stain test confirmed this, as did readings of the pH at several positions in the container (data not shown).

While a broad range of alkaline pH levels can be obtained in this set-up, during this experiment the pH was to be kept at a constant value of 8.0. This pH is a typical average value in cow urine (e.g., Monteny et al., 2002) and at this pH, the NH_4^+/NH_3 balance lies at approximately 5% NH_3 (Court et al., 1964), which is sufficient to produce a steady and measurable NH_3 release. To accomplish this, a buffer solution was prepared with equal amounts of Na_2CO_3 and $NaHCO_3$, i.e. 6.9 kg, in a total volume of 75 L, which led to a buffer solution concentration of 184 g L^{-1}. This buffer solution was stored in a separate container. The pH of the NH_4Cl solution was monitored using a type HI 1006-32 electrode (Hanna Instruments) fitted in the circulation system and was recorded on a Squirrel type 2040 data logger (Grant Instruments, Cambridge, UK).

When the pH of the NH_4-solution dropped below a threshold value, in this case pH 8.0, a valve controlled by a pH controller (type pH 500, Hanna Instruments, Temse, Belgium) dosed

buffer solution into the circulatory system in order to keep the pH constant. The temperature of the NH_4Cl solution was measured with a resistance temperature detector (RTD) (Jumo GmbH & Co. KG, Fulda, Germany) and was logged at 1-minute intervals.

The duration of the current experiment was 10 days. During the course of the experiment, NH_3 evaporated from the NH_4Cl solution, but enough NH_3 was available for prolonged evaporation and a minimal reduction of concentration in the source solution. The latter was observed through daily sampling of the NH_4^+-N concentration (data not shown).

5.2.3. EXPERIMENTAL CONDITIONS

The purpose of the performed experiment was to determine the stability of performance of EmiL, i.e., the ability to maintain a constant solution pH, as well as reproducible NH_3 emissions.

The characteristics of the ammonium solution were described in Section 5.2.2. Furthermore, during this experiment, the headspace height (*HH*) in the pit was set at an intermediate height, i.e. 0.50 m, and the airflow rate (*AR*) at 945 m^3 h^{-1}. Here, this resulted in an air velocity of 0.46 m s^{-1} above the slatted floor. In this case the Reynolds number (*Re*) was 30 000, using a hydraulic diameter of 1.07 m for the wind tunnel. Indoor air from the workshop was drawn into the wind tunnel. This led to a typical daily variation in air temperature.

5.2.4. MONITORING OF AMMONIA CONCENTRATIONS, AIR VELOCITIES, AND AIR TEMPERATURES

NH_3 concentrations were monitored at eight positions: three at the bottom of the floor slits, at 1.0-meter intervals (C_1 to C_3), four at mid-height of the wind tunnel, again at 1.0-meter intervals (C_4 to C_7) and one at the wind tunnel outlet, just in front of the suction fan (C_8) (see Figure 3). Per position three 80-s measurement cycles were carried out by an Innova photoacoustic multi-gas monitor (model 1314, AirTech Instruments, Ballerup, Denmark) connected to an 8-channel sampler (CBISS Intelligent Sampling System MK2, Denmark). All sample tubes were made from Teflon and 8-m long. To prevent sample crossover, the multi-gas monitor provided cleansing of the tubes and the internal measurement chamber. The first two cycles were introduced for stabilisation purposes, and only the third cycle was used for measurement purposes. Consequently, one concentration value was retained per

measurement position approx. every 30 minutes. These data were recorded on a PC through a Telnet interface.

Air velocities and temperatures were also monitored throughout the setup (see Figure 4). One unidirectional hot-film anemometer of type EE66 (E+E Elektronic, Engerwitsdorf, Germany) and one type U thermistor (Grant Instruments, Cambridge, UK) were positioned in the wind tunnel on top of the slatted floor, and two more anemometers in the most leeward floor slits, in a position able to capture the vertical flows.

NH_3 concentrations, air velocities and temperatures were always recorded during the same 3-hour interval every day (6–9 a.m.), for a period of 10 days. The start of the experiment was marked "Day 0" and was considered as a stabilisation phase for the system. Days 5 and 6 were week-end days, where no measurements were performed. Table 1 summarises the measured parameters, measuring intervals, numbers of samples during each 3-hour interval and their precision.

Table 1 – The measured parameters, measuring interval, number of samples per interval, and measuring precision.

Parameter	Measuring interval	N° of samples/interval	Precision
pH	10 s	1080	0.01
u_{WT}	60 s	180	0.01 m s^{-1}
$u_{slit\ L\ \&\ R}$	60 s	180	0.01 m s^{-1}
T_{WT}	600 s	18	0.01 °C
T_{sol}	60 s	180	0.1 °C
$C_{1\text{-}8}$ = [NH_3]	approx. 80 s between each of the 8 positions	6 for each of the 8 positions	0.1 mg m^{-3}

5.2.5 CALCULATIONS

NH_3 emission rate

The wind tunnel outlet concentration ($C_{out} = C_8$) was used to calculate the NH_3 emission rate, through multiplication with the airflow rate, Q, as:

$$E = Q \times (C_{out} - C_{in}) \quad (1)$$

assuming the concentrations are homogenous over the respective in- and outlet surfaces.

C_{out} is the NH_3 concentration measured at the outlet of the wind tunnel. The concentration at the inlet of the wind tunnel, C_{in}, can be set to zero.

Pit transfer coefficient (PTC) for NH_3

In the literature, the NH_3 mass transfer coefficient (*AMTC* or k_c, m s^{-1}) is often used to describe the NH_3 release rate from manure or an ammonium solution (e.g., Arogo et al, 1999; Ye et al., 2008). The *AMTC* is known to be a function of manure temperature, air temperature, wind velocity, and relative humidity (Ad Hoc Committee on Air Emissions from Animal Feeding Operations, Committee on Animal Nutrition, National Research Council, 2003). Generally, the *AMTC* equation takes the form of a constant that relates the emission rate, emitting surface area, and (as the driving force) the concentration difference, as shown by Ye et al. (2008a):

$$AMTC = \frac{E}{A_S \times (C_S - C_a)}, \text{ in m s}^{-1} \quad (2)$$

where E is the emission rate, mg s^{-1}; A_s is the solution surface area of 2.40 m^2; C_s is the equilibrium NH_3 concentration at the immediate solution surface, mg m^{-3}; C_a is the bulk air concentration in the wind tunnel.

In order to quantify the mass transfer rate from the solution surface in EmiL, the *PTC* is proposed. The difference with the general *AMTC* equation is that the bulk air concentration in the wind tunnel (C_a) is neglected. This is justified because of its low value compared to the high concentration at the solution surface (C_s). The pit transfer coefficient averaged over the entire set-up can then be determined as:

$$PTC = \frac{E}{A_S \times C_S}, \text{ in m s}^{-1} \quad (3)$$

The surface concentration, C_s, is calculated using Henry's constant, K_H, the dissociation constant, K_D, the TAN concentration and the pH value (as described by Saha et al., 2010, p. 331).

$$K_H = 10^{-1.69 + (1477.7/T)} \quad (4)$$

$$K_D = 10^{-(0.0897 + 2729/T} \quad (5)$$

For TAN = 33.7 g L^{-1}, pH 8 and T = 16°C, this would result in a C_s value of 359 mg m^{-3}. Variations in solution temperature and pH have a direct effect upon the calculation of the dissociation coefficient, K_D, and Henry's constant, K_H. Therefore, the calculation of C_s and

PTC has always been adapted to the average values of the solution temperature and pH as measured during each interval.

5.3. Results and discussion

5.3.1. SOLUTION pH AND TEMPERATURE MONITORING

The desired pH of 8.0 was reached within an hour after starting the experiment. Figure 5 shows the pH of the ammonium solution, beginning from the start-up of the experiments until 13 hours later (the morning of day 1). It is clear that the time between consecutive buffer dose intakes (indicated by arrows in Figure 5) increased, implying the solution was gradually buffered towards pH 8.0. Figure 5 also shows the importance of having a period of time in which the NH_3 source set-up is allowed to stabilize. Beyond the period shown in Figure 5 no additional buffer was taken during the immediately following 3-hour interval presented in Figure 6, where the solution pH is given for the measuring interval at day 1. That day the pH range was already predominantly limited to 8.00–8.02, as intended. The solution temperature during each day is given in Table 2. Both the pH and temperature measurements showed limited variation, as indicated by the standard deviations over the period of days 1–10.

Table 2 – Measured parameters, averaged for the experimental days. Notation: average ± SD.

Parameter	Day 1	Day 2	Day 3	Day 4	Day 7	Day 8	Day 9	Day 10
pH	8.01 ± 0.02	8.00 ± 0.02	8.01 ± 0.01	8.01 ± 0.01	8.09 ± 0.01	8.00 ± 0.00	8.00 ± 0.01	8.01 ± 0.01
T_{sol} (°C)	16.1 ± 0.1	16.1 ± 0.1	16.2 ± 0.1	17.0 ± 0.1	16.9 ± 0.1	16.8 ± 0.1	17.0 ± 0.1	17.0 ± 0.1
T_{WT} (°C)	18.0 ± 1.1	17.3 ± 1.3	17.0 ± 1.3	18.3 ± 1.1	16.8 ± 1.3	16.5 ± 1.2	16.0 ± 0.3	16.1 ± 0.6
u_{WT} (m s^{-1})	0.47 ± 0.02	0.47 ± 0.02	0.47 ± 0.02	0.48 ± 0.03	0.44 ± 0.01	0.46 ± 0.03	0.47 ± 0.02	0.47 ± 0.01

However, during day 7 a relatively high pH value of 8.09 (SD: 0.01) was reached (see Table 2), probably due to the long-lasting effect of an erroneous excessive intake of buffer solution, or rather badly dissolved constituents. This did allow to see the effect on the measured NH_3 concentrations and the *PTC*, as discussed in sections 5.3.3 and 5.3.4, respectively. Also, the automatic control system ensured that the pH later returned to the desired value, as can be seen from day 8 onward.

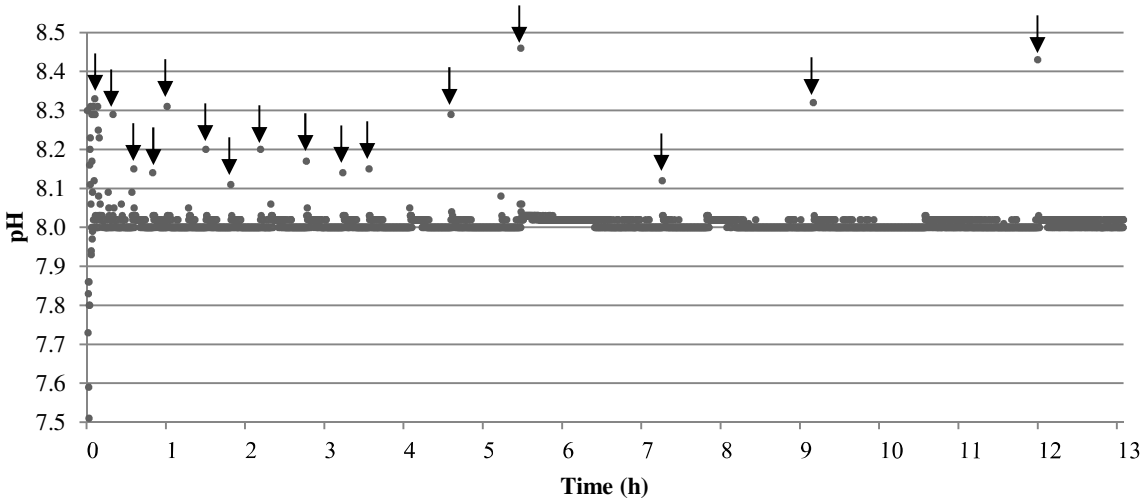

Figure 5 – Solution pH from the start-up of the experiment until 13 hours later (morning of day 1). The peaks above 8.1, indicated by arrows, denote dosage events of buffer solution.

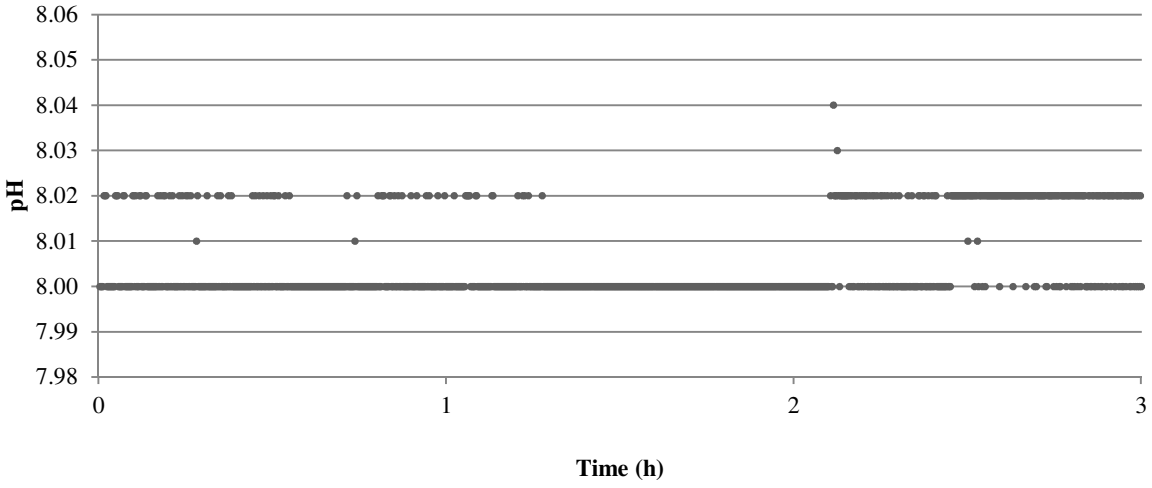

Figure 6 – Solution pH during the 3-hour measuring interval at day 1.

5.3.2. WIND TUNNEL AIR VELOCITY AND TEMPERATURE

The airflow rate of 945 m^3 h^{-1} theoretically resulted in an air velocity of 0.46 m s^{-1} above the slatted floor. The air velocity measurements, T_{WT}, in Table 2 indeed show average values of approx. 0.46 m s^{-1}. The air velocities measured in the floor slits, i.e., $u_{slit\ L}$ and $u_{slit\ R}$, were always lower than 0.10 m s^{-1}. The temperature in the wind tunnel, T_{WT}, exhibited a larger variation than the solution temperature (see Table 2), owing to the natural variation of the temperature in the workshop.

5.3.3. AMMONIA CONCENTRATIONS AND EMISSION RATES

The NH_3 concentrations measured at eight positions in the set-up are shown in Figure 7, for days 1 and 10. The average NH_3 concentrations during the others days are given in Table 3. The variation of the values is presented as a standard deviation. Relatively stable values were found from day 1 to day 10.

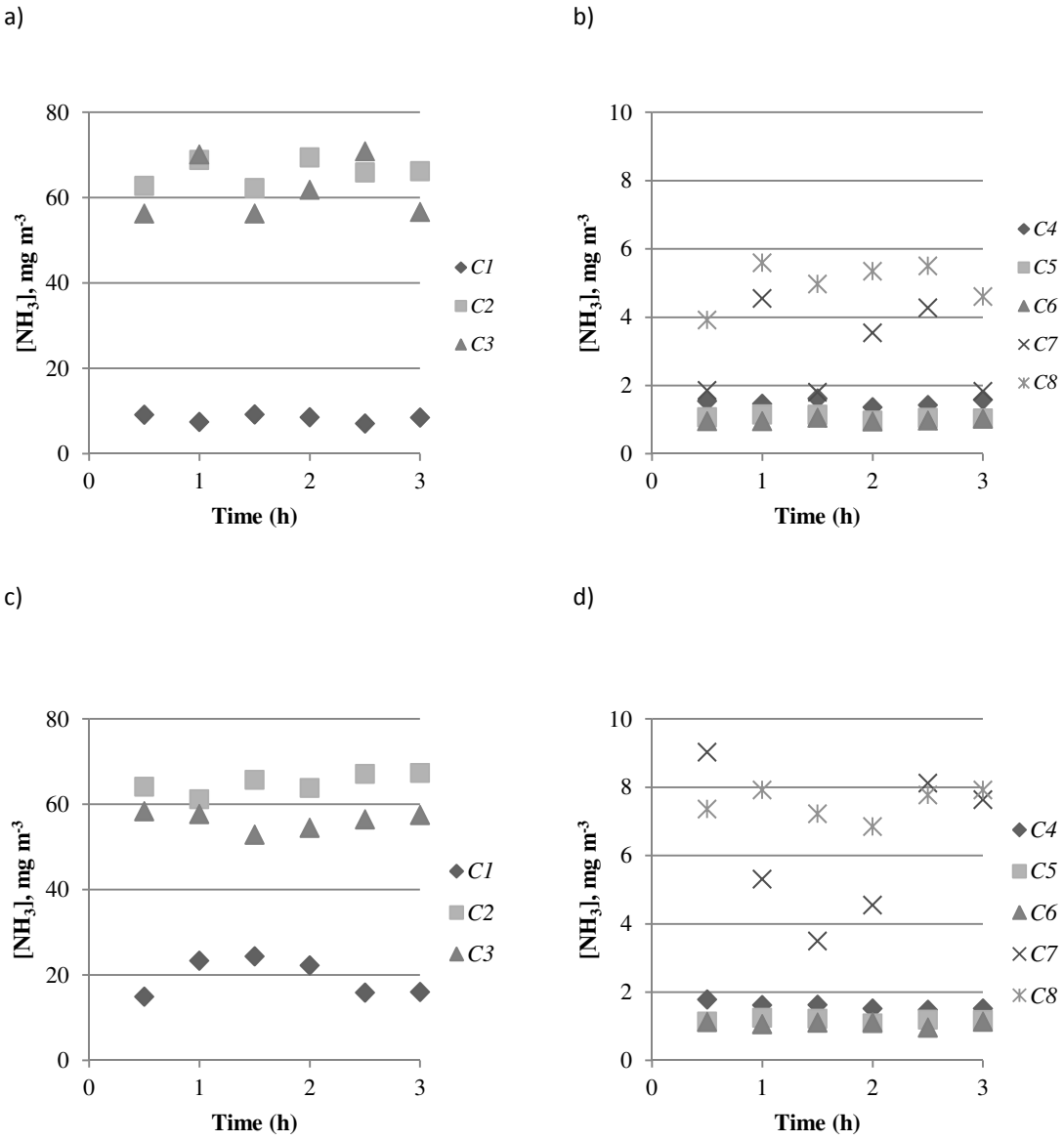

Figure 7 – Examples of raw NH_3 concentration data, in mg m^{-3}, measured at eight locations (C_{1-8}) during day 1 (a-b) and day 10 (c-d).

Table 3 – NH_3 concentrations, in mg m^{-3}, averaged for the week days. Notation: average ± SD.

	Day 1	Day 2	Day 3	Day 4	Day 7*	Day 8	Day 9	Day 10
C_1	8 ± 1	12 ± 2	21 ± 3	20 ± 3	17 ± 6	26 ± 6	19 ± 5	19 ± 4
C_2	66 ± 3	63 ± 3	65 ± 4	69 ± 3	42 ± 6	60 ± 10	71 ± 5	65 ± 2
C_3	62 ± 7	51 ± 6	58 ± 5	68 ± 5	73 ± 7	44 ± 12	61 ± 3	56 ± 2
C_4	1.5 ± 0.1	1.5 ± 0.1	1.4 ± 0.1	1.5 ± 0.1	2.0 ± 0.1	1.6 ± 0.1	1.7 ± 0.1	1.6 ± 0.1
C_5	1.1 ± 0.1	1.0 ± 0.1	1.1 ± 0.1	1.1 ± 0.1	1.0 ± 0.1	1.1 ± 0.2	1.2 ± 0.1	1.2 ± 0.1
C_6	1.0 ± 0.1	1.0 ± 0.1	1.0 ± 0.1	1.0 ± 0.1	1.0 ± 0.1	1.0 ± 0	1.1 ± 0.1	1.1 ± 0.1
C_7	3.0 ± 1.3	4.4 ± 1.7	5.9 ± 1.9	3.7 ± 1.4	15 ± 5	5.9 ± 1.3	5.6 ± 1.7	6.4 ± 2.2
C_8	5.0 ± 0.6	6.8 ± 0.5	7.2 ± 0.7	6.9 ± 0.9	8.0 ± 1.0	8.2 ± 1.2	7.3 ± 0.5	7.5 ± 0.4

* At the measuring interval during day 7, the average pH was slightly higher (8.09).

Table 3 shows that the highest NH_3 concentrations were found in the floor slits directly above the slurry pit (C_1 to C_3), as the NH_3 source was placed only 0.50 m lower. Concentration C_1 was the lowest, with 18 mg m^{-3} on average. Meanwhile, C_2 and C_3 further along the pit exhibited higher values and very similar in-between, averaging 57 and 65 mg m^{-3}. This indicates that the largest NH_3 mass transfer mainly happened between the positions C_1 and C_2, at the first half of the floor. This also implies that the incoming airflow over the floor slits quickly affected the NH_3 gradient underneath. The concentrations above the slatted floor at C_4 to C_6, were very low. Behind the most leeward floor slits, concentration C_7 again increased to 5 mg m^{-3} on average. At the very end of the wind tunnel, before the air exited through the suction fan, concentration C_8 still averaged at 7 mg m^{-3}. However, a range from 5.0 to 8.2 mg m^{-3} was measured. This variation is possibly due to the accidental changes in the solution pH in combination with the effect of the nearby fan, which can portray a slight variation in the frequency of its rotation, as seen in the measured air velocity (see Table 2).

This outlet concentration can be related to the order of NH_3 concentrations emitted from commercial barns. For example, Herbut & Angrecka (2014) measured year-round indoor NH_3 concentrations from 0 to 8 ppm (0 – 5.6 mg m^{-3}) in a naturally ventilated free-stall dairy barn. This range can of course vary depending on the barn type, ventilation system and management, livestock density, frequency of manure removal, etc.

Using Equation 1, the emission rate, *E*, can be calculated. With an average outlet concentration (C_8) of 7 mg m^{-3} and the constant airflow rate of 945 m^3 h^{-1}, the average emission rate *E* is determined at 6.6 g h^{-1} or 159 g day^{-1}. In practice, NH_3 emission rates for dairy cow cubicle houses are around 20–45 g day^{-1} per cow and for tie stalls 5–27 g day^{-1} per cow (Monteny & Erisman, 1998). Given the relatively small dimensions of EmiL compared to a complete barn, the observed emission rate is higher than would be expected in reality, but in this study a high amount of NH_3 was intended for ease of measurement throughout the complete set-up (see Section 5.2.2.). However, this rate can still be lowered in future studies. At present, EmiL is mainly a platform to provide a stable NH_3 release, which can be used as a standard with which other experimental configurations will be compared (such as in Chapter 6).

5.3.4. PIT TRANSFER COEFFICIENTS

Using Equations 3–5 and the values shown in Tables 2–3, the pit transfer coefficients (*PTCs*) could be calculated. On a daily basis they ranged from 2.1×10^{-3} at the first day to 3.3×10^{-3} m s^{-1}, recorded during day 8 (Figure 8). These values are well within the range of *AMTCs* for laboratory and field experiments of NH_3 release from manure, found in the literature (Ni, 1999).

This exploratory experiment was limited to a single steady-state ventilation and geometrical set-up. Saha et al. (2010) illustrated that the relationship between the mass transfer coefficient and wind characteristics (air velocity and turbulence intensity) is highly device-dependent. Therefore, other values can be expected for different experimental procedures and geometries.

As explained in section 5.2.5, calculating *PTC* automatically considers the effective solution temperature and pH, as well as the daily average for the emission point concentration (C_8 in Table 3). Since the only constants used were the airflow rate, *AR*, and the solution surface area, *A*, the variation witnessed in Figure 8 can mainly be attributed to the varying C_8 values, and to a lesser extent to solution pH and temperature variations. Tables 2–3 indeed show that the minimal and maximal values in Figure 8, respectively on days 1 and 8, can be explained by the respective pH and C_8 values measured during these experiments.

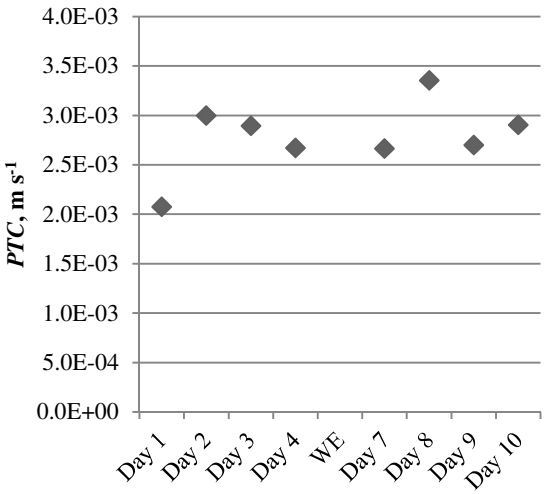

Figure 8 – Calculated pit transfer coefficients (*PTCs*) for NH_3, in m s^{-1}, during the course of the experiment.

Compared to the emission point concentration, solution pH and temperature have a relatively small effect on *PTC* values. When the solution temperature T_{sol} is considered constant, linear relations can be established for the surface concentration C_s and the *PTC*, respectively, as a function of pH alone. Theoretically, a 0.01 increment in pH corresponds in a 5.9 mg m^{-3} rise in C_s and a 1.2×10^{-4} m s^{-1} decrease in *PTC*. Figure 9 shows these effects between pH 8.00–8.10, i.e. the pH range observed during the present experiment, and using a constant T_{sol} of 16.6°C; the average experimental solution temperature. However, as demonstrated in section 5.3.1, with the exception of day 7 the solution pH was maintained between 8.00 and 8.02. Therefore, the expected variation upon C_s and *PTC* during this experiment would be as small as 2%.

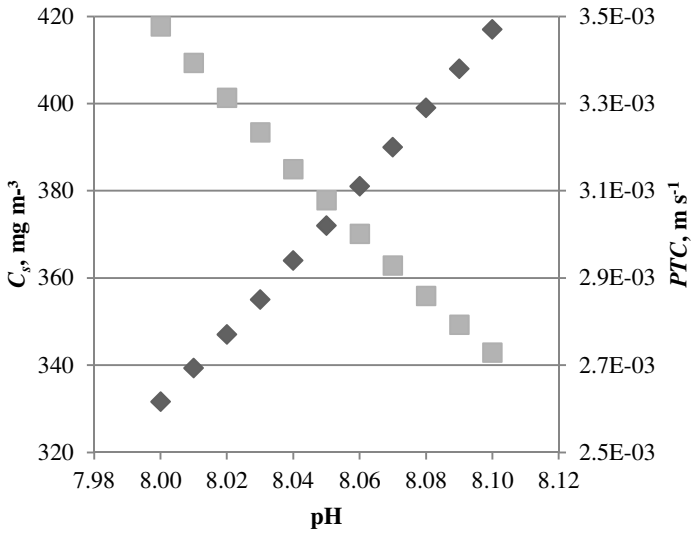

Figure 9 – Theoretical pH dependency of C_s (♦) and PTC (■), for the pH range 8.00–8.10 and T_{sol} = 16.6 °C.

The solution temperature T_{sol} also fluctuated. Likewise, its theoretical effect on the calculation of C_s and *PTC* can be shown. A 0.1°C increase leads to a 4.2 mg m^{-3} increase in C_s, and a 3.9×10^{-5} m s^{-1} decrease in *PTC*. Figure 10 shows this temperature dependency for the range of 16.0–17.0 °C and using a constant pH of 8.00.

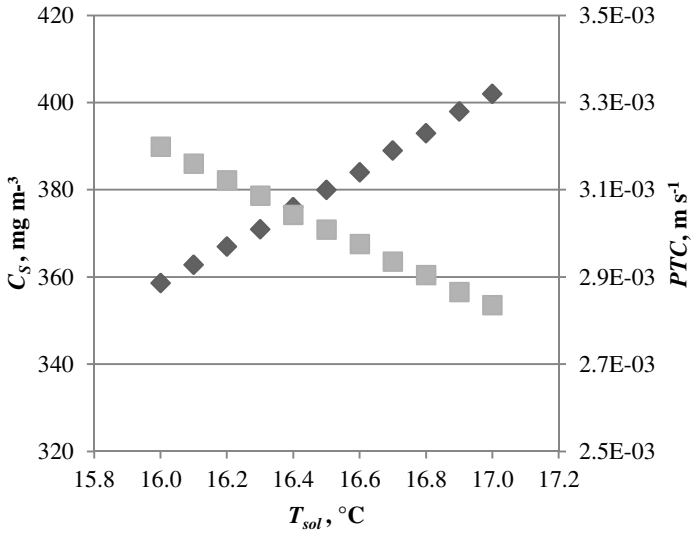

Figure 10 – Theoretical temperature dependency of C_s (♦) and *PTC* (■), for the T_{sol} range 16.0–17.0 °C and pH = 8.00.

In our experiments, however, simultaneous variations of both pH and temperature were observed. The recorded ranges were 8.00–8.09 and 16.1–17.0 °C, respectively. Using Figures 9–10, this would result in theoretical variation coefficients (=SD/average) up to 6.6% for C_s and 7.0% for *PTC*. Our experiment portrayed a coefficient of the same order, i.e. 13.1%, as calculated from the *PTC* values given in Figure 8. This confirms that the test installation EmiL provided an adequate pH and T control of the NH_3 emitting solution.

5.4. Conclusions and implications

The objective of this chapter was to develop a large-scale test installation ('Emission Lab' or 'EmiL') for the study of the NH_3 mass transfer process between the slurry pit and the slatted floor, with the additional aim to keep the pH of the NH_4Cl source solution constant. The set-up was consequently subjected to a 10-day long test, to evaluate to what extent parameters such as the pH of the NH_4Cl solution and the emitted NH_3 concentrations could effectively be maintained. Furthermore, the pit transfer coefficient (*PTC*) was introduced in order to objectively describe the emission rate.

The study showed that the pH of the NH_3 emitting solution could be kept stable as intended at 8.0 ± 0.1. On an average, 7 mg m^{-3} NH_3 was measured at the wind tunnel exhaust, which resulted in a higher emission rate than usually observed in practice, but benefited the ease of measurement. Both the measurement results as a theoretical approach showed that the variation on the *PTC* was limited to 13%. The *PTCs* ranged from 2.1×10^{-3} to maximum 3.3×10^{-3} m s^{-1}, which is well within the range of the similar *AMTC* values found in the literature.

It could be concluded that the test installation is reliable and allows other emission experiments with various slurry pit configurations, e.g., different headspace heights and airflow obstructions at floor level. Also, the airflow rate can easily be set at different levels, which allows for various air velocities over the slatted floor and through the floor slits. Furthermore, other solution pH values could be tested with the automated pH control system. In the next chapter EmiL will indeed be valorised by using it as a platform to study the effects of pit headspace height, air velocity and airflow direction at the slatted floor level.

CHAPTER 6. NH_3 MASS TRANSFER IN THE EMISSION LAB ('EMIL'): EFFECTS OF HEADSPACE HEIGHT, AIR VELOCITY AND DIRECTION

6.1. Introduction

In order to further mitigate both indoor air pollution as well as emissions from animal houses with slurry pits, more research is still required, e.g. regarding the air layer above the slurry surface. Understanding what causes different airflow patterns in the slurry pit is therefore essential.

Chapter 5 described the development of EmiL, a large-scale experimental set-up that allows detailed NH_3 mass transfers from the slurry pit. In order to verify the robustness and variability of the test installation, an exploratory experiment was performed with fixed experimental conditions, i.e., a constant ammonium solution pH, airflow rate and pit headspace height.

In this chapter the objective is to use EmiL to study the effect of a selection of important factors that are likely to influence emissions originating from the slurry pit:

(1) the **pit headspace height**, which relates to the height of the accumulated manure. Good practice is to remove the manure regularly. In this set-up, a lift table will provide the variation in headspace height (*HH*).

(2) the **air velocity** above the slatted floor. In practice, during the ventilation process air flows over the floor, whereby the airflow rate can affect pollutant emissions. To this end, the airflow rate (*AR*) of EmiL's wind tunnel section will be altered.

(3) the **airflow direction** above the slatted floor. In this study, this will be simulated by altering a deflector's angle (*DA*) above the floor. The reason to study different airflow direction at floor level is that they can relate to the presence of various obstacles in commercial barns, e.g. animals, pen boards, feeding troughs and passage plates (e.g., Figure 1), which might unintentionally deflect indoor air. So, certain components of the

Chapter after manuscript submitted to *Biosystems Engineering*: De Paepe, M., Pieters, J.G., Merci, B., Demeyer, P. (2014). Ammonia mass transfer in a real-scale slurry pit set-up: effects of headspace height, air velocity and direction.

animal house's interior may lead to airflow entering the slurry pit, resulting in varying emission rates.

In practice, these three factors are simultaneously at work, so it is of importance to study the interaction between the NH_3 source and the integral effect that airflows may have on emissions. In this study, the impact of these studied factors will not only be determined by measuring raw NH_3 concentrations throughout EmiL, but also by providing the pit transfer coefficient (*PTC*); a standardised measure for the emission rate.

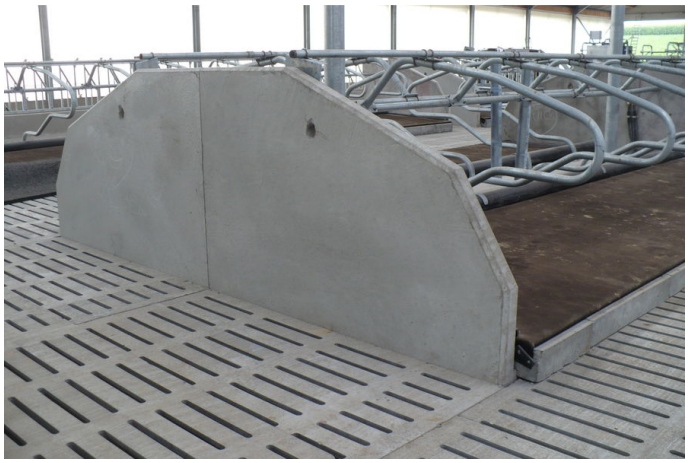

Figure 1 – Example of a low concrete wall near cow cubicles and a slatted floor. Source: Van Hessche BVBA, Egem – Pittem, Belgium.

6.2. Materials and Methods

6.2.1. SLURRY PIT SET-UP

The effects of the pit headspace height, the wind tunnel airflow rate, and the airflow deflector angle on the NH_3 transfer at slurry pit level have been studied using the large-scale Emission Lab ('EmiL'), presented in the previous chapter. For the present study, an airflow deflector was additionally installed in the wind tunnel at 0.43 m from the front end of the slatted floor, i.e. above the first set of floor slits (Figure 2). The deflector consisted of a 1-cm thick polycarbonate shield spanning the wind tunnel area (W 1.15 m × H 0.50 m). A rotational axis at the top of the deflector allowed for a manual positioning at any angle between 0 and 90°. The setting of 0° resulted in no change in airflow direction, since this was the horizontal position, while 90° implied a complete downward airflow deviation towards

the floor slits. Rubber strips were applied to the edges of the deflector to make sure the wind tunnel section was optimally blocked at a 90° angle.

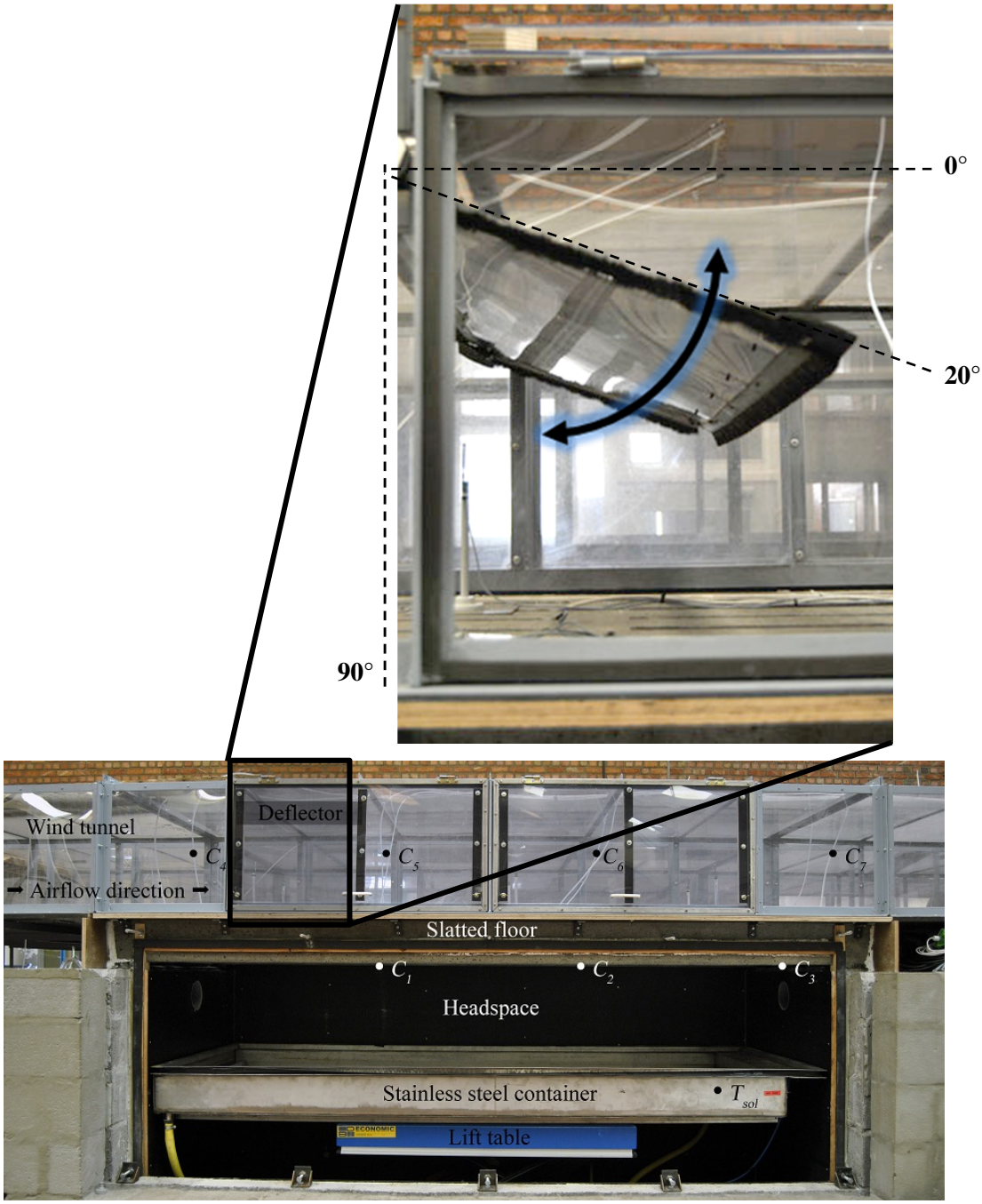

Figure 2 – Bottom: side view of EmiL. Top: detailed side view of the deflector panel positioned in the wind tunnel above the slatted floor (here at a 20° angle). The black edges are rubber strips. The arrow schematically represents the possibility to rotate the deflector between angles of 0° and 90°.

The pit contained a custom built stainless steel container (L 2.65 m × W 1.00 m × H 0.19 m) as a storage facility for the NH_3 emission source in the pit. In this respect, a standardized NH_4Cl solution (100 g L^{-1}) was used, since real manure generally portrays large variations in pH and ammonium concentration. Throughout the experiments, the pH of the ammonium solution was kept constant at a value of 8.00, through automatic addition of a Na_2CO_3/$NaHCO_3$ buffer solution (each at a concentration of 72 g per litre of the total solution). More details about the custom-built circulation and buffer dosage system were given in Chapter 5.

6.2.2. EXPERIMENTAL SERIES

The effect of different headspace heights (*HH*), airflow rates (*AR*) and deflector angles (*DA*) on NH_3 transfer from the pit, was studied during two experimental series which comprised 40 experiments in total.

Experimental series 1 with varying headspace heights and deflector angles (HH*DA)

Varying the headspace height in the pit was accomplished by altering the height between the bottom of the slatted floor and the container that held the emitting solution, using a hydraulic lift (BD Lift & Container International AB, Klippan, Sweden) as shown in Figure 1. The studied headspace heights were 0.10, 0.37, 0.63 and 0.90 m, and reflect different pit manure levels which occur in practice over an animal growing cycle.

At each headspace height, five different airflow deflector angles were imposed through manipulation of the deflector panel inside the wind tunnel: 0°, 20°, 45°, 70° and 90°.

The combination of four headspace heights with five wind deflector angles resulted in 20 experiments. Each experiment lasted 90 min, similar as the time used by Zhang et al. (2008a) for each experimental run. During this first series of experiments a constant airflow rate of 945 m^3 h^{-1} was used, resulting in a free stream air velocity of 0.46 m s^{-1} in the wind tunnel above the slatted floor. The Reynolds number (*Re*) was in this case 30 000, using a hydraulic diameter of 1.07 m for the wind tunnel. Therefore, the mean airflow in the wind tunnel was fully developed and turbulent.

Experimental series 2 with varying airflow rates and deflector angles (AR*DA)

Four different airflow rates (*AR*) were tested: 540, 810, 1080 and 1350 $m^3\ h^{-1}$. These resulted in free stream air velocities in the wind tunnel (u_{WT}) of respectively 0.26, 0.39, 0.52 and 0.65 $m\ s^{-1}$, which relates to the low air velocities expected at floor level in practice (e.g., 0 – 0.5 $m\ s^{-1}$ as stated by Schrade et al., 2012). Although it is best to keep the air speed at animal level as low as possible, preferably below 0.2 $m\ s^{-1}$ (BPEX, 2004), higher air velocities can occur in function of the ventilation regime. At each studied airflow rate, the same five airflow deflector angles were imposed as described under 2.2.1. This combination of four airflow rates with five wind deflector angles again resulted in 20 experiments, each lasting 90 min. During this second experimental series, an intermediate headspace height of 0.50 m was maintained.

6.2.3. MONITORING EQUIPMENT AND PROCEDURES

During all 40 experiments of both experimental series described above, the following parameters were monitored: (1) the pH and temperature of the ammonium solution, (2) the air velocity above the floor and in different floor slits and (3) the NH_3 concentration at different locations in both the pit and wind tunnel head spaces.

The pH of the NH_4Cl-solution was monitored with a type HI 1006-32 electrode (Hanna Instruments) and recorded every 10 s on a Squirrel type 2040 data logger (Grant Instruments, Cambridge, UK). The NH_4Cl solution's temperature was measured with a resistance temperature detector (RTD; Jumo GmbH & Co. KG, Fulda, Germany) and logged at 1-minute intervals.

Air velocities were monitored in the wind tunnel section above the floor (u_{WT}) for control purposes, as well as in the floor slits (u_1 *to* u_6) shown in Figure 3, using unidirectional hot-film anemometers of type EE66 (E+E Elektronic, Engerwitsdorf, Germany), placed in positions able to capture the vertical airflows.

NH_3 concentrations were monitored at eight positions: three at the bottom of the floor slits and at 1.0-meter intervals (C_1 to C_3), four at mid-height of the wind tunnel and at 1.0-meter intervals (C_4 to C_7) and one near the wind tunnel outlet (C_8) (see Figure 3). At each position concentration values were recorded approx. every 30 minutes, and stored on a PC through a Telnet interface.

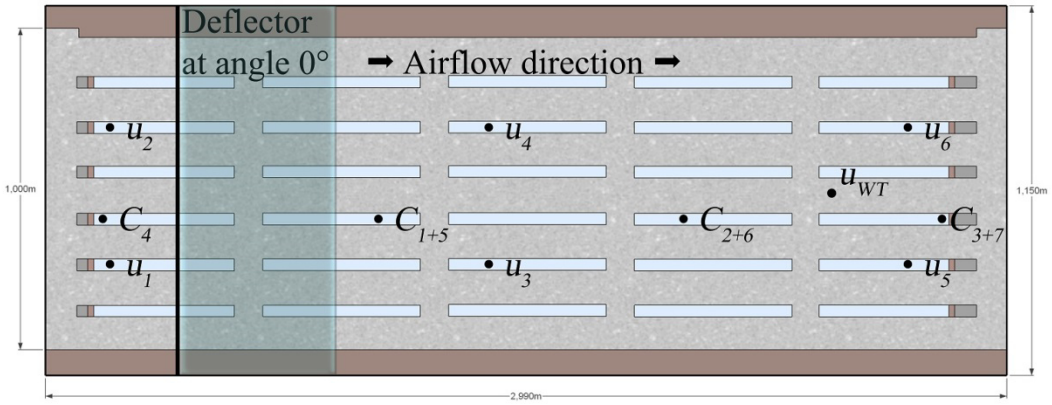

Figure 3 – Top view of the slatted concrete floor with the positions of the deflector panel, anemometers (u_{WT} & $u_{1\text{-}6}$) and the gas sampling positions ($C_{1\text{-}7}$). C_8 was measured at the wind tunnel outlet.

Table 1 summarises for each parameter, the measuring interval, the numbers of samples during a 90-minute interval and the measuring precision. For each parameter, all obtained measuring values were averaged over the total duration of each experiment separately (90 min).

Table 1 – The measured parameters with measuring interval, number of samples per experimental run and sensor precision.

Parameter	Meas. interval	N° of samples/run	Precision
pH	10 s	540	0.01
T_{sol} (°C)	60 s	90	0.1 °C
u (m s^{-1})	60 s	90	0.01 m s^{-1}
$C_=$ [NH_3] (mg m^{-3})	approx. 80 s between each of the 8 positions	3 to 4 for each of the 8 positions	0.1 mg m^{-3}

6.2.4. Calculation of the Pit Transfer Coefficient (*PTC*)

To quantify the NH_3 mass transfer rate from the solution surface in EmiL, the pit transfer coefficient (*PTC*) was used. As explained in our previous study (Section 5.2.5), the *PTC* is derived from the more general NH_3 mass transfer coefficient (*AMTC*) found in the literature (e.g., Ye et al., 2008a). *PTC* is calculated as:

$$PTC = \frac{E}{A_S \times C_S}, \text{ in m s}^{-1} \quad (1)$$

where E is the NH_3 emission rate, A_s is the solution surface area of 2.40 m², and C_s is the equilibrium NH_3 concentration at the immediate solution surface, mg m^{-3}.

The NH_3 emission rate, E , was calculated through the wind tunnel outlet concentration (C_{out} = C_8), the concentration at the inlet (C_{in}, which can be set to zero) and the airflow rate, Q:

$$E = Q \times (C_{out} - C_{in}), \text{ in mg s}^{-1} \quad (2)$$

C_s was calculated using Henry's constant, K_H, the dissociation constant, K_D, the total ammoniacal nitrogen (TAN) concentration and the pH value (Arogo et al, 1999). In our experiments, the TAN value was 33.7 g L^{-1} , which results in a C_s value of 359 mg m^{-3} for pH 8.00 and T = 16°C. However, the calculation of *PTC* was always adapted to the average values of the solution temperature and pH measured for each experiment.

6.2.5. STATISTICS

In order to determine the influence of the set-up's variables (headspace height *HH*, airflow rate *AR*, deflector angle *DA*) on the six measured floor slit air velocities (u_1 to u_6), the NH_3 concentrations at eight positions (C_1 to C_8) and the *PTC* (dependent variables) a general linear regression model (GLM) was performed. For each dependent variable, two different models were built with *HH* (0.10, 0.37, 0.63 and 0.90 m) and *DA* (0,°, 20°, 45°, 70° and 90°) or *AR* (540, 810, 1080 and 1350 m³ h^{-1}) and *DA* (0,°, 20°, 45°, 70° and 90°) as independent continuous variables, respectively. The two-way interaction between the two variables was tested. Next, a new GLM was developed using the combined data from both experimental series described in Section 6.2.2., with *PTC* as dependent variable and *HH*, *DA* and *AR* as independent, continuous variables in order to obtain the best prediction model for *PTC*. Two-way and three-way interactions were tested. The proportion of variation in *PTC* explained by the model was given by R^2 and the predicted *PTC* by the final model was plotted against the observed *PTC*.

All analyses were performed using SAS 9.3 3 (SAS Institute Inc., NC). Statistical significance was considered at $p < 0.05$. The fit of the models was evaluated by examination of the normal probability plots of the residuals and by inspection of the residuals plotted against the predicted values.

6.3. Results and discussion

6.3.1. AMMONIUM SOLUTION PH AND TEMPERATURE

During both experimental series, the ammonium solution's pH and temperature were continuously monitored for stability. Their average values during each measurement interval are given in Table 2. Both parameters showed little variation, as indicated by the standard deviations. At deflector angles of 70° and 90°, the solution temperature always decreased with approx. 1°C. This can be attributed to the fact that the deflector increasingly guided the airflow through the first floor slits, thereby colliding with the ammonium solution and causing evaporative cooling. Other effects of changing the deflector angle are discussed below.

Table 2 – NH_4Cl solution pH and temperature, averaged per measurement interval. Notation: average ± SD.

Experimental series 1				Experimental series 2			
HH (m)	*DA* (°)	*pH*	T_{sol} (°C)	*AR* ($m^3\ h^{-1}$)	*DA* (°)	*pH*	T_{sol} (°C)
0.10	0	8.00 ± 0.01	16.4 ± 0.1	540	0	8.02 ± 0.01	15.2 ± 0.3
	20	8.00 ± 0.01	16.4 ± 0.1		20	8.03 ± 0.01	15.9 ± 0.1
	45	8.00 ± 0.01	16.2 ± 0.1		45	8.03 ± 0.01	16.2 ± 0.1
	70	8.01 ± 0.01	15.6 ± 0.2		70	8.03 ± 0.01	16.2 ± 0.1
	90	8.01 ± 0.02	14.8 ± 0.3		90	8.03 ± 0.02	15.7 ± 0.2
0.37	0	8.00 ± 0.01	16.4 ± 0.1	810	0	8.09 ± 0.01	17.2 ± 0.1
	20	8.00 ± 0.01	16.5 ± 0.1		20	8.09 ± 0.01	17.5 ± 0.1
	45	8.00 ± 0.01	16.4 ± 0.1		45	8.09 ± 0.01	17.3 ± 0.1
	70	8.01 ± 0.01	15.9 ± 0.2		70	8.07 ± 0.01	16.8 ± 0.2
	90	8.00 ± 0.01	15.2 ± 0.2		90	8.03 ± 0.01	16.1 ± 0.2
0.63	0	8.01 ± 0.01	16.5 ± 0.1	1080	0	8.01 ± 0.01	16.9 ± 0.1
	20	8.01 ± 0.01	16.7 ± 0.1		20	8.01 ± 0.01	17.0 ± 0.1
	45	8.00 ± 0.01	16.7 ± 0.1		45	8.01 ± 0.01	17.0 ± 0.1
	70	8.01 ± 0.01	16.3 ± 0.2		70	8.01 ± 0.01	16.5 ± 0.2
	90	8.01 ± 0.01	15.7 ± 0.2		90	8.01 ± 0.01	15.8 ± 0.2
0.90	0	8.00 ± 0.01	17.0 ± 0.1	1350	0	8.01 ± 0.01	17.0 ± 0.1
	20	8.00 ± 0.01	17.1 ± 0.1		20	8.00 ± 0.01	17.0 ± 0.1
	45	8.01 ± 0.01	16.9 ± 0.1		45	8.00 ± 0.01	16.8 ± 0.1
	70	8.01 ± 0.01	16.4 ± 0.2		70	8.01 ± 0.01	16.4 ± 0.1
	90	8.01 ± 0.01	15.7 ± 0.3		90	8.01 ± 0.01	16.1 ± 0.1

6.3.2. FLOOR SLIT AIR VELOCITIES

Air velocities in the floor slits were monitored during both experimental series. Figure 4 shows the effects of headspace height, airflow rate and deflector angle on the air velocities in six of the floor slits, i.e. u_1 to u_6. Headspace heights had no influence on air velocities ($p > 0.05$ for u_1 to u_6) (Fig 4., left column). The varying airflow rates on the other hand, shown in the right column, did have a significant positive effect on floor slit air velocities u_4, u_5, and u_6 ($p < 0.02$, $p < 0.001$ and $p < 0.001$, respectively). Increasing the deflector angle had a significant positive effect on the air velocities in all floor slits ($p < 0.001$). The air entering the slurry pit passed through the first floor slits directly underneath the deflector, where u_1 and u_2 were measured and the largest effects were observed, with exponential increases. Angles > 70° led to velocities above 2.0 m s^{-1}, the maximum measuring range of the anemometers. At the other positions proportional effects were found, with air velocities limited to 0.4 m s^{-1} for deflector angles < 45° and up to 1.1 m s^{-1} for higher angles. Halfway along the slatted floor, u_3 remained zero throughout all experiments, while u_4 did not rise above 0.5 m s^{-1}. (The positions of u_3 and u_4 were placed roughly symmetrically along the slatted floor, so could not differ that much. It has only now become apparent that the anemometer at u_3 was in fact faulty.) At the end of the floor, where the airflow exited the slurry pit again, u_5 and u_6 again showed a gradual increase, to a maximum value of 1.1 m s^{-1}.

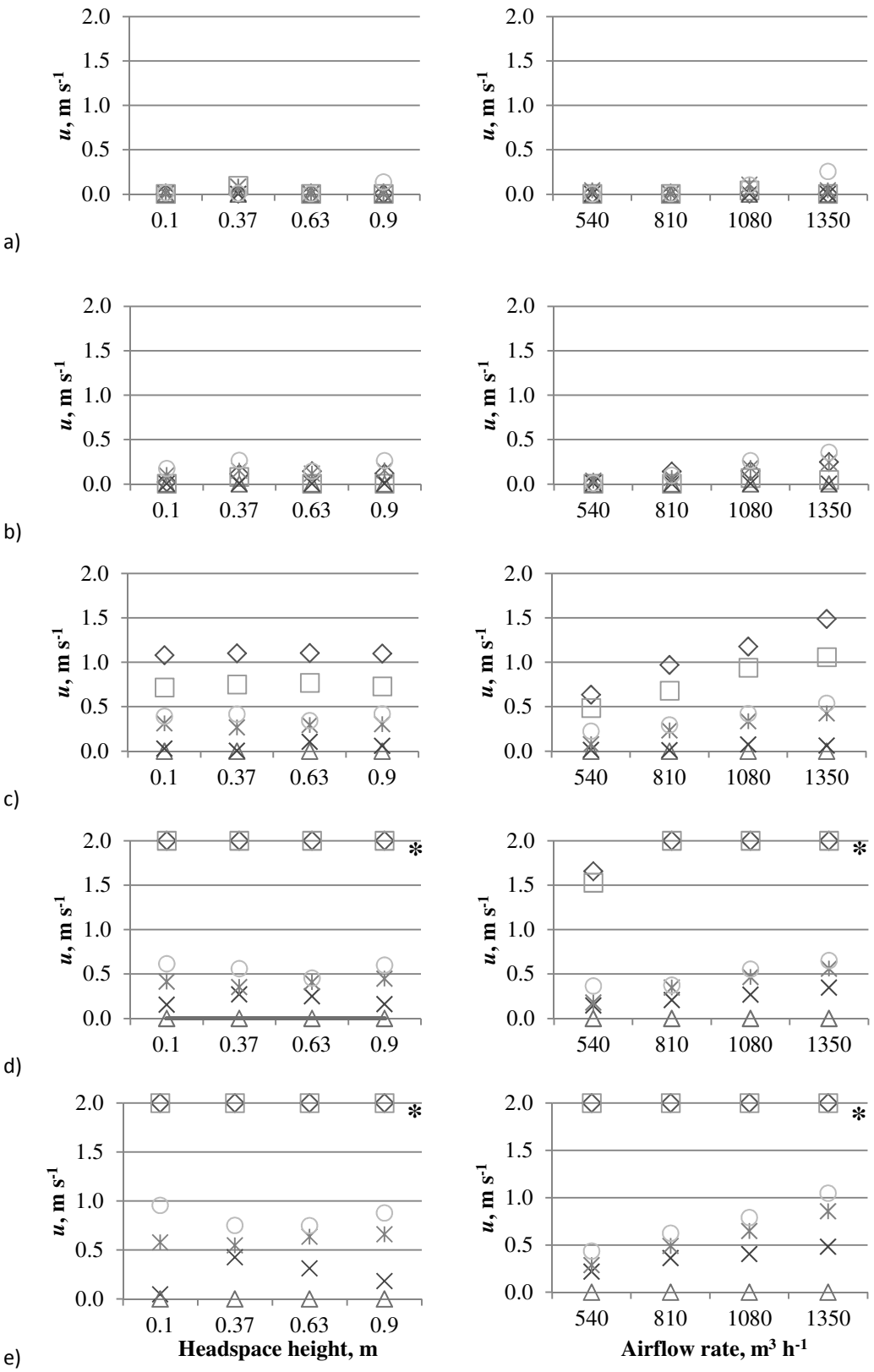

Figure 4 – Effects of headspace height (left column) and airflow rate (right column) on the floor slit air velocities $u_{1\text{-}6}$, for deflector angles (a) 0°, (b) 20°, (c) 45°, (d) 70°, and (e) 90°. ♦ = u_1, ■ = u_2, ▲ = u_3, × = u_4, ж = u_5, • = u_6. (*) Values exceeding the maximum measuring range of 2.0 m s^{-1}.

6.3.3. AMMONIA CONCENTRATIONS IN THE PIT AND WIND TUNNEL HEADSPACES

Experimental series 1 with varying headspace heights and deflector angles (HH*DA)

Figure 5 shows the average NH_3 concentrations measured throughout the slurry pit and wind tunnel headspaces, using the four headspace heights (*HH*) and five deflector angles (*DA*). Using deflector angle 0°, as shown in Figure 5a, the highest concentrations were observed beneath the slatted floor (positions C_1 to C_3), ranging between 9 and 69 mg m^{-3} on average. Directly above the floor, i.e. in the wind tunnel (positions C_4 to C_6), very low values around 1 mg m^{-3} were measured. More leeward of the floor (position C_7), concentrations between 3 and 12 mg m^{-3} were measured. In practice, the lower threshold levels for NH_3 that are considered safe for farm animals are 2 to 7 mg m^{-3} (Tamminga, 1992).

Generally, the concentration values did not show a clear effect of the headspace height ($p > 0.05$ for positions C_1 *to* C_6). However, at positions C_7 and C_8 near the outlet a decreasing trend was noticed as the headspace increased ($p = 0.008$ and $p = 0.055$, respectively). Using a fixed airflow rate, this phenomenon suggests lower emissions at larger pit headspaces, i.e. deeper slurry pits. This can in practice be achieved by cleaning regularly.

Increasing the deflector angle from 0° to 20° or more affected the NH_3 concentrations at all measured positions. Figures 5b–e shows that the concentrations under the floor (C_1, C_2 and C_3) gradually decreased, before slightly increasing again at angles > 70°. Meanwhile, the concentrations at C_2 and C_3 significantly decreased with approx. 50% ($p = 0.0008$ and 0.0002, respectively) for all deflector angles between 20 and 90°. This was a direct consequence of guiding more air into the pit, which resulted in expelling NH_3 out of the pit. This resulted in significant increases (all p-values < 0.01) in the NH_3 concentrations above the floor at positions C_5, C_6 and C_8. Position C_4 remained unaffected due to its location still in front of the deflector.

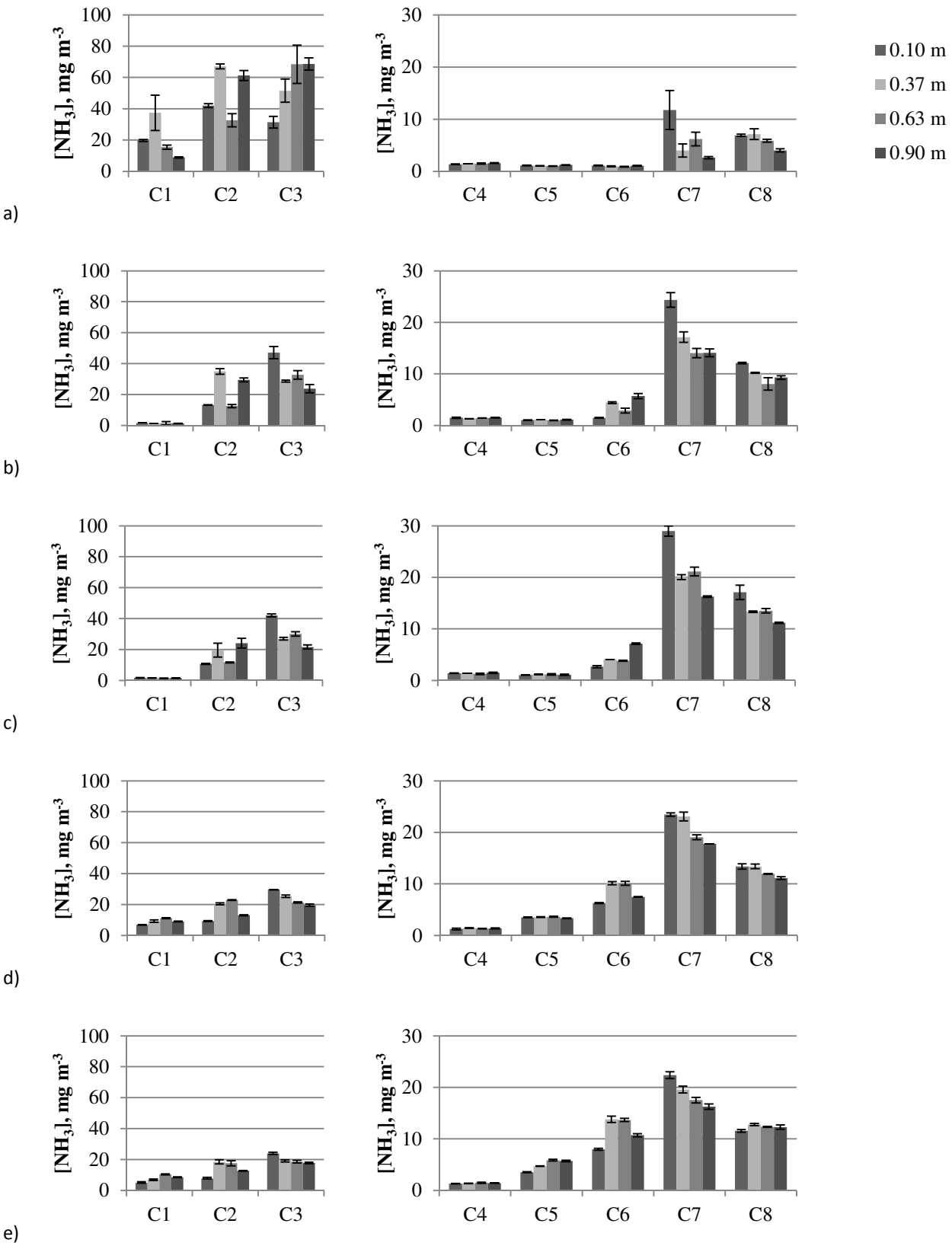

Figure 5 – Average NH_3 concentrations in mg m^{-3}, measured at positions $C_{1\text{-}8}$, using four headspace heights and five deflector angles (a) 0°, (b) 20°, (c) 45°, (d) 70° and (e) 90°. Error bars represent one standard deviation.

Experimental series 2 with varying airflow rates and deflector angles (AR*DA)

The average NH_3 concentrations measured using varying airflow rates and deflector angles are given in Figure 6. Generally, increasing the airflow rate led to a decrease in concentrations by approx. 25 to 75%, except for the values C_2 and C_3 upon testing deflector angle 0° (see Figure 6a). At this angle, the concentrations under the floor (C_1 to C_3) ranged between 8 and 97 mg m^{-3} on average. Above the floor (C_4 to C_6), low concentrations around 1 mg m^{-3} were measured, while at the more leeward positions (C_7 and C_8) concentrations between 2 and 8 mg m^{-3} were found, which is in the order of values found during the headspace height experiments (Series 1). Significant effects of the airflow rate were found for the NH_3 concentrations measured at C_6 and C_8 ($p = 0.0018$), which were positioned in the wind tunnel.

These findings could be expected. For example, West (1977) already showed that the ventilation rate affected the amount of air mixing in a ventilated space. When a gas source was located in a stagnant zone (as is likely the case in an under-floor slurry pit), decreasing the ventilation rate increased the average gas concentration in the room.

As was also observed previously, guiding more air into the slurry pit by increasing the deflector angle once again resulted in lower NH_3 concentrations under the slatted floor (C_1 to C_3), with values dropping by more than 50% (Figures 6b-e), whereas values C_5 to C_8 were doubled (significant effect; all p-values < 0.004), which would lead to higher emissions.

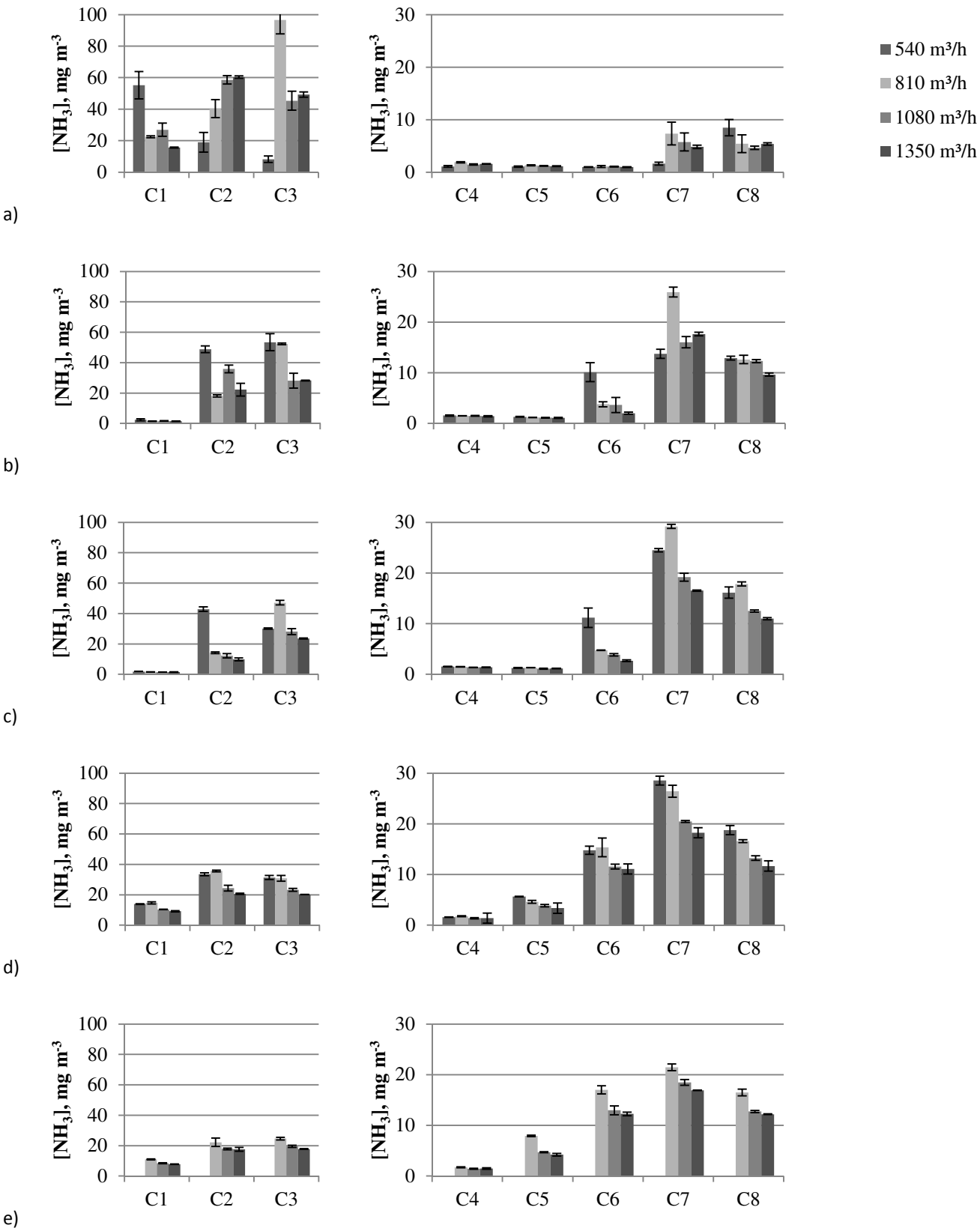

Figure 6 – Average NH_3 concentrations, in mg m^{-3}, measured at positions $C_{1\text{-}8}$, using four airflow rates and five deflector angles (a) 0°, (b) 20°, (c) 45°, (d) 70° and (e) 90°. Error bars represent one standard deviation. Due to an artefact, in Fig. 6e no data are available for the lowest airflow rate (540 m³/h).

6.3.4. PIT TRANSFER COEFFICIENTS (*PTCs*)

Experimental series 1 with varying headspace heights and deflector angles (HH*DA)

Figure 7 shows the calculated *PTCs* as influenced by the headspace height and deflector angle. Despite having found no effect of the headspace height on the floor slit air velocities, higher *PTC* values were found for the low headspace heights ($p = 0.005$), particularly at the minimal value of 0.10 m (see Figure 7). Without altering the airflow direction in the wind tunnel, i.e. with the deflector positioned at a 0° angle, increasing the headspace height to its maximum of 0.90 m led to a linear decrease in *PTC* of up to 45%. At greater deflector angles the decreasing trend remained, although less pronounced. This indicates that care should be taken not to let the manure build-up in the slurry pit reach excessive heights. In the research performed by Ye et al. (2008b & 2009a) emission rates also increased very slightly with decreasing headspace height, although due to the relatively small difference in tested headspace heights, more research was advised.

At all headspace heights, increasing the airflow deflector from its initial 0° angle has shown an increase in *PTC*, with an important effect already witnessed at the angle of 20°. At higher angles the emission rates did not return below the values observed at the 20° angle. At 0.10 m headspace height, of all values tested, 45° was found to give rise to the highest *PTC*. A possible explanation for this is the position where the airflow impacted on the ammonium solution surface. An angle of 45° resulted in the air colliding with the solution at a further (leeward) distance than was the case with angles 70° and 90°, which may have influenced the solution's turbulence and evaporation to a greater extent. The *PTC* values during the 90° angle are similar for the four headspace heights (see Figure 7). This implies that when the deflector guided the maximal amount of air through the floor, the height of the solution surface had much less influence.

Overall, the highest *PTC* value, i.e. 5.1×10^{-3} m s^{-1}, was observed during the experiment with *DA* 45° combined with the lowest headspace height of 0.10m. At 1.1×10^{-3} m s^{-1}, the minimum *PTC* value was almost five times lower, and was observed at *DA* 0° combined with *HH* 0.90m, where the air was not forced through the floor opening at all and the NH_4Cl solution was placed at its lowest point, thus being affected much less.

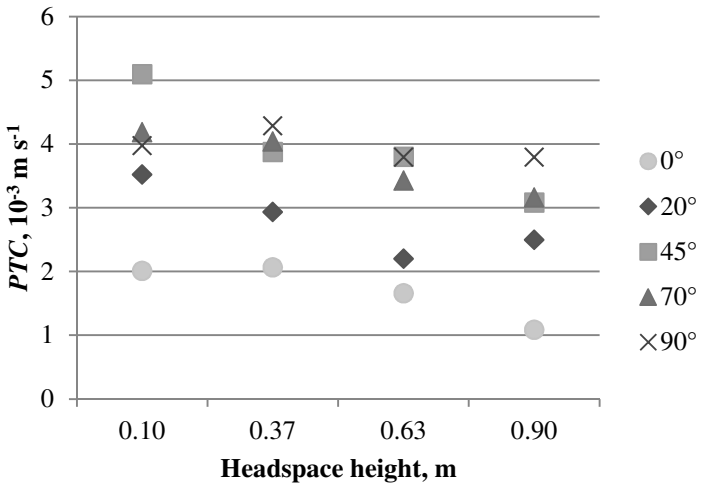

Figure 7 – Effect of the headspace height and the deflector angle on the pit transfer coefficient (*PTC*), using a constant airflow rate of 945 m^3h^{-1}.

Experimental series 2 with varying airflow rates and deflector angles (AR*DA)

Figure 8 shows the pit transfer coefficients (*PTC*) as affected by varying airflow rates and deflector angles. *PTCs* were found to increase in a linear way with rising airflow rates ($p < 0.001$), e.g. a 25% increase between the minimum and maximum airflow rate, using deflector angle 0°. This was to be expected, since the *PTC* is proportional to the airflow rate (see equation in Section 6.2.4). In the literature, emission rates in scale-model and wind tunnel experiments were also proven to increase linearly with the airflow rate (Ye et al., 2008a; Saha et al., 2010). The *AMTCs* determined by Ye et al. (2008a) increased with rising airflow rates for all three of their tested control strategies (constant inlet opening area, constant inlet velocity and constant inlet jet momentum).

As seen previously in experimental series 1, the *PTC* values also increased with rising deflector angles. At a deflector angle of 0°, *PTCs* ranged between 1 and 2×10^{-3} m s^{-1}, whereas the slight change to the angle of 20° already led to values roughly twice as high. As more air was guided into the pit, more NH_3 particles will have been pushed out again as well, leading to higher emissions.

The current range of *PTC* values was the same as for experimental series 1. The maximal *PTC* value, 5.1×10^{-3} m s^{-1}, was observed at a deflector angle of 90° combined with the highest airflow rate of 1350 $m^3 h^{-1}$. In this case the air was guided directly towards the ammonium solution surface, with the highest airflow rate that was tested. The lowest *PTC* value was five

times lower, 9.8×10^{-4} m s^{-1}, and was observed at deflector angle 0°, where the deflector could not force the air through the floor opening. However, looking at the linear trend of the other data in Figure 8, it is more likely that the *PTC* during *AR* = 540 m^3 h^{-1} and *DA* = 0° (in short '540;0' for easy reference) should have been lower than currently observed, and thus be the real minimal value instead of $PTC_{810;0.}$ The overestimation can be attributed to two factors that participate in the calculation of *PTC*: (1) the difference in C_8 concentrations during airflow rates of 540 and 810 m^3 h^{-1} was relatively higher than observed during the other tests (see Figure 6), and (2) the solution temperature was on average 2°C lower during 540;0 when compared with 810;0, due to daily fluctuations (see Table 2). Changing these two parameters to the values observed at 810;0 would indeed decrease $PTC_{540;0}$ to a value of 0.8×10^{-3} m s^{-1}. In that case, the expected linear trend between *AR* and *PTC* would be followed.

In general, all *PTC*s were situated well within the range of *AMTCs* for laboratory and field experiments of NH_3 release from manure found in the literature, i.e. 1.3×10^{-6} to 11.7×10^{-3} m s^{-1} (Ni, 1999). In recent scale-model studies, values of 1.0×10^{-3} to 19×10^{-3} m s^{-1} were found (Saha et al, 2010; Ye et al., 2008a), yet it is always indicated that these coefficients are geometry-dependent.

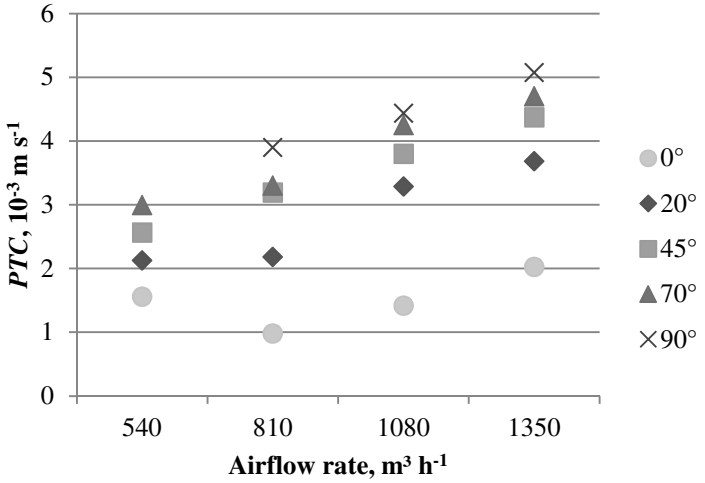

Figure 8 – Effect of the airflow rate (and thereby also of the air velocity at floor level) and deflector angle on the pit transfer coefficient (*PTC*), using a constant headspace height of 0.50 m.

Statistical modelling

In order to be able to predict *PTC* from the defector angle (*DA*), the airflow rate (*AR*) and the headspace height (*HH*), a GLM was built using the data from all experiments. Using this model, 82% of the total variation witnessed in the observed *PTC* values could be explained by the model. The majority of the variation in *PTC* is explained by *DA* (63%), while adding *AR* and *HH* to the model additionally explains 11% and 8 %, respectively. Separately, *DA* explained 63% of the model, *AR* accounted for 16% and *HH* for 6.8%.

Table 3 shows the characteristics of the model. In Figure 9 the correlation between the observed and model-predicted *PTC* values are presented, along with the model's 95%-confidence limits.

Table 3 – General linear model for *PTC*.

Parameter	Estimate	Standard error	P-value
Intercept	9.97E-04	4.20E-04	0.0233
AR	1.81E-06	3.80E-07	< 0.0001
HH	-1.32E-03	3.66E-04	0.0009
DA	2.57E-05	2.43E-06	< 0.0001

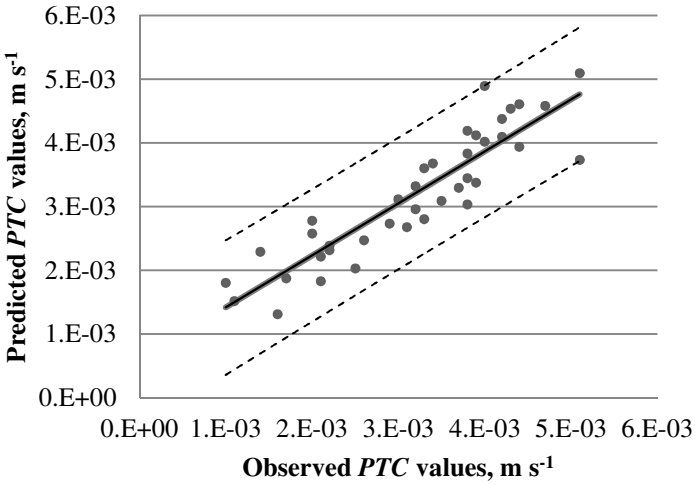

Figure 9 – Correlation between the observed and model-predicted *PTC* values. The full line indicates predictions by the model. The dotted lines indicate the 95%-confidence limits.

6.4. Conclusions and implications

The large-scale experimental set-up 'EmiL' was used to study the impact of varying headspace heights, air velocities and direction on NH_3 mass transfer from the slurry pit through a typical cow housing floor. It was shown that:

(1) Increasing the **headspace height** did not affect the NH_3 concentrations in the pit but led to significantly lower NH_3 concentrations measured leeward of the slatted floor. The implication for the practice is that deeper slurry pits would result in lower emission rates. This can be achieved by cleaning regularly, which is a logical mitigation strategy.

(2) NH_3 concentrations in the pit were not affected by increasing the **air velocity** above the floor up to 0.65 m s^{-1}. Higher air velocities did significantly reduce the wind tunnel outlet concentrations. However, high ventilation rates are likely to result in high emission rates, which should be avoided if possible. In practice, under-ventilation may of course endanger the indoor air quality, so finding a compromise remains necessary.

(3) Changing the **airflow direction** above the floor led to clear effects. A more downward guidance (higher deflector angles) generally led to decreasing NH_3 concentrations in the pit and increasing concentrations above the pit, resulting in higher emissions. In practice this relates to animals, pen boards or other constructions that might unintentionally deflect incoming air into the pit. Therefore, this should not be neglected in the future research towards low-emission barn design.

The above conclusions related to NH_3 concentrations. In order to obtain a standardised measure for the emission rate during the various experiments, the NH_3 pit transfer coefficient (*PTC*) was calculated. *PTC* was indeed found to decrease with increasing headspace height (1), but to increase with higher airflow rates (2) and deflector angles (3). At a deflector angle of 0°, gradually reducing the headspace height from 0.90 m to its minimum of 0.10 m, led to a linear decrease of the *PTC* by 45%. This trend was also seen at higher deflector angles, but less pronounced. Increasing the deflector angle itself showed an increase in *PTC*, with a maximum value at 45°.

Overall, the *PTC* values ranged between 9.8×10^{-4} and 5.1×10^{-3} m s^{-1}. The effects induced by the different experimental setups led to a variation coefficient of 38% for the *PTC*. A general linear model to predict *PTC* values was presented, which explained a large part of the variation (82%) in the observed *PTCs*.

Although mass transfer coefficients such as the *PTC* are characteristically geometry-dependent (e.g., enlarging the pit would result in a larger emitting surface, and a lower *PTC*), the relative effects of the studied factors could clearly be observed, which indicates their potential impact in practice. Consequently, it is recommended to carry out related validation studies in commercial barns.

CHAPTER 7. CFD SIMULATIONS OF AIRFLOW PATTERNS AND NH_3 MASS TRANSFER IN THE EMISSION LAB ('EMIL'): EFFECTS OF HEADSPACE HEIGHT, AIR VELOCITY AND DIRECTION

7.1. Introduction

To the author's knowledge, until now no CFD models were applied for NH_3 mass transfer involving both a real-scale slurry pit and a fully-modelled slatted floor. Thus, in order to better understand and try to mitigate NH_3 emissions, it is important to further study the airflow patterns and NH_3 distribution at the level of the slurry pit in great detail. This should be accomplished through both experiments (as in Chapter 6) and CFD, since validation of CFD simulations requires experimental results using thoroughly defined enclosures (Zhang et al., 2000). Indeed, as with any approximation of reality, CFD results should be interpreted with caution (Norton et al., 2007). Therefore, there is still a strong need for experimental data to evaluate CFD results and to allow further model improvement where necessary.

The experimental study in Chapter 6 clearly illustrated how the air velocity and direction near the slatted floor surface can affect the NH_3 distribution. The pit transfer coefficient (*PTC*) increased with higher airflow rates and deflector angles (both causing more air to enter the slurry pit), but diminished with increasing headspace height. To obtain more insight and more detailed information on the performances of EmiL, the objectives of the present study are:

(1) to use a CFD modelling approach (using ANSYS Fluent 13.0 software) for the study of EmiL's internal airflow patterns and their effect on NH_3 mass transfer, especially in order to visualise aspects that cannot be measured to the fullest extent during experimental studies;

(2) to verify the model results with the available experimental data;

(3) to potentially optimise EmiL, based on the model results.

Chapter after manuscript prepared for submission: De Paepe, M., Pieters, J.G., Merci, B., Demeyer, P. (2014). CFD simulations of NH_3 mass transfer in an experimental slurry pit set-up: effects of headspace height, air velocity and direction.

7.2. Materials and methods

7.2.1. Experimental background of the performed CFD simulations

CFD simulations were conducted based on the experimental study reported in Chapters 6 There, several experiments were carried out in a section of a large-scale slurry pit, in order to determine the effects of headspace height, air velocity near the slatted floor and airflow direction on the NH_3 emission thereof. The slurry pit section was covered by a typical slatted floor with 30 slits, and in its turn covered by a wind tunnel (L 8.00 m x W 1.15 m x H 0.50 m). Figure 1a shows a cross section of the experimental set-up. A 1-cm thick deflector panel was mounted across the wind tunnel section, above the first set of floor slits (see Figure 2), to allow the alteration of the angle at which the airflow is directed towards the floor slits and thus further down into the slurry pit.

Since real manure generally portrays a large variation in pH and ammonium concentrations, a standardised NH_4Cl solution (100 g L^{-1}) placed at the bottom of the pit was used to act as the source of NH_3 emission. A custom-built stainless steel container was placed in the pit to store the NH_4Cl solution. The pH was kept constant at a value of 8.0 through automatic addition of a $Na_2CO_3/NaHCO_3$ buffer solution. More details about the pH monitoring and buffer dosage system are given in Chapter 5.

In Chapter 6, two series of experiments were conducted: one with varying headspace heights and deflector angles (*HH*DA*) and one with varying airflow rates and deflector angles (*AR*DA*).

In the first series, the headspace heights were varied between 0.10 and 0.90 m. At each headspace height, five different airflow deflector angles between 0° and 90° were imposed through manipulation of the deflector panel inside the wind tunnel. Here, the airflow rate was kept constant at 945 m^3 h^{-1}. In the second series, airflow rates between 540 and 1350 m^3 h^{-1} were tested. These resulted in free stream air velocities in the wind tunnel (u_{WT}) between 0.26 and 0.65 m s^{-1}. These were again combined with varying deflector angles. Here, a headspace height of 0.50 m was maintained.

During all experiments the following parameters were monitored: (1) the ammonium solution's pH and temperature (2) the air velocity above the floor and in various floor slits and (3) the NH_3 concentration at eight positions: three at the bottom of the floor slits, at 1.0-

meter intervals (C_1 to C_3), four at mid-height of the wind tunnel, at 1.0-meter intervals (C_4 to C_7) and one near the wind tunnel outlet (C_8), as shown in Figure 1a and 2.

To quantify the NH_3 mass transfer rate from the solution surface in EmiL, the pit transfer coefficient (*PTC*) was used, which was determined as:

$$PTC = \frac{E}{A_S \times C_S}, \text{ in m s}^{-1} \quad (1)$$

where *E* is the emission rate ($AR \times C_8$) in mg s^{-1}; A_s is the solution surface area (2.40 m^2); C_s is the equilibrium NH_3 concentration at the immediate solution surface, in mg m^{-3}, and was calculated using Henry's constant K_H, the dissociation constant K_D, the total ammoniacal nitrogen (TAN) concentration, the solution temperature T_{sol} in K, and the pH value. The details of the used sensors, sampling procedures, calculations and statistical modelling are given in the previous chapters.

7.2.2. CFD MODEL

Cases

Twelve of the experimental cases described in Section 7.2.2. were modelled in CFD. Six cases stemmed from experimental series 1 (*HH*DA*) and six from series 2 (*AR*DA*), as shown in Table 1. Two different headspace heights (*HH*) were studied: both extremes of the experimental study, i.e. 0.10 and 0.90 m. For each *HH* level, three different deflector angles (*DA*) were imposed: 0, 45 and 90°. Also the minimal and maximal experimental airflow rates (540 and 1350 $m^3\ h^{-1}$) were tested, again in combination with the three deflector angles 0, 45 and 90°.

Table 1 – Overview of the experimental cases modelled in CFD.

Series 1 (*HH*DA*)

Case	*HH* (m)	*AR* ($m^3\ h^{-1}$)	*DA* (°)	*pH*	T_{sol} (°C)	C_s (mg m^{-3})
1	0.10	945	0	8.00	16.4	376
2	0.10	945	45	8.00	16.2	367
3	0.10	945	90	8.01	14.8	319
4	0.90	945	0	8.00	17.0	402
5	0.90	945	45	8.00	16.9	398
6	0.90	945	90	8.01	15.7	354

Series 2 (*AR*DA*)						
Case	*HH* (m)	*AR* ($m^3\ h^{-1}$)	*DA* (°)	*pH*	T_{sol} (°C)	C_s ($mg\ m^{-3}$)
7	0.50	540	0	8.02	15.2	342
8	0.50	540	45	8.03	16.2	393
9	0.50	540	90	8.03	15.7	371
10	0.50	1350	0	8.01	17.0	412
11	0.50	1350	45	8.00	16.7	389
12	0.50	1350	90	8.01	16.1	371

Mesh structure

The model of the geometry in the simulations corresponded to the experimental set-up and included –from top to bottom– the slurry pit, the slatted floor with 30 slits, and the wind tunnel section, which contained the airflow deflector panel and a cylindrical fan at the outlet. The boundaries that served as input for the computations are indicated in Figure 2. In Table 2 the dimensions of all major components are presented, as well as their properties in the corresponding computational domain. The virtual origin in the mesh, O_v ,was positioned at the front-left-bottom of the slatted floor, as indicated by the coordinate system in Figure 1b. In all cases hexahedral cells were used in the mesh, with a mesh size of approx. 1.365 x 10^6 cells (see Table 2). The smallest cells were situated in the floor slits (with interval sizes of 0.35 cm × 0.70 cm × 0.80 cm). The largest cells were near the wind tunnel ceiling, where they gradually increased to 4 cm × 4 cm × 8 cm. Interval sizes intermediate to these were used in the remaining regions.

A mesh refinement study was also performed, by using another mesh with twice as small interval sizes for case 3 (i.e., the case where the deflector guided all the air through the smallest pit headspace). Results from the simulation with the finer mesh showed no significant difference with the results from the coarser mesh e.g. a value of 43 $mg\ m^{-3}$ for the outlet concentration C_8; a position vital for the *PTC* calculations. Therefore, it can be argued that the used mesh is sufficiently fine.

Table 2 – Key dimensions of the components in the experimental set-up and in the computational domain.

Component	Length [*x*], m	Width [*y*], m	Height [*z*], m	N° of computational cells
Wind tunnel	7.99	1.15	0.50	573,742 for *DA* = 0° (depends on the chosen *DA*)
Outlet fan	0.30	0.35	0.35	672
Slatted floor	2.99	1.00	0.18	210,000
Floor slit (n = 30)	0.49	0.035	0.08	7000 (total: 210,000)
Slurry pit	2.67	1.00	0.10–0.90 (variable *HH*)	361,800 for *HH* = 0.90 m (100,500 for *HH* = 0.10 m)
Container with NH_3 source	2.47	0.92	0.20 (exp.); 0 (CFD)	0 (modelled as a flat surface)

Cell zone and boundary conditions

The fluid in the total cell zone was a mixture of air and NH_3 vapour. The NH_3 source consisted of a 2.40 m² surface area at the bottom of the pit, which was modelled as a wall boundary that emits an NH_3 mass fraction, m. This mass fraction was adapted for each simulation and was based on the air density, ρ_a, determined at 1.2 kg m^{-3}, and C_s, which was in turn based on the average solution pH and temperature measured during the corresponding experimental run (see Chapter 6):

$$m = \frac{C_s}{\rho_a} \times 10^{-6} \quad (2)$$

As C_s ranged from 319–412 mg m^{-3} in the twelve modelled cases, m ranged from 261–381 × 10^{-4}. The solution boundary temperature, T_{sol}, was adapted to the average value measured during the corresponding experiment.

The wind tunnel outlet was fitted with a suction fan, modelled as a cylinder with a velocity inlet boundary. The velocity magnitude, in m s^{-1}, was calculated from the applied airflow rate in the wind tunnel, as shown in Table 1. Here, the turbulence conditions were specified through the hydraulic diameter, D, and the turbulence intensity, I. For D, the fan diameter of 0.35 m was taken. The turbulence intensity at the center of a fully-developed duct flow can be estimated from the following equation (Pope, 2003):

$$I = 0.16\, Re^{-0.125} \quad (3)$$

For the highest used airflow rate of 1350 m^3 h^{-1}, where *Re* = 42 000, *I* could then be determined at 4 %. At the wind tunnel's inlet, a pressure-inlet boundary type was used, with *I* again determined at 4 %, while *D* was rounded to 2 m, based on the inlet's dimensions. Default-type mesh interfaces were used to link volume meshes with different cell sizes, i.e. between the floor slits and the pit section below, as well as the wind tunnel section above.

Solution methods

The pressure-based simulations were performed in 3D for a steady state, in single precision. The used code was Fluent 13.0 (ANSYS Inc., 2010), which ran on a Linux 64 bit platform. As the turbulence model, the two-equation realisable k-ε model was chosen; with k the turbulent kinetic energy in m^2 s^{-2}, and ε the turbulent dissipation in m^2 s^{-3}. Although the standard k-ε model has been the default in the modelling of air movement in agricultural buildings (Norton, 2007) and rooms in general (Sørensen, 2003), the realizable model is a newer variant that is recommended for the modelling of flows featuring separation and recirculation (Ansys Inc., 2010), as was the case near the floor slits and the pit's borders.

Standard wall functions were used for the near-wall treatment. The gravitational constant of 9.81 m s^{-2} was implemented in the *-z* direction. The NH_3 mass transfer was simulated with the species transport function, without the use of volumetric reactions. For the pressure-velocity coupling, the SIMPLE method was used. The spatial discretisation used the least-squares cell-based gradient. The momentum, turbulent kinetic energy, *k*, and the turbulent dissipation rate, ε, were solved with the second-order-upwind scheme (*). Under-relaxation factors were kept at their default values.

Solution residuals (i.e., the relative difference with the previous iteration) were monitored and plotted, using iterative convergence criteria of at least 10^{-3}. Furthermore, air velocities and species concentrations were considered additional target quantities for convergence monitoring, hence the calculations were continued until stable solutions were acquired.

(*) Upwinding schemes are a family of discretization methods with the specific purpose of reducing or suppressing the spatial oscillations that are at times encountered in certain solution results of convection equations (Fletcher, 1988; Spalding, 1972).

Result presentation and experimental verification

All CFD solutions were considered converged before reporting the results. First the general air velocity patterns (magnitudes and directions) as induced by the applied headspace heights, airflow rates and deflector angles, will be discussed. Second, since the focus of our interest lies in the NH_3 mass transfer, both the NH_3 concentration distributions and the pit transfer coefficients (*PTC*s) will be presented. The calculation of *PTC* values is detailed above and described in Chapter 5.

The developed CFD model will be quantitatively assessed by comparing the computed NH_3 concentration values with the average values ± 2 standard deviations (SD) observed during the experiments performed in Chapter 6. The *PTC* values calculated from the model results will be compared directly and will also be expressed as a ratio to the experimental values.

a)

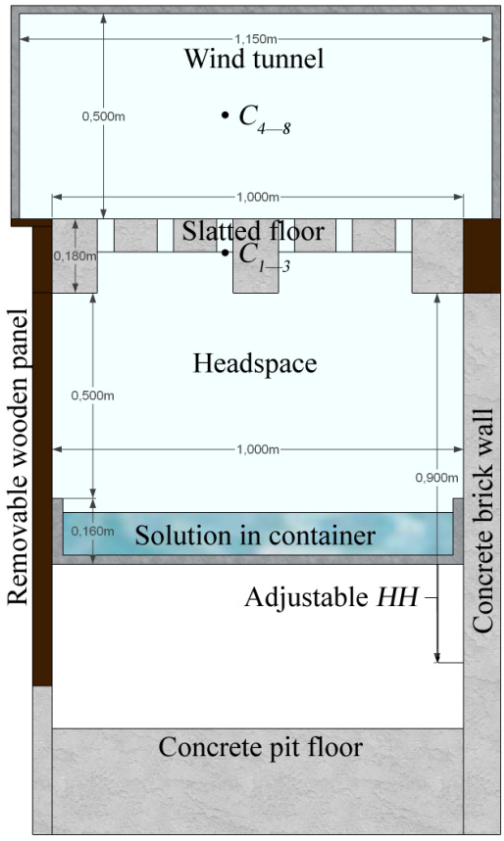

b)

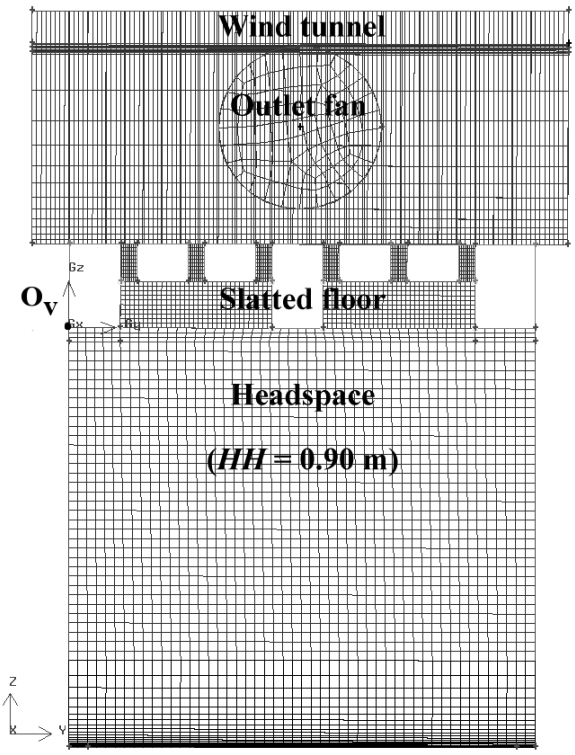

Figure 1 – Cross-sections (*y*,*z*-plane) of (a) the experimental set-up and (b) the computational mesh, with notation of the virtual origin, O_v.

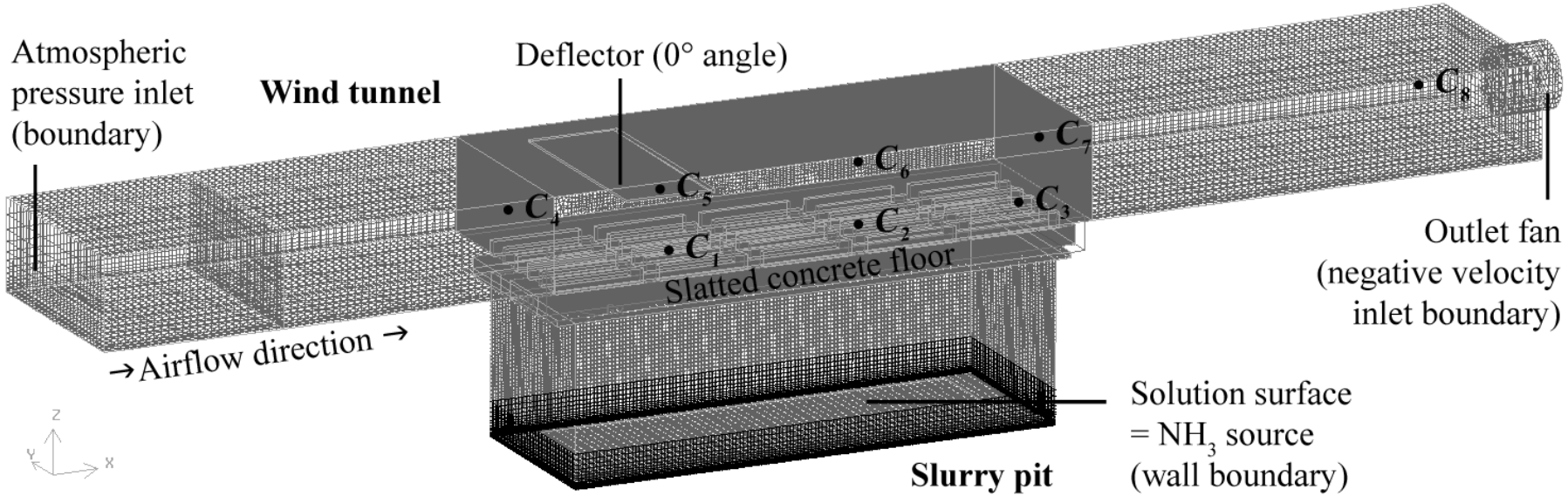

Figure 2 – Complete computational mesh in 3D-view, with notation of the used boundaries and the experimental NH_3 measurement positions, C_1 to C_3 in the floor slits and C_4 to C_8 in the wind tunnel.

7.3. Results and discussion

7.3.1. Overall airflow patterns and NH_3 concentrations

Figure 3a shows an example of a post-processing result of the air velocity contours in the case of *HH* = 0.90 m (the maximal *HH*) and *DA* = 0° (no airflow deflection). It can be seen that during *DA* = 0°, some air from the wind tunnel entered the pit at velocities of up to 0.5 m s^{-1}, due to the pressure difference that occurs over the slatted floor. The airflow separated from the wind tunnel's main flow to small jet formations through the slits in the first half of the floor (S_1 and S_2 in Figure 3a).

Higher deflector angles (*DA* = 45° in Figure 3b and 90° in Figure 3c) led to a greater amount of air entering the slurry pit, with velocities up to 1.0 and 4.3 m s^{-1}, respectively. This also resulted in more air being expelled upwards again through the floor slits in the back half (S3 to S5) at a faster rate, i.e., at velocities up to 0.5 and 1.2 m s^{-1}, respectively. Almost complete mixing of the air in the pit headspace was obtained with *DA* = 90° (see Figure 3c), where all the air generated by the wind tunnel was forced to enter the slurry pit.

The NH_3 concentration distribution was directly linked to these airflow patterns, in the way that higher local air velocities generally led to smaller NH_3 concentrations, and vice versa. This can be seen upon comparing the aforementioned Figure 3 with Figure 4, which shows the contours of NH_3 concentrations for the same cases. Generally, the highest NH_3 concentrations in the slurry pit were in the cases where *DA* was 0°, as this angle left the pit largely undisturbed from air entering the pit. At the top of the slurry pit, near the slatted floor, concentrations up to 120 mg m^{-3} were still present, while *DA* 45° and 90° led to lower concentrations near the bottom of the slatted floor (at most 105 and 55 mg $m^{-3,}$ respectively), as the NH_3 was expelled from the pit to a greater extent (see Figure 4b-c).

Fig 5 shows the NH_3 distribution across the top surface of the slatted floor for the same cases. Using *DA* = 0° (Figure 5a), it is clear that NH_3 emerged from all the floor slits, yet mostly through those at the back half of the floor. For *DA* = 45° (Figure 5b), the first half of the floor showed no NH_3. Here the NH_3 is likely kept under the floor by the precisely guided airflow imposed by the deflector (see also Figure 3b & 4b). Finally, for *DA* = 90° (Figure 5c), a similar low-concentration zone was found directly beneath the deflector, which now guided all air down into the pit. On the other hand, this led to higher concentrations near the other

floor slits, since the increased airflow that emerged from the pit was able to drag more NH_3 particles upward (see also Figure 3c & 4c).

The modelled mass transfer for all the other cases will be discussed in the following sections.

a)

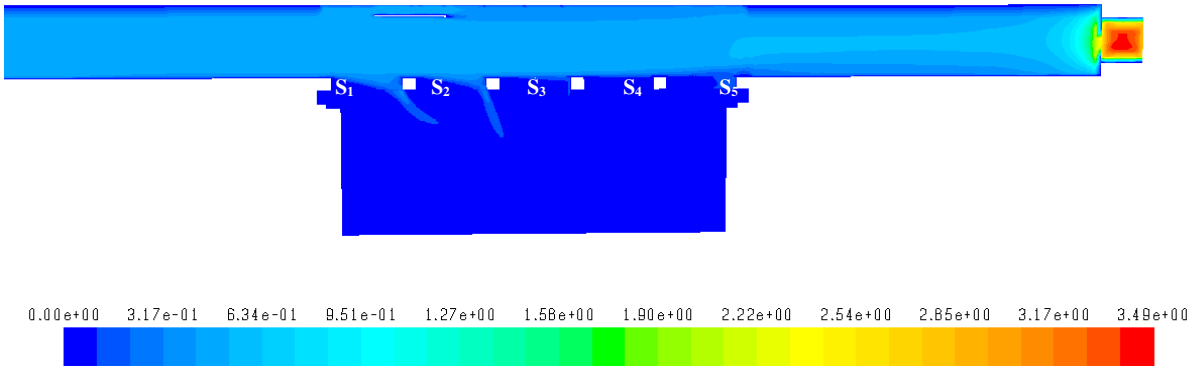

b)

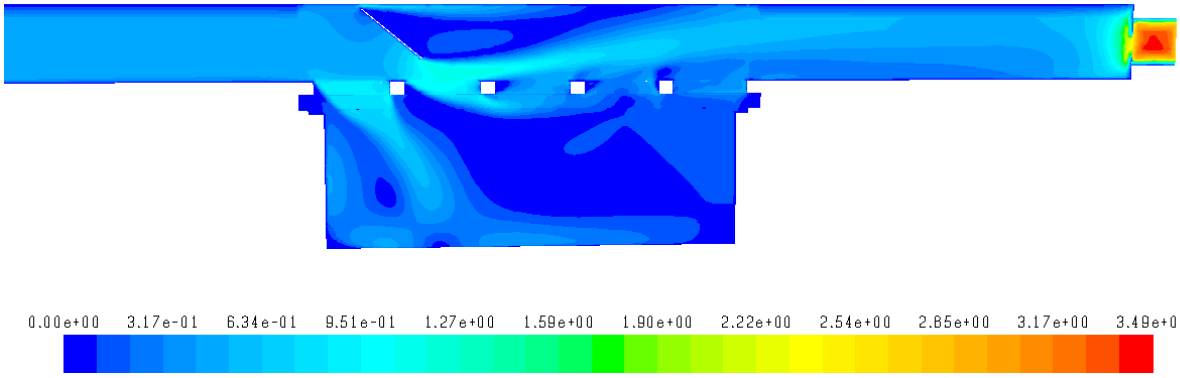

c)

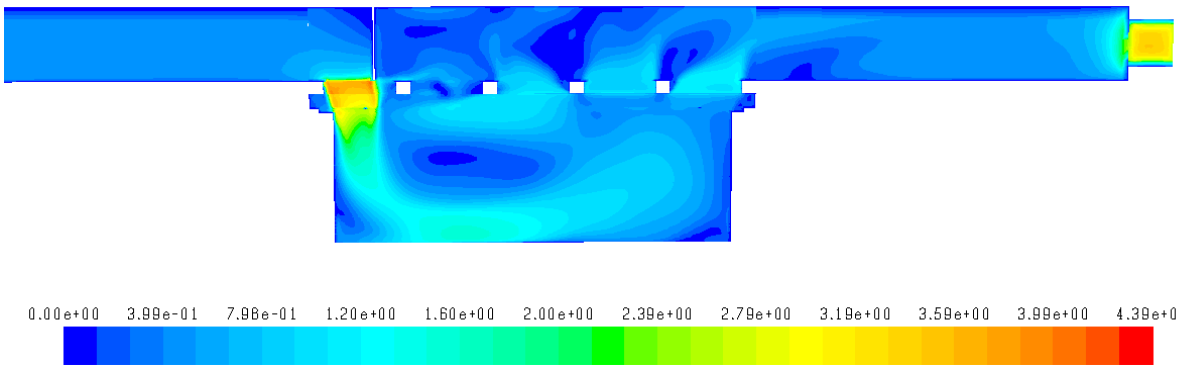

Figure 3 – Contour plot of air velocity magnitudes (in m s^{-1}) in the mid-longitudinal section of the set-up for cases 4, 5 and 6, for the deflector angle (DA) of (a) 0°, (b) 45°, and (c) 90°. S_1 to S_5: sets of floor slits starting from the windward side of the wind tunnel.

a)

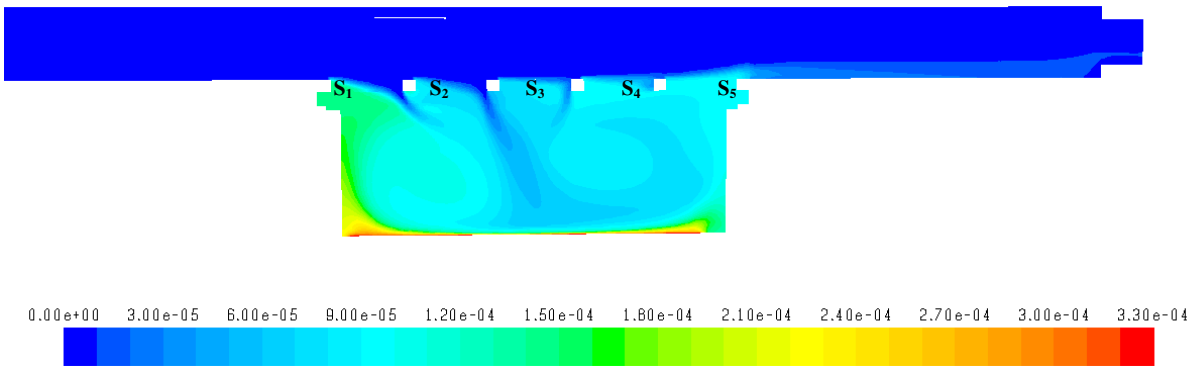

b)

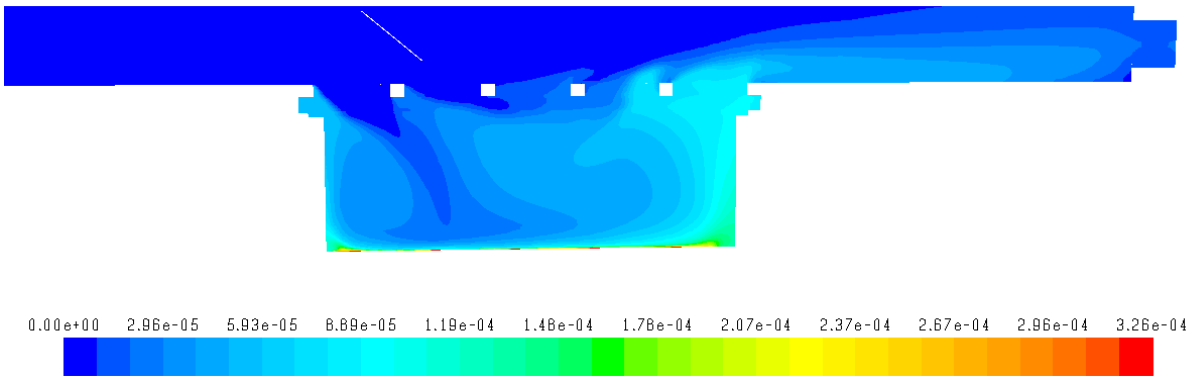

c)

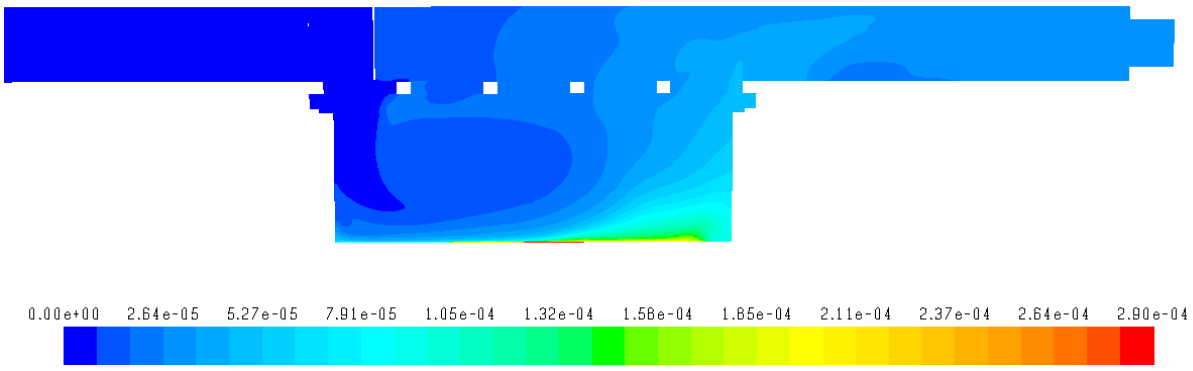

Figure 4 – Contour plot of NH_3 mass fractions in the mid-longitudinal section of the set-up for cases 4, 5 and 6, for the deflector angle (*DA*) of (a) 0°, (b) 45°, and (c) 90°. S_1 to S_5: sets of floor slits starting from the windward side of the wind tunnel.

a)

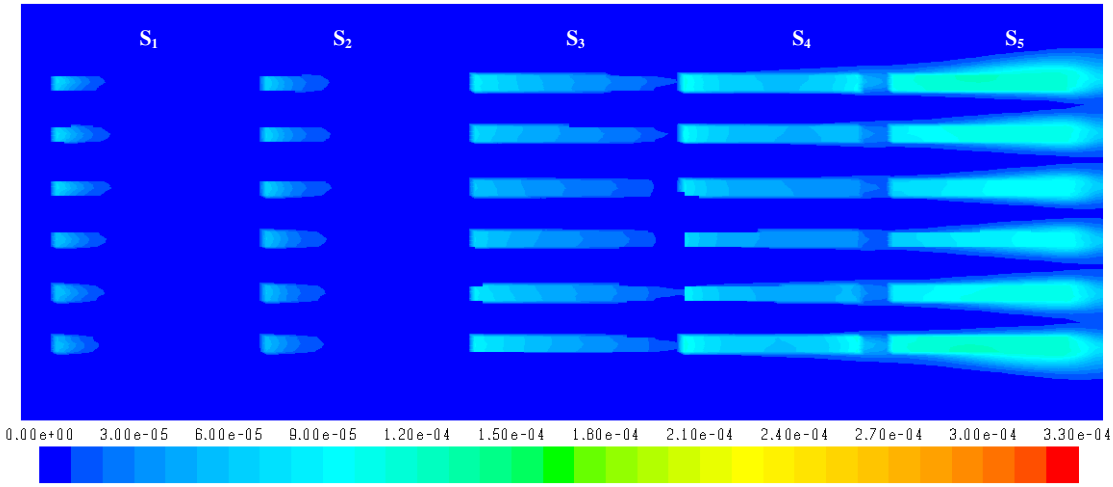

b)

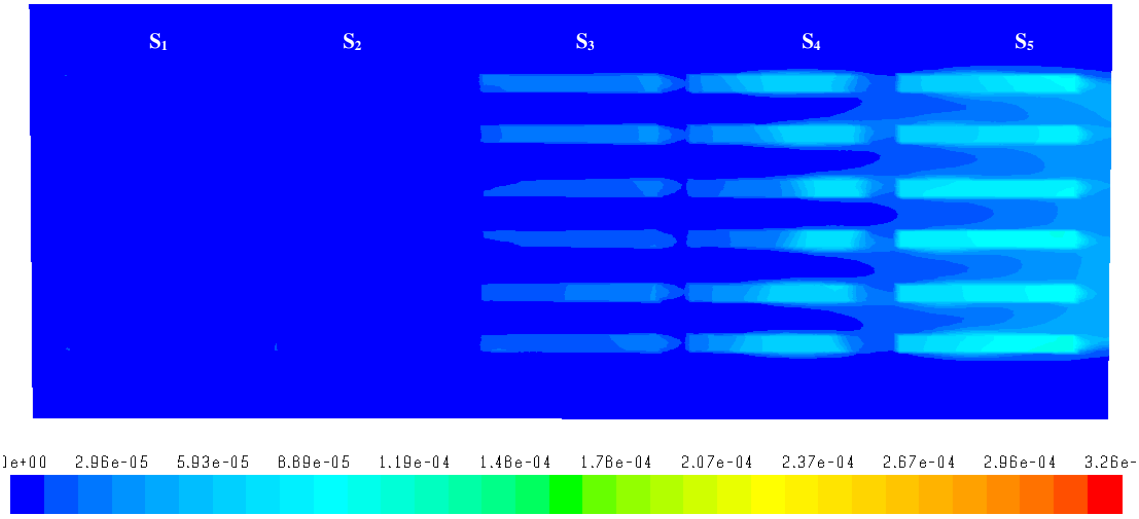

c)

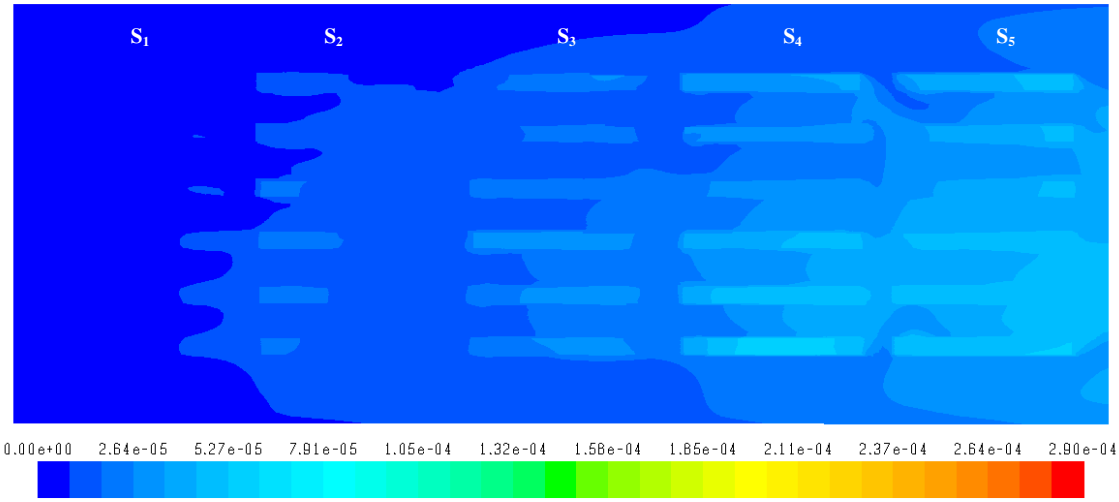

Figure 5 – Contour plot of NH_3 mass fractions at the top surface of the slatted floor for cases 4, 5 and 6, for the deflector angle (*DA*) of (a) 0°, (b) 45°, and (c) 90°. S_1 to S_5: sets of floor slits starting from the windward side of the wind tunnel.

In four of the twelve simulated cases, specifically where *DA* = 0°, it became clear that the solved variables (e.g., air velocity, NH_3 concentration) at some of the eight positions of interest (C_1 to C_8) were found to oscillate around a certain average. The oscillations could be attributed to purely numerical effects of the used steady-state method, since unsteady simulations involving time-stepping methods have proven that the oscillations gradually dampened and reached stables values (data not shown).

Also, as in any model solution, a spatial variation was often witnessed throughout the computational domain, since even a few neighbouring mesh cells can already portray a strong gradation in air velocities and NH_3 concentrations (e.g., Figure 4b). This notion should be remembered upon scrutinising the results in the following sections.

7.3.2. SIMULATED VERSUS MEASURED NH_3 CONCENTRATIONS

Figure 6 shows graphical comparisons of the NH_3 concentrations at the eight positions as measured in the experiments and derived from the numerical solution, for the first six cases,. i.e., using two different headspace heights (*HH*) and three deflector angles (*DA*). The quantitative evaluation criterion for the CFD model was the agreement of the computed values with the range of the experimentally determined NH_3 concentrations ± 2 SD. As can be seen in Figure 6, the model did not lead to values within these ranges. However, the overall trends between positions $C_{1–8}$ in the model were in line with the experimental data, which at the very least indicates that the positional effects between C_{1-8} could be captured. Particularly position C_3 showed much lower experimental values. But, as it is positioned at the back corner of the pit, this is essentially a forward-facing step problem. In that case the airflow characteristics are known to be much more difficult to model (e.g., Abu-Mulaweh, 2003; Barbosa-Saldaña et al., 2006) and can thus be disregarded in the further discussion.

For both tested headspace heights, the numerical model mostly overestimated the NH_3 concentrations when *DA* = 90° (Figure 6c). However, the trend in the experimental values over positions $C_{1–8}$ can still be recognized.

In the experiments, increasing the headspace height led to significantly lower concentrations only at position C_7, i.e., immediately leeward of the slatted floor. Although only the minimal and maximal headspace heights (0.10 m and 0.90 m) have been simulated, the numerical results confirmed the general lack of effect of the headspace height on the NH_3

concentrations at all of the studied positions, since largely similar values were found for both modelled heights; 0.10 m and 0.90 m (see Figure 6).

As confirmed by the experimental data, the CFD model also showed that guiding more air into the pit, through the increase of the deflector angle (*DA*), led to decreasing NH_3 concentrations in the pit (C_1 to C_3) and increasing concentrations above the pit, which would eventually result in higher emissions.

In the second series (cases 7-12), two airflow rates (*AR*) and three deflector angles (*DA*) were modelled. Here, the numerical solutions also generally overestimated the NH_3 concentrations as observed during the experiments (Figure 7). The cases using *AR* = 540 $m^3\ h^{-1}$ are shown in Figure 7's left column, while those using *AR* = 1350 $m^3\ h^{-1}$ are shown on the right. Again, the largest discrepancy could be found at position C_3, where the forward-facing step problem is situated, as discussed above.

In the experiments, the NH_3 concentrations measured in the pit (C_1 to C_3) were not significantly affected by increasing *AR*, or in other words by increasing the air velocity over the slatted floor. However, significant effects of *AR* were found for the NH_3 concentrations measured at C_6 and C_8, which were both negatively affected. For the outlet concentration C_8 this trend could be confirmed through verification with the numerical results.

The numerical results again confirmed that higher deflector angles led to decreasing NH_3 concentrations in the pit (C_1 to C_3) and increasing concentrations elsewhere, as shown for *DA* = 0° (Figure 7a), 45° (Figure 7b), and 90° (Figure 7c).

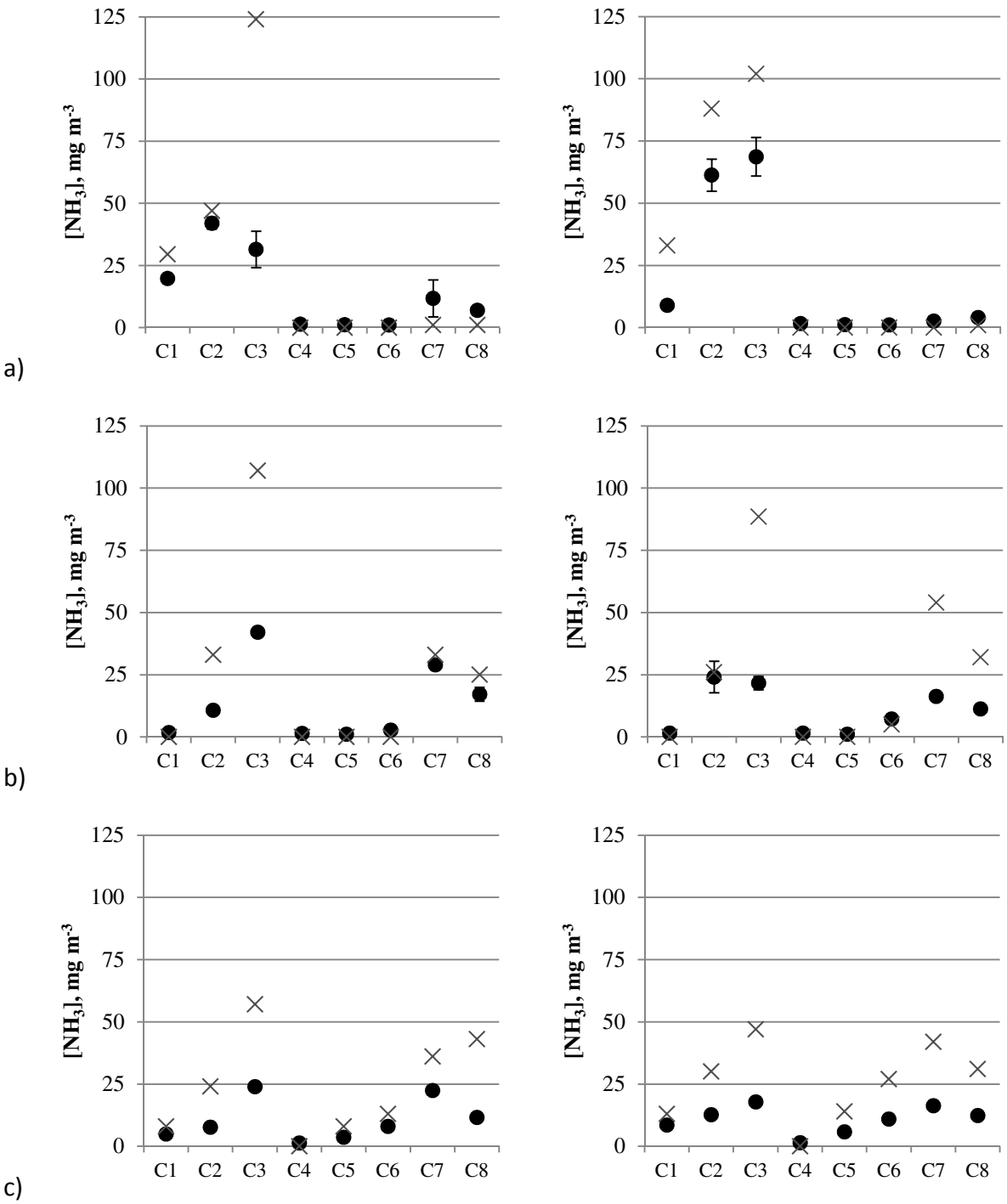

Figure 6 – NH_3 concentrations using deflector angle (a) 0°, (b) 45°, (c) 90°, combined with a headspace height of 0.10 m (left) and 0.90 m (right). The black dots denote the experimental data, with errors bars representing 2x standard deviation. The symbol × denotes the numerical values.

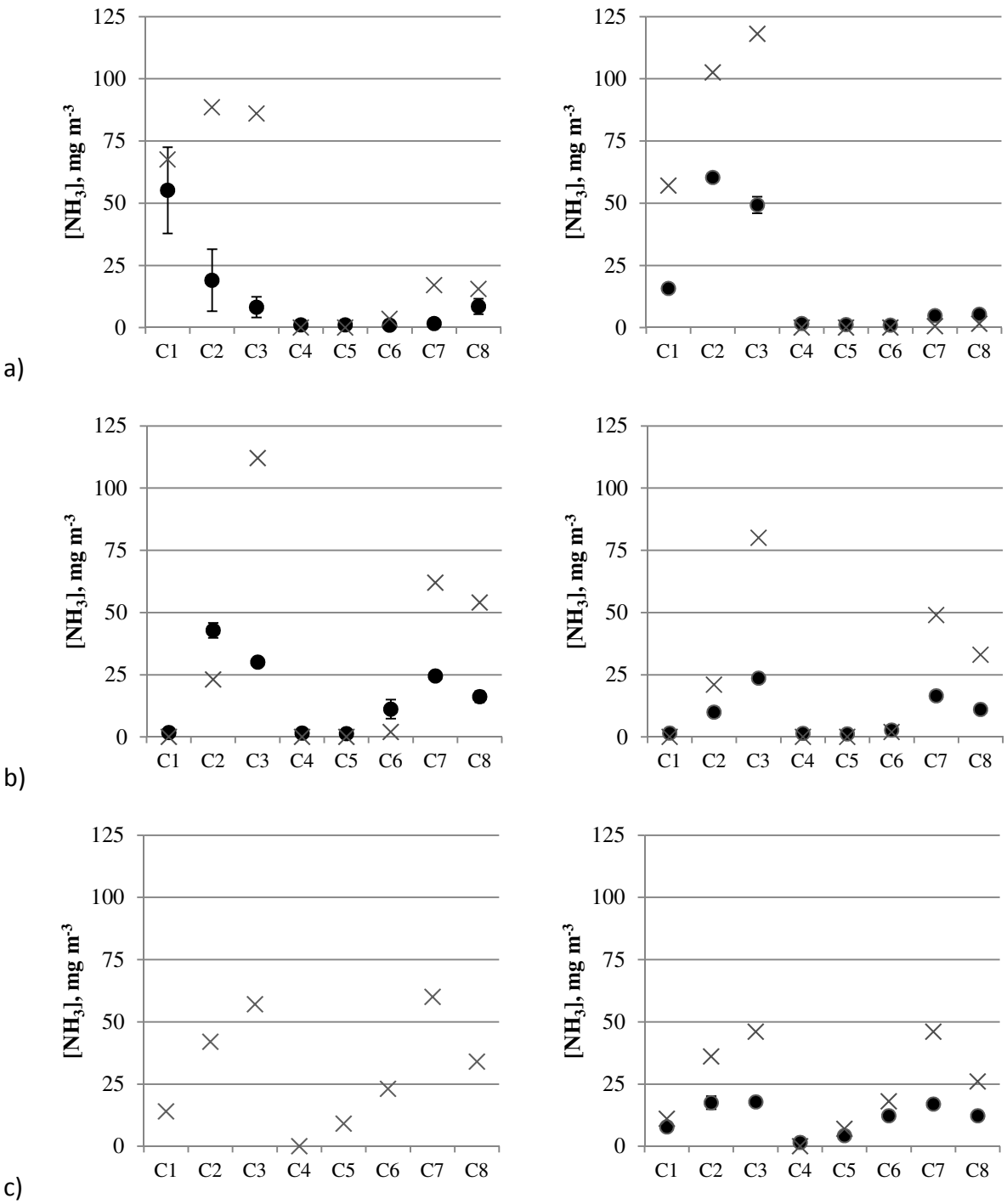

Figure 7 – NH_3 concentrations using deflector angle (a) 0°, (b) 45°, (c) 90°, combined with an airflow rate of 540 $m^3\ h^{-1}$ (left) and 1350 $m^3\ h^{-1}$ (right). The black dots denote the experimental data, with errors bars representing 2x standard deviation. The symbol × denotes the numerical values.

The present results have demonstrated the influence of the airflow rate and direction on the internal NH_3 concentration distribution for an experimental slurry pit section. In practice, high concentration differences can also be found throughout the whole barn. For instance, in recent research by Van Ransbeeck (2013), where sixteen indoor locations were monitored in a pig fattening facility in Oeselgem (Belgium), the highest concentrations were measured at animal height, which can be related to the emission sources (i.e., the slurry pit, wet floors and the animals themselves), followed by the location of the ventilation exhaust. For NH_3, a relative concentration difference of 80% was found between the minimum and maximum concentrations. Furthermore, a clear interaction was seen between ventilation rate and measurement location, indicating the significant effect of the ventilation pattern. Blanes-Vidal et al. (2008) have also shown that gas concentrations in practice are influenced by the ventilation pattern and air velocity over the emitting surfaces. Sun et al. (2002 & 2004) have also demonstrated the variable NH_3 distribution in a hog building, via both experiments and CFD models.

It can thus be concluded that, as in any set-up, the simulated and measured values in the present set-up are sensitive to the exact position, and should therefore be viewed with certain caution. The numerical model showed that the airflow patterns clearly determine the concentration gradients. Therefore, in order to obtain a reference method for the determination of NH_3 emissions, the present set-up should be further optimised. To better capture the emission, a recommendation for future research would be to measure at several more positions near the outlet. This observation should also be taken into account during emission measurements in practice, as mostly only one point location is sampled near an air outlet.

7.3.3. SIMULATED VERSUS MEASURED PIT TRANSFER COEFFICIENTS (*PTCs*)

In Table 3 a comparison between numerical and experimental results is given for all the tested cases, regarding the outlet concentration C_8 and *PTC*s, with an indication of the outcome of linear regressions. It must be noted that in all cases the numerical outlet concentration $C_{8,\ CFD}$ differed from the experimental values $C_{8,\ exp}$. Of course, this has implications regarding the calculation of emission rates and *PTC*'s. In Table 3's last column the ratio of the numerical to the experimental *PTC* value is given as a fraction. This showed underestimations (< 1) for the cases 1, 4 and 10, which used *DA* 0°. This angle resulted in

only a minority of the wind tunnel air passing through the slatted floor, and emitting very little NH_3 at position C_8, while C_8.is a major factor in the calculation of *PTC* (see Equation 1). On the other hand, as more air was guided into the pit, using *DA* 45–90°, complex airflow patterns were formed in the slurry pit, which were likely difficult to model. This was reflected in the overestimation of *PTC* values by the CFD model (50 to 270% higher). However, as the shown contour plots of the vertical NH_3 distribution (Figure 4a-c) suggest, the CFD simulations give the appearance that the experimental sampling position C_8 was situated too far above the wind tunnel floor in order to coincide with the zone of the largest NH_3 concentrations that exit the set-up. If this is indeed the case, this could explain the mostly lower (underestimated) experimental emission rates and *PTC*'s. Nevertheless, this aspect merits further investigation in the emission lab. Furthermore, for control purposes, emission studies in general would all benefit from measurements at several more locations near the outlet.

Table 3 – Numerical and experimentally measured outlet concentrations, *C*, and *PTC* values.

Case	*HH* (m)	*AR* ($m^3\ h^{-1}$)	*DA* (°)	C_s ($mg\ m^{-3}$)	$C_{8,\ CFD}$ ($mg\ m^{-3}$)	$C_{8,\ exp}$ ($mg\ m^{-3}$)	PTC_{CFD} ($m\ s^{-1}$)	PTC_{exp} ($m\ s^{-1}$)	$\frac{PTC_{CFD}}{PTC_{exp}}$
1	0.10	945	0	376	1	7	2.9E-04	2.0E-03	0.1
2	0.10	945	45	367	25	17	7.5E-03	5.1E-03	1.5
3	0.10	945	90	319	43	12	1.5E-02	4.0E-03	3.7
4	0.90	945	0	402	1	4	2.7E-04	1.1E-03	0.2
5	0.90	945	45	398	32	11	8.8E-03	3.1E-03	2.9
6	0.90	945	90	354	31	12	9.6E-03	3.8E-03	2.5
7	0.50	540	0	342	16	8	2.9E-03	1.6E-03	1.9
8	0.50	540	45	393	54	16	8.6E-03	2.6E-03	3.3
9	0.50	540	90	371	34	n/a	5.7E-03	n/a	n/a
10	0.50	1350	0	412	2	5	7.6E-04	2.0E-03	0.4
11	0.50	1350	45	389	33	11	1.3E-02	4.4E-03	3.0
12	0.50	1350	90	371	26	12	1.1E-02	5.1E-03	2.1
				Linear regression:	$R^2 = 0.67$		$R^2 = 0.63$		

7.4. Conclusions and implications

Twelve 3D-CFD simulations of a slurry pit section were performed, to further analyse the airflow patterns and their effect on the NH_3 emissions. Specifically, two pit headspace heights, two airflow rates and three airflow directions were modelled.

(1) CFD modelling results:

Increasing the headspace height during the experiments did not lead to significant effects for the NH_3 concentrations at the measured locations, with the exception of a significantly decreased concentration immediately leeward of the slatted floor. The numerical results did not show clear effects of the headspace height on concentrations at any position, nor on the pit transfer coefficient (*PTC*).

As was observed both experimentally and numerically, guiding more air into the pit by increasing the deflector angle led to decreasing NH_3 concentrations in the pit and increasing concentrations above the slatted floor, which would eventually result in higher emissions. The numerical results also confirmed the experimental finding that the outlet concentrations were significantly reduced by increasing the airflow rate over the slatted floor. Although further improvements are possible, both the numerical model and the experiments confirmed that different airflow rates and directions clearly determine the NH_3 concentration gradient in and above the pit.

(2) Model verification:

In absolute terms, the modelled NH_3 concentrations did not align with the experimentally observed values at the majority of the measurement positions. However, the overall trends between the experimental and numerical results were in line. It was apparent that this outlet concentration, used for emission calculations, was mostly estimated higher by the CFD model than determined experimentally. This could be due to the representativeness of the one-point measurement.

(3) Optimisation of the experimental setup 'EmiL':

Based on the previous notion, EmiL would benefit from measurements at several more locations near the outlet, as would future emission studies in general. In order to further reveal the complex mechanism of NH_3 transfer from the slurry pit, measurements near the solution surface are another point of recommendation.

Furthermore, the present CFD model can quite easily be extended in further research, e.g. by altering the pit and/or room dimensions and the many different manure properties (evaporative emission rate, composition, temperature, etc.). In this way, potential NH_3 abatement techniques can be subjected to quick tests, without the need for extensive experimentation.

CHAPTER 8. GENERAL DISCUSSION

As stated in Chapter 1, the current knowledge and measurement techniques do not allow for accurate estimates of ventilation rates and emissions from naturally ventilated barns, due to the lack of a standard reference method (with emission uncertainties currently considerably higher than 10–20% (Calvet et al., 2013)). Therefore, further research and development are required to develop measurement techniques that are precise enough to validate simulation models (e.g., CFD models) and to obtain more consistent and accurate emission estimates. To meet these requirements, Takai et al. (2013) argued in favour of a better synergy between mathematical modelling, physical modelling and field measurements of ventilation rates.

The complementary use of experimental platforms in this thesis (whether small or large-scale) with computational modelling proved to be a very useful research approach. The applied techniques show similarities with certain other studies in the literature, but included novel measurement methods and parameters.

Several important aspects of natural ventilation and NH_3 mass transfer processes were studied, using experimental set-ups and CFD models. Controlled scale-model experiments highlighted the large effect of the ventilation opening height and wind incidence angle on the internal air velocities and airflow rates. A newly developed 2D CFD model confirmed the trends of the opening height's effect and additionally revealed the internal airflow patterns. An experimental slurry pit section was used to investigate the effect of the pit's headspace height, the air velocity and the airflow direction on the NH_3 mass transfer through a slatted floor. Additionally, a 3D CFD model was developed to provide more insight in the different (mass) flow patterns.

The acquired results are not always directly transferable to practical applications, but although the findings of this thesis are more a proof of concept, they certainly provide a scientific basis for the development of techniques to optimise the indoor climate and give more insight in ways to reduce emissions from animal houses.

The text below features a further discussion of the applied methods, addresses possible shortcomings and limitations, and elaborates on the acquired results. Some overlap may

occur, because CFD modelling was applied for both the small-scale ventilation studies and the NH_3 mass transfer studies in EmiL.

8.1. Small-scale ventilation studies

Chapter 1 illustrated that a proper barn ventilation system should provide the barn with an adequate indoor air quality. It was shown that many factors can influence the airflow rate, such as the wind velocity, the wind incidence angle and the height of the ventilation opening. The latter two have been studied using scale model designs in wind tunnel experiments, to determine their effect on indoor air velocities and airflow rates (Chapters 2 & 3).

With regard to the performed scale-model ventilation experiments, similarities can be found with studies in the literature (see also Chapter 1). For instance, the Canadians Choinière & Munroe (1994) also studied the effect of wind direction, along with multiple barn design characteristics (centre vs side alley, various walls, ridge opening width and length, windows and doors) for a 1:20 scale swine finishing building, but used smoke for visualisation. This allowed for a visualisation of the various airflow patterns, but no quantitative effects could be observed with this method. In our scale-model studies, anemometry did allow for quantification of the relative effects of ventilation opening configurations and wind incidence angles. As mentioned in Chapter 2, the design of the presently used scale models was inspired by the ones used by Verlinde et al. (1998) in the same Ghent I.C.E. wind tunnel. However, using the pressure difference method, they focussed on calculating ventilation coefficients (C_v) for their scale-model cattle barns under circumstances of either 0° or 90° wind incidence, and the presence or absence of ridge spoilers. C_v was logically found to decrease the more the wind impacted on the end walls. In our study, three more wind incidence angles were studied, for two types of naturally ventilated barns (Chapter 3) and they were more directly related to the consequent airflow rates. In Japan, Ikeguchi & Okushima (2001) used anemometry to investigate the effect of roof shape and wind direction on airflows and predicted the resulting contaminant dispersal for 1:30 scale naturally ventilated dairy houses, even including model cows and stalls, but on the other hand they did not study the effects of opening configuration. Later, Ikeguchi et al. (2005) studied airflows and actual contaminant dispersal (using ethylene gas) in scaled naturally

ventilated pig barns. They determined emission effects of the location of the gas-emitting building and the distance towards another (leeward) barn. However, the same barn design was used twice, whereas it would have been very interesting to also include different designs.

In the interpretation of such small-scale studies, care must always be taken that scale effects do not interfere with the representativeness of the airflows. Also, certain practical information is lost in a wind tunnel environment, such as the often strongly fluctuating character of natural winds. With this in mind, wind tunnel experiments do offer many advantages over field experiments, since the wind incidence angle and wind velocity can be controlled (although this could be regarded as compromising on realism).

The here performed wind tunnel studies on ventilation opening height and wind incidence angle, which are essential parameters in natural ventilation systems, do contribute to a better understanding and prediction of the airflow patterns. In general, the results can be considered logical. For instance, a larger windward ventilation opening (inlet) reduced the inlet air velocity, although higher indoor air velocities were observed near the outlet. Additionally, the effects of five different wind incidence angles on the indoor air velocities were quantified. It was shown, for example, that a rotation of the wind incidence angle up to 45° (compared to a wind perpendicular to the lateral ventilation openings) did not seem to alter the internal air velocities greatly. The small changes in air velocities that did occur, could largely be attributed to the relative position of the end walls to the wind direction. Of course, wind that impacted completely on an end wall (90° angle) resulted in a drastically different airflow pattern. The findings that the angle of wind incidence and the size of the ventilation openings determine the incoming airflow rates, the indoor air velocities and the airflow patterns, are not new. However, the added value of our research is in the generation of quantitative data, and so differences between various design options can be better distinguished. Quantitative data are also useful for the development and verification of CFD models, which has been illustrated in Chapter 4 as well as in the recent work of Tabase (2014), where two of our scale-model designs were used in a 3D CFD model (see below, Section 8.3).

Also, only one wind velocity level was implemented in the present studies, i.e., 3.5 m s^{-1}. Lower wind velocities were currently technically not attainable in the used wind tunnel. Higher velocities were mainly excluded due to time constraints, but the experiments have

been set up in such a way that the Reynolds number exceeded the critical level, beyond which the flow patterns become essentially independent of the wind velocity. Linden (1999), for example, stated: “Because separation is a major factor in determining the wind flow around the building, particularly downstream of the windward face, and most buildings have sharp corners, wind speed plays only a minor part in determining the air flow pattern around the building, which is governed by inviscid dynamics. This independence of Reynolds number is, of course, why wind-tunnel modelling has been so successful in determining airflow characteristics.” Therefore, the chosen air velocity was realistic for the practical situation.

In addition to the air velocity, other parameters could be of interest, such as temperature and pressure differences. For instance, temperature differences can give rise to buoyancy (stack effect). This effect that naturally occurs in practice due to temperature differences was not taken into account during the wind tunnel experiments. In a wind tunnel the flow is forced into a channel by an external device, such as a fan. The convection process is then referred to as forced convection and the flow is normally turbulent, as was the case in our wind tunnel set-up. In this situation, the fluid motion created by the density or temperature difference (i.e., the buoyancy-driven motion) is negligibly small as compared to the forced motion of the fluid (Lewis et al., 2004). Furthermore, due to the low height of the scale models, the impact of the stack effect can be entirely neglected. The thermal effects of natural ventilation are therefore to be studied at real scale under natural conditions, or can be modelled.

Another valid reason for not measuring the temperature in the scale models was because eight anemometers were already in place. The introduction of more sensors would have influenced the airflows within the building. Likewise, the possibility of using simultaneous pressure difference sensors was considered. This study illustrated that limited anemometry is already sufficient to explain the different flow patterns.

The scale of the models, which is 1:60 of a typical cattle barn, depended on the height (2.90 m) and width (1.20 m) of the work section in the used wind tunnel. A larger scale model would have caused a corridor effect between the model and the wind tunnel wall (stated by Verlinde et al. (1998), who used the same wind tunnel), with notable effects on the flow pattern at the ventilation inlet and outlet openings. The thickness of the boundary layer of air in the wind tunnel was also of importance. Under natural conditions the cattle building is situated in the boundary layer. For that reason, the scale model also had to be immersed in

the boundary layer of the wind tunnel. The boundary layer was approximately 0.60–0.65 m in height. So, all in all, the scale model could have been higher but not wider or longer, at least not without distorting the proportions of the typical barn that was modelled. It should be noted that the ventilation openings in the scale models were completely open and not covered by a woven windscreen as is typically done in practice. Although this may seem a limitation, it was necessary to distinguish the effect of the opening size on the air velocities. It would also be very difficult to scale the wind screens to such small dimensions.

To summarise, the main contribution of the present scale-model studies to the current state-of-the-art lies in the generation of quantitative data related to different design choices and wind incidence angles. We emphasise that in this age of CFD modelling it is still of essence to compare those models with data from physical set-ups under controlled conditions. Nevertheless, we and the research community in general, are inclined to abandon the scale-model approach in future ventilation studies, for several reasons: due to the relative difficulty of performing certain measurements accurately (such as temperature, pressure differences, gas transfer), the inevitable cost of constructing and/or operating a wind tunnel, especially if one wishes to carry this out properly, and other practical matters (scheduling experiments, building the scale models, etc.). However, the recent emergence of 3D printing in combination with CAD (computer-assisted design) can be expected to accelerate the scale-model building process. But, the raw materials for 3D printers technique are rather expensive.

8.2. NH_3 mass transfer studies at slurry pit level in EmiL

For cattle buildings, there is still limited application of NH_3 emission abatement technologies. In order to find new low emission technologies for naturally ventilated cattle buildings, quantification of ventilation rates and NH_3 emission rates is generally deemed the first key step (Wu, 2012). In the whole, the study of barn emissions is a particularly complex matter. For instance, there exists a multitude of housing types, containing various pollutants and under varying circumstances (notably airflow effects). Thus, it must be viewed as an overall picture. To this end, several building blocks have been provided in this thesis, in order to isolate the key factors. In contrast, macro measurements in commercial barns are particularly expensive to perform, due to the required equipment, maintenance and long

sample times, which can sometimes cover a whole year or more. Nevertheless, they are often required by policy makers for the determination of emission factors (EF), especially for the assessment of potential low-emission systems. But, the error on real-life measurements can be quite high, as previously discussed.

Therefore, in Chapters 5–6, a number of important factors of NH_3 emissions originating from a cow slurry pit have been tested in a highly controlled lab environment. Both the experiments and the coupled CFD model (Chapter 7) confirmed that different airflow rates (translated as near-floor air velocities) and directions clearly determine the NH_3 concentration gradient in and above the slurry pit. Higher air velocities significantly reduced the wind tunnel outlet concentration, but generally led to higher emission rates. Guiding more air into the pit also had clear effects also: a more downward guidance (higher deflector angles) generally led to decreasing NH_3 concentrations in the pit and increasing concentrations above the pit, resulting in higher emissions. In Denmark, Blanes-Vidal et al. (2006) have shown in field experiments with a pig barn that gas (NH_3, CH_4) concentrations were indeed being influenced by the ventilation pattern and air velocity over the emitting surfaces. Two other parameters that explained most of the variability of the NH_3 and CH_4 emissions from the pig barn they studied, were the type of rooting material and the animal activity.

Similar to our work, Buiter et al. (1998) used a 4-m long section of a typical pig building with slurry pit to examine the effects of ventilation rate, slat orientation, and manure depth on the distribution of NH_3 in the airspace above the floor. The orientation of the floor slats generally did not have a significant effect on average ammonia levels in the occupied zones (i.e., above the floor). Increasing the ventilation rate by a factor of 1.8 reduced average levels of NH_3 in the occupied zones by factors ranging from 2 to 8.

Our emission experiments focussed at the slurry pit level, and partly built further on the work of Elzing & Monteny (1997), who utilised real manure and urine. Our integration of a pH-controlled ammonium solutions as a simulator thereof, can be compared with the scale-model experiments of Morsing et al. (2008), Zhang et al. (2008b), Ye et al. (2008a), Rong et al. (2009) and Saha et al. (2010). For instance, the latter investigated the airflow characteristics above an NH_3 release surface at the bottom of a wind tunnel and evaluated the effect of wind tunnel dimensions on the emission and mass transfer process, but they still used small dimensions for the NH_3 release surface (0.60 m × 0.35 m). These small-scale

studies unanimously confirmed the ongoing need for experiments at a larger scale. The novelty value of the here developed emission set-up does not only lie in its larger scale, but also in the use of a real slatted floor, and the ability to control the ammonium solution's pH via automatic buffer dosing. The pH control system was indeed very effective in keeping this most important NH_3 volatilization parameter at the desired level during the total duration of each experiment. Up to this point, no comparable work was found in literature. The emission rate during the exploratory experiment in Chapter 5 was higher than is to be expected in reality, but a high amount of NH_3 was intended for ease of measurement throughout the complete set-up. Also, this emission rate can still be lowered in future studies.

Another added value of the current research is the flexibility to alter the pit's headspace height via a lift table, as well as the airflow rates via a fan, and the airflow direction above the floor via a deflector panel. These different experimental configurations can be regarded as representative of some important phenomena occurring in barns. With this respect, the configurations can refer to manure build-up in the pit and the displacement of NH_3 in the pit headspace by increased airflow rates above the slatted floor or by deflection of airflows into the pit by interior structures of the barn, respectively.

Remarkably, increasing the headspace height did not lead to significant effects for the NH_3 concentrations at seven of the eight measurement locations. The CFD model results confirmed the insignificant effect of the headspace height on the measured NH_3 concentrations. It also became apparent that the outlet NH_3 concentration, used for the calculation of emission rates and pit transfer coefficients (*PTC)*, was very often estimated higher by the CFD model than it was experimentally determined. This could be due to the one-point measurement during the experiments. The developed CFD model in fact revealed a gradient of NH_3 concentrations near the wind tunnel floor. Future emission studies in general would thus benefit from measurements at several more locations near the outlet, in order to become more accurate.

Measurements near the solution surface, e.g. vertical measurements along the gaseous boundary layer, would also be interesting, but involve some practical issues regarding sensor placement near the aqueous solution. For this reason such measurements were not yet performed.

The inclusion of a real-scale slatted floor element in EmiL of course did not warrant a full-scale representation of an animal house, because the dimensions of the wind tunnel section above the floor do not match a real-life barn. Elzing & Monteny (1997) also provided a real-scale slurry pit with slatted floor section, but with a smaller overhead space of 0.5 m^3, as opposed to 1.73 m^3 above our pit section (i.e., not including the wind tunnel sections before and after the slatted floor). Technically, larger dimensions could be introduced to the present set-up, but this would require more time and work. In the present research also no animals, or abstractions thereof, were included. The heat production and its effect on the internal airflow have not been studied yet. Still, the set-up is already a unique and valuable platform for the study of airflows and mass transfer at the slurry pit level.

Where scale-model emission studies in the literature are difficult to validate under real conditions due to the variability in geometries, as well as with geometries in practice, the large-scale experiments of this study have a stronger link to practice.

Of course, it should be noted that the focus of the emission experiments was only on NH_3 originating from the pit. However, the applied techniques can also be considered useful for the study of emissions from soiled floors (as already studied in detail by Wageningen UR in the Netherlands) and for other important gases, possibly even odorous compounds. Many aspects of mass transport as influenced by airflow patterns are comparable, but notable differences between species do exist, e.g. in density. Therefore these components should be studied separately. So, using EmiL, the release of CO_2, CH_4, N_2O or H_2S from manure can also be simulated, either by swapping the used solution or by placing gas cylinders in the pit and/or at floor level. Furthermore, the presently used gas monitoring technique is already able to measure these gases. Of course it is much easier to accomplish this in the developed CFD model, which further demonstrates the value of this modelling technique.

Also, in order to translate the results into practice, it should be noted that the NH_3 emission from a real animal house is the sum of the emission of all the emitting surfaces, which but include multiple puddles and slurry pit sections. Nevertheless, the main findings of the emission lab experiments can already be related to practice, in the light of further mitigation of NH_3 emissions. However, further validation of the results is thoroughly recommended. In other words, additional testing is required, e.g. in commercial barns occupied with animals, so that possible interactions with the barn type and interior, the animal activity or the fluctuating airflow patterns can also be identified. Whereas we have performed stationary

simulations in EmiL and CFD, in reality naturally ventilated barns have the possibility that the ventilation regime turns over and consequently more or less pollutants will be emitted. But, in mechanically ventilated barns, less variation is expected in the airflow rates, meaning there the emission rates will depend more on other factors, like the number of occupying animals, their species, growth stage, etc.

8.3. CFD modelling

Both the ventilation rate and the distribution of gas concentrations in animal houses depend on the external wind and internal airflow patterns, including air velocities and turbulences. Due to the importance of these airflow properties, CFD is often applied to acquire effective solutions for turbulent flow problems. In many different fields of engineering, it can be seen that CFD is more and more becoming a technology that partly or completely replaces experiments. But, the results of a CFD simulation are never 100% reliable because the input data may involve too much guessing or imprecision, the mathematical model of the problem at hand may be inadequate, and the accuracy of the results is limited by the available computing power or the personal usage error, etc. (Versteeg & Malalasekera, 2007). It is therefore highly recommended to maintain a firm interaction between both, such as envisioned in this thesis. Ultimately, this may allow the research to move much faster towards a practical solution. In combination with other studies, the here presented experimental and model results form a meaningful contribution to the state of the art in ventilation and emission research. This knowledge should eventually impact policy, whether local or international.

CFD modelling techniques can specifically be of valuable help in the optimisation of emission measurements. According to the developed CFD model of the Emission Lab (Chapter 7), the set-up can be optimised by adding measurement locations at the emission side (outlet). This finding leads us to recommend precise emission measurements in commercial barns. More generally in the light of the practice, validated CFD models can be used to investigate various parameters in barns and their environment, which in turn will lead to more insight into (natural) ventilation, outdoor air conduction techniques (e.g., shelterbelts), pollutant abatement technologies, etc. The simulation of wind's natural variability does remain computationally complex.

In Chapter 4, the ventilation opening size's effect on the ventilation (as studied in Chapter 2) was compared with the results of a 2D CFD model. A possible shortcoming of the applied two-dimensional modelling approach is the reduced accuracy of the results. Therefore, further 3D modelling of the cases was deemed useful. This has very recently been performed by Tabase (2014) for two of the six scale-model barns, i.e., SM1 and SM4, which are the standard barn and the low-wall barn. Good agreement was found between the 3D model and our published experimental air velocity data (Chapter 2). A point by point comparison led to qualitative R^2 values of 0.97 for SM1, and 0.90 for SM4.

Our CFD modelling approach regarding the ventilation of animal houses can perhaps best be compared with the works of Norton et al. (2010a-d), who used CFD to investigate different ventilation opening conditions and thermal conditions. Norton et al. (2009) also modelled the effect of wind incidence angle of a naturally ventilated barn with different ventilation opening conditions, which in this thesis was only examined through wind tunnel testing. Parallels were found between our wind tunnel tests and their CFD study, regarding the indoor flow pattern. Specifically, it was similarly revealed that under a 30° wind incidence angle, the side of the barn that is blocked from the wind by the end wall, contained a lower-speed wind-driven vortex. This demonstrates the careful attention that should be given to properly ventilate all animal-occupied zones throughout the barn.

The literature review by Bjerg et al. (2013c) further discusses CFD methods to predict NH_3 emission from naturally ventilated buildings and also highlights the importance of an appropriate skill level when using CFD methods. They see the practical use of such methods mainly in research and design, e.g., with respect to low-emission buildings or techniques. Furthermore, these CFD techniques certainly contribute to the understanding of how the control of ventilation openings may influence NH_3 emissions, but they are not yet applicable to on-line (i.e., rapidly varying) control of ventilation systems.

Our developed 3D CFD model of the NH_3 emission lab (Chapter 7) can be related to other CFD studies found in the literature. For example, Norton et al. (2010a-b) modelled airflow patterns and pollutant dispersion in dairy houses, but this remained limited to the animal occupied zone (AOZ) above the floor. Zhang et al. (2008d) performed both experiments and CFD simulations to determine ventilation rates and emissions, but on a small scale. The here presented study of the fluid dynamics of NH_3 under a real slatted floor is thus refreshing, and contributes to the understanding of NH_3 emission from the slurry surface. Additionally, the

full-detail inclusion of a slatted floor into the model was more realistic than other studies (e.g., Sun et al., 2004; Bjerg et al., 2008a-b), in which the slatted floor is usually simulated as a porous medium.

The CFD model of EmiL especially relates to the attempts made to limit the air exchange between the pit headspace and the barn. This model could be seen as a starting point and could therefore be further extended, for instance by incorporating a full-scale barn geometry, other floor types, an enlarged slurry pit section and also using other emitted gases. Other factors that are easily altered in the CFD model are the source solution's pH, temperature and nitrogen content. Additionally, using this model the emission reduction effect of partial pit ventilation or pit curtains could be studied (cfr. Wu, 2012 and Ye et al. 2011, respectively studied in scale-models). It is however not probable that the unidirectional airflow as currently generated in our and their wind tunnel studies are representative enough for the variable draught effects in commercial slurry pits. As discussed, in reality the airflow patterns can fluctuate rapidly (e.g., Takai et al., 2013). Therefore, the additional simulation of varying wind incidences in the CFD model would be advised. A more detailed geometrical description including animals and partitions would also be interesting, but is difficult to model directly in a CFD simulation. The complexity of such a geometry would require very large meshes and a long time to iterate the calculations (Wu, 2012). But, the ongoing advancement in meshing methods should soon alleviate such problems.

Nevertheless, even in their current form the developed CFD models already contain potential benefits for the improvement of barn emission measurement methods, e.g. by revealing optimal measurement locations, since the ease of monitoring at any desired point or section is a great advantage of this technology. Furthermore, as far as NH_3 abatement techniques are airflow-based, CFD-modelling can play an important role as well. With regard to the ongoing search for accurate and practical ventilation rate techniques for naturally ventilated barns, CFD models can definitely help to clarify the results obtained with actual measurement methods.

CHAPTER 9. FRAMEWORK, GENERAL CONCLUSIONS AND RECOMMENDATIONS FOR FUTURE RESEARCH

9.1. Framework

The present research project was a cooperation between Ghent University and Flanders' research institute ILVO. ILVO's department of Agricultural Engineering focuses on innovative and environmentally friendly agricultural systems. The core research activities are development and evaluation of new and existing techniques, as well as their integration, in order to strive for innovative production systems that can support sustainable agriculture and horticulture. The Environmental Engineering research of this department focuses on indoor climate management and environmental safety in and around agricultural buildings. Specifically, airflows, indoor air quality and emissions (especially NH_3, GHG, PM and odour) are measured, evaluated and modelled. The research group's expertise is also called upon for reference services for Flanders' Environment, Nature and Energy Policy Area (LNE). The main research activities are (1) developing and applying measurement techniques and (2) developing and evaluating sustainable management methods (low-emission and/or with a low energy use). Therefore, the topics raised in this thesis tie in with the main objectives of the research group, and include methods that have been applied for the very first time at ILVO (e.g., CFD modelling), and even internationally, such as the large-scale emission lab featuring an automated pH control of the ammonium source solution. The topics considered in this thesis have also garnered a lot of international interest. For instance, the journal *Biosystems Engineering* recently issued the "Special issue on emissions from naturally ventilated livestock buildings" (vol. 116, 2013), in which the challenges associated with emission measurement from naturally ventilated livestock buildings and the future research needs were reviewed. It was stated that "research to understand and then minimise emissions from this type of livestock buildings is vital to ensure the further reduction of atmospheric pollution, particularly as demand for livestock products continues to grow."

The scope of this thesis was precisely to achieve more insight into the complex airflows under naturally ventilated conditions, and NH_3 mass transfer from the slurry pit. Continuous

measurements of air velocities and gas concentrations are difficult in practice, due to the workload, the technical challenges and the considerable costs. Therefore, this thesis included the development of experimental set-ups that allowed controlled studies under steady-state conditions, as well as the development and verification of related CFD models.

Worldwide, the research community tries to convince policy makers to address the need for accurate measurement and assessment techniques for airflow rates and for emissions of NH_3 and GHGs from naturally ventilated barns.

9.2. General conclusions

The experiments that were run in combination with modelling have contributed to a better understanding of a number of key factors. Additionally, it has been proven that controlled wind tunnel experiments are a valuable technique to accomplish this, especially in combination with CFD modelling. In this way, scientifically sound knowledge and practical insights were acquired, which support the optimisation of the ventilation process in naturally ventilated barns (e.g., by placing new animal houses according to the average wind direction that is best suited) and the understanding of (NH_3) emissions from barns (e.g., the effect of near-floor air velocities and direction). However, before the findings can be applied directly in practice, integration with other studies and further validation will be required (see Section 9.3 for future recommendations).

Part I of the research consisted of air velocity measurements in 1:60 scale model designs of a cattle barn at the I.C.E. wind tunnel. Later, the data were coupled with a 2D CFD model.

Ventilation opening experiments (Chapter 2)

The effect of the ventilation opening height on the indoor air velocities was determined for six scale model designs. From these experiments it can be concluded that altering the ventilation opening heights significantly changes the indoor airflows. In practice, farmers already adjust airflow rates by opening or closing ventilation openings using windbreak screens. This study quantitatively shows how influential these adaptations to openings can precisely be. Our results that were obtained under isothermal conditions, i.e. without buoyancy, indicate that enlarging a windward ventilation opening (inlet) will lower the speed of the inlet air, should this be desired, although higher indoor air velocities were observed near the outlet. Enlarging the inlet opening, or completely opening up the wall, led to 40% lower inlet velocities, yet more than 200% higher outlet velocities. The larger inlet opening caused a higher airflow rate, which was subsequently forced through the outlet opening. Noteworthy, at the centre of the house the air velocities were hardly affected by the design. Only in case of removal of the outlet wall, 3–4 times higher velocities were observed at the centre.

Wind incidence angle experiments (Chapter 3)

The effect of five different wind incidence angles on the indoor air velocities has also been investigated. Two of the previously used scale-model barns were included, i.e. the standard barn with relatively small ventilation openings, and the open-type barn (without front nor back wall, only a roof and end walls). The responses in local air velocities could in both designs largely be attributed to the relative position of the end walls towards the wind. This position is crucial and allows the measured air velocity trends to be explained. Upon rotation, the estimated airflow rates through the inlet and outlet openings gradually decreased in both scale models. Linear regressions were presented that relate the measured air velocities to the wind incidence angle, for angles $\leq 45°$. It became clear that, for wind incidence angles < 45°, the open-type barn is better at maintaining the airflow rate between the inlet and the outlet opening. In practice this would mean that naturally ventilated barns with open sidewalls allow for a more uniform indoor airflow distribution. This of course also depends on other ventilation factors, e.g. the wind speed, surrounding constructions, vegetative barriers, etc.

2D CFD model (Chapter 4)

The sets of wind tunnel experiments also provided data for the verification of a CFD model, in which the effect of ventilation opening height was investigated through two-dimensional CFD modelling. The possibility to adequately describe the airflow patterns in the different barn designs was investigated. The CFD model also showed that larger ventilation openings gave rise to lower air velocities near the inlet opening, but higher velocities at the outlet. The model additionally revealed the main airflow paths, showing mainly ceiling-attached airflows in the cross-ventilation barn designs, except for the open-type barn where a straight flow between the inlet and outlet dominated.

A comparison with the experimental data shows there is still some room for improvement in the model, especially at positions featuring low air velocities. Nevertheless, the great advantage of the CFD approach was the ability to visualise the internal airflows for each of the designs. Eventually, this information, supported with other models, may assist in improving barn design and airflow guidance techniques, especially in the light of the development of pollutant abatement technologies. It can indeed be seen more and more that CFD is becoming a technology that partly or completely replaces experiments. It is

however recommended to maintain a firm interaction between both. For instance, where experiments can at some points be difficult to interpret, a complementary CFD model will often help to clarify them. Ultimately, this may allow the research to move much faster towards a practical solution. This should go hand in hand with the ongoing development of accurate measurement methods for the ventilation rate of naturally ventilated barns, which is currently the focus of the related 'NatVent' project (see Section 1.4).

Part II of our research focused on the NH_3 transfer process at slurry pit level, again both using an experimental situation and a (3D) CFD model.

Development and performance check (Chapter 5)

The first objective was to develop a large-scale test installation ('Emission Lab' or 'EmiL') for the study of the NH_3 mass transfer process between a slurry pit and a slatted floor (for cows), but with the important aim to keep the pH of a manure simulator (NH_4Cl solution) constant. The set-up was subjected to a 10-day long test, to evaluate to what extent parameters such as the pH of the NH_4Cl solution and the emitted NH_3 concentrations could effectively be maintained. Furthermore, the pit transfer coefficient (*PTC*) was introduced in order to objectively describe the emission rate. The study showed that the pH of the NH_3 emitting solution could be kept stable as intended at 8.0 ± 0.1. On an average, 7 mg m^{-3} NH_3 was measured at the wind tunnel exhaust, which resulted in a higher emission rate than usually observed in practice, but benefited the ease of measurement. Both the measurement results as a theoretical approach showed that the variation on the *PTC* was limited to 13%. The *PTCs* ranged from 2.1×10^{-3} to maximum 3.3×10^{-3} m s^{-1}, which is well within the range of the similar *AMTC* values found in the literature.

It could be concluded that the test installation was ready to allow other emission experiments with various configurations, e.g., different headspace heights and airflow obstructions at floor level. Also, the airflow rate can easily be set at different levels, which allows for various air velocities over the slatted floor and through the floor slits. Furthermore, other solution pH values could be tested with the automated pH control system. In the next chapter EmiL was indeed valorised by using it as a platform to study the effects of pit headspace height, air velocity and airflow direction at the slatted floor level.

Pit headspace height, air velocity and airflow direction experiments (Chapter 6)

In a next step, the emission lab was used to study the impact of varying headspace heights, air velocities and direction on NH_3 mass transfer from the pit and through a typical cow housing floor. Increasing the **headspace height** did not affect the NH_3 concentrations in the pit but led to significantly lower NH_3 concentrations leeward of the slatted floor. The implication for the practice is that deeper slurry pits would result in lower emission rates. This can be achieved by cleaning regularly, which is a logical mitigation strategy. NH_3 concentrations in the pit were not affected by increasing the **air velocity** above the floor up to 0.65 m s^{-1}. Higher air velocities did significantly reduce the outlet concentrations. However, high ventilation rates are likely to result in high emission rates, which should be avoided if possible. In practice, under-ventilation may of course endanger the indoor air quality, so finding a compromise remains necessary.

Changing the **airflow direction** above the floor led to clear effects. A more downward guidance (higher deflector angles) generally led to decreasing NH_3 concentrations in the pit and increasing concentrations above the pit, resulting in higher emissions. In practice this relates to animals, pen boards or other constructions that might unintentionally deflect incoming air into the pit. Therefore, this should not be neglected in the future research towards low-emission barn design.

In order to obtain a standardised measure for the emission rate during the various experiments, the NH_3 pit transfer coefficient (*PTC*) was calculated. *PTC* was indeed found to decrease with increasing headspace height, but to increase with higher airflow rates and deflector angles. At a deflector angle of 0°, gradually reducing the headspace height led to a linear decrease of the *PTC* by 45%. This trend was also seen at higher deflector angles, but less pronounced. Increasing the deflector angle itself showed an increase in *PTC*, with a maximum value at 45°. Overall, the *PTC*s ranged between 9.8×10^{-4} and 5.1×10^{-3} m s^{-1}. The effects induced by the different experimental setups led to a variation coefficient of 38% for the *PTC*. A general linear model to predict *PTC* values was presented, which explained a large part of the variation (82%) in the observed *PTCs*.

Although mass transfer coefficients such as the *PTC* are characteristically geometry-dependent, the relative effects of the studied factors could clearly be observed, which indicates their potential impact in practice. Consequently, it is highly recommended to carry out related validation studies in commercial barns.

3D CFD model (Chapter 7)

In order to further analyse the airflow patterns and their effect on the NH_3 emissions, three-dimensional CFD simulations of the emission lab experiments were performed. Specifically, two pit headspace heights, two airflow rates and three airflow directions were tested. Increasing the headspace height during the experiments did not lead to significant effects for the NH_3 concentrations at the measured locations, with the exception of a significantly decreased concentration immediately leeward of the slatted floor. The numerical results did not show clear effects at any position. The overall trends between the experimental and numerical results were in line. Guiding more air into the pit by increasing the deflector angle led to decreasing NH_3 concentrations in the pit and increasing concentrations above the slatted floor, which would eventually result in higher emissions. Finally, the outlet concentrations were significantly reduced by increasing the airflow rate over the slatted floor. Also in this case, the numerical results confirmed the experimental finding.

It was apparent that the outlet concentration, used for emission calculations, was mostly estimated higher by the CFD model than determined experimentally. This could be due to the limited representativeness of the one-point measurement during the experiments.

So, although further improvements are possible, both the numerical model and the experiments showed how different airflow rates and directions can affect the NH_3 concentration gradient in and above the pit.

Furthermore, the present CFD model can be extended in further research, e.g. by altering the pit and/or room dimensions and the many different manure properties (evaporative emission rate, composition, temperature, etc.). In this way, potential NH_3 abatement techniques can be subjected to quick tests, without the need for extensive experimentation.

9.3. Recommendations for future research

- After the present scale-model investigations on natural ventilation, the next logical step would embrace full-scale studies, in which both indoor and outdoor airflow measurements are performed. ILVO/Ghent University's ongoing project 'NatVent' already focusses on a full-scale setup in the field, in which detailed measurements of airflow rates are performed under natural field conditions, i.e. with varying wind velocity and direction. Their objective is to obtain a practical measurement technique for airflow rates in commercial naturally ventilated barns. The 'BLESpig' project also includes various airflow and NH_3 measurements inside occupied barns. Furthermore, it will be of special interest and a challenge to integrate these different studies and attempt to validate them in practice.
- The developed emission lab (EmiL) has already proven to be a valuable platform for the study of airflows and mass transfer at the slurry pit level, especially due to the automated pH control of the manure simulator. However, further optimisation of the set-up is still possible, e.g. by using other NH_3 measurement locations, based on the obtained CFD results. For example, measurements near the slurry surface in the pit would offer more insight into the initial NH_3 boundary layer and the further transport. Also, in its current condition the set-up cannot easily be equipped with other floor sections. Information on a broader range of floor types, e.g. solid floors with a limited opening at the side, which is regarded as a low-emission technique, and floors for other animal categories would be of great interest. Furthermore, only the pit emission was studied so far. The release of NH_3 from soiled floors, which is the main source of emission in the barn (60%), could additionally be simulated, for instance by sprinkling EmiL's floor with an ammonium solution or urine/faeces. This could be coupled to the Wageningen UR research on floor emissions. Existing parameters, such as the pH of the solution, could also be varied to study their effect on emissions under various circumstances. Finally, it would be interesting to determine the effect of the incoming air's temperature, using HVAC techniques.
- Future emission studies in commercial barns would benefit from measurements at several locations near the outlets, in order to determine emission rates more

accurately. This is of exceptional importance for the assessment of animal houses' emissions.

- A great advantage of the CFD modelling used in our research, is the ability to generate a broad and detailed view of the parameters of interest (e.g. air velocities, gas concentrations, temperature, pressure) in any geometry. Thus, the NH_3 transfer from the slurry pit could be further analysed in more detail, by using the established CFD model and by altering the pit, floor or room design, the many different manure properties (evaporative emission rate, composition, temperature, etc. Also, the impact of soiled floors can be studied with relative ease. This is of special interest in finding suitable emission abatement strategies. The additional simulation of varying wind incidences in the CFD model would also be advised, in order to address the reality of fluctuating airflow patterns.

LIST OF REFERENCES

Abu-Mulaweh, H.I. (2003). A review of research on laminar mixed convection flow over backward- and forward-facing steps. *International Journal of Thermal Sciences*, 42, 897-909.

Ansys Inc. (2010). *Ansys Fluent theory guide*. Release 13.0, November 2010.

Ad Hoc Committee on Air Emissions from Animal Feeding Operations, Committee on Animal Nutrition, National Research Council (2003). *Air Emissions from Animal Feeding Operations: Current Knowledge, Future Needs*. 286 pp. ISBN-10: 0-309-08705-8. Available online at http://www.nap.edu/catalog.php?record_id=10586 Webpage accessed 20/08/2013.

Albright, L. (1990). *Environment Control for Animals and Plants*. Publ.: American Society of Agricultural Engineers. 453 pp.

Algers, B., Ekesbo, I., Strömberg, S. (1978). Noise measurements in farm animal environments. *Acta Veterinaria Scandinavica supp.* 68, 1-19.

Allen, M.P. & Tildesley, D.J. (1989). *Computer Simulation of Liquids*. Oxford Science Publications. ISBN: 0198556454.

Anders, G.E. (1994). *Predicting natural ventilation induced by the combined thermal buoyancy and wind*, AgEng, Milano, Report No. 94-C-006.

Aneja, V.P., Blunden, J., Roelle, P.A., Schlesinger, W.H., Knighton, R., Niyogi, D., Gilliam, W., Jennings, G. & Duke, C.S. (2008). Workshop on Agricultural Air Quality: State of the science. *Atmospheric Environment*, *42*, 3195-3208.

ApSimon, H.M., Kruse, M., Bell, J.N.B. (1967). Ammonia emissions and their role in acid deposition. *Atmospheric Environment*, 21(9), 1939-1946.

Arogo, J., Zhang, R.H., Riskowski,G.L., Christianson, L.L., Day, D.L. (1999). Mass transfer coefficient of ammonia in liquid swine manure and aqueous solutions. *Journal of Agricultural Engineering Research*, 73(1), 77-86.

ASHRAE (2009). *ASHRAE Handbook.* American Society of Heating, Refrigerating and Air Conditioning Engineers. Atlanta, Georgia, USA.

Asman, W. A. H. (2008). Entrapment of ammonia, odour compounds, pesticide sprays and pathogens by shelterbelts. *DJF Plant Science,* 135.

Banhazi, T. M., Seedorf, J., Rutley, D. L. & Pitchford, W. S. (2008). Identification of risk factors for sub-optimal housing conditions in Australian piggeries - Part III: Environmental parameters. *Journal of Agricultural Safety and Health*, *14*(1), 41-52.

Banhazi, T. M., Rutley, D. L. & Pitchford, W. S. (2010). Validation and fine-tuning of a predictive model for air quality in livestock buildings. *Biosystems Engineering*, *105*(3), 395-401.

Banhazi, T. M., Stott, P., Rutley, D., Blanes-Vidal, V. & Pitchford, W. (2011). Air exchanges and indoor carbon dioxide concentration in Australian pig buildings: Effect of housing and management factors. *Biosystems Engineering*, *110*(3), 272-279.

Barbosa-Saldaña, J.G., Sánchez-Silva, F., Moreno-Pacheco, L.A., Carvajal-Mariscal, I. (2006). Numerical analysis for the flow structures following a three-dimensional horizontal forward-facing step channel. In: *Mecánica Computacional Vol XXV*, pp. 95-108, (Eds.: Alberto Cardona, Norberto Nigro, Victorio Sonzogni, Mario Storti), Santa Fe, Argentina.

Bartzanas, T., Kittas, C., Sapounas, A.A., Nikita-Martzopoulou, Ch. (2007). Analysis of airflow through experimental rural buildings: sensitivity to turbulence models. *Biosystems Engineering*, 97(2), 229-239

Blanes-Vidal, V., Hansen, M.N., Pedersen, S. Rom, H.B. (2008). Emissions of ammonia, methane and nitrous oxide from pig houses and slurry: effects of rooting material, animal activity and ventilation flow. *Agriculture Ecosystems & Environment*, 124, 237-244.

Bianca, W. (1976). The significance of meteorology in animal production. *International Journal of Biometeorology*, 20(2), 139-156.

Bidleman T. F., Helm P. A., Braune B. M., Gabrielsen G. W. (2010). Polychlorinated naphthalenes in polar environments - A review. *Science of the Total Environment*, 408(15), 2919-2935.

Bitog, J. P., Lee, I. B., Hwang, H. S., Shin, M. H., Hong, S. W., Seo, I. H., Kwon, K. S., Mostafa, E. & Pang, Z. Z. (2012). Numerical simulation study of a tree windbreak. *Biosystems Engineering*, 111 (1), 40-48.

Bjerg, B., Kai, P., Morsing, S. & Takai, H. (2004). CFD analysis to predict close range spreading of ventilation air from livestock buildings. *CIGR E-Journal*, volume VI.

Bjerg, B., Zhang, G., Kai, P. (2008a). CFD investigations of a partly pit ventilation system as method to reduce ammonia emission from pig production units. In: Proceedings of the The Eighth ASABE International Livestock Environment Symposium (ILES VIII).

Bjerg B., Zhang, G., Kai, P. (2008b). Porous media as boundary condition for air inlet, slatted floor and animal occupied zone in numerical simulation of airflow in a pig unit. In: Proceedings of the AgEng2008 International Conference on Agricultural Engineering, Hersonissos, Crete-Greece.

Bjerg, B. & Andersen M. (2010). Numerical simulation of a pit exhausts system for reduction of ammonia emission from a naturally ventilated cattle building. In: Proceedings of the XVIIth world congress of the international commission of agricultural and biosystems engineering (CIGR). Quebec, Canada.

Bjerg, B., Cascone, G., Lee, I.-B., Bartzanas, T., Norton, T., Hong, S.-W., Seo, I.-H., Banhazi, T., Liberati, P., Marucci, A., Zhang, G. (2013). Modelling of ammonia emissions from naturally ventilated livestock buildings. Part 3: CFD modelling. *Biosystems Engineering*, 116(3) (Special Issue: "Emissions from naturally ventilated livestock buildings"), 259-275.

Bottcher, R.W., Willits, D.H. & Baughman, G.R. (1986). Experimental analysis of wind ventilation of poultry buildings. *Transactions of the ASAE*, *29*(2), 571-578.

Boulard T., Kittas C., Roy J.C. & Wang S. (2002). Convective and ventilation transfers in greenhouses. Part 2: determination of the distributed greenhouse climate. *Biosystems Engineering*, 83, 129-147.

Boussery, K. (2002). *Natuurlijke ventilatie rundvee: luchtinlaten en bouwmaterialen (English: Natural ventilation for cattle: air inlets and building materials)*. AgriCONSTRUCT. Ventilatie, 2(2), 4 pp.

Boussery, K. & Christiaens, J. (2002). *Wind: bepalende factor voor natuurlijke ventilatie in rundveestallen (English: Wind – key factor for natural ventilation in cattle barns).* In: AgriCONSTRUCT. Ventilatie, 2 (2), 3 p.

Bowman F. M. & Eskelson K. (2009). Thermodynamic consistency of Raoult's Law and Henry's Law approaches for multiphase organic aerosol partitioning. *Journal of Atmospheric Chemistry*, 64(2-3), 179-193.

BPEX (2004). *Environmental Management for Healthy Pig Production*. Meat and Livestock Commission. www.bpex.org.uk

Braam, C. R., Smits, M.C.J., Gunnink, H., Swierstra, D. (1997). Ammonia Emission from a Double-sloped Solid Floor in a Cubic House for Dairy Cows*. Journal of Agricultural Engineering Research*, 68(4), 375-386.

Broucek, J., Letkovicova, M. & Kovalcuj, K. (1991). Estimation of cold stress effect on dairy cows. *International Journal Biometeorology*, 35 (1), 29–32.

Brouk, M.J., Smith, J.F. & Harner, J.P. (2000). Freestal Barn Design and Cooling Systems. In: M. Brouk (ed.), *Heart of America Dairy Management Conference Proceedings*, June 21-22, 2000, St. Joseph, MO.

Buiter, J.J. & Hoff, S.J. (1998). Ammonia distribution in a pit-ventilated confinement building: one-half scale model study. *Transactions of the ASAE*, 41(6), 1817-1827.

Calvet, S., Gates, R.S., Zhang G.-Q., Estellés, F., Ogink, N.W.M., Pedersen, S., Berckmans, D. (2013). Measuring gas emissions from livestock buildings: A review on uncertainty analysis and error sources. *Biosystems Engineering*, 116(3) (Special Issue: "Emissions from naturally ventilated livestock buildings"), 221-231.

Cambra-López, M., Aarnink, A.J.A., Zhao, Y., Calvet, S., Torres, A.G. (2010). Airborne particulate matter from livestock production systems: a review of an air pollution problem. *Environmental Pollution*, 158, 1-17.

Campen J. B. & Bot G. P. A. (2003). Determination of greenhouse-specific aspects of ventilation using three-dimensional computational fluid dynamics. *Biosystems Engineering*, 84 (1), 9-77.

Choinière, Y., Munroe, J.A. & Blais, F. (1988). A wind tunnel study of airflow patterns in a naturally ventilated building. *Canadian Agricultural Engineering*, 30, 293-297.

Choinière, Y. & Munroe, J.A. (1990). Principles for natural ventilation for warm livestock housing. *Canadian Society of Agricultural Engineers*, Paper No. 90-122, 151 Slater St., Ottawa, Ontario.

Choinière, Y. & Munroe, J.A. (1994). A wind tunnel study of wind direction effects on airflow patterns in naturally ventilated swine buildings. *Canadian Agricultural Engineering*, *36*(2), 93-101.

CIGR (1994). Het ontwerp van melkveestallen. Rapport van Sectie II van het CIGR, Werkgroep Nr. 14, Huisvesting van runderen. *Aanbevelingen van het CIGR in verband met huisvesting van melkvee*. Available online at http://www2.vlaanderen.be/landbouw/downloads/dier/31.pdf Webpage accessed 26/08/2013.

Cnockaert, H. & Sonck, B. (2007). Study of the distribution pattern of the ammonia concentration inside a naturally ventilated dairy house. In: Monteny, G.J. & Hartung, E. (eds.), *Ammonia Emissions in Agriculture*. Wageningen Academic Publishers, pp. 354-356.

Cornelis, W.M., Erpul, G. & Gabriels, D. (2004). The I.C.E. wind tunnel for water and wind interaction research. In: S. Visser, W.M. Cornelis (Eds.). *Wind and rain interaction in erosion*. ESW publications, Wageningen, Netherlands. p. 195-224.

Cornelis, W.M. & Gabriels, D. (2005). Optimal windbreak design for wind-erosion control. *Journal of Arid Environments*, *61*, 315-332.

Court, M.N., Stephen, R.C. & Waid, J.S. (1964). Toxicity as a cause of the inefficiency of urea as a fertilizer. *Journal of Soil Science*, 15, 42-48.

Demmers, T. G. M., Burgess, L. R., Phillips, V. R., Clark, J. A., Wathes, C. M. (2000). Assessment of techniques for measuring the ventilation rate, using an experimental building section. *Journal of Agricultural Engineering Research*, 76(1), 71-81.

Demolder H. & Peymen, J. (2012). Natuurindicatoren 2012. Toestand van de natuur in Vlaanderen: cijfers voor het beleid. *Mededeling van het Instituut voor Natuur- en Bosonderzoek (INBO),* M.2012.2, Brussel.

de Vries, G. (2001). Workshop on Mathematical Modelling. Mathematics Symposium: Focus on Applied and Pure Mathematics, June 2001, Edmonton Regional Consortium. Available online at: http://www.math.ualberta.ca/~devries/erc2001/slides.pdf

Dierickx, W., Cornelis, W.M. & Gabriels, D. (2003). Wind tunnel study on rough and smooth surface turbulent approach flow and on inclined windscreens. *Biosystems Engineering*, *86*(2), 151-166.

Dierickx, W., Gabriels, D & Cornelis, W.M. (2001). A wind tunnel study on wind speed reduction of technical textiles used as windscreen. *Geotextiles and Geomembranes*, *19*, 59-73.

Donea, A., Huerta, A. (2003). *Finite Element Method for Flow Problems.* John Wiley & Sons, Chichester.

Drummond, J.G., Curtis, S.E., Simon, J., Norton, H.W. (1980). Effects of aerial ammonia on the growth and health of young pigs. *Journal of Animal Science*, 50, 1085–1091.

EEA (2013). *Air pollution fact sheet 2013 – Belgium.* Available online at http://www.eea.europa.eu/themes/air/air-pollution-country-fact-sheets/belgium-air-pollutant-emissions-country-factsheet/view

Elzing, A. & Monteny, G.J. (1997). Ammonia emission from a scale model of a dairy-cow house. *Transactions of the ASAE*, 40, 713-720.

EPA (Ireland). (2008). *Draft BAT Guidance Note on Best Available Techniques for the Intensive Agriculture Sector*. Available online at http://www.epa.ie/downloads/consultation/Intensive%20Agriculture%20draft%20BAT%20V4%20Jan%202008.pdf Webpage Accessed 15-03-13.

EPA (U.S.) (2013). *Overview of greenhouse gases.* U.S. Environmental Protection Agency, Washington, DC, USA. Available online at http://epa.gov/climatechange/ghgemissions/gases/

EU (1998). Council Directive 98/58/EC of 20 July 1998 concerning the protection of animals kept for farming purposes. *Official Journal of the European Communities*, 20.07.1998, L221-227. Available online at:
http://eur-lex.europa.eu/LexUriServ/LexUriServ.do?uri=OJ:L:1998:221:0023:0027:EN:PDF
Webpage last accessed on 17/12/2013.

European Environment Agency (2012). *Ammonia (NH_3) emissions (APE 003) - Assessment published Dec 2012*. Available online at http://www.eea.europa.eu/data-and-maps/indicators/eea-32-ammonia-nh3-emissions-1/assessment-2 Webpage accessed 20/08/2013.

FAO (2011). *Rural structures in the tropics. Design and development.* Rome.

Fiedler, M., Berg, W., Ammon, C., Loebsin, C., Sanftleben, P., Samer, M., et al. (2013). Air velocity measurements using ultrasonic anemometers in the animal zone of a naturally ventilated dairy barn. *Biosystems Engineering*, 116(3) (Special Issue: "Emissions from naturally ventilated livestock buildings"), 276-285.

Fisk, J.W. & Rosenfeld, A.H. (1997). Estimates of improved productivity and health from better indoor environments. *Indoor Air*, 7(3), 158-172.

Fletcher, C.A.J. (1988). *Computational Techniques for Fluid Dynamics, Vol. 1, Fundamentals and General Techniques.* Springer-Verlag.

Gabriels, D., Cornelis, W., Pollet, I., Van Coillie, T., Ouessar, M. (1997). The I.C.E. wind tunnel for wind and water erosion studies. *Soil Technology*, *10*, 1-8

Gay, S.W. & Knowlton, K.F. (2009). *Ammonia Emissions and Animal Agriculture*. Virginia Cooperative Extension, publication 442-110. Available online at http://pubs.ext.vt.edu/442/442-110/442-110_pdf.pdf Webpage accessed 20/08/2013.

Gebremedhin, K.G. & Wu, B. (2005). Simulation of flow field of a ventilated and occupied animal space with different inlet and outlet conditions. *Journal of Thermal Biology*, *30*, 343-353

Graves, R.E. & Brugger, M. (1995). *Natural Ventilation for Freestall Barns*. Fact Sheet by the Pennsylvania State University, PA 16802, USA. Available online at: http://pubs.cas.psu.edu/freepubs/pdfs/G75.pdf Webpage last accessed on 22/05/2012.

Groot Koerkamp, P. W. G., Metz, J. H. M., Uenk, G. H., Phillips, V. R., Holden, M. R., Sneath, R. W., Short, J. L., White, R. P. P., Hartung, J., Seedorf, J., Schröder, M., Linkert, K. H., Pedersen, S., Takai, H., Johnsen, J. O. & Wathes, C. M. (1998). Concentrations and emissions of ammonia in livestock buildings in Northern Europe. *Journal of Agricultural Engineering Research*, 70 (1), 79-95.

Hahn, G. L. (1999). Dynamic responses of cattle to thermal heat loads. *Journal of Animal Science*, 77(2), 10-20.

Harral, B. B., & Boon, C. R. (1997). Comparison of predicted and measured air flow patterns in a mechanically ventilated livestock building without animals. *Journal of Agricultural Engineering Research*, 66, 221-228.

Hellickson, M.A & Walker, J.N. (1983). Ventilation of Agricultural Structures. Monograph No. 6, *American Society of Agricultural Engineers*, St. Joseph, MI 49085, USA, pp. 81-102.

Herbut, P. & Angrecka, S. (2014). Ammonia concentrations in a free-stall dairy barn. *Annals of Animal Science*, 14(1), 153–166.

Hinz, T. & Linke, S. (1998). A comprehensive experimental study of aerial pollutants in and emissions from livestock buildings. Part 2: Results. *Journal of Agricultural Engineering Research*, 70(1), 119-129.

Hoff, S.J., (2004). Automated control logic for naturally ventilated agricultural structures. *Transactions of the ASAE*, 20(1), 47–56.

Ikeguchi, A. & Okushima, L. (2001). Airflow patterns related to polluted air dispersion in open free-stall dairy houses with different roof shapes. *Transactions of the ASAE*, 44(6), 1797-1805.

Ikeguchi, A., Okushima, L., Zhang, G. & Strom, J.S. (2005). Contaminant air propagation between naturally ventilated scale model pig buildings under steady-state conditions. *Biosystems Engineering*, *90*(2), 217-226.

IPCC (2013). *Climate Change 2013: The Physical Science Basis.* Working Group I contribution to the IPCC 5th Assessment Report. Available online at http://www.ipcc.ch/report/ar5/wg1/#.UlUG5lB7KSp

IPPC (2013). *Best Available Techniques (BAT) Reference Document for the Intensive Rearing of Poultry and Pigs*. Industrial Emissions Directive 2010/75/EU. Integrated Pollution Prevention and Control. European Commission, 854 pp.

Jardinier, P. (1980). Ventilation and free area of openings of the exterior of dwellings. *Cahiers Techniques du Bâtiment*, 27.

Ji, L., Tan, H., Kato, S., Bu, Z. & Takahashi, T. (2011). Wind tunnel investigation on influence of fluctuating wind direction on cross natural ventilation. *Building and Environment*, *46*, 2490-2499.

Jiang, Y., Alexander, D., Jenkins, H., Arthur, R., Chen, Q. (2003). Natural ventilation in buildings: measurement in a wind tunnel and numerical simulation with large eddy simulation. *Journal of Wind Engineering and Industrial Aerodynamics*, *91(3)*, 331-353.

Jones, D.D., Friday, W.H., DeForest, S.S. (1980). *Natural Ventilation for Livestock Housing.* Extension circular - Purdue University, Cooperative Extension Service, AE-97. West Lafayette, IN 47907. Available online at http://www.extension.purdue.edu/extmedia/AE/AE-97.html Webpage Accessed 28-10-13.

Jordan, E. R. (2003). Effects of heat stress on reproduction. *Journal of Dairy Science*, *86*, 104-114.

Jungbluth, T., Hartung, E., Brose, G. (2001). Greenhouse gas emissions from animal houses and manure stores. *Nutrient Cycling in Agroecosystems*, 60, 133-145.

Khan, N., Su, Y. & Riffat, S.B. (2008). A review on wind driven ventilation techniques. *Energy and Buildings, 40*, 1586–1604.

Khanduri, A.C., Stathopoulos, T. & Bédard, C. (1998). Wind-induced interference effects on buildings – a review of the state-of-the-art. *Engineering structures*, *20*(7), 617–630.

Ki Y. Kim, Han J. Ko, Kyung J. Lee, Jae B. Park & Chi N. Kim (2005). Temporal and spatial distributions of aerial contaminants in an enclosed pig building in winter. *Environmental Research*, 99(2), 50-157.

Kim, K.Y., Ko, H.J., Kim, H.T., Kim, Y.S., Roh, Y., Lee, C.M., Kim, C.N. (2008). Quantification of ammonia and hydrogen sulfide emitted from pig buildings in Korea*. Journal of Environmental Management*, 88, 195-202.

Kiwan, A. K., Brunsch, R., Özcan, S. E., Berg, W., & Berckmans, D. (2010). Tracer gas technique in comparison with other techniques for ventilation rate measurements through naturally ventilated barns. In: Proceedings of the CIGR XVIIth World Congress (CSBE100975).

Kiwan, A.K., Berg, W., Fiedler, M., Ammon, C., Gläser, M., Müller, H.J., Brunsch, R. (2013). Air exchange rate measurements in naturally ventilated dairy buildings using the tracer gas decay method with ^{85}Kr, compared to CO_2 mass balance and discharge coefficient methods. *Biosystems Engineering*, 116(3) (Special Issue: "Emissions from naturally ventilated livestock buildings"), 286-296.

KMI (Royal Meteorological Institute, Belgium). (2012). *De maandnormalen te Ukkel (English: The monthly normals in Uccle, Belgium*). Available online at: http://www.kmi.be/meteo/view/nl/360955-Maandelijkse+normalen.html#ppt_5238229 Webpage last accessed on 22/05/2012.

KNMI (2001). *Handboek Waarnemingen.* Available online at: http://www.knmi.nl/samenw/hawa/

Kuijken, E. (2006). *Landschapsecologie en Natuurbehoud (Natuur- en Groenbeheer) (aangepaste versie 2006).* Syllabus 2e Licentie Biologie. Universiteit Gent, Belgium, 179 pp.

Lambert, T.W., Goodwin, V.M., Stefani, D, Strosher, L. (2006). Hydrogen sulfide (H_2S) and sour gas effects on the eye. A historical perspective. *Science of the Total Environment,* 367, 1-22.

Landbouwrapport (2005). Brussel 2006, eerste druk, 240 blz. Depotnummer: Landbouwbeleidsrapport 2005 D/2006/3241/155.

Lane-Serff, G.F. (1989). *Heat flow and air movement in buildings*. PhD thesis. Cambridge University, UK.

Larsen, T.S., Nikolopoulos, N., Strotos, G. & Nikas, K.-S. (2011). Characterization and prediction of the volume flow rate aerating a cross ventilated building by means of experimental techniques and numerical approaches. *Energy and Buildings*, *43*, 1371-1381.

Lee, I, Sase, S., Okushima, L., Ikeguchi, A., Choi, K., Yun, J. (2003). A wind tunnel study of natural ventilation for multi-span greenhouse scale models using two-dimensional particle image velocimetry (PIV). *Transactions of the ASAE*, *46(3)*, 763-772.

Lee, I., Lee, S., Kim, G., Sung, J., Sung, S., Yoon, Y. (2005). PIV verification of greenhouse ventilation air flows to evaluate CFD accuracy. *Transactions of the ASAE*, *48(6)*, 2277-2288.

Lewis, R.W., Nithiarasu, P., Seetharamu, K.N. (2004). *Fundamentals of the Finite Element Method for Heat and Fluid Flow*. Publ.: John Wiley & Sons, Ltd. ISBNs: 0-470-84788-3 (HB); 0-470-84789-1 (PB).

Linden, P.F. (1999). The fluid mechanics of natural ventilation. *Annual Review of Fluid Mechanics*, *31*, 201-238.

LNE (2006). *NEC reduction programme Belgium*. Departement Leefmilieu, Natuur en Energie, Belgium. Available online at http://www.lne.be/themas/luchtverontreiniging/6nec-programma_belgie_2006.pdf Webpage accessed 03/09/2013.

LNE (2013). *Instrumenten inzetten voor de realisatie van de instandhoudingsdoelstellingen*. Available online at http://www.lne.be/themas/beleid/mina4/leeswijzer/projecten/ihd/instrumenten-inzetten-voor-de-realisatie-van-de-instandhoudingsdoelstellingen Webpage accessed 25/09/2013.

Maton, A., Daelemans, J., Lambrecht, J. (1985). *Housing of animals*. Elsevier Science Publishing Company Inc. ISBN: 0-444-42528-4.

McCutcheon, G. (2013). Energy use on Irish pig farms. In: *Conference Proceedings of the Pig Farmers' Conference*. October 23-24, 2012, Thurles and Cavan, Ireland.

McGinn, S.M., Janzen, H. H. & Coates, T. (2003). Atmospheric Ammonia, Volatile Fatty Acids, and Other Odorants near Beef Feedlots. *Journal of Environmental Quality*, 32, 1173-1182.

Monteny, G.J. & Erisman, J.W. (1998). Ammonia emission from dairy cow buildings: a review of measurement techniques, influencing factors and possibilities for reduction. *NJAS Wageningen Journal of Life Sciences*, 46(3/4).

Monteny, G. J., M. C. J. Smits, G. Van Duinkerken, H. Mollenhorst, I. J. M. De Boer. (2002). Prediction of ammonia emission from dairy barns using feed characteristics part II:

Relation between urinary urea concentration and ammonia emission. *Journal of Dairy Science*, 85(12), 3389-3394.

Morsing, S., Ikeguchi, A., Bennetsen, J.C., Strøm, J.S., Ravn, P. & Okushima, L. (2002). Wind induced isothermal airflow patterns in a scale model of a naturally ventilated swine barn with cathedral ceiling. *Applied Engineering in Agriculture*, 18(1), 97-101.

Morsing, S., Strøm, J.S, Zhang, G., Kai, P. (2008). Scale model experiments to determine the effects of internal airflow and floor design on gaseous emissions from animal houses. *Biosystems Engineering*, 99, 99-104.

Müller, H.-J., Möller, B., Wanka, U., Heidenreich, T., Erik, V., Ozcan, S. E., et al. (2007). Measuring methods of determination of air exchange rates and ammonia emission mass flows in naturally ventilated livestock buildings. In G. Monteny (Ed.), International ammonia conference in agriculture. Wageningen, Netherlands: Wageningen Academic Publishers.

NEC Directive (2001). Directive 2001/81/EC of the European Parliament and of the Council of 23 October 2001 on national emission ceilings for certain atmospheric pollutants. *Official Journal of the European Communities*, 27.11.2001, L309, 22-30. Available online at http://eur-lex.europa.eu/LexUriServ/LexUriServ.do?uri=OJ:L:2001:309:0022:0030:EN:PDF Webpage accessed 20/08/12.

Ni, J. (1999). Mechanistic models of ammonia release from liquid manure: a review. *Journal of Agricultural Engineering Research*, 72, 1-17.

Ni, J.-Q., Heber, A.J., Diehl, A.J., Lim, T.T. (2000). Ammonia, hydrogen sulphide and carbon dioxide release from pig manure In under-floor deep pits. *Journal of Agricultural Engineering Research*, 77(1), 53-66.

Nieuwejaers, B., De Splenter, N., Knight, D., Lauwereins, S., Meulepas, P., Van Laer, G., Van Mierlo, T. en Goossens, A. (2004). *NEC-reductieprogramma – Emissiereductie-programma voor het Vlaamse Gewest voor de polluenten SO2 , NOx , VOS en NH3 in het kader van Richtlijn 2001/81/EG. (English: NEC reduction programme – Emission reduction programme for Flanders, for the pollutants SO2 , NOx , VOC and NH3 in the context of Guideline 2001/81/EG.)* Ministerie van de Vlaamse Gemeenschap, Departement Leefmilieu en Infrastructuur, Administratie Milieu-, Natuur-, Land- en Waterbeheer, Afdeling Algemeen Milieu- en Natuurbeleid, Sectie Lucht. Publisher: Jean-Pierre Heirman,

Ministerie van de Vlaamse Gemeenschap, AMINAL, Koning Albert II-laan 20, bus 8, 1000 Brussels, Belgium.

Nikas, K.-S. P., Nikolopoulos, N., Nikolopoulos, A. (2009). Numerical study of a naturally cross-ventilated building. *Energy and Buildings, 42(4),* 1191-1202.

Nikolopoulos A., Nikolopoulos N., Larsen, T.S., Nikas, K.-S. (2012). Experimental and numerical investigation of the tracer gas methodology in the case of a naturally cross-ventilated building. *Building and Environment*, *56*, 379-398.

Norton, T., Sun, D.W., Grant, J., Fallon, R. & Dodd, V. (2007). Applications of computational fluid dynamics (CFD) in the modelling and design of ventilation systems in the agricultural industry: a review. *Bioresource Technology*, *98*, 2386-2414.

Norton, T., Grant, J., Fallon, R. & Sun, D.-W. (2009) Assessing the ventilation effectiveness of naturally ventilated livestock buildings under wind dominated conditions using computational fluid dynamics. *Biosystems Engineering*, *103*, 78-99.

Norton, T., Grant, J., Fallon, R., Sun, D-W. (2010a). Assessing the ventilation performance of a naturally ventilated livestock building with different eave opening conditions. *Computers and Electronics in Agriculture*, 71, 7-21.

Norton, T., Grant, J., Fallon, R., Sun, D-W. (2010b). A computational fluid dynamics study of air mixing in a naturally ventilated livestock building with different porous eave opening conditions. *Biosystems Engineering*, 106, 125-137.

Norton, T., Grant, J., Fallon, R., Sun, D-W. (2010c). Optimising the ventilation configuration of naturally ventilated livestock buildings for improved indoor environmental homogeneity. *Building and Environment*, 45, 983-995.

Norton, T., Grant, J., Fallon, R., Sun, D-W. (2010d). Improving the representation of thermal boundary conditions of livestock during CFD modelling of the indoor environment. *Computers and Electronics in Agriculture*, 73, 17-36.

Ogink, N.W.M. & Kroodsma, (1996). Reduction of ammonia emission from a cow cubicle house by flushing with water or a formalin solution. *Journal of Agricultural Engineering Research*, 63, 197-204.

Ogink, N.W.M. & Aarnink, A.J.A. (2003). Managing Emissions from Swine Facilities: Current situation in The Netherlands and Europe. *Proceedings of the University of Illinois Pork Industry*. Available online at:

http://www.livestocktrail.uiuc.edu/sowm/paperDisplay.cfm?ContentID=6526 Webpage last accessed on 22/05/2012.

Ogilvie, J.R. & Boyd, K.G. (1985). Tracer gas analysis of ventilation due to wind in models of a modified open-fronht (MOF) swine finishing barn. *CSAE Paper,* No. 85-413, Saskatoon.

Ogink, N., Ogink, N. W. M., Mosquera, J., Calvet, S., Zhang, G. (2013). Methods for measuring gas emissions from naturally ventilated livestock buildings: developments over the last decade and perspectives for improvement. *Biosystems Engineering*, 116(3) (Special Issue: "Emissions from naturally ventilated livestock buildings"), 297-308.

Ozcan, S. E., & Berckmans, D. (2010). A critical evaluation of the accuracy of tracer gas measurements in ventilated spaces. In: Proceedings of the CIGR XVIIth World Congress (CSBE100467).

Ozcan, S. E. (2011). *Techniques to determine ventilation rate and airflow characteristics through naturally ventilated buildings.* Dissertation, Katholieke University Leuven.

Pankow J. F. (1994). An Absorption-Model of Gas-Particle Partitioning of Organic-Compounds in the Atmosphere. *Atmospheric Environment*, 28(2): 185-188.

PCM (2008). *Hoe omgaan met ammoniak, geur en (fijn) stof in de veeteelt?* (English: How to deal with ammonia, odour and particulate matter in cattle rearing?) Provinciaal Centrum voor Milieuonderzoek, dienst Landbouw en Platteland, Gent, Belgium. Depotnummer: D/2008/5139/18.

Pedersen, S., Takai, H., Johnsen, J.O., Metz, J.H.M., Koerkamp, P.W.G.G., Uenk, G.H., Phillips, V.R., Holden, M.R., Sneath, R.W., Short, J.L., White, R.P., Hartung, J., Seedorf, J., Schroder, M., Linkert, K.H., Wathes, C.M. (1998). A comparison of three balance methods for calculating ventilation rates in livestock buildings. *Journal of Agricultural Engineering Research*, 70(1), 25-37.

Philippe, F.X., Cabaraux, J.F., Nicks, B. (2011). Ammonia Emissions from Pig Houses: Influencing Factors and Mitigation Techniques. *Agriculture, Ecosystems and Environment,* 141, 245-260.

Pollet, I. (2009). *Agrarische constructies*. Syllabus 1e Master in de Bio-ingenieurswetenschappen. Vakgroep Biosysteemtechniek, Universiteit Gent, Belgium.

Pope, S.B. (2003) *Turbulent Flows*. Cambridge University Press.

Preller, L. (1995). *Respiratory health effects of pig farmers. Assessment of exposure and epidemiological studies of risk factors*. PhD thesis, Agricultural University Wageningen, pp.173.

Pronk, A., Ogink, N., Holterman, H. J., Hofschreuder, P. & Vermeij, I. (2013). *Effecten van groenelementen op de luchtkwaliteit*. Plant Research International, rapport 493, Wageningen UR.

Quarteroni, A. (2009). Mathematical Models in Science and Engineering. *Notices of the AMS*, 56(1), 10-19.

Radon K., Danuser B., Iversen M., Monso E., Weber C., Hartung J., Donham K. J., Palmgren U. & Nowak D. (2002). Air contaminants in different European farming environments. *Annals of Agricultural and Environmental Medicine*, 9, 1-48.

Ravagnolo, O. & Misztal, I. (2000). Genetic component of heat stress in dairy cattle, parameter estimation. *Journal of dairy science*, *83*, 2126-2130.

Retz, S. K., Georg, H., Godbout, S., Van den Weghe, H. F. A. (2010). Impact of the manure removal from slatted floor in a dairy barn on the ammonia emission. In: Proceedings of the CIGR XVIIth World Congress (CSBE100616).

Roeloffs, J. G. L. & Houdijk, A. L. M. (1991). Ecological effects of ammonia. In: *Ammonia and Odour Emission from Livestock Production* (Nielson, V C; Pain, B F; Hartung, J, eds), pp 10–16. Elsevier Applied Science, London.

Rong, L., Nielsen, P.V., Zhang, G. (2009). Effects of airflow and liquid temperature on ammonia mass transfer above an emission surface: experimental study on emission rate. *Bioresource Technology*, 100, 4654-4661.

Saha, C.K., Zhang, G., Ni, J.-Q. (2010). Airflow and concentration characterisation and ammonia mass transfer modelling in wind tunnel studies. *Biosystems Engineering*, 107, 328-340.

Sapounas, A.A., Campen, J.B., Smits, M.C.J., Dooren, H.J.C. (2009). Simulating the effect of forced pit ventilation on ammonia emission from a naturally ventilated cow house with CFD. In: *4th European Conference on Precision Livestock Farming*; Precision livestock farming 09; 81-90.

Savardekar K. (1990). *Aspects of passive cooling. A study on natural ventilation*. MPhil thesis. Cambridge University, UK.

Schild, P.G. & Mysen, M. (2009). *Recommendations on specific fan power and fan system efficiency*. AIVC Technical Note 65. Air Information and Ventilation Centre, Belgium.

Scholtens, R. & Van 't Ooster, A. (1994). Performance and accuracy of methods for measuring natural ventilation rates and ammonia emissions. In: *Proceedings of the International Conference on Agricultural Engineering*, AGENG '94. 240 pp.

Schrade, S., K. Zeyer, L. Gygax, L. Emmenegger, E. Hartung, M. Keck. (2012). Ammonia emissions and emission factors of naturally ventilated dairy housing with solid floors and an outdoor exercise area in Switzerland. *Atmospheric Environment*, 47, 183-194.

Schuurkes, J.A.A.R. & Mosello, R. (1998). The role of external ammonium inputs in freshwater acidification, *Aquatic Sciences*, *50*(1), 71-86

Seppänen, O.A., Fisk, W.J. en Mendell, M.J. (1999). Association of ventilation rates and CO2 concentrations with health and other responses in commercial and industrial buildings. *Indoor Air*, 9, 226-52.

Shearer, J.K., Beede, D.K., Bucklin, R.A. & Bray, D.R. (1991). Environmental Modifications to Reduce Heat Stress in Dairy Cattle. *Agri-Practice*, *12*(4).

Scheffé, H. (1959). *The Analysis of Variance*. Wiley, New York. (reprinted 1999, ISBN 0471345059)

Shames, I.H. (1982). *Mechanics of fluids*. Publisher: McGraw-Hill.

Silanikove, N. (2000). Effects of heat stress on the welfare of extensively managed domestic ruminants. *Livestock Production Science*, 67, 1-18.

Smith, H. J., Boon, C. R., Webster, A. J. F., & Wathes, C. M. (1999). Measurements of the effect of animals on airflow in an experimental piggery. *Journal of Agricultural Engineering Research*, 72, 105-112.

Snell, H.G.J., Seipelt, F., Van den Weghe, H.F.A. (2003). Ventilation rates and gaseous emissions from naturally ventilated dairy houses, *Biosystems Engineering*, *86*(1), 67-73.

Snoek, D.J.W., Ogink, N.W.M., Stigter, H., Groot Koerkamp, P.W.G. (2012). Sensitivity analysis of a mechanistic model for the ammonia emission of dairy cow houses. In: Proceedings of the Ninth International Livestock Environment Symposium, Valencia, Spain, July 8 - 12, 2012.

Sørensen, D.N. & Nielsen, P.V. (2003). Quality control of computational fluid dynamics in indoor environments. *Indoor Air*, 13, 2-17.

Spalding, D.B. (1972). A novel finite difference formulation for differential equations involving both first and second derivatives. *International Journal for Numerical Methods in Engineering*, 4, 551-559.

Spoolder, H.A.M., Edwards, S.A., Armsby, A.W. & Corning, S. (2000). A within farm comparison of three different housing systems for finishing pigs. In: *Proceedings of the First International Conference on Swine Housing*, Des Moines, Iowa, pp. 40-48.

St-Pierre, N., Cobanov, B. & Schnitkey, G. (2003). Economic losses from heat stress by U.S. livestock industries. *Journal of Dairy Science*, 86, 52-77.

Stevens, R. (2007). Verse lucht bij de varkens: zes inlaatsystemen met eigen eisen. *Boerderij/Varkenshouderij*, 92(19), 4-7.

Strøm, J.S., (1978). *Heat loss from cattle, swine and poultry as basis for design of environmental control systems in livestock buildings*. Danish Research Institute, Denmark.

Swierstra, D., Smits, M.C.J., Kroodsma, W., (1995). Ammonia Emission from Cubicle Houses for Cattle with Slatted and Solid Floors. *Journal of Agricultural Research*, 62, 127-132.

Sun, H., Stowell, R.R., Keener, H.M., Michel, F.C.-Jr. (2002). Two–dimensional computational fluid dynamics (CFD) modeling of air velocity and ammonia distribution in a High–Rise™ hog building. *Transactions of the ASAE*, 45(5), 1559–1568.

Sun, H., Keener, H.M., Deng, W., Michel, F.C.-Jr. (2004). Development and Validation of 3-D CFD Models to Simulate Airflow and Ammonia Distribution in a High-Rise™ Hog Building during Summer and Winter Conditions. *Agricultural Engineering International: the CIGR Journal of Scientific Research and Development*. Manuscript BC 04 004, vol. VI.

Tabase, R.K. (2014). *Climate change adaptation of pig buildings: development of novel designs and energy conservation strategies to reduce carbon footprint*. Mphil thesis. Department of engineering, Harper Adams University, Newport, United Kingdom.

Takai, H., Nimmermark, S., Banhazi, T., Norton, T., Jacobson, L.D., Calvet, S., Hassouna, M., Bjerg, B., Zhang, G.-Q., Pedersen, S., Kai, P., Wang, K., Berckmans, D. (2013). Airborne pollutant emissions from naturally ventilated buildings: Proposed research directions. *Biosystems Engineering*, 116(3) (Special Issue: "Emissions from naturally ventilated livestock buildings"), 214-220.

Tamminga, S. (1992). Gaseous Pollutants Produced by Farm Animal Enterprises. In: *Farm Animals and the Environment*. Phillips C., Piggins, D. (Eds). CAB International, pp. 345-357.

Taylor, C., Hughes, T.G. (1981). *Finite Element Programming of the Navier-Stokes Equations*. Pineridge Press Ltd., Swansea.

Teye, F.K., Hautalla, M. (2008). Adaptation of an ammonia volatilization model for a naturally ventilated dairy building. *Atmospheric Environment*, 42, 4345–4354.

van 't Klooster, C.E. (1994). *Implementation of natural ventilation in pig houses*. PhD thesis, Wageningen, ISBN 90-5485-285-2.

Van 't Ooster, A. (1994). Using natural ventilation theory and dynamic heat balance modelling for real time prediction of ventilation rates in naturally ventilated livestock houses. In: *Proceedings of the International Conference on Agricultural Engineering*, AGENG '94, 206-207.

Van Buggenhout, S., Eren Özcan, S., Vranken, E., Van Malcot, W. & Berckmans, D. (2007). Acoustical ventilation rate sensor concept for naturally ventilated buildings. *Transactions of ASHRAE*, 113(2), 192-199.

Van Buggenhout, S., Van Brecht, A., Eren Özcan, S., Vranken, E., Van Malcot & W., Berckmans, D. (2009). Influence of sampling positions on accuracy of tracer gas measurements in ventilated spaces. *Biosystems Engineering, 104*, 216-223.

Vande Ryse, L., de Hulster, A., Depraetere, D., Dieleman, W., Dochy, O., Mahieu, J., Mermuys, K., Storme, K., Verdonckt, P. & Willemsen, J. (2007). *Boeren bouwen aan het landschap*. Interreg IIIa-project.

Vandille, G. & Janssen, L. (2012). De Belgische milieurekeningen - Milieu-economische rekeningen 1990-2008., Federaal Planbureau, Planning Paper 111, pp. 43-44. Available online at http://www.plan.be/publications/publication_det.php?lang=en&TM=30&IS=63&KeyPub=1156 Webpage accessed 20/08/13.

Van Ransbeeck, N. (2013). *Particulate matter, ammonia and greenhouses gases in pig fattening facilities: measuring strategies, indoor concentrations and emissions.* PhD thesis. Ghent University, Belgium.

van Wagenberg, A., Bjerg, B., Bot, G. (2004). Measurement and simulation of climatic conditions in the animal occupied zone in a door ventilated room for piglets. *Agricultural Engineering International: the CIGR Journal of Scientific Research and Development*. Manuscript BC 03 020. April, 2004.

Verlinde, W., Gabriels, D. & Christiaens, J.P.A. (1998). Ventilation coefficient for wind-induced natural ventilation in cattle buildings: a scale model study in a wind tunnel. *Transactions of the ASAE*, *41*(3), 783-788.

Venkatram, A., Shiva Nagendra, S.M. en Amita, T., (2003). Comparison and performance evaluation of CFD based numerical model and Gaussian based models for urban air quality prediction. In: *Proceedings of the 96th Annual Conference and Exhibition of Air and Waste Management Association*, San Diego, California, USA, June 23-25,2003.

Versteeg, H.K. & Malalasekera, W. (2007). *An Introduction to Computational Fluid Dynamics - the finite volume method*. Second edition. Publ.: Pearson Education Limited, Essex, England.

VLM (2013). *Emissiearme stallen (English: Low-emission barns).* Available online at http://www.vlm.be/SiteCollectionDocuments/Mestbank/Emissiearme%20stallen/mb_stallen_.pdf Webpage accessed 03/09/2013.

VMM (2011). *Lozingen in de lucht 1990–2011 (English: Atmospheric emissions 1990–2011).*

Weeks, C.A. (2008). A review of welfare in cattle, sheep and pig lairages, with emphasis on stocking rates, ventilation and noise. *Animal Welfare, 17*(3), 275-284.

West, D.L. (1977). Contaminant dispersion and dilution in a ventilated space. *ASHRAE Transactions*, 83(1), 125-140.

West, J.W. (2003). Effects of heat-stress on production in dairy cattle. *Journal of Dairy Science*, *86*(6), 2131-2144.

Wu, W. (2012). *Modelling and reducing gas emissions from naturally ventilated livestock buildings.* Technical report BCE-TR-2, Department of Engineering, Aarhus University. Denmark. 151 pp.

Wu, W., Kai, P., Zhang, G. (2012a). An assessment of a partial pit ventilation system to reduce emission under slatted floor – Part 1: Scale model study. *Computers and Electronics in Agriculture*, 83, 127-133.

Wu, W., Zhai, J., Zhang, G., Nielsen, P.V. (2012b). Evaluation of methods for determining air exchange rate in a naturally ventilated dairy cattle building with large openings using computational fluid dynamics (CFD). *Atmospheric Environment,* 63, 179–188.

Wu, W., Zhang, G., bjerg, B., Nielsen, P.V. (2012c) An assessment of a partial pit ventilation system to reduce emission under slatted floor – Part 2: Feasability of CFD prediction using RANS turbulence models. *Computers and Electronics in Agriculture*, 83, 134-142.

Ye, Z., Zhang, G., Li, B., Strøm, J.S., Tong, G., Dahl, P.J. (2008a). Influence of airflow and liquid properties on the mass transfer coefficient of ammonia in aqueous solutions. *Biosystems Engineering*, 100, 422-434.

Ye, Z., Zhang, G., Li, B., Strøm, J.S., Dahl, P.J. (2008b). Ammonia emissions affected by airflow in a model pig house: effects of ventilation rate, floor slat opening, and headspace height in a manure storage pit. *Transactions of the ASABE*, 51(6), 2113-2122.

Ye, Z., Zhang, G. Seo, I.-H., Kai, P. Saha, C.K., Wang, G. Li, B. (2009a). Airflow characteristics at the surface of manure in a storage pit affected by ventilation rate, floor slat opening, and headspace height. *Biosystems Engineering*, 104, 97-105.

Ye, Z., Saha, C.K., Li, B., Tong, G., Wang, C., Zhu, S. Zhang, G. (2009b). Effect of environmental deflector and curtain on air exchange rate in slurry pit in a model pig house. *Biosystems Engineering*, 104, 522-533.

Ye, Z., Zhu, S., Kai, P., Li, B., Blanes-Vidal, V., Pan, J., Wang, C., Zhang, G. (2011). Key factors driving ammonia emissions from a pig house slurry pit. *Biosystems Engineering*, 108, 195-203.

Yu, H., Hou, CH. en Liao, CM. (2002). Scale model analysis of opening effectiveness for wind-induced natural ventilation openings*. Biosystems Engineering*, 82, 199-207.

Zhang, J.S., Janni, K.A. & Jacobson, L.D. (1989). Modeling Natural Ventilation Induced by Combined Thermal Buoyancy and Wind. *Transactions of the ASAE*, 32(6), 2165-2174.

Zhang, G., Morsing, S, Bjerg, B., Svidt, K., Strøm, J.S. (2000). Test room for validation of airflow patterns estimated by Computational Fluid Dynamics. *Journal of Agricultural Engineering Research*, 76, 141-148.

Zhang G., Strom, J.S., Li, B., Rom, H.B., Morsing, S., Dahl, P., Wang C. (2005). Emission of ammonia and other contaminant gases from naturally ventilated dairy cattle buildings. *Biosystems Engineering*, 92(3), 355–364.

Zhang, Y., Wu, S.-Y., Krishnan, S., Wang, K. Queen, A., Aneja, V.P., Arya, S.P. (2008a). Modeling agricultural air quality: Current status, major challenges, and outlook. *Atmospheric Environment*, 42, 3218–3237.

Zhang, G., Bjerg, B., Strøm, J.S., Morsing, S., Kai, P., Tong, G., Ravn, P. (2008b). Emission effects of three different ventilation control strategies–a scale model study. *Biosystems Engineering*, 100, 96-104.

Zhang, G., Tong, G., Ravn, P., Rong, L., Nielsen, P. (2008c). Effect of environmental deflector on air exchange in slurry pit and concentration distribution in a two-dimensional ventilation chamber. *Proceedings of the International Conference on Agricultural Engineering*, Hersonissos, Crete, Greece, 23-25 June 2008.

Zhang, G., Bjerg, B., Strøm, J.S., Kai, P. (2008d). Reducing odor emission from pig production buildings by ventilation control. *Proceedings of the 31 August - 4 September 2008 Conference (Iguassu Falls, Brazil)*. ASABE Publication Number 701P0408. Available online at: https://elibrary.asabe.org/abstract.asp?aid=25570&t=2

CURRICULUM VITAE

PERSONAL DATA

Name	**Merlijn De Paepe**
Date of birth	July 5th, 1984
Place of birth	Ghent
Nationality	Belgian
Address	Nekkersputstraat 128, 9000 Gent, Belgium
E-mail	merlijn@telenet.be

EDUCATION

2009 – 2014	Doctoral Schools of Bioscience Engineering, Ghent University, Ghent
2007 – 2008	MSc in Applied Informatics (Master after Master), Faculty of Engineering and Architecture, Ghent University, Ghent
2002 – 2007	MSc in Biology, option Zoology, Faculty of Sciences, Ghent University, Ghent
1996 – 2002	Secondary school, Latin – Mathematics, K.A. III Voskenslaan, Ghent

PROFESSIONAL CAREER

2009 – 2013	Researcher at the Institute for Agricultural and Fisheries Research (ILVO), Technology and Food Science Unit, Agricultural Engineering Research subject: 'Experimental and model-based study of airflows and ammonia distributions in and around animal houses'

PUBLICATIONS

INTERNATIONAL JOURNALS WITH PEER REVIEW

De Paepe, M., Pieters, J.G., Cornelis, W.M., Gabriels, D., Merci. B., Demeyer, P. (2014). CFD simulations of NH_3 mass transfer in an experimental slurry pit set-up: effects of headspace height, air velocity and direction. (Prepared for submission.)

De Paepe, M., Pieters, J.G., Cornelis, W.M., Gabriels, D., Merci. B., Demeyer, P. (2014). Ammonia mass transfer in a real-scale slurry pit set-up: effects of headspace height, air velocity and direction. (Submitted for review at *Biosystems Engineering.*)

De Paepe, M., Pieters, J.G., Cornelis, W.M., Gabriels, D., Merci. B., Demeyer, P. (2014). Real-scale test installation for the study of ammonia transfer processes at slurry pit level. (Submitted for review at *Biosystems Engineering.*)

De Paepe, M., Pieters, J.G., Cornelis, W.M., Gabriels, D., Merci. B., Demeyer, P. (2013). Airflow measurements in and around scale model cattle barns in a wind tunnel: effect of wind incidence angle. *Biosystems Engineering*, 115(2), 211-219.

De Paepe, M., Pieters, J.G., Cornelis, W.M., Gabriels, D., Merci. B., Demeyer, P. (2012). Airflow measurements in and around scale model cattle barns in a wind tunnel: effect of ventilation opening height. *Biosystems Engineering*, 113(1), 22-32.

CONFERENCE PROCEEDINGS (FIRST AUTHOR)

De Paepe, M., Pieters, J.G., Merci. B., Demeyer, P. (2013). A real-scale test facility for the study of ammonia emissions from a slurry pit - Effect of airflow rate and airflow direction at the slatted floor level. In: Proceedings of the 11th International Congres 'Bau, Technik und Umwelt in der landwirtschaftlichen Nutztierhaltung', 2013, Vechta, Germany.

De Paepe, M., Pieters, J.G., Cornelis, W.M., Gabriels, D., Merci. B., Demeyer, P. (2013). Computational modelling and scale model validation of airflow patterns in naturally ventilated barns. In: ISHS Acta Horticulturae, 1008 – 1st International Symposium on CFD Applications in Agriculture. CIGR-AgEng, 2012, Valencia, Spain. Editor: Suay, R. ISBN: 978-90-66056-76-3. Available online at: http://www.actahort.org/books/1008/1008_22.htm

De Paepe, M., Pieters, J.G., Cornelis, W.M., Gabriels, D., Merci. B., Demeyer, P. (2010). Modelling airflow patterns and the behaviour of ammonia in and around naturally ventilated barns. In: Proceedings of the 13th Faculty of Engineering and Architecture (FEA) PhD Symposium, Ghent, Belgium.

NATIONAL JOURNALS

De Paepe, M. (2012). Gasemissies uit de mestkelder in kaart gebracht. *Landgenoten*, 32, 18-19.

De Paepe, M. (2009). Optimaal gebruik van natuurlijke ventilatie. *Landbouw & Techniek*, 9, 45.

De Paepe, M. (2009). Onderzoek naar het optimaal gebruik van natuurlijke ventilatie in agrarische gebouwen. *Mededeling ILVO (Nieuwsgolf),* 61, 84-87.

De Paepe, M. & Polet, C. (2007). "Numerous and tall": a revision of the Late Neolithic human remains found in a collective burial site at Sclaigneaux (prov. Namur), Belgium. *Notae Praehistoricae*, 27, 163-168.

SCIENTIFIC ACTIVITIES

ORAL PRESENTATIONS AT CONFERENCES

July 8th, 2012 — Computational modelling and scale model validation of airflow patterns in naturally ventilated barns.
CIGR-AGENG 2012 International Conference of Agricultural Engineering, Valencia, Spain.

September 17th, 2009 — A study on the optimal use of natural ventilation in agricultural buildings.
Conference of the UNESCO Chair on Eremology, International Centre for Eremology (I.C.E.), Ghent, Belgium.

May 7th, 2009 — Onderzoek naar het optimaal gebruik van natuurlijke ventilatie in agrarische gebouwen.

Studienamiddag 'Samen naar rationeel energiegebruik in land- en tuinbouw', Melle, Belgium.

December 15th, 2007 "Talrijk en groot": een herziening van de laat-neolithische menselijke resten uit een collectief graf te Sclaigneaux (prov. Namen).
Congres van de Contactgroep "Prehistorie", Koninklijk Belgisch Instituut voor Natuurwetenschappen, Brussels, Belgium.

POSTER PRESENTATIONS AT CONFERENCES

December 5th, 2010 Modelling airflow patterns and the behaviour of ammonia in and around naturally ventilated barns.
13th Faculty of Engineering and Architecture (FEA) PhD Symposium, Ghent, Belgium.

DANKWOORD

Dit werk was niet mogelijk zonder mijn promotoren dr. Peter Demeyer, prof. dr. ir. Jan Pieters en prof. dr. ir. Bart Merci. Bedankt voor jullie geduldige inzet en vele suggesties om mijn teksten te kunnen verbeteren. Ook dr. Lieve Herman en prof. dr. ir. Erik Van Bockstaele wens ik te bedanken om mij deze uitzonderlijke kans te bieden bij ILVO. Tevens bedank ik de voltallige leescommissie voor hun inzet.

Aangezien men een doctoraat maar zelden alleen uitvoert, en al zeker niet zonder het geschikte materiaal, ben ik de technici van ILVO-T&V (Ronny, Olav, Bart'en E. & L., Tim, Eric, Davy, Jan, Robert) bijzonder dankbaar voor hun waardevolle hulp bij het helpen bouwen van de diverse testopstellingen, het verifiëren van de meettoestellen en tenslotte om mij gebruik te laten maken van het deskundig ingerichte atelier, wat toch een beetje hun heilige grond is. Nele, Eva en de thesisstudenten Dieter Lesaffre en Ben Hautekeete, bedankt voor het helpen op punt stellen van allerlei componenten van het emissielab ("de mestput", zoals we voor het gemak zeggen).

Het onderzoeksluik in de I.C.E. windtunnel kon gebeuren dankzij de enthousiaste medewerking en de kennis van prof. dr. ir. Wim Cornelis en prof. dr. ir. Donald Gabriels, waarvoor veel dank. Dr. ir. Reni Demeester en ir. Nicholas Agon, jullie hebben mij veel kneepjes van het complexe CFD-vak bijgeleerd, zonder dewelke dit doctoraat ook niet mogelijk zou geweest zijn. Dr. Stephanie Van Weyenberg, bedankt voor jouw hulp met de statistiek. Ook al was ik de zoveelste collega die jou hiermee kwam lastigvallen wegens een-beetje-te-moeilijk-om-er-snel-nog-bij-te-nemen, je deed het zichtbaar met veel plezier.

Uiteraard bedank ik ook alle andere vrollega's (!) bij ILVO-T&V voor hun steun en nooit aflatende medeleven. Energietechnologe, zeg maar eco-warrior, Veerle: jij was er sinds dag 1 op mijn toenmalig bureau (en ook jouw toenmalig bureau, eigenlijk feitelijk – wat wordt daar veel verhuisd…) en jij toonde meteen aan dat het goed zat met de sfeer op onze gang, alsook met de kabouters… Bedankt voor de vele fijne momenten en nuttige tips! In dezelfde categorie: big shout out to Dieter, doctor D.! Jij ontfermde je niet alleen snel over mij, maar weet ook aan iedereen de soms onontbeerlijke ontspanning over de middag te brengen, zij

het met je gitaar, poker, schaken, (extreme) petanque of ander verantwoord speelgoed (zo heet dat dan) als viking kubb. Ecollega nummer 3, Gerlinde, jij bent er nog niet zó heel lang bij, maar je hoorde er wat mij betreft ook meteen thuis, wat zeker veel te maken heeft met je nooit aflatende vrolijkheid en jouw recht-door-zee-heid. Tim U. en Nathalie, jullie heb ik ook nog weten beginnen op mijn toenmalig bureau. Jullie goed gezelschap was ook altijd een plus! Verder wens ik de hele groep te bedanken voor de vele geanimeerde gesprekken en activiteiten: Ingrid, Rolinde, Bert B., Liesbeth, Jarissa, Jürgen, Koen, Annelies, Sarah, Sophie, Filip, Els, Johan, Katrien, Tim VDG, Simon, David, Donald, Sofija, Marleen, Els, Claudia, Elsy, Sofie, Magda, … (Altijd spannend om niemand te vergeten in zulke lijstjes! Mocht ik het toch doen, sorry! Het moest snel gaan.) Zodus, Philippe, je dacht toch niet dat ik jou zou vergeten? De reden dat ik jou nu pas vermeld heeft natuurlijk alles te maken met de nodige zorg voor structuur, want jij bent veel meer dan een collega - ja, zelfs vrollega - geworden. Zonder jouw warme vriendschap, zwemcoaching en voortdurende motivatie was dit echt niet mogelijk geweest, dat meen ik. Jessy, blijf goed voor hem zorgen he (en omgekeerd). ILVO kan zo'n toffe gangmaker niet missen, zelfs alleen al voor de steeds goed bedachte personeelsactiviteiten!

Femke en Gwen, allebei echte globetrottende biologen met een gezond hoekje af, jullie brachten tijdens mijn jaren op het unief onnoemelijk veel plezier, zeker tijdens de talloze excursies. Het behalen van jullie mooie doctoraten en verder onderzoek motiveerde mij altijd om verder vol te houden, en daarna ook terug wat meer van de wereld te gaan zien!

Bart M.(iauw), jij was er voor mij op een moeilijk moment met een lach en een traan, maar gelukkig voor de rest van de tijd altijd met een lach, hoe flauw de mopjes soms ook mogen zijn ;) (Ik bedoel maar, heb jij nu wel of niet een broer met een camionette? De volgende persoon alvast wel!) Hendrik, tevens medebioloog, toegepaste informaticus en (hier houdt de vergelijking helaas op) all-round talent: wij hebben op tal van vlakken uncharted territories mogen ontdekken, het liefst van al vanop een snowboard op één of andere misty mountain (hier moet ik ook Stijn en tektonik vermelden) of als buddies tijdens een stevige portie gamegeweld. Ik kijk er ongelooflijk naar uit om binnenkort een van jouw eigen creaties te mogen spelen! Kwinten, de man-geworden basgitaar, bij jou kan ik ook altijd terecht voor eender wat. Jouw warme persoonlijkheid en gastvrijheid is echt een voorbeeld.

XXX. Fanny, Valerie, Veerle, Maria, Tommeke, Sarah, Claire en co., ook allen bedankt voor de leuke gesprekken en het nodige entertainment.

Natuurlijk wens ik mijn ouders Ann en Luc niet alleen te bedanken voor hun jarenlange zorg en steun, maar ook voor hun geloof in mij toen ik het zelf weer maar eens kwijt was. En we zijn nog niet helemaal klaar, want: Eline, liefje, jou bedank ik natuurlijk ook voor je steun (pomponnetjes!) en om het zo al 3 jaar vol te houden met mij, gezien de drukte die er geweest is. Het wordt nu dringend tijd om er samen nog iets veel mooier van te maken. :)

Ook zonder muzikale motivatie was dit werk niet mogelijk. De betere schrijfsessies gebeurden met een soundtrack van klassieke grootheden als Chopin, Beethoven en Satie, maar ook The Smiths, Editors, Metallica, Amenra en vele anderen...

Aan allen nog eens eeuwige dank!

– Merlijn